Hampshire Water Transfer & Water Recycling Project

Environmental Statement Appendix 19.11 Havant Thicket Reservoir water quality modelling

VOLUME NUMBER: 6

PLANNING INSPECTORATE SCHEME NUMBER: WA010002

APPLICATION DOCUMENT REFERENCE: 6.2

APFP REGULATION: 5(2)(a)

May 2026

Version 0

from Southern Water

Havant Thicket Reservoir

2025 Interim Update to Water Quality Modelling of Recycled Water Inputs

Future Water MJJV Limited

August 20, 2025

→ The Power of Commitment

Project name		Havant Thicket Reservoir Project					
Document title		Havant Thicket Reservoir | 2025 Interim Update to Water Quality Modelling of Recycled Water Inputs					
Project number		12547181					
File name		HTR-GHD-RZ-RE-RP-Y-XXXX (Revised 2025-08-20 RevA - Not FW Reviewed).docx					
Status Code	**Revision**	**Author**	**Reviewer**		**Approved for issue**		
			Name	**Signature**	**Name**	**Signature**	**Date**
S0	Prelim Draft	[redacted]					8-20-25
S1	Final Draft						
Rev0	Final						

[redacted]uatic Sciences

Executive Summary

Portsmouth Water are planning a new water supply reservoir, Havant Thicket Reservoir (HTR), with an expected completion date by 1 October 2029, and subsequent filling over 3 consecutive wet periods (October-May). HTR was originally intended to serve as an emergency water supply storage in the event of drought conditions. Southern Water are planning a new recycled water plant to serve as an additional regional water source with an expected onset of continuous inputs of recycled water (RW) to HTR on 1 October 2033. The effect of RW inputs on the future water quality (WQ) of HTR relative to the originally planned (also referred to as reference) operational regime (i.e. maintain at/near Top Water Level [TWL] with ~1 month of winter inputs of springs water) is evaluated in this investigation.

The Aquatic Ecosystem Model – Three Dimensional (AEM3D) has been applied to HTR to design a bubble plume destratification system for the original HTR reference design (GHD 2023) and updated design (GHD 2025a), and a RW and springs inlet location options analysis (GHD 2025b). This modelling framework was tailored by GHD (2024) and was again used in this investigation to simulate a 12 year baseline scenario of filling (~2 years over 3 winters, 'fill' stage), and maintaining reservoir at/near TWL prior to (~1 year, the 'classic' stage) and after the onset of (~9 years, the 'recycled' stage) RW inputs.

This investigation is an interim update to the GHD (2024) model forecasts that accounts for the following:

– The RW and spring inlet location into the reservoir has moved from the north basin (eastern borrow pit) to the south basin (western borrow pit) in closer proximity to the withdrawal infrastructure.
– An updated bubble plume destratification system design, in particular the layout of the bubbler lines in the south basin.
– Improved characterisation of the RW WQ with the planned implementation of a High Rejection Rate Membrane (HRRM) that substantially decreases nutrient concentrations of this water source.
– Improved characterisation of the Bedhampton Springs and Havant Springs WQ.
– Inclusion of calcium (Ca), sodium (Na), chloride (Cl) and sulphate (SO_4) into the modelling framework.
– A later planned onset of reservoir filling on 1 October 2029 (previously 1 November 2026).
– A later planned onset of RW inflows into the reservoir on 1 October 2023 (previously 1 June 2032).
– Changes to the 'normal' and 'drought' operational scenarios in terms of RW and springs inputs, and water supply withdrawals.

As with GHD (2024), the objectives of this interim updated modelling investigation are to provide quantitative forecasts of the future reservoir and withdrawal WQ to inform drinking water safety planning (DWSP) and to evaluate their environmental acceptability.

Typically, WQ monitoring data is used to calibrate and verify a 3D WQ model. As there is no monitoring data of the future HTR, a generic set of model parameter values was established from published AEM3D applications.

The model was configured as follows:

– Scenarios were simulated with a coarse model grid (50 m horizontal and 1 m vertical resolution) for time efficiency, which yield very similar predictions as 2 scenarios with a fine model grid (20 m horizontal and 1 m vertical resolution).
– The current bathymetry design relative to the reference design has a larger and deeper north basin, and smaller and deeper south basin that are separated by a sill. The deepest portion of the south basin is a hole with a maximum depth that is ~5 m below the design elevation of the bubble plume lines of the mixing system.
– Withdrawals for water supply and environmental compensation flows to Riders Lane Stream were primarily from the high draw-off, though the middle draw-off was used in 1 scenarios with substantial drawdown of the reservoir's surface during drought conditions. Inflows include 3 local streams into the wetland along the

northern boundary of the reservoir, and an inlet structure that discharges springs water and/or RW into the deep waters of the south basin at a horizontal distance of ~200 m from the withdrawal infrastructure at a depth well below the high and middle draw-off openings. Rainfall is a model input and evaporation is simulated. The WQ model inputs of the streams, RW and springs were based on measurements and estimates. Nitrogen (N) and phosphorus (P) rainfall estimates were included as model inputs along with N, P and carbon (C) load estimates from birds.

– A range of WQ variables were modelled including:
  - P determinands of phosphate, dissolved and particulate organic P, algal internal P and total P.
  - N determinands of nitrate, ammonia, dissolved and particulate organic N, algal internal N and total N.
  - C determinands of dissolved inorganic carbon, alkalinity, pH, dissolved and particulate organic C, total algal biomass (as chlorophyll-a) and total organic C.
  - Metals determinands of reduced dissolved and oxidised particulate manganese and iron.
  - Other determinands include temperature, dissolved oxygen, inorganic suspended particles of clay and silt, calcium, sodium, chloride and sulfate.
– The GHD (2025a) design of the bubble plume destratification system for the current HTR bathymetry was adopted. All scenarios were simulated with nighttime (1800-0600, operational cost reduction measure) bubbler operations to demonstrate the effectiveness of this in-reservoir control measure across a number of operational scenarios. Additionally, the 12 year baseline scenario was run without bubbler operations to forecast reservoir and withdrawal WQ in the absence of this control measure.
– The stabilisation effect (occurrence of high in-reservoir dissolved inorganic and organic matter, and low DO, from the decomposition and mineralisation of inundated above and below ground terrestrial organic matter) during the initial 4 years of reservoir filling was estimated and modelled.

The key findings from this investigation include:

– Simulations with fine (20x20x1 m) and coarse (50x50x1 m) grids with nighttime bubbler operations over the 12 year baseline scenario compared well over the ‘fill’, ‘classic’ and ‘recycled’ stages.
– Because of its modest size (~1.5 km fetch), the horizontal WQ variability in the reservoir’s main body is forecast to be very low. However, the sill that separates the two basins is a physical barrier that allows the WQ of the bottom waters to diverge. The larger (~18 ha with depths >~15 m) but shallower (maximum depth 17 m) north basin is forecast to have greater wind-induced vertical mixing than the smaller (~4.5 ha with depths >~15 m) but deeper (maximum depth 22.5 m) south basin. Hence, in the absence of mixing system operations during seasonal stratification (~April-~August) the deep waters of the south basin are forecast to undergo anoxia (DO of ~0 mg/L), whereas DO will remain higher in the north basin due to differences in basin scale vertical mixing. The occurrence of anoxia in the south basin’s deep hole is forecast to cause high sediment fluxes and elevated bottom water concentrations of dissolved iron (~5 mg Fe/L) and manganese (~0.5 mg Mn/L), and 2-3 fold increases of dissolved inorganic (phosphate, ammonia) and dissolve organic (P, N, C) matter relative to the north basin.
– Nighttime (1800-0600) bubbler operations from April-August (seasonal stratification period) are an effective ‘in-reservoir’ control measure to maintain a well-mixed and well-oxygenated water column with low bottom water concentrations of dissolved metals, and dissolved inorganic and organic matter. Bubbler operations are also forecast to moderately decrease total algal biomass. Bubbler operations are the primary in-reservoir control measure that is stipulated in the DWSP.
– Interestingly, the withdrawal WQ is not forecast to be overly sensitive to bubbler operations. This is largely due to the limited volume of poor WQ that is forecast with the coarse model grid in the bottom waters of the south basin’s deep hole, which is effectively diluted by the large volume in the remainder of the reservoir. As noted beforehand, the fine grid simulation of the baseline scenario did not predict deleterious WQ in the bottom waters of the south basin’s deep hole, which indicates that the coarse grid simulations do not properly resolve the hydrodynamics (and associated vertical mixing) in this limited region.

– Stabilisation effects on reservoir WQ are forecast to only be material during the first year of filing. As filling of the reservoir will be over 3 consecutive winters, freshly inundated soils and terrestrial biomass with higher deleterious effects on WQ are staggered in time. Additionally, because much of the inundation area is comprised of borrow pits to source material to construct the embankments, the remnant terrestrial organic biomass (and its contribution to the stabilisation effect) will be relatively low.
– A comparative analysis of the baseline scenario's 'recycled' stage relative to the extended classic scenario (minimal springs inputs and withdrawals), 3 'normal' operational scenarios (surface maintained at/near TWL, but with substantially higher RW/springs inputs and withdrawals) and 3 'drought' operational scenarios (very high RW/springs inputs with a period of reservoir drawdown well below TWL) indicated the following:
    - The 'extended classic' scenario and the 'recycled' stage of the baseline scenario are predicted to have very similar WQ. In part, the combination of the ~50% total P of the RW (0.017 mg P/L) than the springs (0.03 mg P/L), and the total P losses via the sizeable continuous withdrawals (~15 MLD), result in similar WQ forecasts as the 'extended classic' scenario.
    - Increased inputs into and withdrawals from the reservoir for the 'normal' operational scenarios were forecasted to also have a relatively modest difference from the baseline 'recycled' stage WQ. Further, the final year of these 'normal' operational scenarios utilised the baseline 'recycled' stage hydrology as model inputs, which are forecast to rapidly converge to the baseline WQ. In short, these operational scenarios demonstrate that increases of the inflows into and withdrawals from the reservoir, and variations in the proportion of source waters (i.e. springs versus RW), have a relatively modest effect on WQ and that the response time to return to baseline 'recycled' stage WQ with baseline 'recycled' stage hydrology is on the order of ~1 year.
    - Similarly, very large increases in the 'drought' operational discharges into and from the reservoir were not forecasted to dramatically change the reservoir WQ. A minimum retention time of ~50 days was forecast for the scenario over the period with the most sizeable reservoir drawdown of the surface, the only scenario with water extracted from the middle draw-off. This was the most extreme drought scenario considered in terms of drawdown of the surface level, which indicates a minimal risk of short-circuiting with the current reservoir morphology, inlet location and withdrawal operational rules.

Model forecasts of the future WQ of HTR and its withdrawals have been provided in digital format to support the preparation of the DWSP and other environmental considerations. This report provides the following supporting information for these objectives:

– Tables of minima and maxima of selected determinands to inform the withdrawal WQ envelope for the DWSP.
– Tables of the forecasted ecological status on the basis of the 2015 Water Framework Directive Directions of the:
    - Withdrawals for releases as environmental compensation flows to Riders Lane Stream immediately downstream of HTR. All scenarios forecast a 'high' ecological status of downstream releases in terms of dissolved oxygen, ammonium, pH, phosphate and water temperature, which supports the comparative analysis assessment that variations in WQ across the scenarios are relatively modest.
    - Reservoir WQ is forecast as 'good' to 'high' ecological status in terms of ammonium, total phosphorus, algal biomass, and dissolved oxygen of the bottom waters of the north basin. The dissolved oxygen in the bottom waters of the deep hole in the south basin are forecast as a 'moderate' to 'good' ecological status on the basis of the coarse grid simulations, which have been identified to not adequately resolve the hydrodynamics within this limited volume of the reservoir.

The current design of the reservoir bathymetry is undergoing updates in effort to source appropriate material for the dam embankments, which will likely include:

– A large channel through the sill between the two basins that will provide connectivity and a horizontal exchange pathway.
– Elimination of the south basin's deep hole so that the lakebed in this region is at the same elevation as the north basin, which will allow:

- The bubble plume destratification system to effectively maintain vertically well mixed conditions throughout the main body of the reservoir.
- Natural basin scale mixing processes to function effectively across the entirety of the reservoir's deep bottom waters.

This change to the reservoir bathymetry is anticipated to remove the WQ risks (albeit minor) associated with the current design with a deep hole in the south basin, and overcome the coarse grid simulations deficiencies in adequately reproducing the hydrodynamics (vertical mixing) of this small volume.

Upon finalisation of the reservoir bathymetry design, it is recommended that the scenarios in this investigation are re-run and provided in a Final Update Report.

This report is subject to, and must be read in conjunction with, the limitations set out in Section 1.3 and the assumptions and qualifications contained throughout the Report.

Contents

Table index

Figure index

Appendices

Abbreviations, acronyms and units

Abbreviation, acronym or unit	
3D	Three-Dimensional
°C	Degrees Celsius
ηm	Nanometers
µg	Microgram
AEM3D	Aquatic Ecosystem Model – Three Dimensional
ANC	Acid Neutralising Capacity
BOD	Biological Oxygen Demand
BTO	British Trust for Ornithology
C	Carbon
Ca	Calcium
$CaCO_3$	Calcium Carbonate
CAD	Computer Aided Design
CFSv2	Climate Forecast System, version 2
Chl-a	Chlorophyll-a
CO2	Carbon Dioxide
Cl	Chloride
CS	Current Speed
d	Day
DFe	Dissolved Iron
DIC	Dissolved Inorganic Carbon
DIM	Dissolved Inorganic Matter
DMn	Dissolved Manganese
DO	Dissolved Oxygen
DO_{Sat}	Percentage Saturation of Dissolved Oxygen
DOC	Dissolved Organic Carbon
DOM	Dissolved Organic Matter
DON	Dissolved Organic Nitrogen
DOP	Dissolved Organic Phosphorus
DWSP	Drinking Water Safety Plan
$EQR_{Chl\text{-}a}$	Ecological Quality Ratio for Chl-a
EQR_{PTI}	Ecological Quality Ratio for Phytoplankton Trophic Index
EQR_{Cyan}	Ecological Quality Ratio for Cyanobacteria Blooms
Fe	Iron
FRP	Filterable Reactive Phosphorus (≈PO_4)
g	Gram
ha	Hectare

Abbreviation, acronym or unit	
HMWB	Heavily Modified Water Body
HRRM	High Rejection Rate Membrane
HTR	Havant Thicket Reservoir
IN	Internal Nitrogen
IP	Internal Phosphorus
km	Kilometer
km^2	Square Kilometer
L	Liter
m	Meter
m^2	Square Meter
MA	Monthly Moving Average
meq	Milliequivalent
mg	Milligrams
min	Minute
ML	Megaliters
MLD	Megaliters per Day
mm	Millimeter
Mn	Manganese
N	Nitrogen
Na	Sodium
NH_3	Ammonia
NH_4	Ammonium
NH_X	Total Ammonia (=NH_4 + NH_3)
NO_3	Nitrate
NO_2	Nitrite
NO_X	Oxidised Inorganic Nitrogen (=NO_3+NO_2)
OD	Ordnance Datum
NCEP	National Centers for Environmental Prediction
P	Phosphorus
PAR	Photosynthetic Active Radiation
pCO2	Partial Pressure of CO2 in water
PFe	Particulate Iron
PO4	Phosphate
PMn	Particulate Manganese
POC	Particulate Organic Carbon
POM	Particulate Organic Matter
PON	Particulate Organic Nitrogen
POP	Particulate Organic Phosphorus

Abbreviation, acronym or unit	
Precip-Net	Precipitation Network
PW	Portsmouth Water
RT	Retention Time
RW	Recycled Water
s	Second
SiO2	Silicon Dioxide
SO4	Sulfate
SOD	Sediment Oxygen Demand
SS	Suspended Solids
STP	Sewage Treatment Plant
SW	Southern Water
T	Temperature
TA	Total Alkalinity
TAC	Total Algal Concentration
TFe	Total Iron
TMn	Total Manganese
TN	Total Nitrogen
TOC	Total Organic Carbon
TP	Total Phosphorus
TWL	Top Water Level
UKEAP	United Kingdom Eutrophying and Acidifying Network
UK-TAG	Water Framework Directive – United Kingdom Technical Advisory Group
WFD	European Commission Water Framework Directive 2006/60/EC
WQ	Water Quality
WQSG	Water Quality Steering Group for the Havant Thicket Reservoir Project
WSW	Water Supply Works

1. Introduction

1.1 Purpose of this report

Portsmouth Water (PW) is constructing a new water supply reservoir, Havant Thicket Reservoir (HTR), to the north of Havant and immediately to the southwest of Rowlands Castle with an anticipated filling date of 1 October 2029 (Figure 1.1). The reservoir will be filled over three consecutive winters (October-March) to Top Water Level (TWL). Initially, HTR was intended to serve as an emergency water supply storage in the event of drought conditions. As the local catchment is small, the primary source of water to fill and to maintain the reservoir at/near TWL was to be excess water yield from Bedhampton Springs and Havant Springs. Atkins (2020) developed a model to predict total phosphorus (TP) and the reservoir trophic status during the filling and maintenance of HTR as an emergency water supply storage.

Southern Water (SW) are planning a new recycled water plant to serve as an additional regional water source, which is to be routed through the future HTR. This investigation provides updated forecasts of recycled water (RW) inputs on the water quality (WQ) of the future HTR. The facility will have capacity to provide a continuous inflow of ~10-60 megaliters per day (MLD) of RW to HTR from 1 October 2033 under typical operational regimes with continual withdrawals of ~20-100 MLD for water supply. Maintenance of HTR at/near TWL with the appropriate balance between RW and spring water inflows, and withdrawals for water supply and compensation flows to Riders Lane Stream, will also achieve the original objective for the planned storage to serve as an emergency water supply during future droughts.

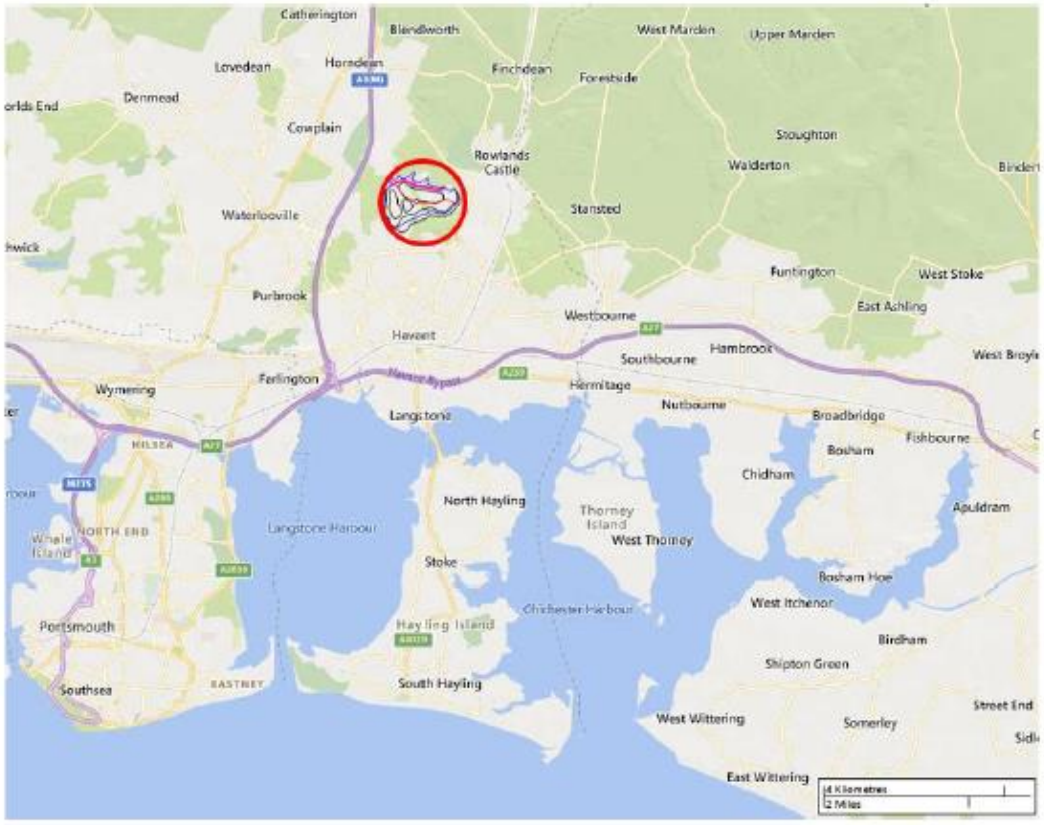

Figure 1.1 Location of the future Havant Thicket Reservoir.

GHD (2023) developed and applied a three-dimensional (3D) WQ model of the future reservoir over a period of ~8 months that encompassed the spring to autumn seasons when seasonal thermal stratification will occur in the

absence of a destratification system. The GHD (2023) objective was to design a bubble plume destratification system as the primary in-reservoir WQ management measure to prevent seasonal thermal stratification, and associated low dissolved oxygen (DO) conditions and deleterious WQ. GHD (2023) also demonstrated that the bubble plume destratification design will prevent persistent thermal stratification with continuous RW inflows of ~7.5 MLD. The GHD (2023) predictions were based on the HTR's reference design bathymetry, which has undergone substantive updates in the interim.

GHD (2024) tailored the GHD (2023) modelling framework to simulate a 15 year period (2027-2041) that included the stages of filling (~3years, the 'fill' stage), maintaining the reservoir at/near TWL prior to (~3 years, the 'classic' stage) and after the onset of (~10 years, the 'recycled' stage) RW inputs to inform drinking water safety planning (DWSP) and environmental considerations in regards to in-reservoir and withdrawal WQ. The inflow location of RW and springs inputs into HTR was located in the north basin (eastern borrow pit) with a substantive separation distance (~500 m) from the withdrawal infrastructure for water supply and environmental compensation flows in the south basin (western borrow pit)[1]. Additionally, scenarios with an alternate inlet location in the south basin and reductions in the phosphorus content of RW were also considered.

This investigation is an interim update of the GHD (2024) model forecasts that accounts for:

– The RW and spring inflow location has been moved to the south basin in closer proximity to the withdrawal infrastructure.
– An updated bubble plume destratification system design, in particular the layout of the bubble lines in the south basin.
– Improved characterisation of the RW WQ with the planned implementation of a High Rejection Rate Membrane (HRRM) that substantially decreases nutrient concentrations from this water source.
– Improved characterisation of the WQ of Bedhampton Springs and Havant Springs.
– Inclusion of calcium (Ca), sodium (Na), chloride (Cl) and sulphate (SO_4) into the modelling framework.
– A later planned onset of reservoir filling on 1 October 2029 (previously 1 November 2026).
– A later planned onset of RW inflows into the reservoir on 1 October 2023 (previously 1 June 2032).
– Changes in the operational and drought scenarios in terms of RW and springs water inputs, and water supply withdrawals, over the 12 year simulation period from 1 January 2030 to 31 December 2041.

1.2 Scope

The scope of this investigation includes:

– Update the GHD (2024) model configuration and inputs.
– Carry out 3D WQ simulations of updated scenarios.
– Update GHD (2024) WQ forecasts of the:
  - Withdrawals to inform DWSP and environmental acceptability of downstream releases.
  - Reservoir to inform whether the forecast WQ will have an acceptable ecological status.
– Recommend management measures to mitigate potential WQ risks.

1.3 Limitations

This report has been prepared by GHD for Future Water MJJV Limited and may only be used and relied on by Future Water MJJV Limited for the purpose agreed between GHD and Future Water MJJV Limited as set out in Section 1.1 of this report.

[1] From a construction point of view, because material to build the HTR dam embankment is sourced from two pits in the eastern and southwestern regions of the future reservoir, they are referred to as the eastern and western borrow pits, respectively. Once the dam is constructed an operational the appropriate terminology is to refer to these borrow pits as basins. Hence, in this report the eastern borrow pit is referred to as the northern basin and the western borrow pit as the southern basin.

GHD otherwise disclaims responsibility to any person other than Future Water MJJV Limited arising in connection with this report. GHD also excludes implied warranties and conditions, to the extent legally permissible.

The services undertaken by GHD in connection with preparing this report were limited to those specifically detailed in the report and are subject to the scope limitations set out in the report.

The opinions, conclusions and any recommendations in this report are based on conditions encountered and information reviewed at the date of preparation of the report. GHD has no responsibility or obligation to update this report to account for events or changes occurring subsequent to the date that the report was prepared.

The opinions, conclusions and any recommendations in this report are based on assumptions made by GHD described in this report (refer Section 1.4 of this report). GHD disclaims liability arising from any of the assumptions being incorrect.

1.4 Assumptions

The following assumptions have been made in this investigation:

– No spillway is incorporated into the 3D model as simulated water levels are maintained at/below TWL with no uncontrolled discharge over the dam spillway crest.

– The GHD (2023) bubble plume destratification system was designed on the basis of the reference design bathymetry, which has undergone material revisions in the interim. GHD (2024) utilised the GHD (2023) design specifications except for a reorientation of the south basin bubble plume line. GHD (2025a) updated the design specifications of the bubble plume destratification system for the current design bathymetry, which are evaluated in this investigation.

– The potential effect of future climate change on HTR WQ without a bubble plume destratification system is likely to manifest as stronger and more persistent seasonal thermal stratification. Persistent seasonal thermal stratification will increase the risk of deoxygenated hypolimnetic waters with associated WQ risks (e.g. elevated nutrient and metals fluxes). The primary 'in-reservoir' control measure to manage the effects of seasonal (and persistent) thermal stratification and associated deleterious WQ is the bubble plume destratification system. The bubble plume destratification system was intentionally 'over' designed by GHD (2023) and GHD (2025a) to maintain a future HTR condition with only short periods (days, if any) of thermal stratification during extended periods of low winds and high surface heat fluxes. Hence, a potential temperature increase of several degrees over the entire water body may occur due to climate change driven atmospheric warming, but the destratification system (if operated appropriately) will prevent the occurrence of seasonal (and persistent) thermal stratification. As such, climate change effects are not considered explicitly in this investigation due to this key 'in-reservoir' management measure.

– The GHD (2024) assessment focused on an inlet location for the inputs of RW and spring water in the north basin (eastern borrow pit). GHD (2025b) carried out an inlet location options assessment for the current design bathymetry and determined that moving the inlet site to the south basin (western borrow pit) did not pose a material WQ risk. The south basin inlet location is evaluated in this investigation.

– GHD (2024) implicitly assumed that prior to the filling of HTR, the soils are not dispersive. Hence, dispersive fluxes of inorganic particles from the soils were not considered by GHD (2024). This investigation explicitly states this assumption of non-dispersive material in the upper ~30 cm of the soil horizon. If dispersive soils occur in the upper horizons of the soil profile within the HTR footprint, this investigation assumes that these regions will be capped by ~30 cm of non-dispersive material.

– Recognising the reservoir does not yet exist and the forecasts of in-reservoir and withdrawal WQ cannot be verified, the model has been configured in a generic manner in effort to provide indicative predictions of the future HTR (see Section 2.1.2). Therefore:

  - The forecasts of HTR WQ should be used as an 'additional available estimate' of the future in-reservoir and withdrawal WQ. Solely the use of the WQ forecasts of the raw water supply from this investigation as the basis of design for water treatment processes of the future HTR withdrawals is discouraged.
  - There is a degree of predictive confidence in regards to the forecasted total phytoplankton biomass as three generic groups (i.e. green algae, blue-green algae, diatoms) have been configured into the modelling framework with productivity characteristics that span typical seasonal variations in water

temperatures and WQ in temperate lakes and reservoirs. However, predictive confidence is low in terms of seasonal and interannual variations in the forecasted composition of the phytoplankton assemblage (i.e. relative proportion of algal groups at any given time). Therefore, only total phytoplankton biomass (i.e. simulated as total algal chlorophyll-a) is reported and evaluated in this investigation.

– Additional assumptions and further clarifications of the above assumptions in terms of model configuration and inputs are provided in relevant sections of this report.

2. Model description

2.1 Model capability

2.1.1 Hydrodynamics and morphology

Modelling of the future HTR needs to reasonably predict the spatial-temporal WQ variability in the reservoir and temporal variability of the withdrawals to inform environmental and DWSP considerations, respectively. The adopted modelling framework of this investigation (Section 2.2) simulates the following hydrodynamic and morphological related processes to provide credible forecasts of the future HTR WQ:

– Seasonal (and persistent) vertical thermal stratification will occur in the absence of a destratification system in the future HTR because of its depth (average ~9 m, maximum ~22 m). Further, because of its relatively modest size (~1.5 km length scale), horizontal variations in the surface waters of the main body will be constrained due to horizontal dispersion. Hence, the greatest degree of spatial WQ variability in the future HTR in the absence of a destratification system will be vertical variations during seasonally stratified periods. In fact, a vertical one-dimensional (1D) model would likely be sufficient to predict the WQ throughout most of the future HTR volume. However, the sill that separates the deep waters of north and south basins (see Section 4.1) provides a morphological setting for spatial WQ differences to evolve because:
  - Seasonal stratification during spring/summer in the absence of a destratification system is likely to occur and the WQ of the deeper waters in each basin will diverge (spatial variability) because:
    – The greater areal extent of the north basin's deep waters could potentially cause greater sediment fluxes into the bottom waters than the south basin's smaller deep water area if both had the same low dissolved oxygen (DO) levels.
    – The greater depth of the south basin, deep waters would likely have a longer duration of seasonal thermal stratification with lower DO levels and associated poorer WQ than the north basin.
    – The inflow structure location for RW and spring inputs in the deep waters of the south basin will further promote differing WQ relative to the north basin.
    – Though not a planned operational measure, or considered in this investigation, deep water withdrawals from the bottom scour in the south basin may lead to horizontal WQ variability relative to north basin through the extraction of bottom waters from this volumetrically smaller size basin.
  - With an appropriately operated destratification system these horizontal WQ variations in the deep waters of both basins will be greatly reduced as elevated DO will be maintained through the water column with bottom (near-sediment) WQ similar to the surface. As such, application of a 1D model is likely to give adequate WQ predictions within HTR and its withdrawals with bubbler operations.

– The wetland along the northern margin of the north basin will have a relatively minor effect on the hydrodynamics of the main body of the reservoir because of:
  - Its small volume relative to the future HTR's main body.
  - The local catchment discharge through the wetland is small relative to the planned RW and springs inflows through a dedicated inflow structure into the south basin.
  - Limited exchange with the reservoir's main body due to the five anthropogenic control structures that connect the wetland (i.e. invert elevations of 38.8 m ordnance datum [OD], which is 0.7 m below TWL at 39.5 m OD). Further, wetland-derived waters will be rapidly diluted/dispersed in HTR's main body. Hence, though the WQ of the wetland may differ from the reservoir due to morphology (shallow) and wetland vegetation (e.g. macrophytes), the spatial extent of wetland waters on the reservoir's main body WQ will be restricted due to limited exchange (via the control structures).

2.1.2 Water quality

A range of WQ determinands (e.g. DO, dissolved manganese [DMN], total algal concentrations [TAC]) are simulated in this investigation to inform DWSP and environmental considerations. The modelling framework's representation of the dominant WQ processes of these determinands (e.g. nitrification, particle settling, photosynthetic oxygen production) has been applied to simulate annual and interannual observations in reservoirs and lakes across a variety of settings (Ghane 2022, Caramatti 2021, Gharechchaman 2021, Trammer et al 2018, Missaghi & Hondzo 2010, Romero et al 2004). Spatial and temporal WQ variability in the future HTR will be driven by:

– Interactions between the physical aspects of the reservoir (e.g. bathymetry, inflow and withdrawal locations) with hydrodynamics as described in Section 2.1.1.
– Variability in the external loads of WQ determinands (i.e. external inputs of springs and RW, local streams, bird loads, rainfall).
– Variability in the internal loads (i.e. sediment fluxes) of WQ determinands (e.g. nutrients, dissolved metals) that will largely be driven by bottom water DO variations immediately overlying the sediments.
– Reservoir management (e.g. destratification system design and operation, quantity and quality of RW and springs inputs, withdrawal strategy).

Typically, WQ monitoring data of an existing reservoir is used to calibrate (i.e. reproduce a temporal subset of monitoring data satisfactorily) and to verify (i.e. reproduce satisfactorily another temporal subset of monitoring data with no additional 'tuning' of model parameters or inputs) a model. If the model reproduces the verification period adequately, then subsequent scenario simulations to forecast future states in response to changes in operations (e.g. variations in inflow and withdrawal discharge and/or WQ) and management (e.g. destratification operations) have a high degree of confidence. As clearly there is no monitoring data available of the future HTR, the following approach was adopted to provide a degree of confidence to forecasts:

– A catalogue of parameter values (e.g. nitrification rate, sediment oxygen demand [SOD], diatom growth rate) of primarily published Aquatic Ecosystem Model – Three Dimensional (AEM3D) applications across a wide range of lakes and reservoirs was collated.
– The catalogue of literature-based parameter values was primarily restricted to AEM3D applications to minimise bias from differences in WQ process parameterisations that can vary between models.
– A 'generic' model parameter set was established to reasonably forecast HTR WQ (Appendix B).

2.2 AEM3D model

2.2.1 Overview

AEM3D is a 3D numerical model that includes hydrodynamic and WQ modules to simulate the temporal behaviour of stratified water bodies from environmental forcing (Hodges & Dallimore 2023). AEM3D simulates the velocity, temperature and salinity of surface waters that are subjected to environmental and anthropogenic forcing such as wind, tides, surface heating and cooling, inflows, withdrawals, bubblers and mixers.

AEM3D can also be configured to simulate a range of WQ dynamics with a biogeochemical module that was adapted from the Computational Aquatic Ecosystem Dynamics Model (Hipsey & Hamilton 2008). The WQ module includes process representations of the carbon (C), nitrogen (N), phosphorus (P) and DO cycles, inorganic suspended solids behaviour, and phytoplankton and metals dynamics. In this application three phytoplankton groups (diatoms, green algae, blue-green algae) were simulated, which generally reproduce typical seasonal patterns of total algal biomass (as micrograms of chlorophyll-a [chl-a] per liter [µg chl-a/L]) in temperate lakes and reservoirs. The algal groups were configured with dynamic internal N and P stores and constant C:chl-a ratios. Five dissolved inorganic nutrients (phosphate [PO4], nitrate [NO3], ammonium [NH4], dissolved inorganic carbon [DIC], silicate [SiO2, for diatoms only]), three dissolved (dissolved organic C [DOC], dissolved organic N [DON], dissolved organic P [DOP]) and three particulate (particulate organic C [POC], particulate organic N [PON], particulate organic P [POP]) organic matter

groups, two inorganic suspended solid (SS) types (clay, silt), DO, and pH were simulated. Oxidised particulate (PMN, PFE) and reduced dissolved (DMN, DFE) forms of manganese and iron are simulated as well. All of these state variables undergo hydrodynamic dispersion and transport within the reservoir. Carbonate alkalinity (CA) is derived from DIC and pH. Total nitrogen (TN) and total phosphorus (TP) are derived as the total of all modelled N and P state variables.

2.2.2 Summary of key modelled processes

A summary of key modelled processes include:

- Photosynthetic available radiation (PAR, 400-700 ηm, meteorological input) was estimated as 45% of incident shortwave radiation (280-2800 ηm) (Jellison & Melack 1993), which is assumed to penetrate through the water column according to the Beer-Lambert Law with a vertically varying PAR extinction coefficient to account for variability in underwater light absorbing constituents including algal biomass, inorganic and detrital particles, and dissolved organic matter.
- The model tracks the mass of the particle components (POC, PON, POP, SS [clay, silt], PFE, PMN) in the sediment layer of each horizontal grid cell at the bottom of the water column due to accumulation from settling, losses from resuspension, and transformations in the sediment compartment (e.g. algal mortality). Particle resuspension is dependent on the model parameters of critical shear stress, maximum resuspension rate and half saturation constant for sediment mass concentration.
- The sediment fluxes of dissolved inorganic nutrients (DIC, PO4, NH4, NO3, SiO2), dissolved organic matter (DOM) (DOC, DOP, DON), reduced dissolved metals (DFE, DMN) and sediment oxygen demand (SOD) are based on parameter values (e.g. maximum [or minimum] sediment flux rate) of WQ process formulations.
- DO processes include atmospheric exchange, SOD, DOM mineralisation, nitrification, reduction of oxidised particulate metals, oxidation of reduced dissolved metals, photosynthetic oxygen production and respiratory oxygen consumption. Atmospheric exchange is based on the model of Wanninkhof (1992) and the flux equation of Riley and Skirrow (1974). Simulated SOD varies as a function of the overlying water temperatures and DO, and emulates the decomposition of DOM to DIC with a stoichiometrically equivalent amount of DO removal.
- Both the inorganic and organic, and dissolved and particle forms of C, N and P are modelled explicitly along the degradation pathway of particulate organic matter (POM) to DOM to dissolved inorganic matter (DIM). The N cycle includes the additional processes of denitrification and nitrification that are not in the C and P cycles. The silica cycle is simpler and includes the processes of biological uptake of dissolved silicon dioxide (SiO2), dissolved SiO2 sediment fluxes, settling of diatoms with internal SiO2 stores and accumulation in the sediments, and resuspension of diatoms from the sediments with internal SiO2 stores. The DIC cycle includes atmospheric fluxes of carbon dioxide (CO2) (driven by differences between the atmospheric and partial pressure of CO2 in water [pCO2]) via the Wanninkhof (1992) relation and the solubility product of CO_2 estimated from Weiss (1974). Alkalinity is assumed to be a conservative state variable with variations due to inflows, withdrawals, evaporative concentration and rainfall dilution. To estimate dissolved CO_2, pH is estimated from DIC and alkalinity at each time step with the Butler (1982) relation with the gaseous and aqueous phase CO_2 values related by Henrys Law. Simulated pH is an output to inform water treatment aspects of the raw water from the reservoir, but has not been configured in this investigation to influence any other modelled processes (e.g. sediment fluxes).
- Both reduced dissolved (DFE, DMN) and oxidised particle (PFE, PMN) forms of manganese and iron are modelled. Simulated DMN and DFE processes included sediment fluxes, oxidation to particle forms, and reduction of particle to dissolved forms. Simulated PMN and PFE processes included sediment resuspension, settling, reduction to dissolved forms, and oxidation of dissolved to particle forms.
- Three phytoplankton groups that are typical in temperate lakes/reservoirs (i.e. diatoms, chlorophytes [green algae], cyanophytes [blue-green algae]) were configured into the model and tracked in units of chl-a (as µg chl-a/L). For each phytoplankton group, the maximum potential growth rate (corrected for the simulated water temperature within a grid cell) is multiplied by the minimum value of expressions for limitation by PAR, P and

N (and SiO2 for diatoms). While there may be some interaction between limiting factors, a minimum expression likely provides a realistic representation of growth limitation (Rhee and Gotham, 1981). The internal P (IP) and N (IN) dynamics of the phytoplankton were modelled as dynamic intracellular stores (Droop 1974) where variable internal nutrient concentrations with dynamic nutrient uptake are bounded by minimum and maximum nutrient to chl-a ratios. Loss terms for respiration, natural mortality and excretion are modelled with a single 'respiration' rate coefficient, which is apportioned to pure respiratory losses (DO consumption balanced by DIC increase), and losses due to mortality (senescent algal biomass to POM) and excretion (excreted algal biomass to DOM). Typical settling rates were configured for each of the three phytoplankton groups, which are dynamically adjusted depending on the calculated viscosity. As stated in the assumptions of Section 1.4, the simulated total algal biomass as chl-a of the 3 modelled phytoplankton groups are presented in this report.

Schematics of the nutrient (P, N and C) and algae, DO, and inorganic particles (SS) and metals/metalloids are illustrated in Figure 2.1, Figure 2.2 and Figure 2.3, respectively.

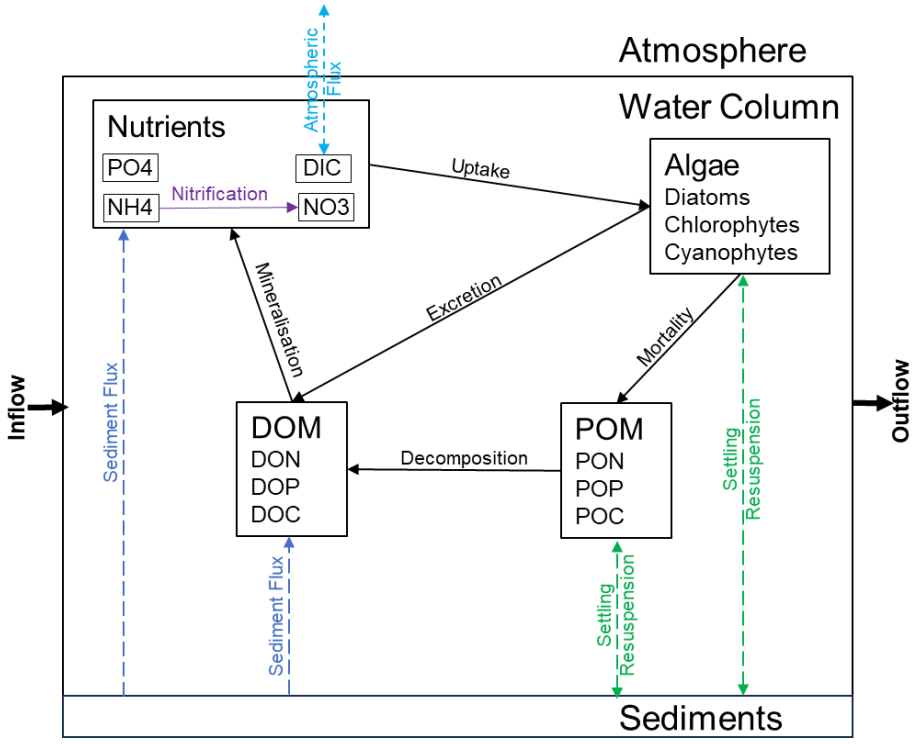

Figure 2.1 Schematic of P, N and C cycles.

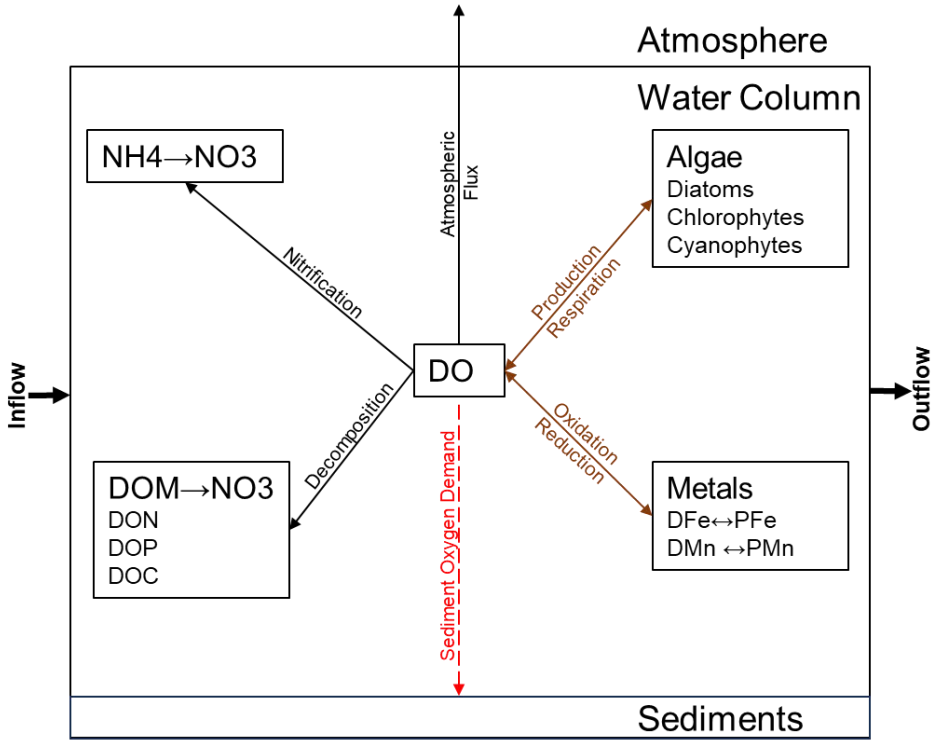

Figure 2.2 Schematic of DO cycle.

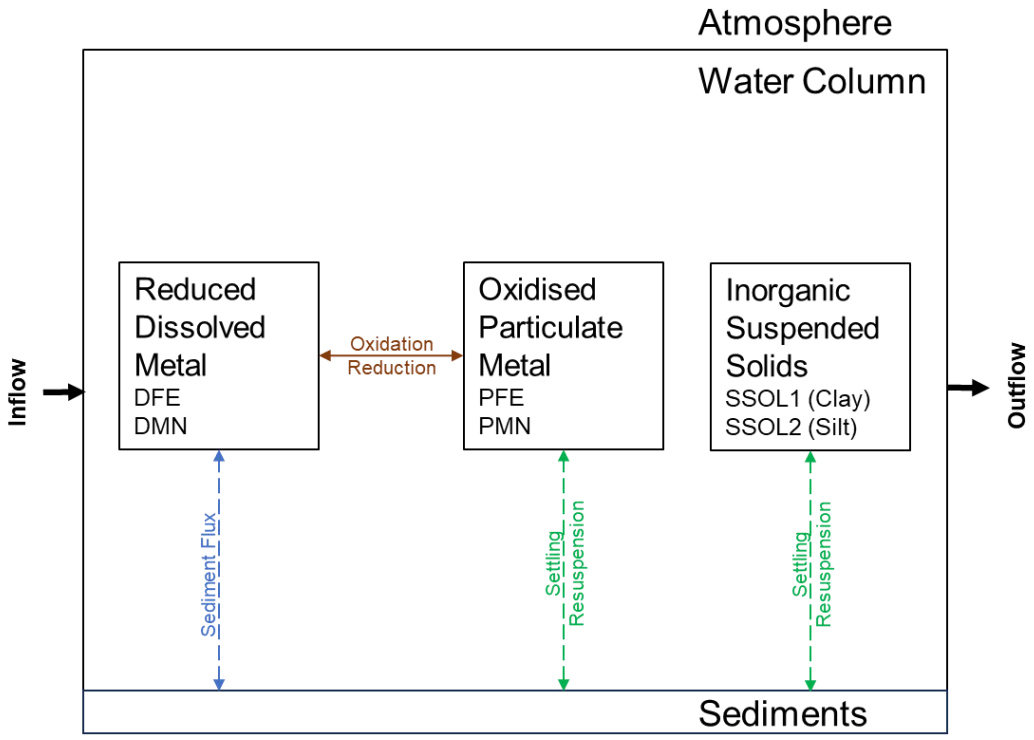

Figure 2.3 Schematic of the inorganic particle and metals cycles.

3. Overview of scenarios

An overview of the scenarios evaluated in this investigation are summarised in Table 3.1. These scenarios were endorsed by the HTR Water Quality Steering Group (WQSG) to evaluate a range of potential operational scenarios of this future water body. All scenarios were run with seasonal (April-August) nighttime operations of the GHD (2025a) bubble plume destratification system design (see Section 4.1.2). The bubble plume destratification system is the key in-reservoir control measure in the DWSP to ameliorate water treatment risks of this future raw water supply source. WQ forecasts within the reservoir and its withdrawals for baseline scenario 1B with and without the bubble plume destratification system are described in Section 6 to demonstrate its effectiveness as a the primary control measure. The remaining scenarios in this report assume that this primary in-reservoir control measure is implemented as specified in Section 4.1.2.

Table 3.1 Overview of scenarios.

Scenario ID	Scenario Name	Description	Purpose
1B	Baseline with and without mixing system operations	Simulation of the following stages of the initial 12 years of reservoir operation: – 'Fill' stage (2030-March 2032) – 'Classic' stage with winter springs flows to maintain TWL with minimal withdrawals (i.e. maintain as an emergency water supply during drought conditions) (April 2032-September 2033) – 'Recycled' stage with the onset of continual inputs of RW and periodic inputs of springs water, and continual withdrawals for water supply (i.e. maintain as an operational water supply source) (October 2032-2041)	Forecast WQ within the reservoir to characterise the likely Water Framework Directive (WFD) ecological status of the future water body and acceptability of environmental compensation flow releases to Riders Lane Stream Forecast WQ of the outlet(s) withdrawals to evaluate the acceptability of the WQ envelope of the raw water supply in line with the DWSP Demonstrate effectiveness of the mixing system as the primary control measure to maintain acceptable reservoir WQ from DWSP and environmental perspectives
1BS	Baseline with stabilisation effect over initial 4 years	As scenario 1B simulation with estimates of increased sediment fluxes of dissolved inorganic and organic WQ constituents to emulate the decomposition of inundated terrestrial biomass over the first 4 years of reservoir operations	Ascertain sensitivity of WQ predictions to estimates of the stabilisation effect during initial four years following reservoir completion
2E-G	Operational variations in the discharge of inlet RW and springs inputs and withdrawals from the reservoir	Three year simulations from 1 June 2037-31 May 2040 with variations in the operational discharges of RW and springs inflows and outlet withdrawals with an additional year from 1 June 2040 to 31 May 2041 of representative baseline hydrology (i.e. scenario 1B hydrology) to evaluate the time scale for the reservoir to return to typical baseline (scenario 1B) WQ where: – Scenario 2E is high yield (~50 MLD withdrawal) – Scenario 2F is moderate yield (~30 MLD withdrawal) that maximises springs inputs and minimises RW inputs – Scenario 2G is moderate yield (~30 MLD withdrawal) that	Ascertain sensitivity of predicted reservoir WQ to operational variations in RW and springs inflows and withdrawals, and evaluate the response time afterwards to return to baseline conditions similar to scenario 1B

Scenario ID	Scenario Name	Description	Purpose
		minimises springs inputs and maximises RW inputs Note typical scenario 1B yield during the 'recycled' phase is ~20 MLD	
2H-J	Operational variations with a very high withdrawal period with concomitant sizeable decreases in water levels during drought conditions	Nearly 5 year simulations from 1 June 2037-28 February 2042 with variations in operational RW and springs inflows and very high withdrawals and concomitant reservoir drawdown during drought conditions	Forecast WQ in reservoir and withdrawals during a combination of changes in operational RW and springs inputs and a short period of very high withdrawals during drought conditions with a sizeable decrease in water levels
4A	Extended classic phase	Simulations from 1 April 2032-31 December 2041 where the reservoir is maintained as an emergency water supply source with no RW inputs	Forecast long-term reservoir and withdrawals WQ in the absence of RW inputs

4. Model configuration and inputs

4.1 Configuration: bathymetry, inflows, withdrawals and bubbler system

Figure 4.1 and Figure 4.2 illustrate the fine (20 m horizontal resolution) and coarse (50 m horizontal resolution) model grids of the HTR bathymetry of this investigation and GHD (2024), respectively. GHD (2025a) updated the GHD (2023) bubble plume destratification system design due to changes in the reference design of the HTR bathymetry. The GHD (2025a) and GHD (2023) simulations with fine and coarse grids reproduced very similar hydrodynamics and WQ. Similarly, a GHD (2025b) options analysis of the inlet location for RW and springs into the reservoir demonstrated that the coarse and fine horizontal grids predict nearly identical WQ through the water column at 2 deep water locations in the north and south basins, and the withdrawal WQ for water supply and environmental compensation flows.

Simulations of the long-term (up to 13 years duration) scenarios to inform DWSP and environmental considerations were carried out with the coarse 50 m grid at a 1 m vertical resolution. A comparison of fine (20x20x1 m) and coarse (50x50x1 m) grid simulations of scenario 1B demonstrate very similar WQ forecasts (see Section 5).

Further details in regards to this investigation's and the GHD (2024) model bathymetries include:

– The GHD (2024) bathymetry was generated from a computer aided design (CAD) drawing (Coffeys HTR-COF-EM-RE-M3-C-0009, 12 December 2023) that has subsequently only undergone minor modifications, so it was again used in this investigation. The CAD drawing contours were at 0.5 m intervals, which were interpolated onto a horizontal grid of ~1 m. The fine and coarse model bathymetry files were then prepared.
– AEM3D's 'levee' functionality[2] was used to represent the wetland retention structures between the 4 wetland compartments, and between the wetland and the open waters. The width of the three spillways (openings) between the 4 wetland compartments, and the 5 spillways from the wetland to the reservoir's main body (2 openings for westernmost wetland compartment), were set to a width of 1 horizontal grid cell. The reference design width of these openings is 28 m (Atkins drawing: HTR-ATK-EM-RE-DR-C-3804 Rev C01, 20 August 2020), which is similar to the fine grid size of 20 m. However, these opening widths are approximately twice as wide for the single grid representation with the coarse grid (50 m), hence horizontal exchange is expected to be overestimated. The elevations of the 3 opening inverts between the 4 wetland compartments, and the 5 opening inverts between the wetlands and the reservoir main body, were set to 38.8 and 38.7 m OD, respectively, as per the reference design (Atkins drawing: HTR-ATK-EM-RE-DR-C-3804 Rev C01, 20 August 2020).
– Local stream inputs from the 3 local catchments were configured to enter the northern extent of the 3 westernmost wetland compartments when reservoir levels were at/near TWL. Stream inflows were configured to discharge at appropriate locations in the wetland and/or in the main body of the reservoir depending on the simulated water level.
– GHD (2024) primarily evaluated the RW and springs inlet location in the western portion of the north basin, ~500 m from the withdrawal structures. The location of this inlet was changed to the southern portion of the south basin, ~250 m from the withdrawal structures on the basis of an options analysis by GHD (2025b). The inlet discharge elevation was set to ~1 m above the local reservoir bottom at a depth of ~24 m OD (-15.5 m TWL).
– The vertical placements of the operational outlets (high draw-off, middle draw-off) were set to 5.5-5 and 10.5-11 below TWL as per the updated design (GHD drawing: HTR-GHD-CU-RE-DR-S-0021 Rev P04, 8 December 2023). The bottom scour outlet was set at level of ~5 m of the maximum depth of the south basin,

[2] The levee functionality allows a barrier of infinite thinness to be defined between grid cells. As the wetland retention structure is ~4 m wide at TWL, this model functionality was implemented as the most practical manner to emulate the much shorter widths of this infrastructure relative to the fine (20 m) and coarse (50 m) horizontal grid sizes.

and was only used during the 'fill' stage for environmental compensation flows until the reservoir surface attained a level where the middle draw-off could be used..

– GHD (2024) configured the bubble plume destratification system on the basis of the GHD (2023) mixing system design that was based on the reference design bathymetry (Atkins drawing: HTR-ATK-EM-RE-DR-C-3907 Rev C01, 20 August 2020). GHD (2025a) updated the mixing system design (i.e. each line of 360 m length at ~0.3 m above the local HTR bottom with 180 openings at 2 m intervals and a free air flow rate of 87.5 L/s) that is used in this investigation (Figure 4.1).

– This investigation used the same approach for bird loading as GHD (2024). Atkins (2020) estimated that bird loading will be an important source of nutrient loading into the future HTR. Stantec (2022) estimated that considerable spatial variability in these loadings is likely between wetlands, margins of the reservoir's open waters, and deep (interior) reservoir's open waters. Bird loading model inputs were configured at 1 location in each of the 4 wetland compartments, 2 open water margin locations at the western and eastern extents of the reservoir, and 4 deep water locations. HTR will be a relatively small reservoir (open water distance of ~1.5 km) where horizontal dispersion of bird nutrient loads will be relatively rapid, so the number of bird loading locations that have been configured is sufficient.

– Atkins (2020) identified that rainfall inputs of N are likely to be important to the overall nutrient budget, but less so for P. Rainfall inputs of NO3, NH4 and PO4 were configured into the surface waters of the model to account for this nutrient source.

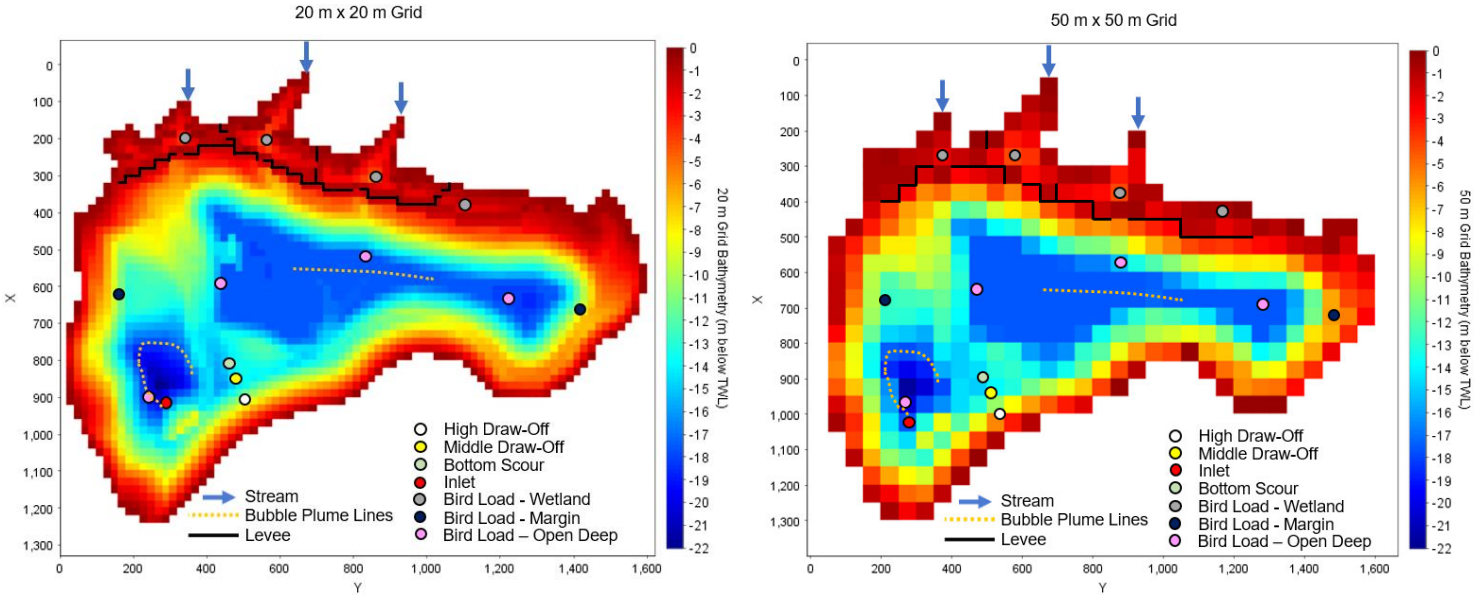

Figure 4.1 ***Fine (20 m, left) and coarse (50 m, right) horizontal model grid resolutions of the current HTR bathymetry with locations of stream confluences (at TWL), updated location of the springs and RW inlet, withdrawal outlets (high and middle draw-offs, bottom scour), bird loading locations (4x wetland, 2x open water margins, 4x open water deep [interior]), and updated design of the two bubble plume destratification lines.***

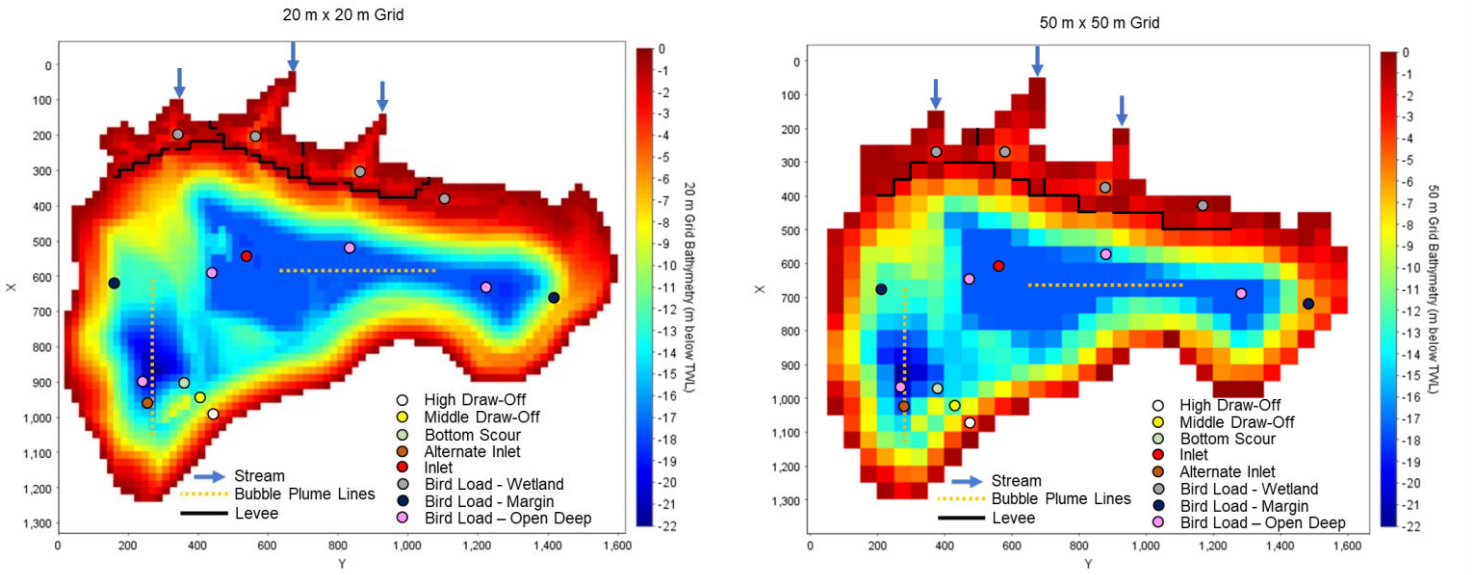

Figure 4.2 ***As Figure 4.2 for the original GHD (2023) mixing system design along with the north basin and alternate south basin locations for the RW and springs inlet locations that were evaluated by GHD (2024)[4].***

4.1.1 Withdrawal operational rules

It is assumed that all withdrawals over a particular simulation time step to the Otterbourne and Farlington water supply works (WSWs), and for environmental compensation flows to Riders Lane Stream, are from a single outlet (e.g. high draw-off, middle draw-off or bottom scour). The configuration of the model operational rules to select the outlet from which withdrawals are extracted were as follows:

– The bottom scour outlet is only used during the initial filling period to supply environmental compensation flows when simulated water levels are below 30 m OD (-9.5 m TWL).

– The middle draw-off is used if simulated water levels are between 30 m OD and 35.5 m OD (-9.5 m to -4 m TWL).

– The high draw-off is used if simulated water levels are greater than 35.5 m OD (-4 m TWL).

4.1.2 Bubble plume destratification system operations

Rather than continuous operation of the bubbler system from April-September as GHD (2023), GHD (2024) configured nighttime (0600-1800) operations from April-August in effort to reduce future power costs, which has been further demonstrated as an appropriate strategy by GHD (2025a). This reduces the cumulative duration of mixing system operations (i.e. 24 hour to nightly, no September operations) relative to GHD (2023), yet adequately maintains vertically well-mixed conditions throughout the main body of the reservoir (see Section 6).

4.2 Model state and derived variables

Table 4.1 provides a summary of the state (i.e. directly simulated by AEM3D) and derived (i.e. calculated from state variables) variables that have been configured for this modelling investigation. A high level overview of the data sources for the external loading model inputs (i.e. measurements, estimates or assumptions) of the state variables is also provided in Table 4.1.

[4] The GHD (2023) south basin plume line was oriented east-west.

Table 4.1 State and derived variables in the AEM3D HTR modelling application and the source of the external loading model inputs.

Model Variable	Variable Name	Justification for Inclusion in Modelling Investigation	Source of External Load Model Inputs				
			Bird Loads	Rain	Springs	Streams	Recycled Water
State Variables							
WTR_TEMP	Water Temperature	Stratification and WQ dependency	No input		Measurements		
SALINITY	Salinity	Stratification dependency	No Input		Estimated from measured EC		Estimate
RETENTION_T	Retention Time	Track water age in reservoir	All water inputs into the reservoir are automatically introduced with retention time of 0 days				
TRACER_1, TRACER_2, TRACER_3, TRACER_4	Conservative Numerical Tracers of Inlet Streams, Springs and RW Inputs	Stream, springs and RW source composition of reservoir waters	Stream and inlet numerical tracers input with value of 1 Springs and RW numerical tracer input values are the fraction composition of inlet inflows				
SSOL1, SSOL2	Clay, Silt	PAR attenuation	No input		Measured turbidity	Measured SS	Estimate
DO	Dissolved (Diss.) Oxygen	Carbon (inorganic, organic), pH and oxygen dynamics	No input		Measured DO		Estimate
DIC	Diss. Inorganic C		No input		Calculated from alkalinity & pH measurements/estimates		
pH	pH		No input		pH measurements		Estimate
ALK	Alkalinity		No input		Alkalinity measurements		Estimate
DOC, POC	Diss. & Part. (Particulate) Organic C		N input scaling	No Input	Estimated from measured TOC		Estimate
FDIAT, CHLOR, CYANO	Diatoms, Green & Blue-Green Algae	Phytoplankton and nutrient dynamics	No input		Assume ~0 µg chl-a/L		
IN_FDI, IN_CYA, IN_CHL	Internal N in Phytoplankton		No input		Assume ~0 mg N/L		
IP_FDI, IP_CYA, IP_CHLP	Internal P in Phytoplankton		No input		Assume ~0 mg P/L		
NO3, NH4	Nitrate, Ammonium		% of TN load estimate	Measured NH_4 and NO_3			Estimate
DON, PON	Diss. & Part. Organic N			No input	% of measured TN for DON, assume ~0 mg N/L for PON		
PO4	Phosphate		% of TP load estimate	Measured PO_4	% of measured TP		Estimate
DOP, POP	Diss. & Part. Organic P			No input	% of measured TP for DOP, assume ~0 mg P/L for POPL		
SiO2	Silicon Dioxide		No input		Estimate		
PMN, DMN	Oxidised Part. & Reduced Diss. Mn	Iron and manganese dynamics	No input		% of measured TMn		TMn estimate
PFE, DFE	Oxidised Part. & Reduced Diss. Fe		No input		% of measured TFe		TFe estimate
TRACER_5, TRACER_6, TRACER_7, TRACER_8	Conservative Tracers of Ca, Na, Cl and SO4 Stream and Comingled Inputs	Inform corrosivity assessment	No input	Measurements			Estimates
Derived Variables							
PAR_EXT, TSS, DOSAT, BOD, TOC, TCHLA, TN, TP	PAR Extinction Coefficient, Total Suspended Solids, Percentage DO Saturation, Biological Oxygen Demand, Total Organic C, Total Chl-a, Total N, Total P	WQ determinands to inform DWSP and environmental considerations	Not applicable, derived from State Variables				

4.3 Model inputs

4.3.1 Hydrodynamic inputs

4.3.1.1 2012-2022 CFSv2 meteorology

Hourly meteorology from the National Centers for Environmental Prediction's (NCEP's) Climate Forecast System, version 2 (CFSv2) (Suranjana *et al.* 2014) over 2012-2022 (11 years) served as inputs into the 3D hydrodynamic model (Figure 4.3). The CFSv2 data from 2012-2022 was configured to occur from the start 2024[5] to the end of 2034, and then was repeated to allow simulations to extend through 2042.

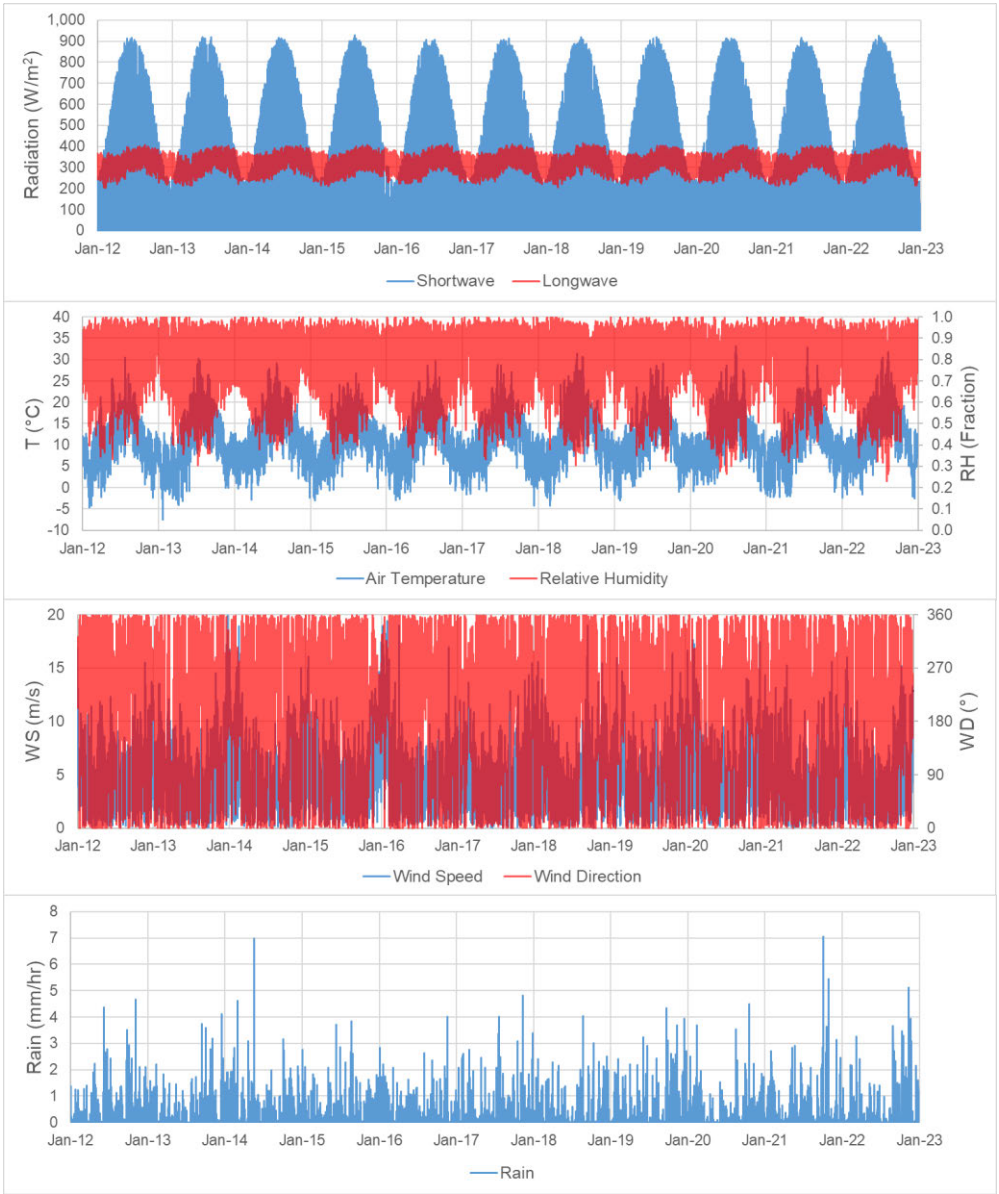

Figure 4.3 ***Hourly CFSv2 meteorological inputs to the 3D model from 2012-2022. CFSv2 rainfall is reduced by 23.5% (see Section 4.3.1.2.2).***

[5] 2012 meteorology mapped to start of 2024 as both years leap years.

4.3.1.2 Daily water balance

Daily water balances were developed by SW to estimate the south basin's inlet discharge into the reservoir and withdrawals to WSWs and environmental compensation flows for the scenarios in this investigation. The baseline scenario 1B daily water balance spanned 12 years over the planned stages of reservoir filling (January 2030-March 2032, 'fill' stage), the maintenance of the reservoir at/near TWL prior to RW inputs with minimal water supply withdrawals (April 2032-September 2033, 'classic' stage), and maintenance of the reservoir at/near TWL with a combination of RW and springs inflows with sizeable water supply withdrawals (October 2033-December 2041, 'recycled' stage). The SW daily water balance model was adapted to prepare daily hydrological model inputs of the inlet inflows (springs and RW) and withdrawals for water supply and environmental compensation flows. This adapted daily water balance model is described next.

4.3.1.2.1 Evaporation

Monthly evaporation in the SW daily water balance consisted of measured daily pan evaporation adjusted for open water. The monthly evaporation of the water balance was updated with daily averages of the simulated 1 min evaporation rates over preliminary model runs from 2030-2041[6]. The average annual modelled AEM3D evaporation of ~625 mm/year is ~20% lower than SW adjusted average annual pan evaporation estimate of ~775 mm/year in the original water balance. The daily AEM3D evaporation was used in the updated water balance model.

4.3.1.2.2 Rainfall

Monthly rainfall in the SW daily water balance was used to determine an adjustment factor for the hourly CFSv2 rainfall that served as model inputs. The ratio of the average annual rainfall of measurements at the Southampton and Eastbourne meteorological sites (778 mm/year) to the CFSv2 hourly values (1,016 mm/year) was 0.754. Hence, a 24.6% reduction was applied to the hourly CFSv2 rainfall data. Daily totals of these adjusted CVSv2 hourly rainfall data were used in the updated water balance model.

4.3.1.2.3 Stage-volume-area relations

Stage-volume-area relations for the Atkins (2020) original reference design, and the fine (20 m) and coarse (50 m) model bathymetries are illustrated in Figure 4.4. The SW daily water balance used the Atkins (2020) stage-volume-area relations, which was modified to use those of the fine (20 m) bathymetry in the updated water balance model.

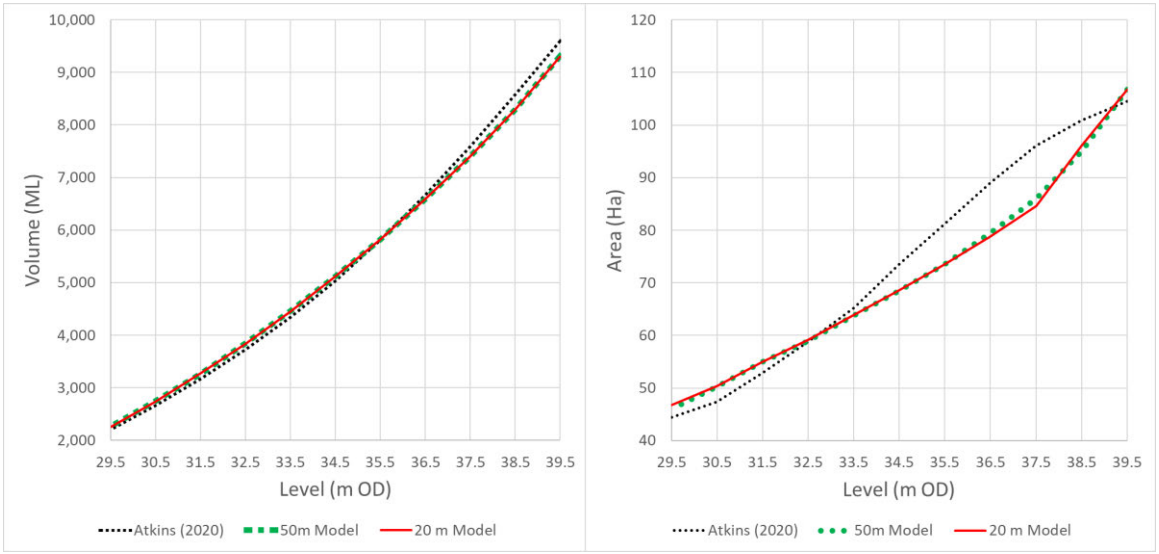

Figure 4.4 Stage-area-volume relations.

[6] AEM3D calculates evaporation from hourly inputs of relative humidity, air temperature and wind speed, and simulated surface water temperatures.

The SW water balance used the Atkins (2020) stage-volume-area relations to estimate the surface area at 90%, 80%, 43% and 20% of the full HTR volume, which were then used to estimate the daily volumes of rainfall onto and evaporation from the reservoir. The updated water balance uses the surface area at the projected water level on a given day on the basis of the fine (20 m) bathymetry hypsographic relation to determine the rainfall and evaporation volumes.

4.3.1.2.4 Operational rule for winter spring inputs when reservoir near TWL

In the daily water balance, springs water is used to 'top-up' the HTR during the winter to maintain seasonal peaks in the surface levels at/near TWL. The SW daily water balance was modified to cease this winter 'top-up' once the predicted surface level is greater than 39.2 m OD (TWL). This is the only water balance parameter that was 'calibrated' to ensure that reservoir water levels did not increase above the TWL of 39.5 m OD (i.e. ensure no spills over the spillway crest occur).

4.3.1.2.5 Other water balance terms

No further adjustments were made were made to any other water balance terms of the SW daily water balance (i.e. recycled water plant inflows, water supply extractions to Otterbourne and Farlington WSWs, stream inflows, environmental compensation releases).

4.3.1.2.6 Overview of model hydrology inputs for scenario 1B

Figure 4.5 illustrates the components of the daily water balance for scenario 1B where:

– Over the 'recycled' phase from 1 October 2033 to 31 December 2041:
  - The 3 primary streams are relatively small inputs with an annual average of ~1 MLD.
  - Rainfall is a relatively small component of the water balance with average losses of ~1.8 MLD.
  - Evaporation is a relatively small component of the water balance with average gains of ~2.2 MLD.
– Winter spring inputs over the first 3 years of the water balance fill the reservoir ('fill' stage).
– During the 'classic' stage winter spring water 'top-ups' and relatively low withdrawals maintain water levels near TWL.
– During the 'recycled' stage the water balance is primarily driven by RW (~16.7 MLD) and springs (~2.7 MLD) largely balanced by withdrawals (20 MLD), which maintain surface levels at/near TWL.

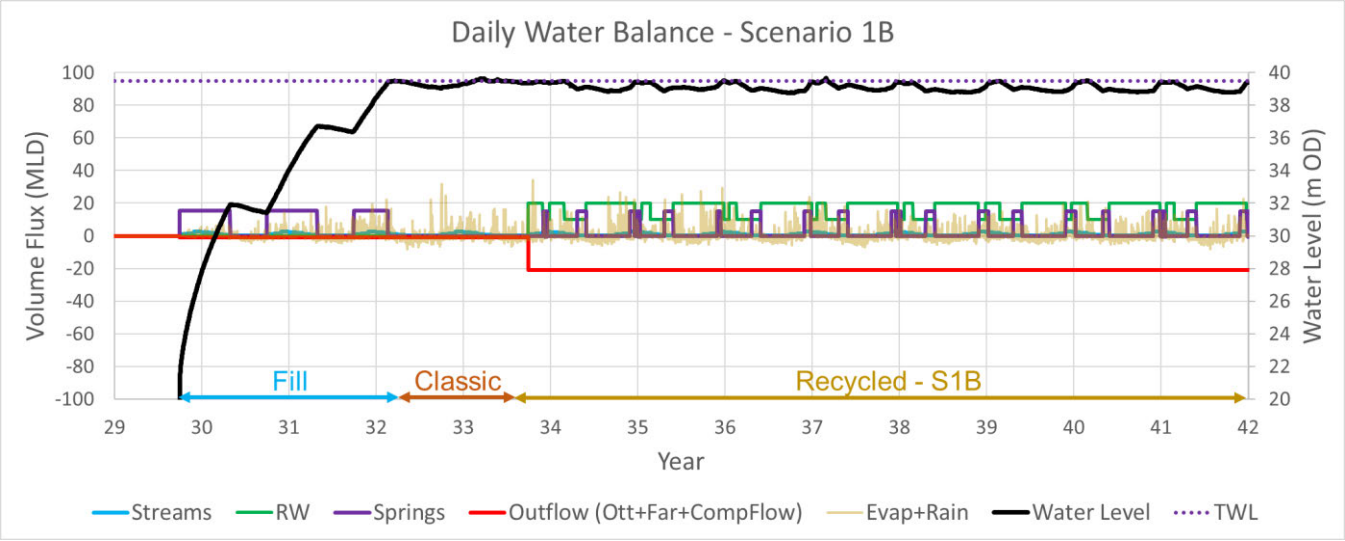

Figure 4.5 Overview of daily water balance over the three stages (fill, classic, recycled) of scenario 1b.

The following daily discharge estimates from the updated water balance served as the hydrology model inputs:

– RW and spring inflows via the inlet in the south basin.
– Stream inflows via the 3 local catchments into the 3 western wetland compartments.
– Withdrawals for water supply and environmental compensation releases primarily from the high draw-off (though the middle draw-off is used for low water levels during drought conditions in other scenarios), and the bottom scour and middle draw-off during the 'fill phase' for compensation flows.

AEM3D directly simulates evaporation. Hourly CFSv2 rainfall (adjusted by annual average correction factor) served as model input.

4.3.1.2.7 Model hydrology inputs for operational scenarios 2E-G

The simulation period of the 3 additional operational scenarios (2E, 2F, 2G) was from 1 June 2037-31 May 2040, which span 3 years after 3.67 years of the 'recycled' phase of scenario 1B. An additional 1 year of simulation from 1 June 2040-30 May 2041 with the scenario 1B inputs over this period was also included to evaluate the time scales for a return to baseline WQ conditions The key differences between these 3 operational scenarios and 1B are:

– All 3 operational scenarios have higher inlet inputs into and withdrawal discharge from HTR than 1B.
– 2E had extended periods of ~50-60 MLD RW and 40 MLD springs inflows into the reservoir and continually ≥50 MLD withdrawal extraction from the reservoir.
– 2F had extended periods of ~30-40 MLD RW and 40 MLD springs inflows into the reservoir. This scenario maximises springs inputs for an operational scenario with withdrawals typically of ~40 MLD.
– 2G is similar to 2F in terms of withdrawals of ~40 MLD and extended periods of ~30-40 MLD RW inflow except the spring water contribution is minimised with several brief periods of springs inflows .

The daily water balances of operational scenarios 2E-2G are illustrated in Figure 4.6 along with baseline scenario 1B. Daily time series of RW and springs inflows through the south basin inlet and the high draw-off withdrawals served as model inputs for scenarios 2E-G.

4.3.1.2.8 Model hydrology inputs for drought scenarios 2H-J

The simulation period of 3 additional drought scenarios (2H, 2I, 2J) was from 1 June 2037-28 February 2042. The key differences between these 3 drought scenarios and 1B include:

– As with the 3 operational scenarios, all 3 drought scenarios have higher inlet inputs into and withdrawal discharge from HTR than 1B. However, whereas the operational scenarios maintain surface levels at/near TWL, they decrease substantially due to reservoir drawdown to meet water supply needs during emergency drought conditions for the drought scenarios. Specifically, low water levels occur from June 2039-April 2040 where:
    - The lowest level of 31 m OD (-8.5 m TWL) for scenario 2H occurs in December 2039 due to withdrawals of ~80-120 MLD from June-December 2039 well in excess of the 60 MLD RW inputs.
    - A minimum level of 36 m OD (-3.5 m TWL) occurs for scenario 2I from October-November 2039 due to withdrawals of ~60-90 MLD from June-October 2039 well in excess of the 30-60 MLD RW inputs.
    - A modest minimum level of 37 m OD (-2.5 m TWL) occurs for scenario 2J from October-November 2039 due to similar withdrawals as scenario 2I of ~60-90 MLD from June-October 2039, but with greater duration of RW inputs at ~60 MLD over this period.

The daily water balances of drought scenarios 2H-J are illustrated in Figure 4.7 along with baseline scenario 1B. Daily time series of RW and springs water discharge through the south basin inlet and the high and middle (when water levels decreased to below 35.5 m OD [4 m below TWL] for 2H as per withdrawal operational rules in Section 4.1.1) draw-off withdrawals from the reservoir served as model inputs for scenarios 2H-J.

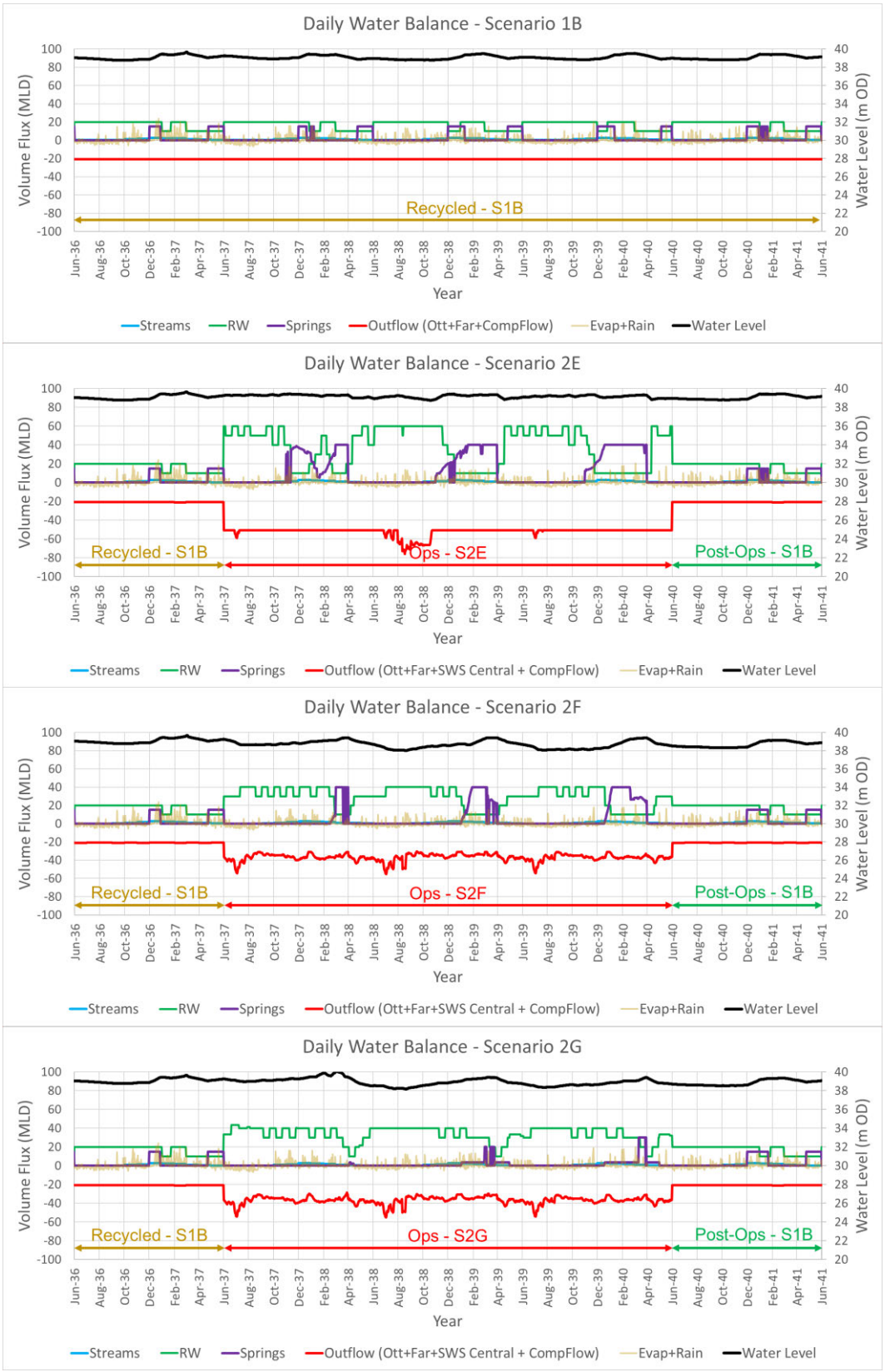

Figure 4.6 ***Overview of daily water balances of operational scenarios 2E-G over the period of 1 June 2037 to 31 May 2040 and comparison to scenario 1B.***

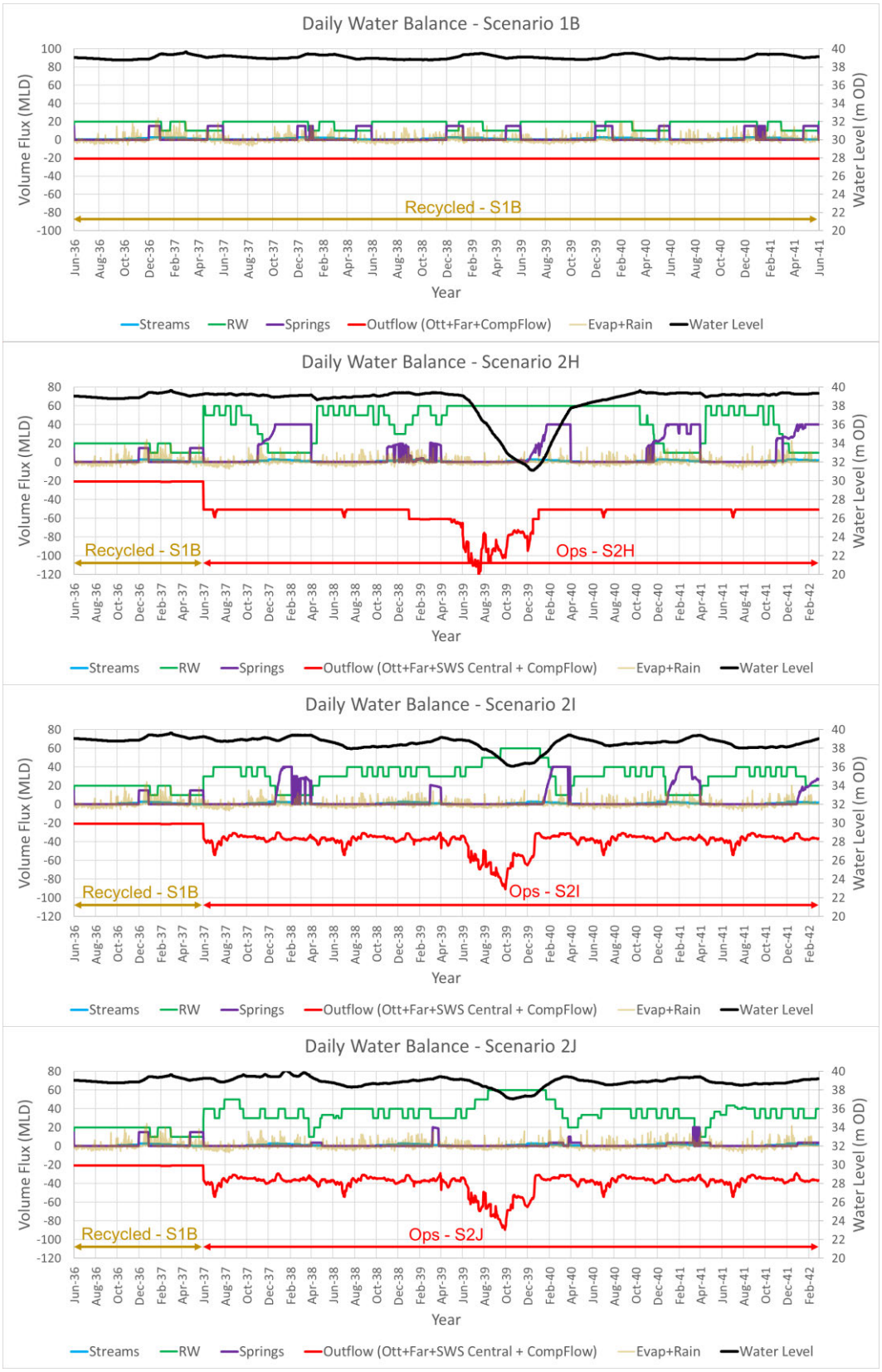

Figure 4.7 ***Overview of daily water balances of drought scenarios 2H-J over the period of 1 June 2037 to 1 March 2042 and comparison to scenario 1B.***

4.3.1.2.9 Model hydrology inputs for scenario 4A

Figure 4.8 illustrates the components of the daily water balance for scenario 4B where 'top-ups' to maintain the reservoir level at/near TWL from springs occur over ~1-3 months duration a year at ~15 MLD.

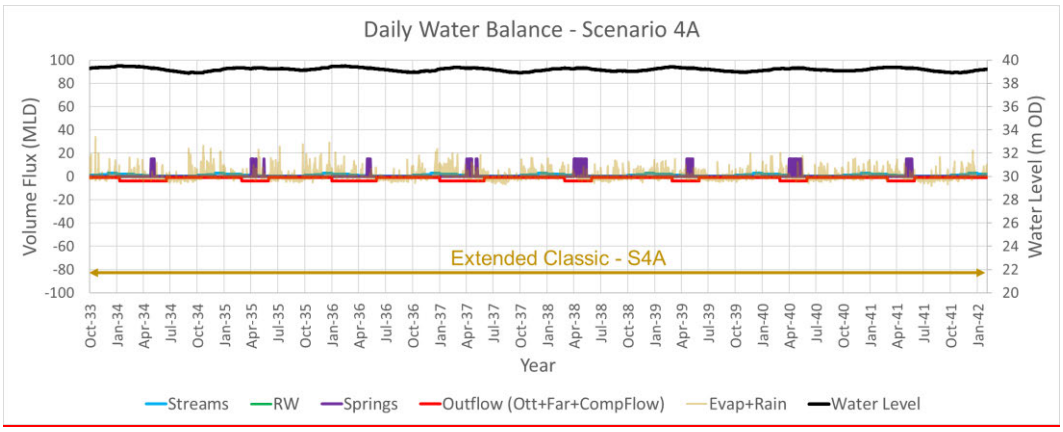

Figure 4.8 ***Overview of daily water balance of scenario 4A with extended classic phase from 1 October 2033 in lieu of RW phase of scenario 1B.***

4.3.1.3 Recycled water and springs temperatures

Water temperatures (T) of sewage effluent data that was provided by SW, which is illustrated in Figure 4.9, where:

- The timing of monthly T measurements of sewage effluent from Budds Farm and Peel Common sewage treatment plants (STPs) from 2012-2022 were offset by ~2 weeks over the measurement record, thereby the combined dataset has approximately a bi-weekly sampling frequency.
- A monthly moving average that was centred on each ~bi-weekly sampling date (generally three consecutive measurements with an interval between the first and last date of measurements of ~30 days) was applied to smooth the time series and to reduce the influence of outliers.
- Generally, minimum seasonal winter T was cooler prior to 2017 (~9-10°C) than afterwards (~11-12°C).

Linear interpolation between the time series of monthly moving averages of sewage effluent T from 2012-2022 (which corresponds to the meteorological record of Section 4.3.1) were used to estimate the RW T model inputs into HTR.

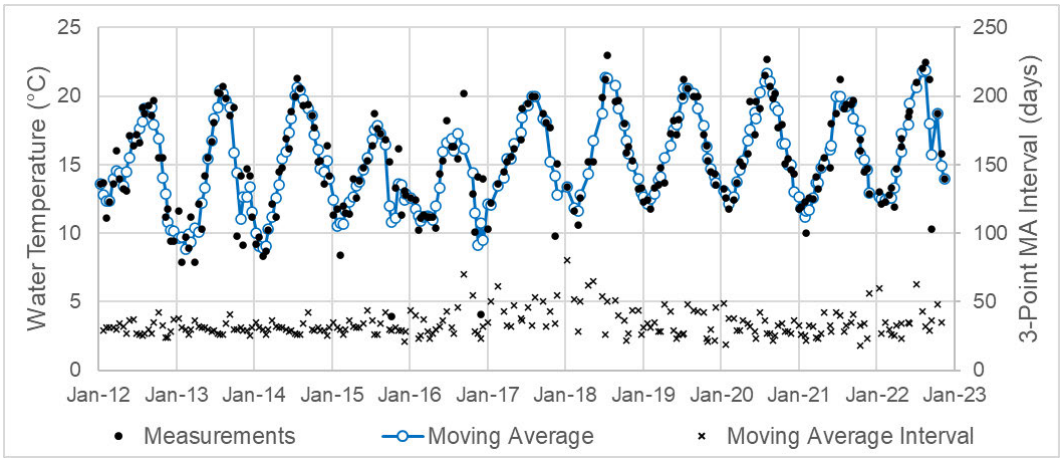

Figure 4.9 ***Water T measurements of Budds Farm and Peel Common STPs effluent, ~monthly moving averages (MA) of 3 ~bi-weekly measurements, and the time interval between the first and last dates of each moving average (2nd y-axis).***

Springs T data that was provided by PW, which is illustrated in Figure 4.10, where:

– The frequency of measurements ranged from weekly (2012-2018, 2022) to monthly (2019-2021) at sites RWBH1 and RWHAS.
– Monthly to bi-monthly moving averages were calculated that were centred on each sampling date (generally 3 monthly measurements from 2019-2021 to 5 weekly measurements from 2012-2019 and 2022) to smooth the time series of measurements and to reduce the influence of outliers.
– The interval between the first and last date of measurements in the moving average was generally ~28 days from 2012-2018 and 2022, and ranged from ~20-60 days from 2019-2021.
– Generally, peak seasonal summer T was cooler prior to 2019 (~11.5-12°C) than afterwards (~12.5°C).

Linear interpolation between the time series of monthly moving averages of springs T from 2012-2022 (which corresponds to the meteorological record of Section 4.3.1) were used to estimate the springs T model inputs into HTR.

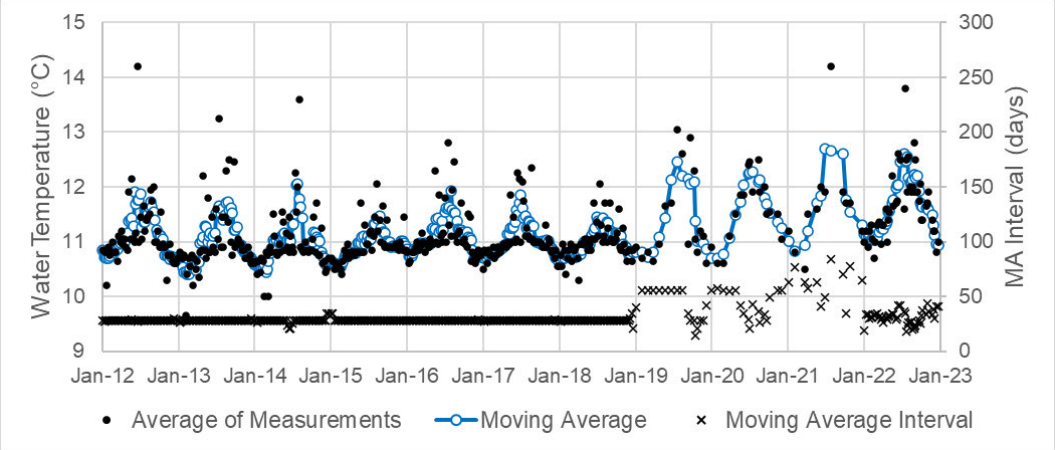

Figure 4.10 ***Water T measurements at two springs sites, monthly to bi-monthly moving averages of 3-5 consecutive sampling dates, and time intervals between the first and last dates of each moving average (2nd y-axis).***

The comingled (RW and springs) inflow model inputs of T were calculated as the volume-weighted average of the daily RW (Figure 4.9) and springs (Figure 4.10) water T for each scenario, which is illustrated for baseline scenario 1B in Figure 4.11.

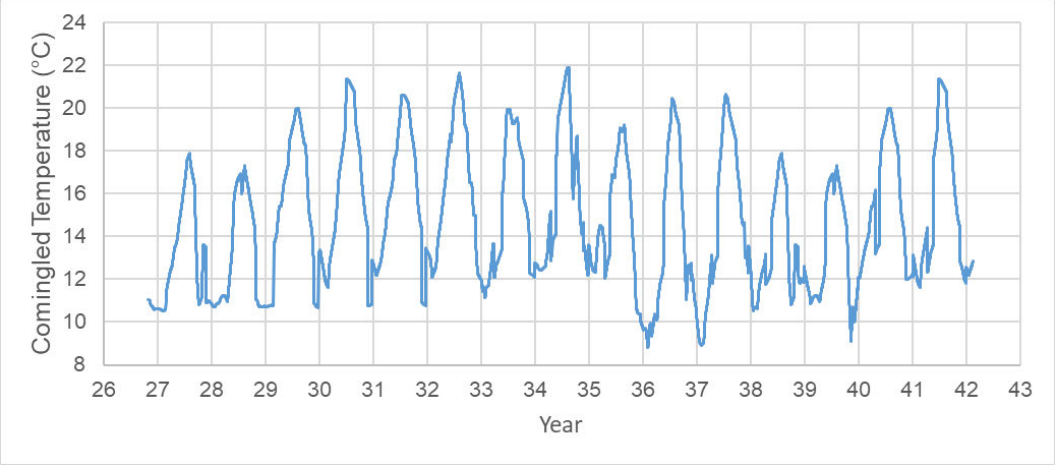

Figure 4.11 ***Daily interpolated time series of comingled inflow T from the volume-weighted 2012-2022 moving averages of springs and TW for scenario 1B.***

4.3.2 Water quality inputs[7]

4.3.2.1 Streams

As GHD (2023) and GHD (2024), WQ data of the 3 local catchments (sites S1, S2 and S3) of the future HTR were based on available monitoring data at approximately monthly intervals (with some gaps) from August 2008-December 2010, May-June 2018, and November 2018-March 2019. Monthly medians of all measurements are summarised in Table 4.2. Stream WQ measurements from November-April are representative of conditions when streams are typically flowing, whereas higher concentrations during other months typically correspond to no/low discharge conditions.

Table 4.2 Summary of monthly medians of stream WQ data where shading denotes use to estimate model inputs.

Month	T (C)	EC (uS/cm)	pH	SS (mg/L)	NH_x (mg N/L)	NO_3 (mg N/L)	TP (mg P/L)[8]	TOC (mg C/L)	Alkalinity (mg $CaCO_3$/L)	TMn (mg Mn/L)	TFe (mg Fe/L)	Ca (mg Ca/L)	Na (mg Na/L)	Cl (mg Cl/L)	SO_4 (mg S/L)
January	4.8	159	5.28	3.6	0.016	0.113	0.005	7.4	11.6	0.240	0.601	8.3	16.4	33.7	10.2
February	6.5	154	5.12	4.2	0.016	0.113	0.006	10.5	11.8	0.181	0.507	6.9	18.0	32.5	10.0
March	8.1	170	5.33	8.2	0.016	0.113	0.005	7.8	12.8	0.175	0.397	7.4	18.7	36.6	10.2
April	12.5	159	5.30	12.0	0.016	0.260	0.0075	9.1	-	0.228	0.879	6.6	16.8	34.5	12.0
May	11.5	166	5.98	35.6	0.121	0.237	0.032	10.9	22.2	0.712	4.268	11.3	18.3	36.4	10.2
June	13.5	279	6.52	602.0	0.418	0.294	0.056	21.2	35.8	1.348	14.094	17.2	23.0	42.1	26.5
July	16.6	243	6.43	20.8	0.308	0.113	0.050	16.7	-	0.707	8.648	18.3	23.5	37.9	13.8
August	15.3	203	5.78	125.7	0.113	0.226	0.0255	12.8	-	0.392	4.878	12.5	19.9	43.5	14.2
September	13.7	257	6.19	62.0	0.277	0.113	0.028	12.2	-	0.844	6.494	16.4	16.5	37.1	16.4
October	11.8	262	6.33	11.8	0.016	0.113	0.010	9.1	-	0.441	2.162	14.3	17.6	37.7	10.9
November	8.9	187	5.28	5.4	0.016	0.113	0.005	9.3	14.5	0.201	0.636	9.1	20.1	40.2	10.0
December	4.9	186	4.94	3.2	0.016	0.113	0.005	8.1	11.1	0.161	0.388	6.6	18.5	38.9	10.2
Oct.-Apr.	8.1	176	5.25	5.8	0.016	0.113	0.005	8.8	12.5	0.198	0.567	7.3	18.6	36.8	10.5

4.3.2.2 Inlet inflow

The primary sources of water into HTR will be springs and RW via the inlet location into the south basin. As with T (Section 4.3.1.2.7), salinity (S) and other WQ determinands of the inlet discharge were estimated with a mass balance approach on the basis of the daily discharge (from the daily water balance) and the adopted analyte concentrations of the springs and RW. The WQ concentrations of the RW and springs are described next.

4.3.2.2.1 Springs

There is an extensive measurement record of the springs from ~2012-2023 for many of the determinands considered in this investigation. As springs are a major component of the water balance, a time series of monthly averages of measurements from the 2 available sites served as model inputs. The 2012-2022 monitoring data is presented in Figure 4.12 along with the averages of determinands (i.e. turbidity, TOC, NOX, NH4, PO4, TP) at both measurement sites (RWBH1, RWHAB). Those WQ determinands with a shorter measurement record (i.e. DO, TMn, TFe, pH, TA[9])

[7] Laboratory measurements of determinands of less than the Limit of Detection (<LOD) assigned a value of 50% of LOD.
[8] Orthophosphate (PO4) not reported as limit of reporting (i.e. analytical detection limit typically very high <0.085 mg P/L.
[9] DIC is a state variable, which was estimated from alkalinity and pH.

that also exhibited seasonal variability utilised monthly medians over the shorter 3 year record from 2020-2022 as model inputs.

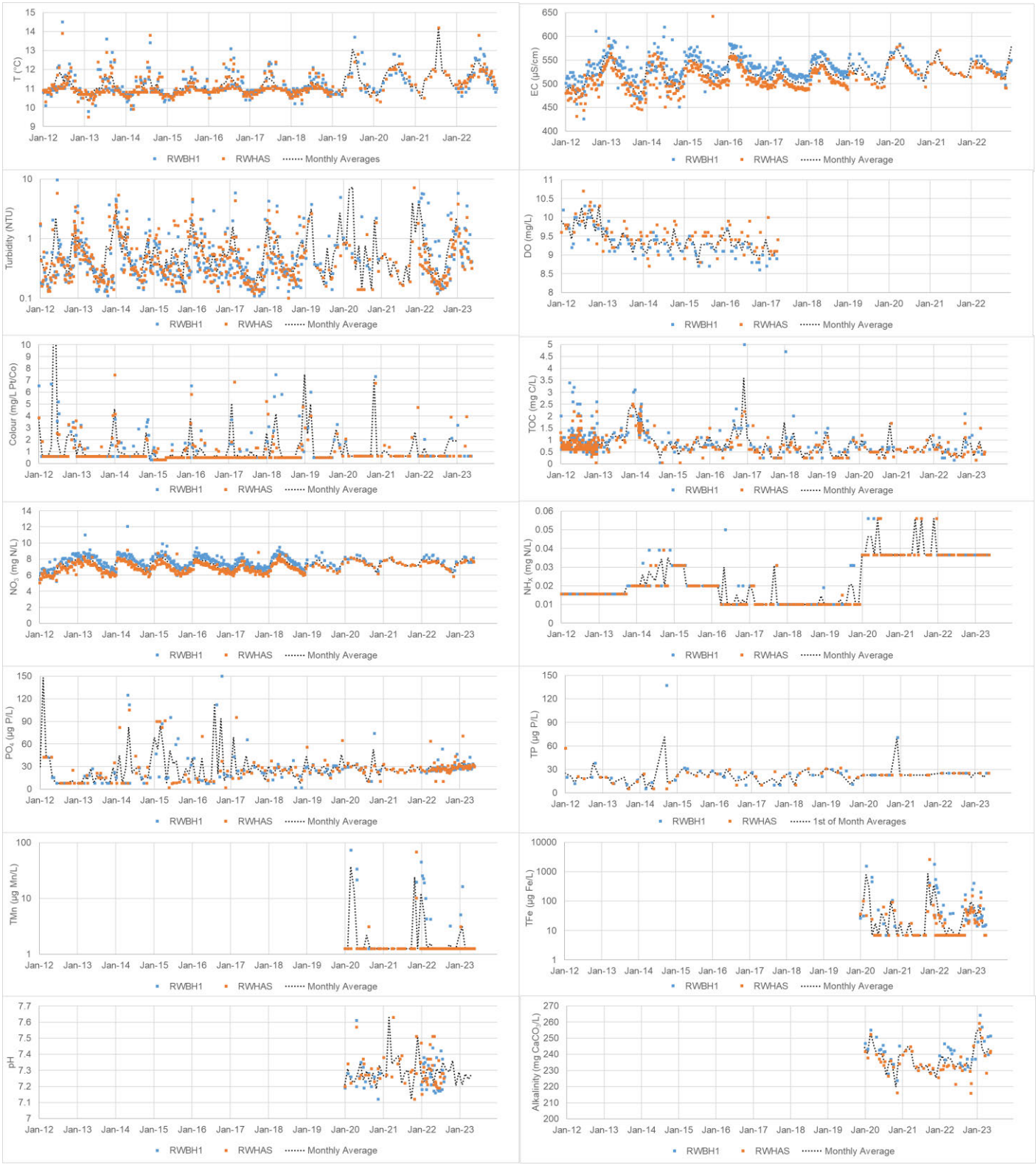

Figure 4.12 2012-2023 springs monitoring data at sites RWBH1 and RWHAS along with monthly averages (black dotted lines).

A table of the monthly median values of the available 2020-2022 data for pH, TMn and TFe is provided in Table 4.3, which served to inform model inputs (see Table 4.10). Additionally, the median of 235 mg $CaCO_3$/L of the alkalinity from the available 2020-2023 data served as a model input (see Table 4.10).

Table 4.3 Monthly median springs concentrations of pH, TMn and TFe.

State Variable (Determinand)	Jan	Feb	Mar	Apr	May	Jun	Jul	Aug	Sep	Oct	Nov	Dec
pH	7.28	7.27	7.39	7.30	7.29	7.35	7.25	7.31	7.27	7.23	7.28	7.35
TMn (mg Mn/L)	0.0052	0.0025	0.0133	0.0057	0.0013	0.0013	0.0013	0.0016	0.0013	0.0013	0.0089	0.0013
TFe (mg Fe/L)	0.152	0.058	0.271	0.103	0.010	0.012	0.008	0.018	0.012	0.010	0.339	0.046

Two major cations (sodium [Na] and calcium [Ca]) and 2 major anions (chloride [Cl] and sulfate {SO4]) were also simulated as conservative substances to indicatively forecast the corrosivity potential of the withdrawals on the downstream water supply infrastructure. SW provided monthly springs concentrations for these major anions and cations to serve as model inputs, which are summarised in Table 4.4.

Table 4.4 Monthly springs concentrations of major anions and cations.

State Variable (Determinand)	Jan	Feb	Mar	Apr	May	Jun	Jul	Aug	Sep	Oct	Nov	Dec
Calcium (Ca) (mg Ca/L)	112.3	119.0	115.4	114.9	113.6	115.3	114.1	111.3	110.8	112.3	106.1	114.3
Sodium (Na) (mg Na/L)	9.8	10.5	11.0	10.4	9.9	9.1	9.7	9.6	9.4	9.4	9.8	9.9
Chloride (Cl) (mg Cl/L)	22.2	22.9	22.6	22.5	22.0	21.4	20.8	20.6	20.4	20.4	20.7	21.3
Sulfate (SO4) (mg SO_4/L)	17.8	19.6	19.6	19.2	18.3	16.8	15.2	14.4	13.9	13.2	13.9	15.6

4.3.2.2.2 Recycled water

SW provided WQ estimates of RW after treatment with a high anti-fouling resistance membrane (HFRM) and a high rejection rate membrane (HRRM). A comparison of HFRM, HRRM and GHD (2024) RW WQ estimates by SW is provide in Table 4.5. SW also provided HFRM and HRRM estimates of monthly RW concentrations for PO4, alkalinity and major anions (Na, Ca) and cations (Cl, SO4), which is reproduced Table 4.6 and Table 4.7, respectively. GHD (2025c) carried out simulations with the GHD (2024), HFRM and HRRM RW WQ on the basis of the GHD (2024) hydrology scenario 1 (baseline). Generally, total algal biomass, and P and C determinands were considerably lower for the HRRM case than the GHD (2024) and HFRM cases because of the considerably lower RW P concentrations. Because of the forecasted material improvement in the WQ of the reservoir and withdrawals in terms of many P, N and C determinands, SW committed to the application of the HRRM process for RW treatment because of the large reduction in PO4 (Table 4.7) relative to the HFRM process (Table 4.6) even though operational costs will be greater.

*Table 4.5 SW estimates of the RW WQ estimated used by GHD (2024), and recently provided for the high fouling resistance membrane (HFRM) and high rejection rate membrane (HRRM). **Red** values to be run for the Final Update Report.*

State Variable (Determinand)	GHD (2024)	HFRM	HRRM	Comment
Salinity (S) (g/L)	0.3			
Suspended Solids Inorganic (SS_{Inorg}) (mg/L)	0			
Alkalinity (mg $CaCO_3$/L)	150	Monthly in Table 4.6	Monthly in Table 4.7	Average HFRM and HRRM 161.1 and 154.1 mg $CaCO_3$/L, respectively
pH	8.0	7.8	7.8	
Dissolved Inorganic Carbon (DIC) (mg C/L)	36.6	Monthly in Table 4.6	Monthly in Table 4.7	Calculated from alkalinity and pH
Particulate Organic Carbon (POC) (mg C/L)	0			
Dissolved Organic Carbon (DOC) (mg C/L)	0.37		0.37 (0.39)	HRRM of 0.37 mg C/L used, final update to use 0.39 mg C/L

State Variable (Determinand)	GHD (2024)	HFRM	HRRM	Comment
Dissolved Oxygen (DO) (mg/L)	100% Saturation at Simulated T			
Total Ammonia (NH4) (mg N/L)[10]	0.008		0.008 (0)	HRRM of 0.008 mg N/L used, final update to use 0 mg N/L
Total Oxidised Inorganic Nitrogen (NO3) (mg N/L)[11]	0.639	0.661	0.661 (0.301)	HRRM of 0.661 mg N/L used, final update to use 0.301 mg N/L
Particulate Organic Nitrogen (PON) (mg N/L)	0			
Dissolved Organic Nitrogen (DON) (mg N/L)	0.162[12]	0	0	
Orthophosphate (PO4) (mg P/L)	0.035[13]	Monthly in Table 4.6	Monthly in Table 4.7	Average total phosphorus (TP) of GHD (2024), HFRM and HRRM are 0.07, 0.047 and 0.017 mg P/L, respectively
Particulate Organic Phosphorus (POP) (mg P/L)	0			
Dissolved Organic Phosphorus (DOP) (mg P/L)	0.035[13]	0		
Silicate (SiO_4) (mg Si/L)	3	1.4	1.4 (0.14)	HRRM of 1.4 mg Si/L used, final update to use 0.14 mg Si/L
Particulate Iron (PFE) (mg Fe/L)	0		0.017	
Dissolved Iron (DFE) (mg Fe/L)	0.05		0.033	
Particulate Manganese (PMN) (mg Mn/L)	0		0.0012	
Dissolved Manganese (DMN) (mg Mn/L)	0.017		0.016	

SW provided monthly RW concentrations for PO4, alkalinity and major anions (Na, Ca) and cations (Cl, SO4) for the HRRM and HFRM RW WQ as summarised in Table 4.7 and Table 4.6, respectively.

Table 4.6 Monthly RW concentrations of PO4, alkalinity, DIC, and major anions and cations after HFRM treatment.

State Variable (Determinand)	Jan	Feb	Mar	Apr	May	Jun	Jul	Aug	Sep	Oct	Nov	Dec
Phosphate (PO4) (mg P/L)	0.0196	0.0261	0.0196	0.0522	0.0620	0.0587	0.0652	0.1044	0.0587	0.0489	0.0196	0.0294
Alkalinity (mg $CaCO_3$/L)	157.4	158.8	158.1	162.2	162.5	163.2	163.6	167.5	163.1	161.2	157.2	158.7
Dissolved Inorganic Carbon (DIC) (mg C/L)	38.9	39.2	39.1	40.1	40.2	40.3	40.4	41.4	40.3	39.8	38.8	39.2
Calcium (CA) (mg Ca/L)	60.2	60.3	60.2	60.3	60.3	60.4	60.3	60.5	60.4	60.3	60.2	60.2
Sodium (NA) (mg Na/L)	18.0	25.5	22.6	38.5	35.9	38.7	44.3	65.4	47.2	40.6	21.7	23.9
Chloride (CL) (mg Cl/L)	22.0	33.4	29.0	50.8	46.6	50.4	59.2	88.9	63.5	54.1	27.4	30.3
Sulfate (SO4) (mg S/L)	0.44	0.61	0.56	0.92	0.84	0.92	1.02	1.57	1.14	1.00	0.54	0.60

Table 4.7 Monthly RW concentrations of PO4, alkalinity, DIC, and major anions and cations after HRRM treatment.

State Variable (Determinand)	Jan	Feb	Mar	Apr	May	Jun	Jul	Aug	Sep	Oct	Nov	Dec
Phosphate (PO4) (mg P/L)	0.0087	0.0087	0.0087	0.0174	0.0217	0.0217	0.0217	0.0391	0.0217	0.0174	0.0087	0.0087
Alkalinity (mg $CaCO_3$/L)	152.8	153.2	153.0	154.5	154.6	154.8	154.9	156.4	154.9	154.1	152.7	153.2
Dissolved Inorganic Carbon (DIC) (mg C/L)	37.7	37.8	37.8	38.2	38.2	38.2	38.3	38.6	38.3	38.1	37.7	37.8
Calcium (CA) (mg Ca/L)	60.1	60.1	60.1	60.2	60.2	60.2	60.2	60.2	60.2	60.2	60.1	60.1
Sodium (NA) (mg Na/L)	5.3	7.2	6.5	10.8	10.2	11.0	12.4	18.4	13.3	11.5	6.4	6.8

[10] NH4 is total ammonia (NH_4^++NH_3).
[11] NO3 is total oxidized inorganic nitrogen (NO_3^-+NO_2^-).
[12] GHD (2024) assumed DON was 25% of NO_3^-+NH4.
[13] GHD (2024) assumed TP was 0.07 mg P/L with an allocation of 50% as PO4 (0.035 mg P/L) and 50% as DOP (0.035 mg P/L).

State Variable (Determinand)	Jan	Feb	Mar	Apr	May	Jun	Jul	Aug	Sep	Oct	Nov	Dec
Chloride (CL) (mg Cl/L)	6.0	8.9	7.8	13.5	12.4	13.5	15.6	23.7	17.0	14.5	7.5	8.1
Sulfate (SO4) (mg S/L)	0.05	0.07	0.07	0.10	0.09	0.10	0.11	0.17	0.13	0.11	0.07	0.07

4.3.2.2.3 Example time series of inlet WQ concentrations for scenarios 1B, 2H and 4A

Time series of inlet determinand concentrations of scenarios were calculated on a mass balance basis of the springs and RW discharge (Sections 4.3.1.2.6 to 4.3.1.2.9) and concentrations (Sections 4.3.2.2.1 and 4.3.2.2.2) for all scenarios. Examples of the time series of inlet WQ concentrations for selected determinands for scenarios 1B (baseline), 2H (drought) and 4A (extended classic) are shown in Figure 4.13.

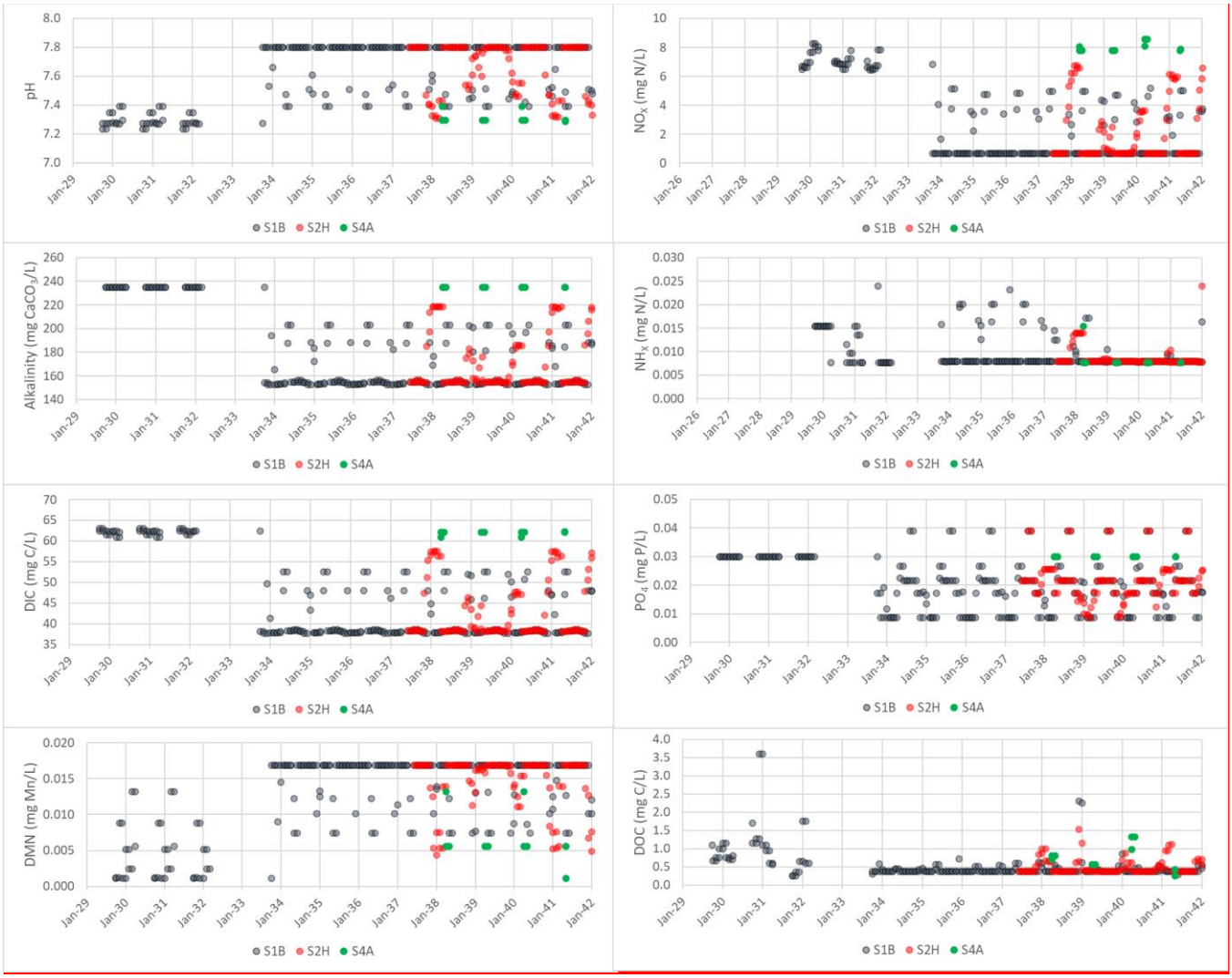

Figure 4.13 Example time series of pH, alkalinity, DIC, DMN, NO3, NH4, PO_4 and DOC inlet concentrations for scenarios 1B, 2H and 4A.

4.3.2.3 Rain

pH, conductivity, NO3, NH4, PO4, Ca, Na, Cl and SO4 concentrations in rain from the Lullington Heath site of the United Kingdom Eutrophying and Acidifying Network (UKEAP) Precipitation Network (Precip-Net) were used to estimate characteristic values to apply as model inputs. Determinand concentrations of samples with less than 5 mm of rainfall over the ~2 week measurement intervals typically had much higher analyte concentrations than periods with

higher rainfall (likely from dry deposition that caused a concentration bias during low rainfall periods). Most of the PO4 measurements were below the limit of reporting (<0.01 mg P/L), so a value of 0.005 mg P/L (half of the laboratory analytical detection limit) was assumed (note this may still be an overestimate with even lower PO4 on these occasions). This nutrient (NO3, NH4, PO4) data set is illustrated in Figure 4.14. The rainfall-weighted averages ($= (\sum r_i \times c_i) / \sum r_i$ where r_i is rainfall and c_i is the concentration over measurement interval i) were adopted as the characteristic concentrations for the rainfall inputs because high concentrations during low rainfall intervals are appropriately scaled (Table 4.8). For example, the averages of NO3, NH4 and PO4 (0.763 mg N/L, 0.473 mg N/L and 0.008 mg P/L, respectively) are much higher than the medians (0.371 mg N/L, 0.261 mg N/L and 0.005 mg P/L, respectively) and rainfall-weighted averages (0.331 mg N/L, 0.260 mg N/L and 0.007 mg P/L, respectively).

Table 4.8 Rainfall-weighted averages, medians and averages of determinand concentrations in rainfall

Determinand	Rainfall-Weighted Average	Median	Average
pH[14]	5.41	5.68	5.39
Conductivity (µS/cm)	43.3	39.7	52.7
NO3 (mg N/l)	0.331	0.371	0.763
NH4 (mg N/L)	0.260	0.261	0.473
PO4 (mg P/L)	0.0071	0.0050	0.0080
Ca (mg Ca/L)	0.414	0.379	1.010
Na (mg Na/L)	5.25	4.49	6.40
Cl (mg Cl/L)	9.09	7.91	10.95
water supply on	0.545	0.529	0.812

[14] pH volume-weight average, average and median calculated on hydronium ion concentrations and then transformed to pH.

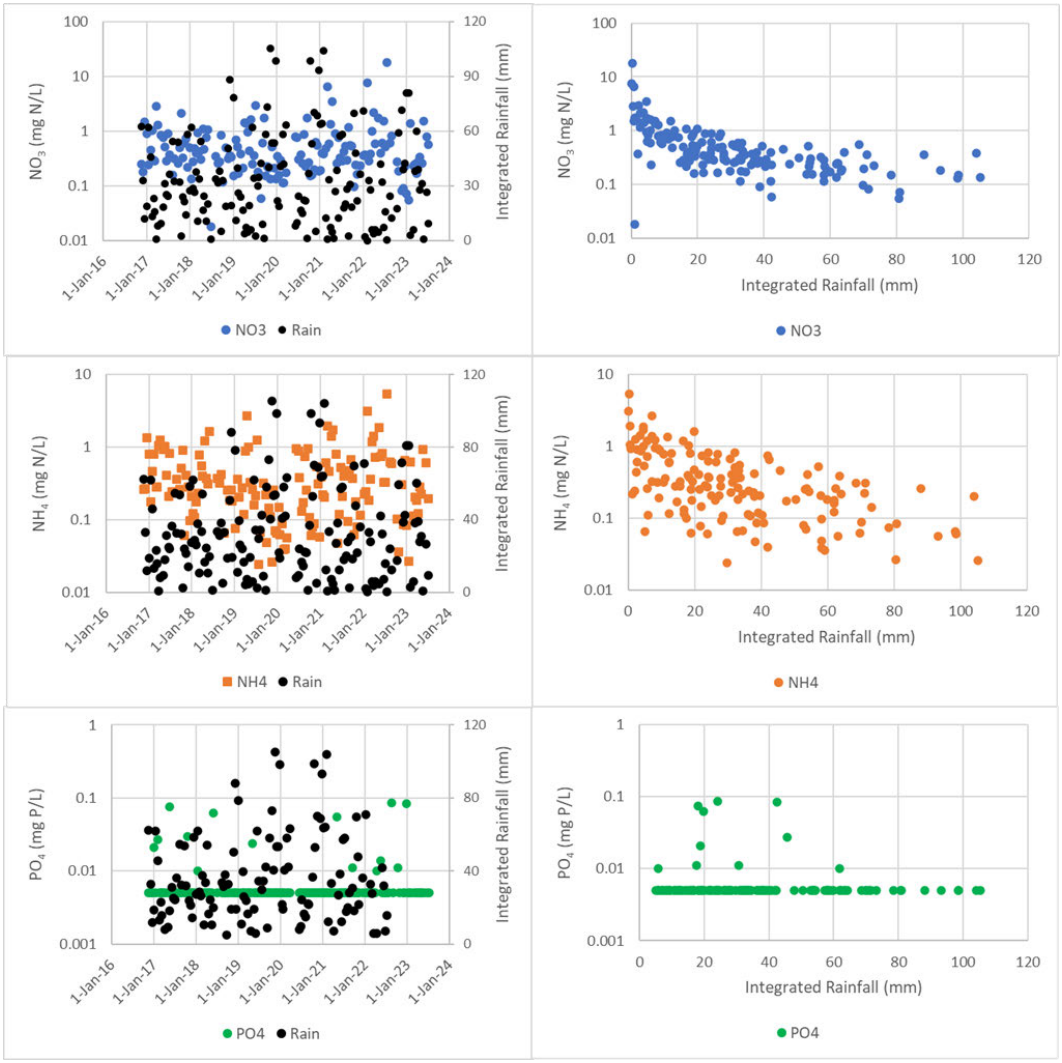

Figure 4.14 ***UKEAP Precip-Net NO3 (top), NH4 (middle) and PO4 (bottom) concentrations in rain over time (left) and correlated to integrated rainfall amount at the Lullington Heath site (right).***

4.3.2.4 Bird loading

The GHD (2023) methodology to estimate external loading of N and P from birds was updated in GHD (2024), and is described next. Some elements of the GHD (2023) methodology were retained, namely:

– Dissolved inorganic, dissolved organic and particulate organic inputs of N and P from birds were estimated on the basis of information in Atkins (2020) including:
  - The medians[15] of the peak monthly density of bird species in representative lakes and reservoirs within 10 km of the southern England coast were scaled to the area at TWL (1.06 km^2) (as Table 3.3 in Atkins (2020)).
  - The use of typical P and N export rates per bird (as Table 3.4 in Atkins (2020)).
– Partitioning of P and N loading from birds was as follows:
  - Assumed 20% of loading was PO4 and NH4.
  - Assumed 60% of loading was DOP and DON, as much of bird excrement is uric acid.

[15] Note that the 'average' density of birds reported in Stantec (2022) yields an over-estimate of loading due to a large outlier in one of the lakes/reservoirs in the dataset for the Lesser Black-Backed Gull (average ~1,240 birds/km^2, median ~12 bird/km^2). The median density of each of the bird species across the eleven (11) reservoirs/lakes was chosen as the appropriate baseline for this investigation.

- The remaining 20% was assumed to be POP and PON.
- NO3 was assumed to be zero.

– DOC and POC loads were assumed to be 20-fold greater than DOP and POP loads, respectively.

GHD (2024) updates to the GHD (2023) methodology included the following:

– Incorporating estimates of the seasonal variability (average monthly) of peak median densities of each species with the monthly bird index (British Trust for Ornithology [BTO] data) collated by Stantec (2022)[16]. These indices ranged from 0 (absence of species at HTR for the month) to 100 (peak median density of species attained for the month). The peak median density of each species was scaled as the monthly index value divided by 100. Estimates of loading from each species during each month were then multiplied by the N and P loading rates per bird species by the scaled bird species density for the month. The sum of all bird loadings per month then constituted the monthly bird loading rates. Total daily P and N loads across the twelve months ranged from ~76-230 g P/day and ~347-1,039 g N/day, respectively. The annual phosphorus and nitrogen loading rates were 58.5 kg N/year (160.2 g P/day) and 274.4 kg N/year (751.7 g N/day), respectively, substantially lower than the GHD (2023) estimates of 94.7 kg P/year (259.4 mg P/day) and 442.8 kg N/year (1,213.3 mg N/day), respectively. Atkins (2020) in their Figure 3.2 only illustrate the annual P loading rates for the 6 individual bird species with the largest loadings, which compare well with this investigation's estimates (Table 4.9).

– Stantec (2022) classified the bird species to habitat types, namely, deep open water, open water at the reservoir margins, wetland and no habitat preference. This spatial approach was adopted whereby the species with no habitat preference were assumed to be distributed evenly among the 3 habitat types. Approximately 76-81%, 5-8% and 11-16% of the total monthly varying P loads were into the deep waters, reservoir margins and wetland habitats, respectively, whereas for the N loads the ranges were 58-68%, 8-16% and 21-28%, respectively. Simulated locations of bird loading for the three habitat types are shown in Figure 4.2.

Table 4.9 Comparison of six species with the greatest annual P loadings (kg P/year) in this study and Atkins (2020).

Species	This Investigation's Estimate	From Atkins (2020) Figure 3.2
Cormorant	20.1	~25
Black-headed Gull	12.48	~12
Mediterranean Gull	2.5	0
Canada Goose	4.2	~2.5
Great Crested Grebe	3.5	~3.5
Greylag Goose	2.8	~2
Total of Top 6 Species	**45.6**	**~45**

The monthly estimates P and N bird loading are illustrated in Figure 4.15, which shows that the majority of the loads occurs in the open deep waters of the reservoir.

[16] Note Atkins (2020) included seasonality of bird species on this basis as well.

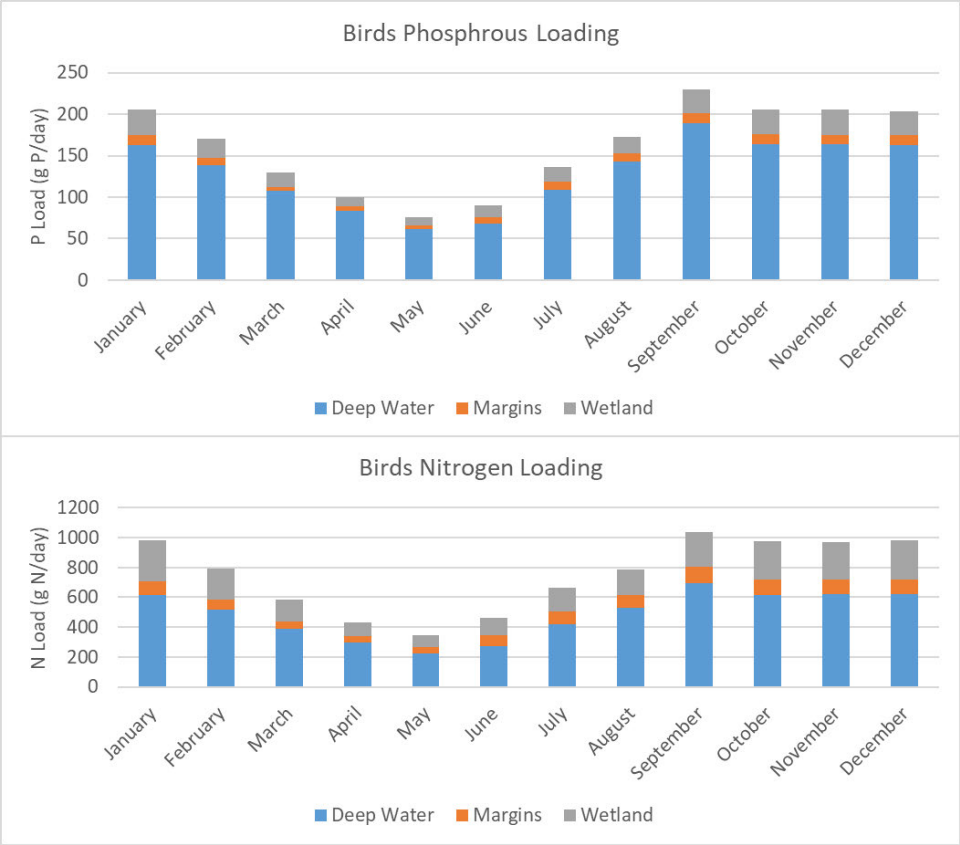

Figure 4.15 Monthly P (top) and N (bottom) bird loading estimates.

4.3.2.5 Summary of external model inputs

Table 4.10 summarises the external WQ modelling inputs on the basis of available information as described in previous Sections 4.3.2.1 to 4.3.2.4 and professional judgement.

*Table 4.10 Model input WQ concentrations for streams, bird loading and rainfall, and those to calculate the comingled inputs from springs and recycled water. **Red** values to be run for the Final Update Report.*

State Variable	Streams	Springs	Recycled Water	Bird Loading	Rain
T	Monthly T medians (Table 4.2)	Time series (TS) of 2012-2023 T monthly averages from 2 sites (Figure 4.12)	RW remineralisation TDS of 302 mg/L (Table 4.5)	Assume same T as waters in which inputted	Assume same T as surface waters
S	S estimate from Oct.-Nov. median Table 4.2 specific conductance (EC)[17]	S estimate from median of monthly averages of EC[17] at 2 sites (Figure 4.12)	RW remineralisation TDS of 302 mg/L (Table 4.5)	Assume no load	Assumed no load
NO3	Monthly NO_3 medians (Table 4.2)	TS of 2012-2023 NO3 monthly averages from 2 sites (Figure 4.12)	HRRM NO3 of 0.661 (0.301) mg N/L (Table 4.5)	Assume 0% of TN bird loading	Rainfall weighted average of 0.331 mg N/L (Table 4.8)
NH4	Monthly Total NH_X medians (Table 4.2)	TS of 2012-2023 NH4 monthly averages from 2 sites (Figure 4.12)	HRRM NH4 of 0.008 (0) mg N/L (Table 4.5)	Assume 20% of TN bird loading (~10% chicken urine and faeces in literature)	Rainfall weighted average of 0.260 mg N/L (Table 4.8)

[17] S = c x EC where c adopted as 0.625 in range of typical values between 0.55-0.7.

State Variable	Streams	Springs	Recycled Water	Bird Loading	Rain
DON, PON	Both assumed 0.05 mg N/L	PW estimated DON and PON as 0 mg N/L	SW estimated DON and PON as 0 mg N/L (Table 4.5)	Assume 60% and 20% of TN bird loading for DON (primarily uric acid, ~80% chicken urine and faeces) and PON (urea, ~5% chicken urine and faeces, >50% for goose droppings in literature)	Assumed no load
PO4	Assume 50% of monthly TP[18] medians (Table 4.2)	Constant PO4 of 0.03 mg P/L on basis of 2021-2023 TP and PO4 monthly averages from 2 sites (Figure 4.12)	HRRM PO4 of 0.03 mg P/L (Table 4.5)	Assume as NH4 with 20% of TP bird loading	Rainfall weighted average of 0.007 mg P/L (Table 4.8)
DOP, POP	Assume DOP and POP are each 25% of monthly TP medians (Table 4.2)	PW estimated DOP and POP as 0 mg P/L	SW estimated DOP and POP as 0 mg P/L (Table 4.5)	Assume as DON and PON with 60% and 20% of TP bird loading for DOP (uric acid) and PON (urea)	Assumed no load
DOC, POC	Assume DOC and POC are each 50% of monthly TOC medians (Table 4.2)	Assume DOC as 100% of TS of 2012-2023 TOC monthly averages (Figure 4.12) Assume POC 0 mg C/L	DOC of 0.37 (0.39) mg C/L (Table 4.5) POC of 0 mg C/L (Table 4.5)	Assume 5 fold the load of DON and PON (C:N of poultry excreta ~5 in literature)	
SiO2	Assume 3 mg Si/L (Neal et al 2005)	Characteristic regional chalk springs of 6 mg Si/L (Stuart & Smedley 2009)	Assume SiO2 of 1.4 (0.14) mg Si/L (Table 4.5)	Assume no loads	
FDIAT, CHLOR, CYANO	Assume each group 0.01 µg chl-a/L				
DO	Assume DO 100% saturated on basis of monthly median T	Assume DO is 100% saturated	Assume DO is 100% saturated (Table 4.5)		
SSOL1, SSOL2	Assume SSOL1 (clay) and SSOL2 (silt) are 75% and 25% of monthly SS medians (Table 4.2)	TS of 2012-2023 SSOL1 (clay) monthly average estimates from monthly averages of turbidity[19] at 2 sites (Figure 4.12) SSOL2 (silt) assumed 0 mg/L	SSOL1 (clay) and SSOL2 (silt) 0 mg/L (SS_{Inorg} 0 mg/L in Table 4.5)		
pH	Monthly pH medians (Table 4.2)	TS of 2012-2023 pH monthly averages from 2 sites (Figure 4.12)	pH of 7.8 (Table 4.5)		Rainfall weighted average of 5.41 (Table 4.8)
ALK	Median alkalinity of 12.5 mg $CaCO_3$/L of the Oct.-Apr. measurements (Table 4.2)	Median of 235 mg $CaCO_3$/L from available data at 2 sites (Section 4.3.2.2.1)	Alkalinity of 150 mg $CaCO_3$/L (Table 4.5)		Estimated with relation of Butler (1982) from DIC and pH as 0.94 mg $CaCO_3$/L
DIC	Estimated with relation of Butler (1982) from alkalinity and pH	Estimated with relation of Butler (1982) from alkalinity and pH	DIC of 37.0 mg C/L (Table 4.5)		Assumed 2 mg C/L (Gorka et al 2011)
DMN	Assume 100% of monthly TMn medians (Table 4.2)	Assume DMN 100% of monthly TMn medians of 2020-2023 measurements (Table 4.3)	DMN 0.016 mg Mn/L (Table 4.5)		Assumed no load

[18] PO4 has higher limit of detection than TP, and often PO4 > TP for same sample, so PO4 measurement reliability questionable.
[19] Turbidity to TSS ratio of 2 adopted as requested by PW (H. Thomas, pers. comm.).

State Variable	Streams	Springs	Recycled Water	Bird Loading	Rain
PMN	Assume 0 mg Mn/L	Assume 0 mg Mn/L	PMN 0.0012 mg Mn/L (Table 4.5)		
DFE	Assume monthly TFe medians (Table 4.2)	Assume DFE 100% of monthly TFe medians of 2020-2023 measurements (Table 4.3)	DFE of 0.033 mg Fe/L f (Table 4.5)		
PFE	Assume 0 mg Mn/L	Assume 0 mg Mn/L	PFE of 0.017 mg Fe/L (Table 4.5)		
TRACER_1 (Outfall)	0	1	1	0	0
TRACER_2 (Streams)	1	0	0	0	0
TRACER_4 (Springs)	0	Fraction of inlet discharge comprised of springs water	0	0	0
TRACER_4 (Recycled Water)	0	0	Fraction of inlet discharge comprised of RW	0	0
TRACER_5 (Ca)	Monthly Ca medians (Table 4.2)	Monthly Ca averages (Table 4.4)	Monthly Ca estimates (Table 4.7)	0	Rainfall weighted average (Table 4.8)
TRACER_6 (Na)	Monthly Na medians (Table 4.2)	Monthly Na averages (Table 4.4)	Monthly Na estimates (Table 4.7)	0	Rainfall weighted average (Table 4.8)
TRACER_7 (Cl)	Monthly Cl medians (Table 4.2)	Monthly Cl averages (Table 4.4)	Monthly Cl estimates (Table 4.7)	0	Rainfall weighted average (Table 4.8)
TRACER_8 (SO_4)	Monthly SO_4 medians (Table 4.2)	Monthly SO_4 averages (Table 4.4)	Monthly SO_4 estimates (Table 4.7)	0	Rainfall weighted average (Table 4.8)

4.3.2.6 Scenario 1B external loading estimates

The relative proportions of the 5 TN and TP external loading sources across the entirety of scenario 1B and the 3 phases (fill, classic, recycled) are provided in Figure 4.16, which shows that:

– RW and birds account for ~74% and ~13% of TP loads over the entirety of scenario 1B, respectively, while springs and RW account for ~75%, and ~20% of TN loads, respectively.

– Springs and birds account for ~73% and ~21% of TP loads over the 'fill' stage, respectively, while springs account for ~98% of TN loads.

– Birds account for ~81% of TP loads over the brief 'classic' stage of ~1 year duration because no springs water was discharged into the reservoir via the inlet, while rain and birds account for ~55%, and ~34% of TN loads, respectively. The total TN load during the 'classic' stage is very low because of no springs inputs over this short period (see Figure 4.17).

– RW and birds account for ~81% and ~11% of TP loads over the 'recycled' stage, respectively, while springs and RW account for ~60%, and ~33% of TN loads, respectively.

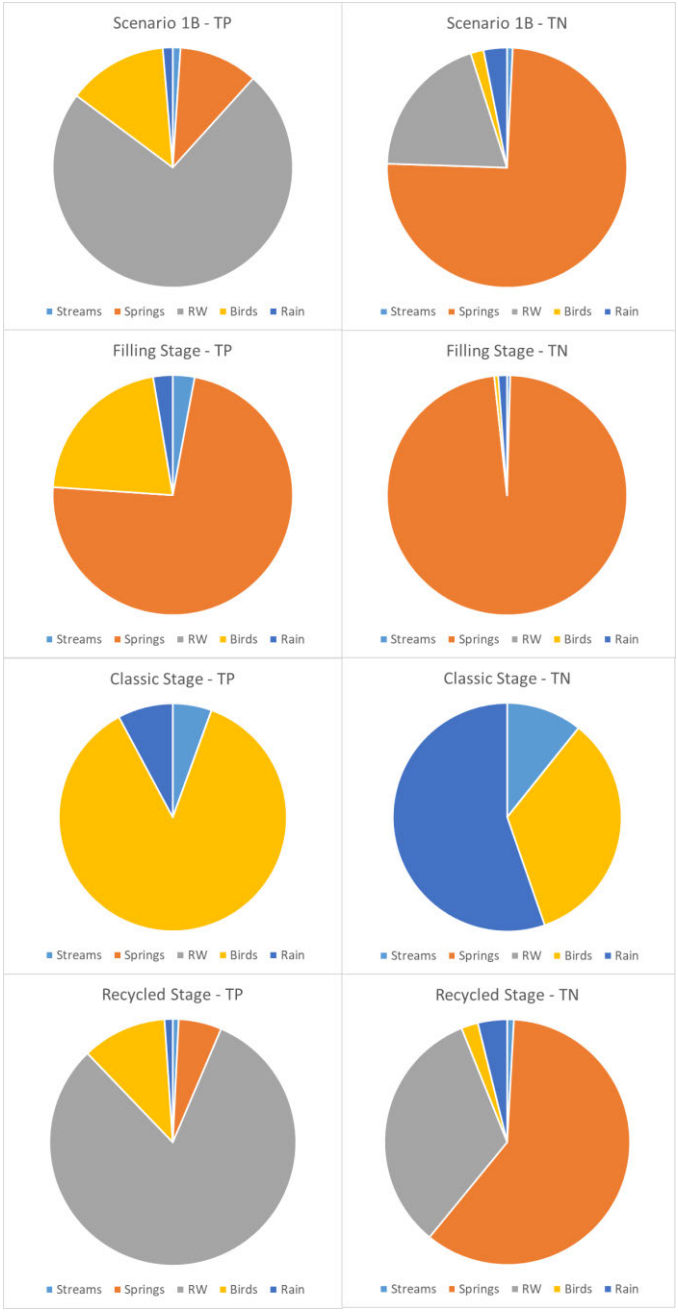

Figure 4.16 ***Relative proportions of the 5 sources of external TP (left) and TN (right) loading over the entirety of scenario 1B (top row), and the 'fill' (2nd row, 1 October 2029 to 31 March 2032), 'classic' (3rd row, 1 April 2032 to 30 September 2033) and 'recycled' (bottom row, 1 October 2033 to 1 January 2042) stages.***

The average daily loading rates (fluxes) from the five TN and TP external loading sources across the entirety of scenario 1B and the three stages (fill, classic, recycled) are provided in Figure 4.17. Average daily TP and TN external loadings are predicted to be much greater during the 'recycled' than 'classic' stage because of the much greater volumetric inputs of RW and springs. For example, the average daily TP load increased by a factor of ~7 for 'recycled' stage. The average daily TN load increased by a factor of nearly ~20 for the 'recycled' relative to the 'classic' stage due to the addition of RW and no springs water inputs during the short 'classic' stage.

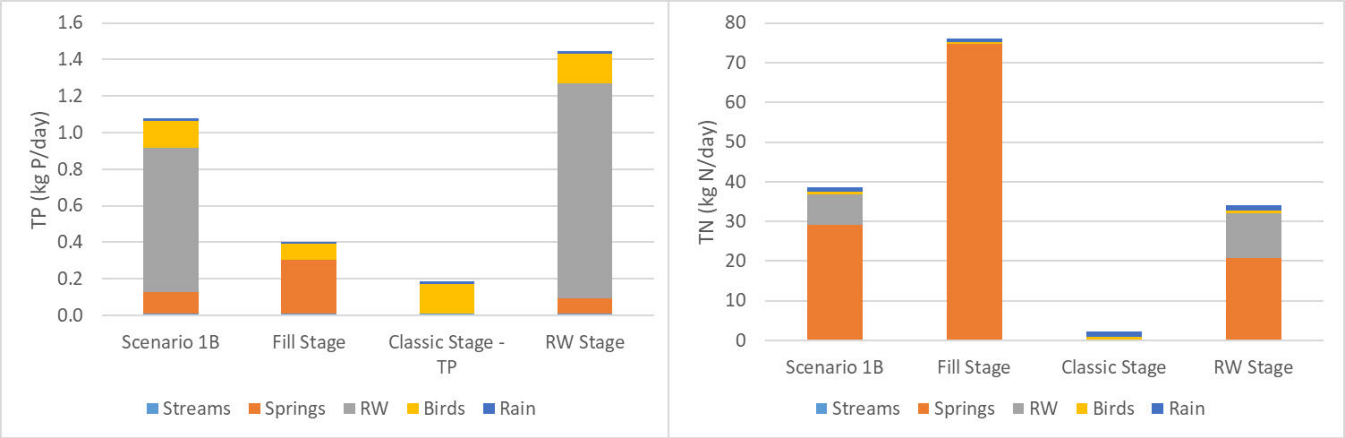

Figure 4.17 ***Average daily loading rates (fluxes) of the five sources of external TP (left) and TN (right) loading over the entirety of scenario 1B, and the fill (1 October 2029 to 31 March 2032), classic (1 April 2032 to 30 September 2033) and recycled (1 October 2033 to 1 January 2042) stages.***

4.4 Initial conditions

4.4.1 Start of reservoir fill for scenarios 1B and 1BS

The initial condition of the state variables at the start of scenarios 1B and 1BS on 1 January 2030 are summarised in Table 4.11. Many of the initial values of the state variables were assumed to be equivalent to the springs WQ estimates because it is the dominant input during the initial 'fill' stage from October-December 2029. The simulation start date is 1 January 2030 with an initial water level of -11.4 m below TWL, which is above the sill elevation of ~-13.5 m below TWL between two basins, so as to minimise numerical errors during the 'fill' stage if the north basin is filled initially and then overflows into an empty south basin.

4.4.2 Start of scenarios 2E-J

Scenarios 2E-J were initialised with the simulated snapshot of the hydrodynamic and WQ conditions of scenario 1B at midnight on 24 March 2037 to allow for model spin-up prior to the onset of RW inputs on 1 June 2017. Hence, changes in the discharge and WQ from the inlet into the reservoir and withdrawal discharge for scenarios 2E-J vary from scenario 1B only after 1 June 2037.

4.4.3 Start of scenario 4A

Scenario 4A was initialised with the simulated snapshot of hydrodynamics and WQ conditions of scenario 1B at midnight on 9 September 2033. Changes in the discharge and/or WQ of the inlet (springs + RW) inflow and withdrawal discharge for scenario 4B only varies from scenario 1B after the onset of RW inputs into the reservoir after 1 October 2033.

Table 4.11 Initial conditions on 1 January 2030 for state variables at the start of the scenario 1B.

State Variable ID	Initial Condition	State Variable Description	Justification
T	7°C	Water Temperature	Typical temperature at beginning of January
S	0.12 psu	Salinity	Assumed
FDIAT (Diatoms) CHLOR (Green Algae) CYANO (Cyanobacteria)	2 µg chl-a/L 2 µg chl-a/L 2 µg chl-a/L	Diatoms Green Algae Blue-Green Algae	Assumed
FDIAT_IN NODUL_IN CHLOR_IN	0.012 mg N/L 0.012 mg N/L 0.012 mg N/L	Internal N in Diatoms Internal N in Green Algae Internal N in Blue-Green Algae	Assume 6 g N/1 g chl-a
FDIAT_IP NODUL_IP CHLOR_IP	0.0012 mg P/L 0.0012 mg P/L 0.0012 mg P/L	Internal P in Diatoms Internal P in Green Algae Internal P in Blue-Green Algae	Assume 0.6 g P/1 g chl-a
NO3	7.51 mg N/L	Nitrate	October-December springs data average
NH4	0.014 mg N/L	Ammonium	
DONL	0.01 mg N/L	Dissolved Organic N	Assume 0.01 mg N/L as 0 mg N/L in springs water
PONL	0.001 mg N/L	Particulate Organic N	Assume 0.001 mg N/L as 0 mg N/L in springs water
PO4	0.03 mg P/L	Phosphate	Characteristic constant value on basis of TP measurements
DOPL	0.001 mg P/L	Dissolved Organic P	Assume 0.001 mg P/L as 0 mg P/L in springs water
POPL	0.0001 mg P/L	Particulate Organic P	Assume 0.0001 mg N/L as 0 mg P/L in springs water
DOCL	1.0 mg C/L	Dissolved Organic C	October-December springs data average
POCL	0.66 mg C/L	Particulate Organic C	Estimate
SSOL1	1.4 mg/L	Clay	October-December springs data turbidity average and NTU conversion to mg/L
SSOL2	0.01 mg/L	Silt	Assumed
DO	9 mg/L	Dissolved Oxygen	Assumed
SiO2	6 mg Si/L	Silica	PW provided characteristic concentration on basis of monitoring data
pH	7.31	Hydronium ion concentration	October-December springs data averages
DIC	61.9 mg C/L	Dissolved Inorganic Carbon	
Alkalinity	235 mg $CaCO_3$/L	Alkalinity	
DMN	0.007 mg Mn/L	Dissolved Manganese	October-December springs TMn data average
PMN	0.001 mg Mn/L	Particulate Manganese	Assume
DFE	0.16 mg Fe/L	Dissolved Iron	October-December springs TFe data average
PFE	0.01 mg Fe/L	Particulate Iron	Assume

4.5 Water quality parameter values

4.5.1 Standard set of values

As HTR does not yet exist (and thereby model calibration and verification cannot occur), establishment of a credible set of values for the parameters (constants) of the model's WQ processes (e.g. nitrification, dissolved organic matter mineralisation, phytoplankton respiratory consumption and photosynthetic generation of DO) must through necessity

largely rely on published literature values, estimates and assumptions. Where possible, published literature values from CAEDYM (prior to 2018) and AEM3D (after 2017) modelling applications served as the primary basis to set parameter values, in part to provide a level of consistency that is not confounded by alternative formulations of WQ processes in other modelling frameworks.[21] A reasonable 'generic' set of WQ parameter values was established on the basis of a number of AEM3D (and CAEDYM) applications that span a range of lake and reservoir settings to allow credible forecasts of future HTR WQ to:

– Identify the primary WQ determinands of potential concern.
– Identify the primary mechanisms that effect WQ over the 'classic' and 'recycled' stages.
– Evaluate the effectiveness of operational strategies (i.e. bubbler operations) on the WQ within the reservoir and withdrawals.
– Estimate the future WQ envelope of withdrawals for water supply to inform DWSP.
– Estimate the environmental acceptability of withdrawals for downstream releases (environmental compensation flows) and in-reservoir WQ.

This 'generic' set WQ parameter values for the AEM3D application to HTR is provided in Appendix B. This parameter set is nearly equivalent to GHD (2024) with several updated parameter values noted in Appendix B on the basis of AEM3D applications by the author to similar systems in the interim.

Lastly, sediment fluxes assume that the inundated soils are not dispersive. GHD (2024) implicitly assumed that the inundated soils are not dispersive. This investigation explicitly assumes non-dispersive material in the upper ~30 cm of the soil horizon. If dispersive soils occur in the upper horizons of the profile within the HTR footprint, this investigation assumes that these regions will be capped by ~30 cm of non-dispersive soil material.

4.5.2 Estimates of sediment fluxes during the stabilisation phase

4.5.2.1 Temporal variation

The primary mechanism that can potentially cause poor WQ during the initial filling of a new reservoir is the mineralisation and decomposition[22] of inundated labile (readily degradable) above and below ground terrestrial-derived organic matter. The stabilisation period is defined as the first several years after the initial inundation of a reservoir when above and below ground labile terrestrial-derived biomass is decomposed and mineralised that results in substantially larger dissolved inorganic (e.g. NH4, PO4 and DIC due to mineralisation) and organic (e.g. DON, DOP and DOC due to decomposition) matter sediment fluxes than typical post-stabilisation rates (i.e. a number of years after reservoir filling when sediment fluxes attain a quasi-equilibrium). The post-stabilisation phase begins after labile terrestrial organic matter in the soils and overlying biomass has largely been decomposed and mineralised.

Both the decomposition and mineralisation of above and below ground labile terrestrial-derived organic matter is represented in the model through changes to the potential maximum sediment flux rates into the reservoir waters immediately overlying the simulated sediments. In particular, the potential maximum sediment flux of a particular dissolved WQ constituent is temporally varied to account for the stabilisation effect. These potential maximum sediment fluxes that are defined at a standard T of 20°C are then corrected for simulated T and the DO conditions of the waters immediately overlying the sediments. Adopted post-stabilisation sediment flux parameters are provided in Appendix B.

The following potential maximum sediment flux parameters are used to forecast the stabilisation effect:

– Maximum potential SOD at 20°C is defined as the DO consumed to mineralise the labile above and below ground terrestrial organic matter during the stabilisation phase, and additionally the 'normal background' decomposition

[21] Many other WQ models (e.g. WASP, CE-QUAL-W2) only model a subset or larger number of state variables and processes than AEM3D. Hence, model parameters for applications by these other models in many cases may not be 'like for like' with AEM3D due to the differences in WQ model architecture (e.g. differences in state variables and processes that are simulated).
[22] Decomposition refers to the breakdown of particulate organic matter to dissolved organic matter, while mineralisation refers to the breakdown of dissolved organic matter to dissolved inorganic mater.

of organic matter in/on the sediments during the post-stabilisation phase. A conservative post-stabilisation potential maximum SOD sediment flux at 20°C of 1.0 g DO/m^2/d has been adopted (Appendix B) and stabilisation estimates are provided in Table 4.12.

– Mineralisation of organic matter within the sediments also results in the release of DIC into the HTR waters. Here, the potential maximum DIC sediment flux at 20°C is assumed to be proportional to the SOD.
– Decomposition of particulate organic matter within the sediments also liberates DOC, DON and DOP into the near-sediment reservoir waters. The typical post-stabilisation and stabilisation potential maximum DOC sediment flux at 20°C is provided in Appendix B and Table 4.12, respectively. The maximum DON and DOP sediment fluxes at 20°C are assumed to be proportional to DOC.
– The inorganic nutrients of NH4 and PO4 typically accumulate in the sediment porewaters via mineralisation of dissolved organic matter within the sediments. Typical post-stabilisation and stabilisation maximum potentialNH4 and PO4 sediment fluxes at 20°C are provided in Appendix B and Table 4.12, respectively.
– The maximum potential sediment flux rates at 20°C of reduced DFE and DMN are assumed to not materially differ between the stabilisation and post-stabilisation phases as the content of these metals in terrestrial above- and below-ground organic matter is relatively low. As such, the typical maximum DFE and DMN sediment fluxes at 20°C over the stabilisation phase is assumed to be the same as the post-stabilisation phases (see Appendix B). However, the higher SOD during the stabilisation phase has the potential to cause lower DO levels of the overlying water immediately above the sediments and thereby indirectly increase the simulated fluxes of DFE and DMN into the water column.

DOC, DON, DOP, NH4, PO4, DFE and DMN sediment fluxes are assumed to be dependent on the simulated DO levels of water immediately overlying the sediments. Typically, an inverse Michaelis-Menton relation is utilised to simulate this DO dependency whereby lower (<~1-2 mg/L) and higher (>5 mg/L) DO levels yield higher and lower fluxes, respectively. Temperature and DO dependent sediment flux model parameters for each of these WQ constituents are provided in Appendix B.

Though the available literature catalogues 'in-water' measurements of WQ degradation in reservoirs during the stabilisation phase, no publications were identified that quantitatively estimate sediment fluxes (in terms of both submerged soils and terrestrial-derived above ground organic matter). Gunnison et al (1984) carried out above-ground terrestrial biomass and below-ground terrestrial organic matter decomposition studies for a reservoir in the southeast USA prior to its construction, and found that at 20°C:

– The SOD of the below-ground terrestrial organic matter in the soil was comparable to other similar reservoirs where it effectively acts as a steady slow-rate of release material. For the purposes of this investigation, the maximum potential SOD was estimated as follows:
    - Post-stabilisation is the adopted potential maximum SOD rate at 20°C of 1 g/m^2/day.
    - Year 1 of inundated soils are estimated as 3x the post-stabilisation potential maximum SOD at 20°C.
    - Year 2 of inundated soils is estimated as 1.5x the post-stabilisation potential maximum SOD at 20°C.
– Labile above-ground terrestrial biomass decomposed much more rapidly over the initial several months of the Gunnison et al (1984) study, however the biomass was macerated in their laboratory study and therefore the time scales of decomposition were likely too short relative to actual conditions. Further, the above-ground vegetation biomass in HTR prior to inundation is anticipated to be very low because it is primarily grassland, the borrow pits to provide material for the construction of the dam embankments will remove a large proportion of the permanent (and seasonal) above-ground vegetation and below-ground organic matter, and it is assumed that some effort in the removal of above-ground vegetation will be made immediately prior to inundation of areas over each of the 3 filling winters to ameliorate the stabilisation effect on HTR's WQ. In this investigation it is assumed that a moderate rate of decomposition of labile above-ground terrestrial biomass occurs during the first year following inundation. Supposing an average typical net annual primary productivity of above-ground terrestrial biomass prior to HTR inundation of 600 g/m^2/year typical of temperate grasslands, and assuming that ~1 year of this net productivity is predominantly 'fresh labile' biomass that is flooded during the inundation of soils during the 'fill' phase, then:

- Assume that 75% of the above-ground terrestrial biomass will be removed from the inundation area.
- A moderate potential maximum SOD rate of above-ground terrestrial biomass decomposition/mineralisation at 15°C (the typical predicted reservoir water temperature over a year) of 0.4 g/m^2/d will decompose/mineralise the remaining 25% of the biomass over the first year of inundation. This is equivalent to a maximum SOD sediment flux of 0.51 g/m^2/d at 20°C (the standard model parameter input temperature), which is 50% of the adopted post-stabilization sediment SOD of 1.0 g DO/m^2/d. This SOD rate is applied to simulated HTR regions over the first year of inundation.

– The total release of carbon (C) into the water column was scaled to the SOD rate. Fifty percent (50%) of the carbon was assumed to be released into the waters immediately overlying the sediments as DOC due to decomposition and the remaining 50% as DIC due to mineralisation. A C:N mass ratio of 21 mg C in leaves/1 mg N in leaves (Zhang et al 2020) was used to convert DOC and DIC fluxes to DON and NH4 fluxes, respectively. Similarly, a N:P mass ratio of 21 mg N in leaves/1 mg P in leaves (Tian et al 2020) was used to convert DOC and DIC fluxes to DOP and PO4 fluxes, respectively.

– Adopted potential maximum sediment fluxes of DMN and DFE of the post-stabilisation phase were assumed to not be influenced by the decomposition and mineralisation of inundated terrestrial-derived organic matter. Similarly, nitrate (NO3) fluxes are typically small from the water column into the sediments, and therefore were not varied from the adopted post-stabilisation maximum sediment flux rate.

The estimated values for the maximum sediment fluxes at 20°C over for the post-stabilisation phase, and the first and second years following soil inundation during the 'fill' stage, are summarised in Table 4.12.

Table 4.12 ***Adopted values for potential maximum sediment rates at 20°C for the post-stabilisation phase, and the first and second years in which sediments are inundated during the stabilisation phase where bold underlined values are estimates of sediment fluxes from the decomposition/mineralisation of both submerged terrestrial biomass and soils.***

	Post-Stabilization			1st Year of Inundation			2nd Year of Inundation			
Parameter	**Sediments**	**Terrestrial Biomass**	**Modelled Rate**	**Sediments**	**Terrestrial Biomass**	**Modelled Rate**	**Sediments**	**Terrestrial Biomass**	**Modelled Rate**	**Description**
SOD @ 20°C (g DO/m^2/d)	1.0	0	**1.0**	3.0	0.5	**3.5**	1.5	0	**1.5**	Sediment: 1st and 2nd years of inundation 3x and 1.5x post-stabilisation fluxes, respectively Vegetation: 1st year of inundation decompose/mineralise ~25% of vegetation at 15°C (typical water T), assume 75% removed
DIC @ 20°C (g C/m^2/d)	0.38	0	**0.38**	1.13	0.10	**1.22**	0.56	0	**0.56**	Sediment: As SOD Vegetation: Assume half vegetation SOD rate is mineralisation to DIC
PO4 @ 20°C (g P/m^2/d)	0.003	0	**0.003**	0.0090	0.0002	**0.0092**	0.0045	0	**0.0045**	Sediment: As SOD Vegetation: Assume N:P ratio of 21 mg N/mg P (Tian et al 2018) times NH_4 flux
NH4 20°C (g N/m^2/d)	0.015	0	**0.015**	0.045	0.005	**0.050**	0.023	0	**0.023**	Sediment: As SOD Vegetation: Assume C:N ratio of 21 mg C/mg N (Zhang et al 2020) times DIC flux
DOC @ 20°C (g C/m^2/d)	0.1	0	**0.1**	0.3	0.1	**0.4**	0.15	0	**0.15**	Sediment: As SOD Vegetation: Assume half SOD rate is decomposition to DOC
DON @ 20°C (g N/m^2/d)	0.018	0	**0.018**	0.052	0.005	**0.057**	0.026	0	**0.026**	Sediment: Assume N:C ratio of 0.121 mg N/mg C (Wang et al 2021) times DOC flux Vegetation: Assume C:N ratio of 21 mg C/mg N (Tian et al 2018) times DOC flux
DOP @ 20°C (g P/m^2/d)	0.0025	0	**0.0025**	0.0075	0.0002	**0.0077**	0.0038	0	**0.0038**	Sediment: Assume P:C ratio of 0.089 mg P/mg C (Wang et al 2021) times DOC flux Vegetation: Assume N:P ratio of 21 mg N/mg P (Zhang et al 2020) times DON flux

4.5.2.2 Spatial variation

The current forecast is for HTR to be filled over 3 consecutive years with spring-summer surface levels at ~31.5 m OD (~8 m below TWL), ~35.5 m OD (~4 m below TWL) and ~39 m OD (~0.5 m below TWL) during years 1 (2030), 2 (2031) and 3 (2032), respectively (refer to Figure 4.5). These inundation areas during the first, second and third years of the 'fill' stage are illustrated in Figure 4.18.

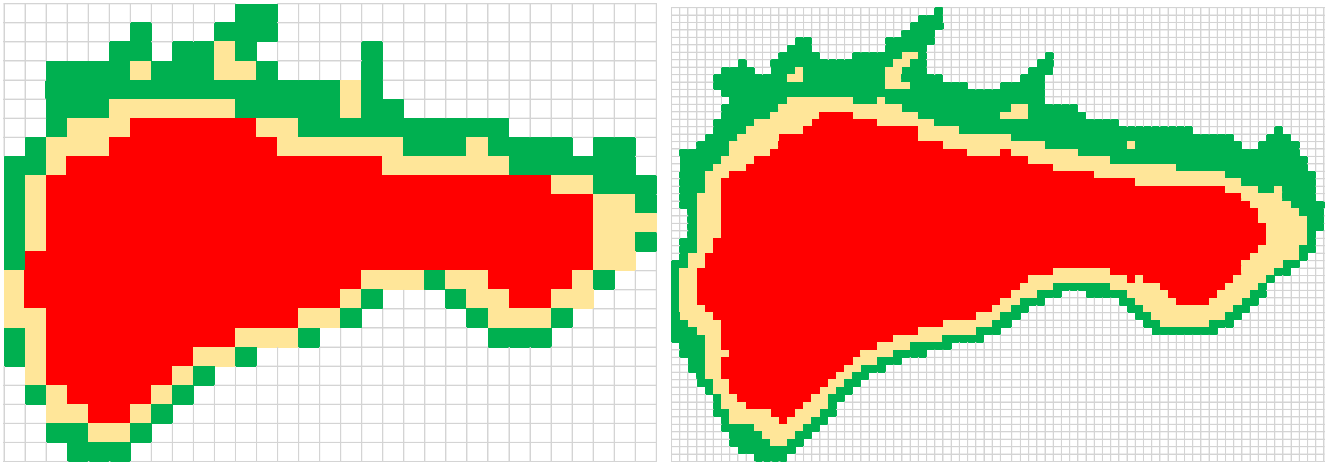

Figure 4.18 ***Inundation regions during the first (red), second (yellow) and third (green) years of reservoir filling of the coarse (50 m, left) and fine (20 m, right) model horizontal grid resolutions.***

4.5.2.3 Spatial and temporal integration

Figure 4.19 illustrates the sequence of ~1 year simulations to emulate potential stabilisation effects on HTR over the first 4 years, and a description of the spatial variation in sediment fluxes across depth/elevation bands.

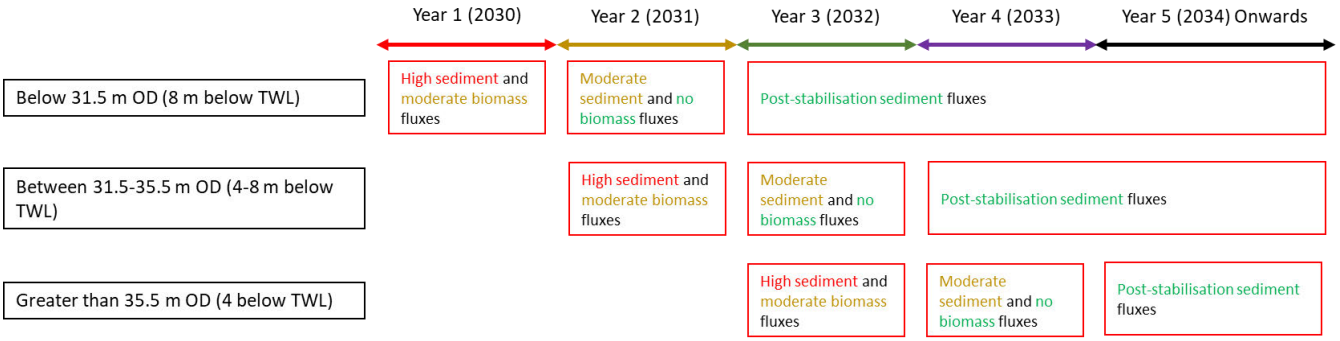

Figure 4.19 ***Schematic of sequence of sediment fluxes across the three reservoir 'fill' depth bands (see Figure 4.18) to estimate the stabilisation process over the initial 4 years of scenario 1BS.***

5. Comparison of coarse and fine grid simulations

As described in Section 4.1, a coarse grid (50x50x1 m) was established to carry out simulations in a more timely manner than was possible with the fine grid (20x20x1 m), but with sufficient spatial and temporal accuracy to meet the objectives of this study, namely the long-term (~12 years, 2030-2041) evolution of WQ within the reservoir and withdrawals for raw water supply and downstream environmental compensation flows.

GHD (2024) Appendix A compared coarse and find grid simulations of the reference design bathymetry for a RW inlet discharge of ~7.5 MLD with and without continuous bubbler operations from April-September and found:

– Though there are some differences in the simulated vertical and horizontal variations in hydrodynamics (T, currents, RW conservative tracer) and WQ between the coarse and fine grids, these differences were minor.
– The simulated T, RW tracer and WQ of the withdrawals matched very well between the fine and coarse grids, which demonstrated that the spatial-temporal in-reservoir variations are not material in terms of the predicted outlet WQ for water supply and downstream environmental releases.
– The coarse grid was deemed more than adequate to meet this investigation's objectives in a timely manner.

There have been several updates in regards to the onset of reservoir operations, the water balance of operational and emergency drought scenarios, RW and springs WQ inputs, RW and springs inlet location, and bubble plume mixing system design since GHD (2024). Additionally, the scenarios were finalised ~2 months prior to the scheduled completion date of this study, so to maintain the delivery schedule to inform downstream water supply design considerations and regulatory engagement, use of a coarse grid for forecasts was necessary.

Appendix A provides an evaluation of the adequacy of the coarse grid (50x50x1 m) simulation of scenario 1B with nighttime bubbler operations relative to the fine grid (20x20x1 m) . The predicted in-reservoir WQ for the most part was very similar except for DO and DMN in the deep waters of the south basin's deep hole. The coarse grid does not resolve the hydrodynamics in this deep hole well, so poor mixing is simulated with insufficient DO fluxes into this volume from overlying waters. In contrast, the fine grid does resolve the hydrodynamics well with DO levels similar to the bottom waters in the north basin over the 12 year duration of scenario 1B (Appendix A). As the south basin's deep hole below -17 m TWL (22.5 m OD, the elevation of the bubble plume destratification system) only represents 1.5% of the reservoirs volume at TWL, the numerical artefact of poor WQ in this deep hole when diluted with the large reservoir volume during autumn mixing yields predicted withdrawal WQ that is very similar to the fine grid simulation. Hence, the coarse (50x50x1 m) grid was used to simulate scenarios to inform DWSP and environmental considerations.

6. Scenario 1B forecasts without and with nighttime bubbler operations

6.1 Hydrodynamics

6.1.1 Water levels

The simulated surface levels (Figure 6.1) reproduced the water levels of the daily water balance well for scenario 1B (Figure 4.5).

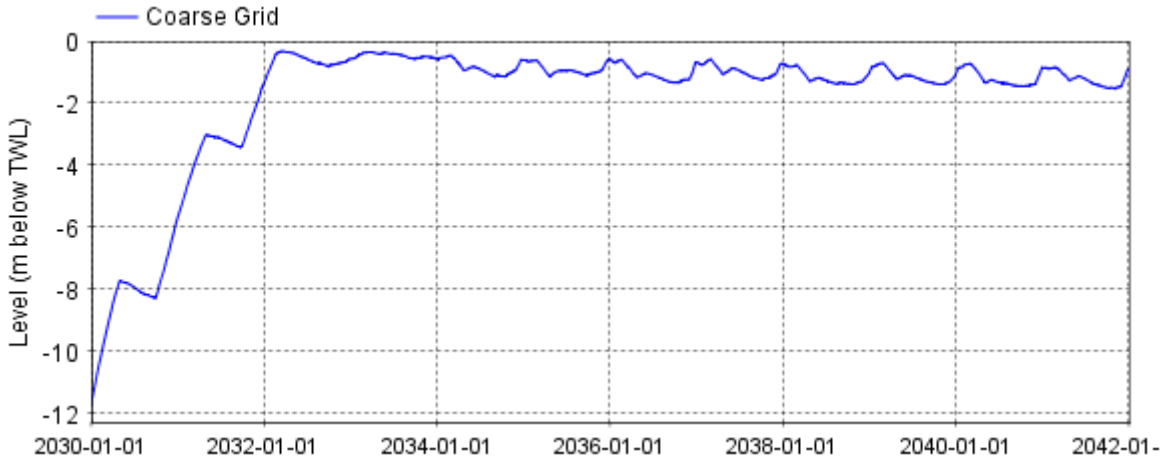

Figure 6.1 Simulated surface level for scenario 1B.

6.1.2 North basin deep water location

Pseudocolour plots[23] of hydrodynamic state variables at a deep north basin location without and with nighttime bubbler operations for scenario 1B (Figure 6.2) predict that:

- Peak T without and with bubbler operations, and the duration of seasonal thermal stratification without bubbler operations, exhibit a modest degree of interannual variability.
- Retention time (RT) peaks at ~3 years at the end of the 'classic' stage and then decreases rapidly during the 'recycled' stage to ~1 year (~400 days).
- During the 'classic' stage, springs are predicted to comprise ~75% of the HTR volume, which decreases to 15-20% during the 'recycled' stage.
- During the 'recycled' phase RW comprises 80-85% of the HTR source water.
- At the end of the 'classic' stage the proportion of stream-derived waters (i.e. stream tracer) in HTR is predicted to peak at ~15%, which then decreases to <5% during the 'recycled' stage.
- Nighttime operations of the bubble plume destratification system maintains reasonably vertically homogenous T through the water column as intended.

[23] Display of variable (e.g. temperature) as a colour gradient (e.g. maximum value red to minimum value blue) with depth through the water column (y-axis) and time (x-axis).

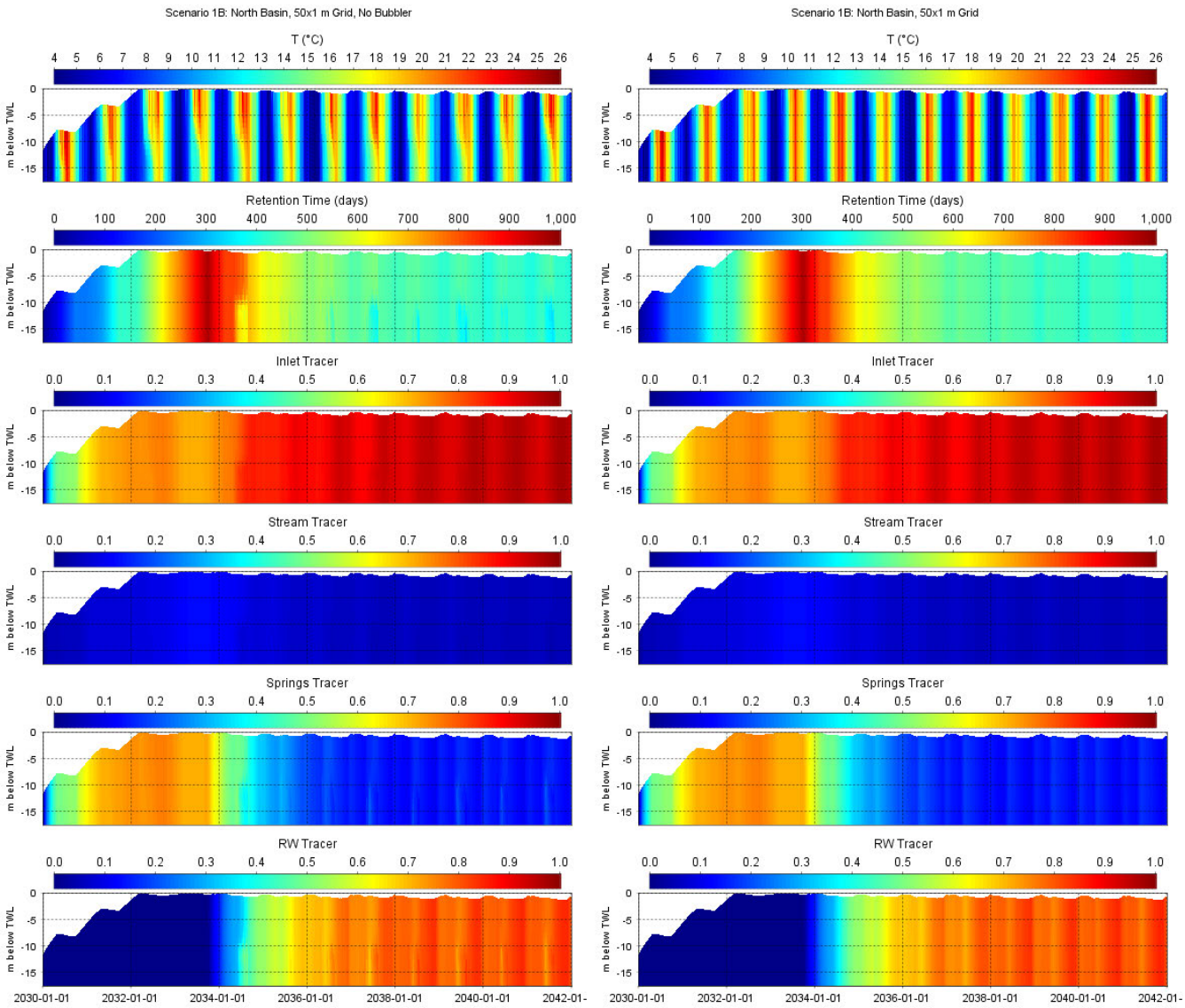

Figure 6.2 ***Pseudocolour plots of T (top), RT (upper middle), and conservative tracers of inlet discharge (lower middle) and streams (bottom) at a deep location in the north basin without (left) and with (right) nighttime bubbler operations for scenario 1B.***

Line plots of simulated T, RT and tracers within the surface and bottom waters at a northern basin deep location (-17 m TWL) without and with nighttime bubbler operations for scenario 1B are illustrated in Figure 6.3. The key differences between the simulations include:

– The elimination of seasonal thermal stratification from ~April-August with bubbler operations.

– Lower RT in the hypolimnion than the epilimnion[24] of the north basin by ~50-100 days over the 'recycled' phase without bubbler operations due to the accumulation of inlet inflows below the seasonal thermocline as illustrated by the bottom inlet tracer levels.

In short, the inlet inflows are simulated to accumulate below the seasonal thermocline of the north basin in the absence of bubbler operations. In contrast nighttime bubbler operations are predicted to maintain vertically homogeneous T, RT and conservative tracers of streams and inlet inflows.

[24] Hypolimnion and epilimnion are limnological terms that refer to the lower and upper portions of the water body below and above the seasonal thermocline, respectively.

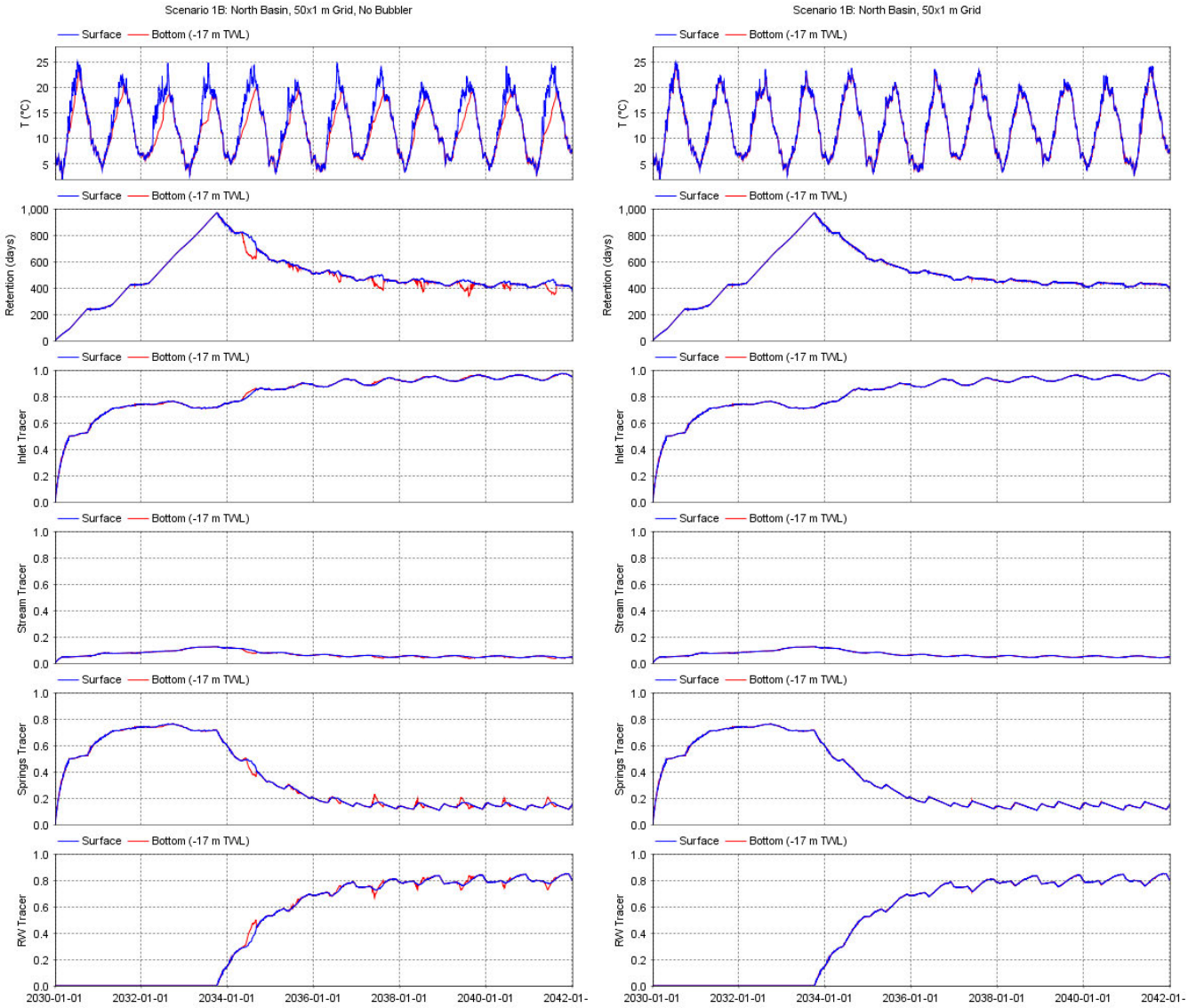

Figure 6.3 ***Simulated T (top), RT (upper middle), and inlet discharge (lower middle) and stream (bottom) tracers at a deep water location in the north basin at the surface and bottom without (left) and with (right) nighttime bubbler operations for scenario 1B.***

6.1.3 South basin deep water location

Pseudocolour (Figure 6.4) and line (Figure 6.5) plots of T, RT and tracers for scenario 1B at the deep water location of the south basin are similar to the north basin (Figure 6.2 and Figure 6.3). Because of the greater depth and smaller basin size of the south basin, seasonal thermal stratification is stronger and several weeks more persistent at the end of summers in the absence of a mixing system.

As with the north basin, nighttime bubbler operations are effective in maintaining a vertical homogeneous water column over the period of potential thermal stratification (~April-August) above the bubbler line elevation at -17 m TWL. However, thermal stratification persists in the small volume of water below the bubble plume lines at -17 m TWL of the south basin due to no provision of artificial mixing by the destratification system.

6.1.4 Withdrawals

The discharge, T, RT, and inlet and stream tracers of the withdrawals for Scenario 1B are illustrated in Figure 6.6 without and with nighttime bubbler operations. Differences between the simulations are minor as water is typically extracted from the epilimnion above the seasonal thermocline in the south basin (i.e. the high draw-off), which are forecasted to have nearly identical hydrodynamic properties (T, RT, tracers) regardless of bubbler operations.

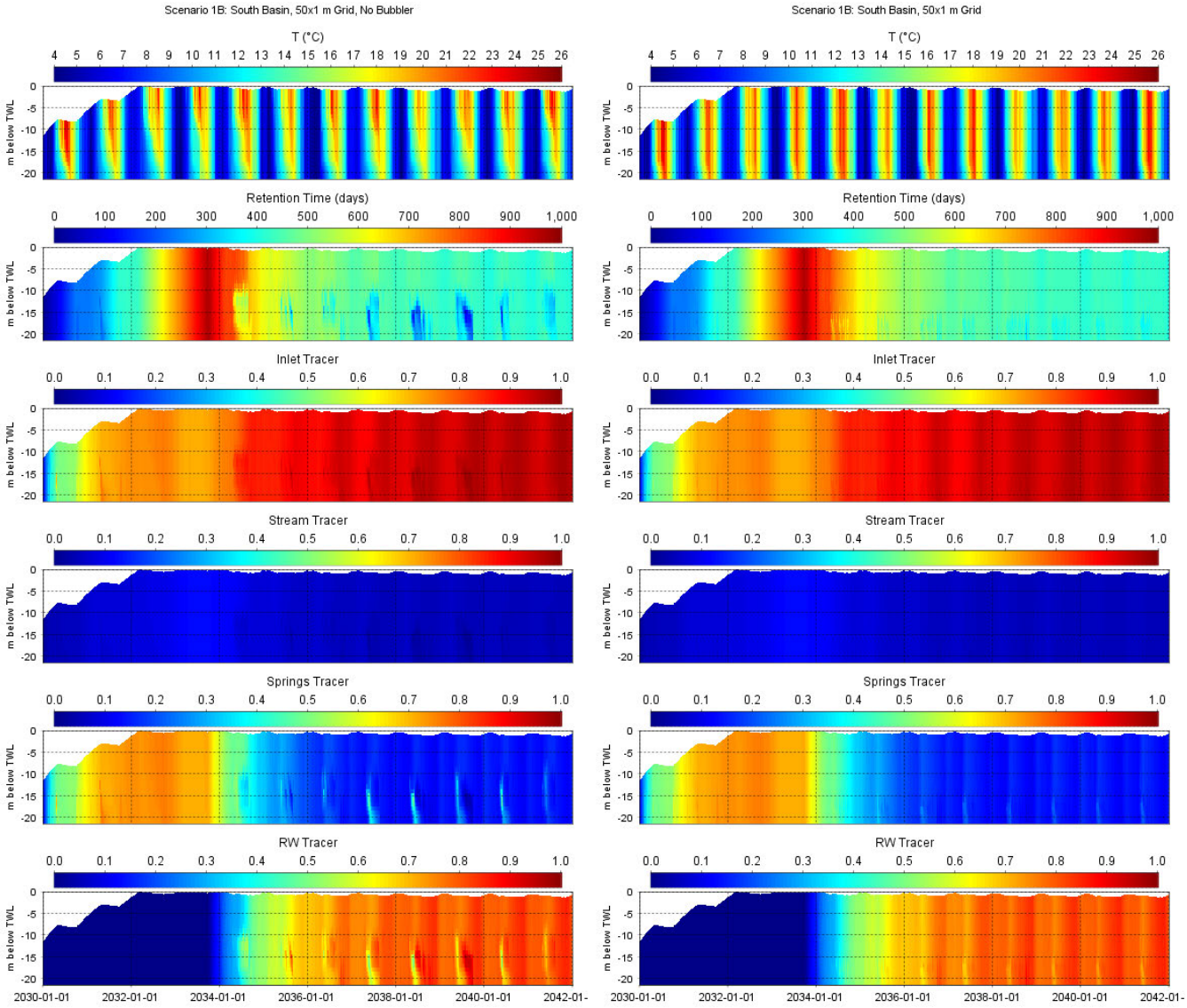

Figure 6.4 As Figure 6.2 for the south basin.

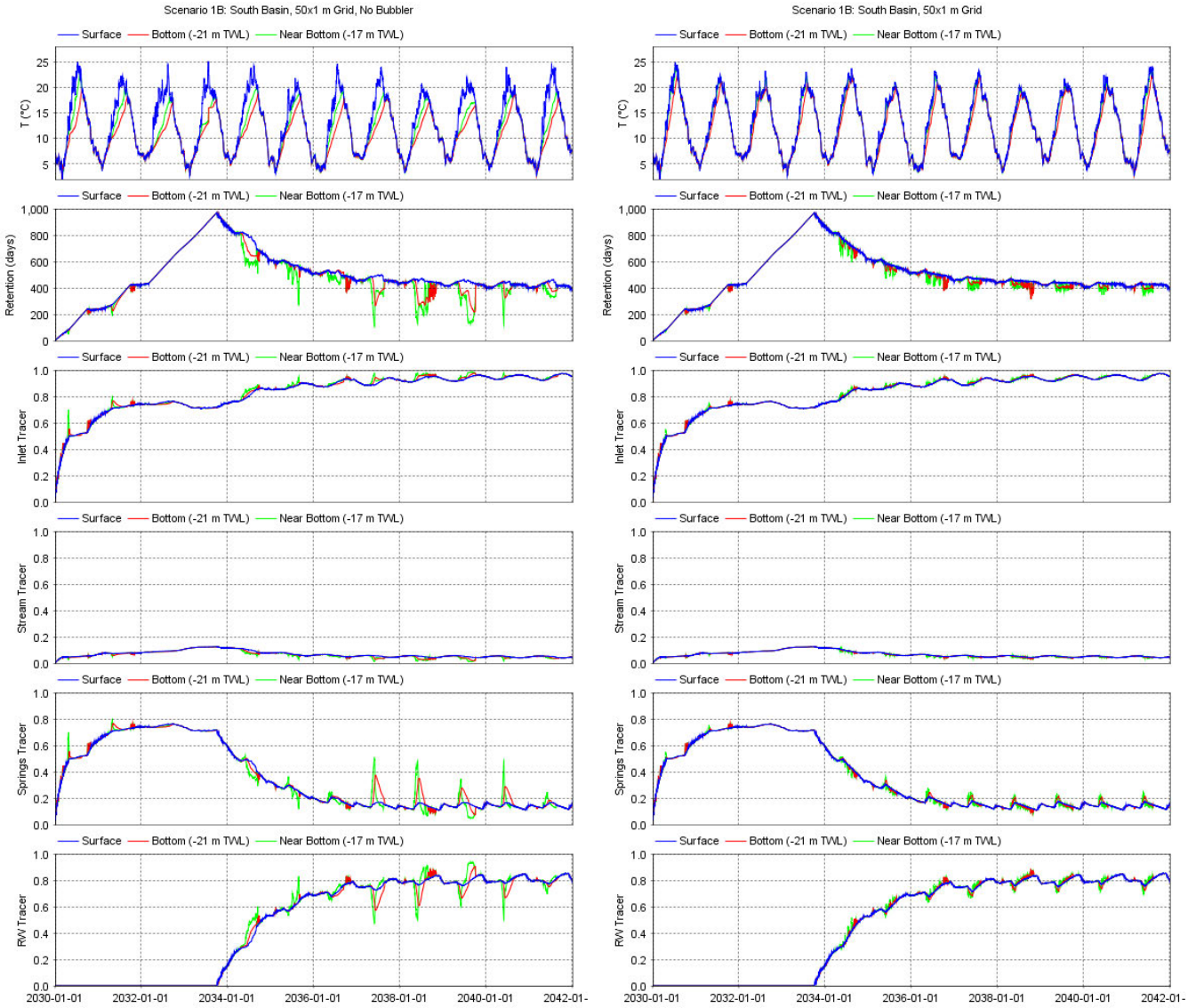

Figure 6.5 As Figure 6.3 for the south basin.

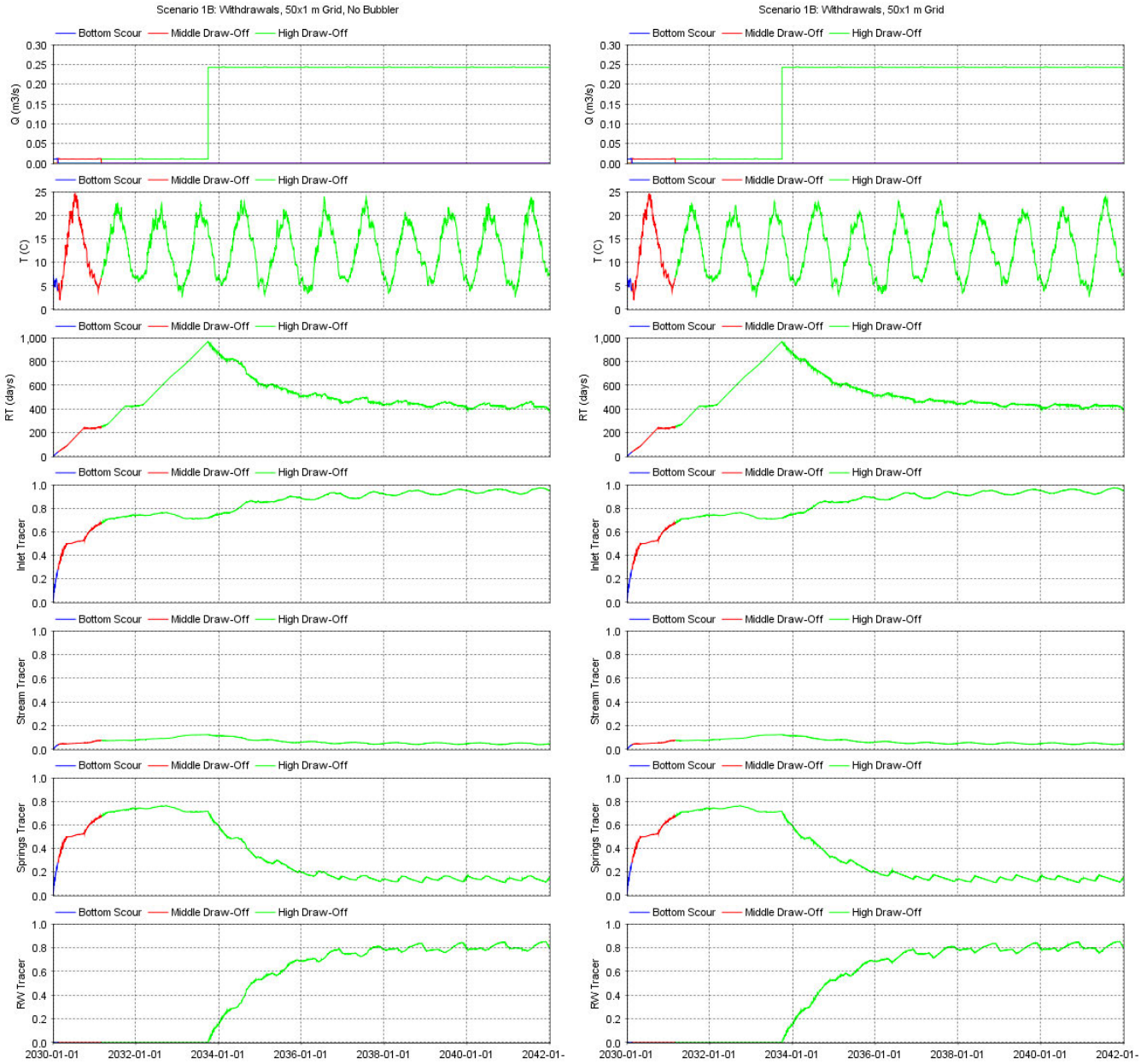

Figure 6.6 ***Simulated T (top), RT (lower middle), and tracers of inlet discharge (lower middle) and streams (bottom) of the withdrawals with no (left) and nighttime (right) bubble operations for scenario 1B.***

6.1.5 Summary

The scenario 1B simulations emulated the daily water balance well in terms of filling HTR to/near TWL over the first 3 winters via springs inputs, maintaining HTR at/near TWL at the end of winter during the 'classic' stage with springs inflows, and maintaining HTR at/near TWL at the end of each winter during the 'recycled' stage with inputs of RW and springs.

The scenario 1B simulations without and with nighttime bubbler operations predict that the destratification system will maintain well-mixed conditions throughout the water column in both basins except for a small volume of deep water in the south basin below the bubbler line elevation of -17 m TWL. However, in the absence of bubbler operations inlet (springs, RW) inflows during seasonal stratification from ~April-August will accumulate to a degree in the hypolimnion below the thermocline of the south basin with a concomitant RT reduction in this portion of the reservoir.

Lastly, the simulations do not predict any short-circuiting of inlet inflows to the withdrawal outlets. Nighttime bubbler operations effectively dilute the inlet inflows each evening that result in relatively homogeneous distributions of the inlet tracer and RT throughout the HTR main body.

6.2 Water quality

6.2.1 Vertical profiles without bubbler operations

Pseudocolour plots of the simulated hydrodynamic state variables described previously in Sections 6.1.2 and 6.1.3 (i.e. T, tracers, RT), and DO (WQ state variable) and DOSAT (derived variable) at deep water locations in both basins without bubbler operations for scenario 1B are illustrated in Figure 6.7. The simulation forecasts that:

– Seasonal thermal stratification will occur every year over the 'classic' and 'recycled' stages once HTR is at/near TWL in the absence of bubbler operations. In part, because the south basin is ~4.5 m deeper than the north basin, the bottom waters will remain cooler for a longer duration and will extend seasonal stratification by several weeks during August.

– Inlet inflows are predicted to comprise ~70% and ~95% of the HTR volume over the 'classic' and 'recycled' stages, respectively, whereas streams (i.e. streams tracer) are predicted to comprise up to ~15% of the HTR volume at the end of the 'classic' stage, and ~5% during the 'recycled' stage. The composition of inlet waters is solely comprised of springs water through the 'classic' stage and then predominantly RW during the 'recycled' stage (80-85%) with a lower proportion of springs water (15-20%). Variations in the magnitude of inflows and withdrawals into/from HTR are forecasted to increase RT to a maximum of ~1, 000 days at the end of the 'classic' stage[25], and ~400 days throughout the 'recycled' stage.

– DO will typically be >10 mg/L through the water column except during seasonal stratification with surface levels of ~7 mg/L, and bottom water levels at seasonal minima of ~0 mg/L (south basin) to ~1-5 mg/L (north basin). There is predicted interannual variability in the duration and volume of low DO bottom waters during seasonal stratification due to variations in climatic forcing. DO in the deeper south basin will be lower than the north basin because:

  - The deeper south basin will have a longer duration of seasonal stratification with concomitant greater DO consumption of bottom waters.
  - Over the seasonally stratified periods of the 'recycled' stage, the inlet discharge will be primarily RW that discharges above the south basin's deep hole and does not materially contribute to downward DO fluxes into this volume of water, so it becomes anoxic.
  - The larger size of the north basin relative to the south basin will yield greater basin scale mixing in response to winds that will generate enhanced boundary mixing across the thermocline and episodic fluxes of surface water (with elevated DO) into the hypolimnion during seasonal stratification. Because of its limited areal extent the south basin's deep hole, vertical mixing from basin scale hydrodynamic processes does not materially transport elevated DO waters from the surface to these depths.

– Temporal variations in DOSAT between the winter well-mixed and spring-summer epilimnion will be less than those of DO because of temperature effects (i.e. lower DO levels yield greater DO saturation for warm relative to cool waters).

[25] RT continues to increase if the 'classic' phase is extended, see Section 8.1.

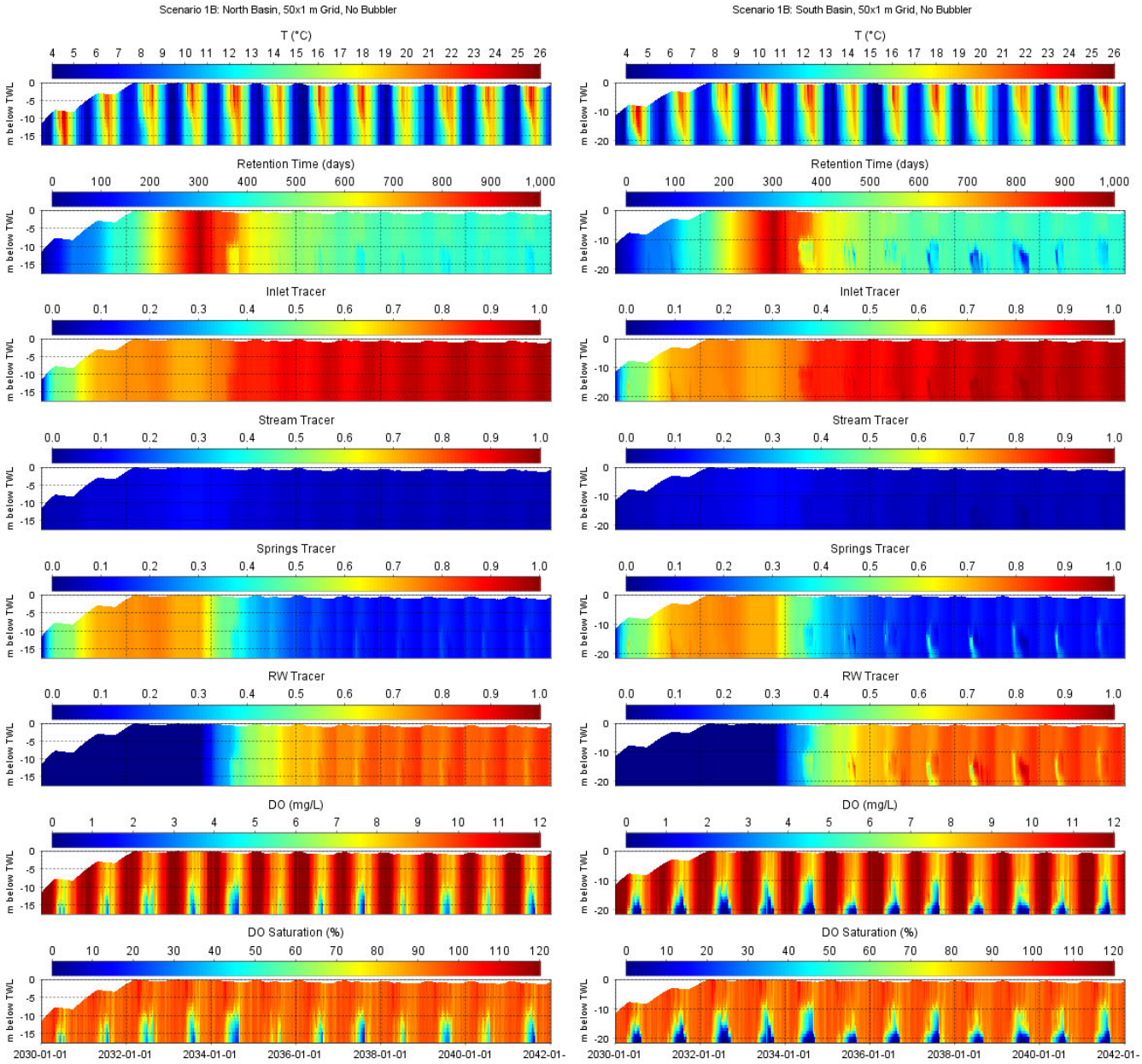

Figure 6.7 ***Pseudocolour plots of T (top), conservative tracers of inlet inflows (2nd panel), streams (3rd panel), springs (4th panel) and RW (5th panel), RT (6th panel), DO (7th panel) and DOSAT (bottom) at deep locations in the north (left) and south (right) basins without bubbler operations for scenario 1B.***

Pseudocolour plots at deep locations in both basins of the simulated state variables of pH, DIC, DFE, PFE, DMN and PMN, and the derived variable of alkalinity in the absence of bubbler operations for scenario 1B are illustrated in Figure 6.8. The simulation forecasts that:

– Peak spring and summer surface pH is similar during the 'recycled' and 'classic' stages (pH of ~8.2-8.5) because of higher algal productivity (see Figure 6.9) and associated greater uptake of dissolved CO_2 than winter (pH of ~7.8-8.1, low algal productivity). In contrast, the deep bottom waters during seasonal stratification are predicted to have pH of ~7.4-7.6 and ~7.3-7.4 in the north and south basins, respectively, because of increased CO_2 levels in the hypolimnion predominantly from DOM mineralisation in the water column and DIC releases from the sediments (i.e. CO_2 from the sediments).

– DFE and DMN are predicted to increase rapidly in the deep hole of the south basin below -17 m TWL (peaks of ~3-5 mg Fe/L and ~0.4-0.7 mg Mn/L, respectively) due to low DO in the deep waters over seasonal stratification that promote substantive sediment fluxes of these dissolved metals into the overlying waters. Subsequent mixing of the water column in late summer/autumn results in the oxidation and coagulation into particulate forms (PFE, PMN), though dilution of this relatively small volume of elevated metals is the primary mechanism that maintains subsequent low levels throughout the reservoir (see Section 9.3.2). Simulated dissolved metals were much lower in the bottom waters of the north basin and above -17 m TWL in the south basin than the deep hole of the south basin below 17 m TWL over seasonal stratification because of the higher DO that limited sediment releases.

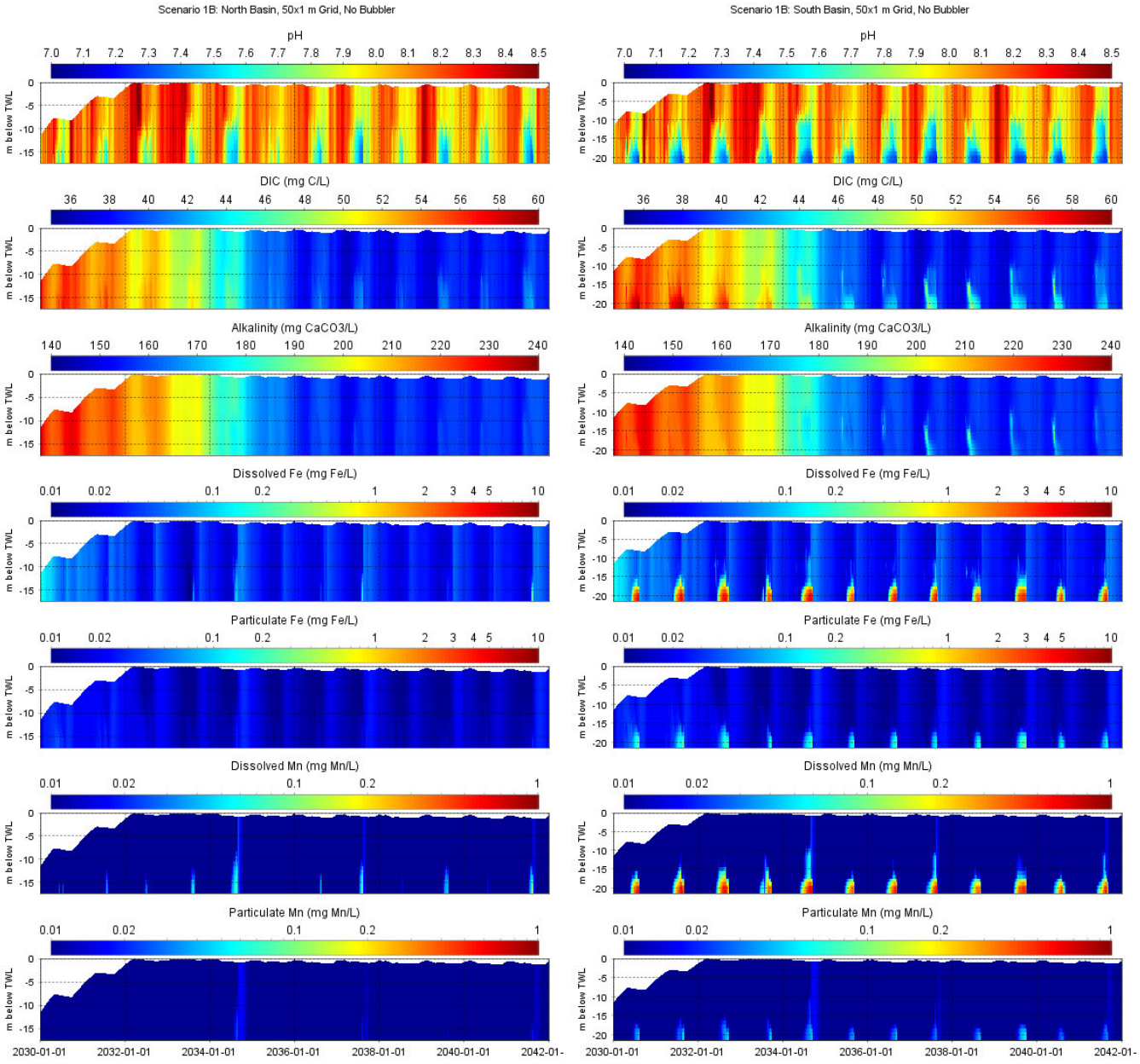

Figure 6.8 *As Figure 6.7 for pH (top), DIC (2nd panel), carbonate alkalinity (3rd panel), DFe (4th panel), PFe (5th panel), DMn (6th panel) and PMn (bottom).*

Pseudocolour plots at deep locations in both basins of the state variables of DOC and POC, and the derived variables of total algae, TOC and BOD in the absence of bubbler operations for scenario 1B are illustrated in Figure 6.9. The

simulation forecasts that total algal biomass, DOC, POC, TOC and BOD were considerably greater during the 'fill' stage than both the 'classic' and 'recycled' stages, which both had similar levels. This was in large part driven by elevated algal biomass in the epilimnion during spring-summer due to greater N external loading during the 6 months from October-March during the 'fill' stage with springs water (NO3 >6 mg N/L). This contrasts with the continuous inlet discharge during the 'recycled' stage with relatively low N external loading by the dominant RW inputs (NO3 of ~0.3 mg N/L), and only ~1 month of winter 'reservoir top-up' flows with springs water during the 'classic' stage. In short, the 'fill' phase is predicted to have the highest algal and organic carbon levels because of high N loading during 6 months of springs water inputs, whereas the 'recycled' and 'classic' stage levels are limited by a continuous relatively low external N supply (because of low RW TN due to the HRRM process) and an annual short (~1 month) period of elevated external N inputs (i.e. reservoir top-up flows), respectively. The TP levels of springs and RW are similar at 0.03 mg P/L, and hence do not drive the differences in organic carbon and algal pools between the stages. At times elevated DOC in the south basin's deep waters relative to the north basin was driven by low DO that promoted elevated sediment releases. POC increased in the surface waters due to algal mortality during seasonal stratification when algal productivity was elevated. BOD patterns mirrored those of TOC.

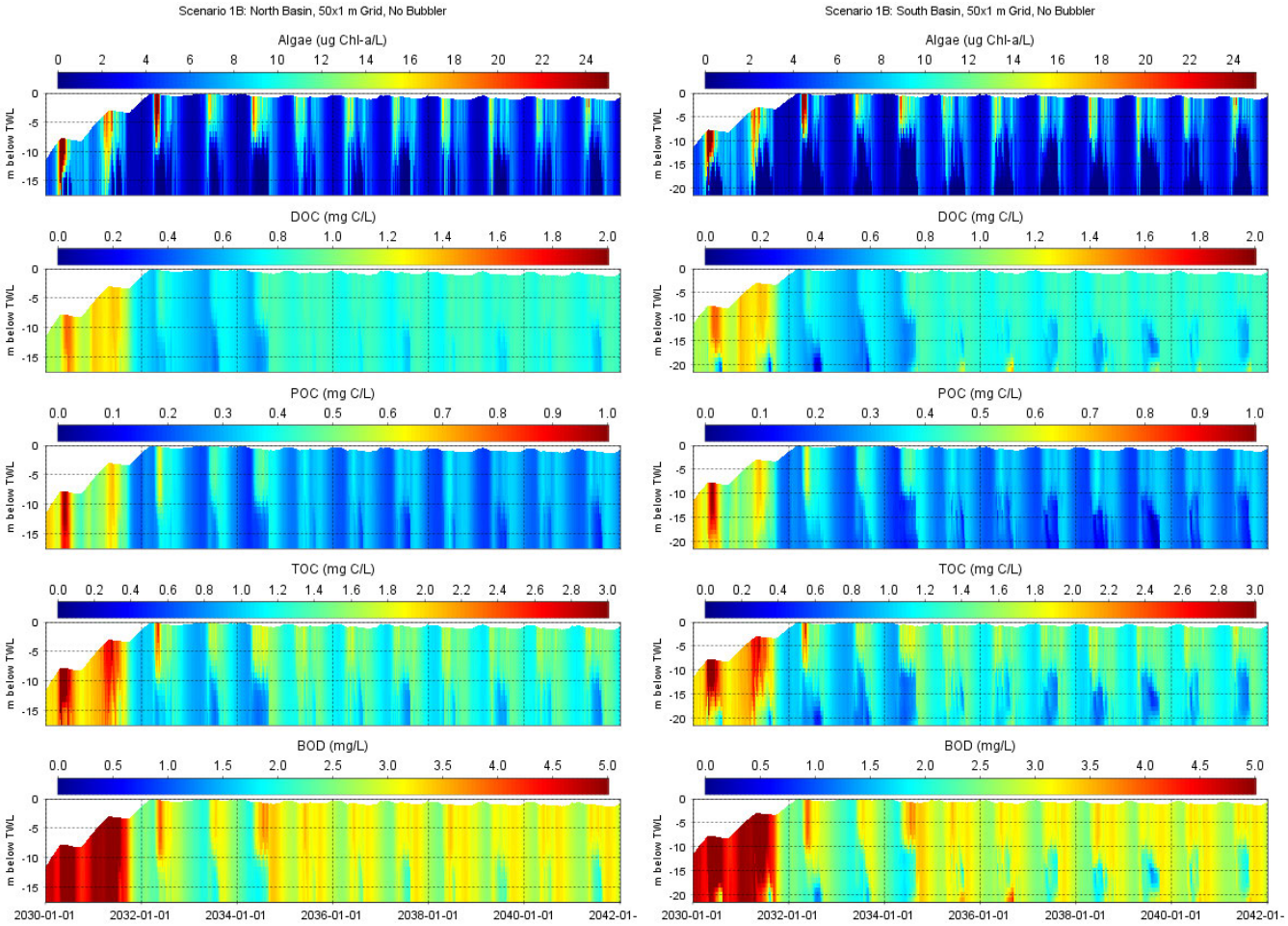

Figure 6.9 As Figure 6.7 for total algal biomass (top), DOC (2nd panel), POC (3rd panel), TOC (4th panel) and BOD (bottom).

Pseudocolour plots at deep locations in both basins of the state variables of PO4, DOP and POP, and the derived variable of TP, in the absence of bubbler operations for scenario 1B are illustrated in Figure 6.10. The simulation forecasts that similar to organic C (Figure 6.9), simulated TP, DOP, POP and PO4 were generally lower during the 'recycled' and 'classic' stages than the 'fill' stage. Similar to POC (Figure 6.9), elevated spring-summer algal levels lead to elevated POP (via mortality) with lower levels over the 'recycled' and 'classic' stages than the 'fill' stage due to lower primary productivity. During summer stratification low POP occurred in the hypolimnion below the thermocline

due to the absence of any primary productivity and algal standing stocks due to underwater light limitation in this portion of the water column. Elevated PO4 and DOP in the deep water pocket of the south basin below -17 m TWL occurred during seasonal stratification because low bottom DO promoted high sediment fluxes. Higher bottom DO and resultant lower sediment fluxes of the north basin resulted in lower bottom PO4 and DOP levels than the south basin during summer seasonal thermal stratification similar to values throughout the water column.

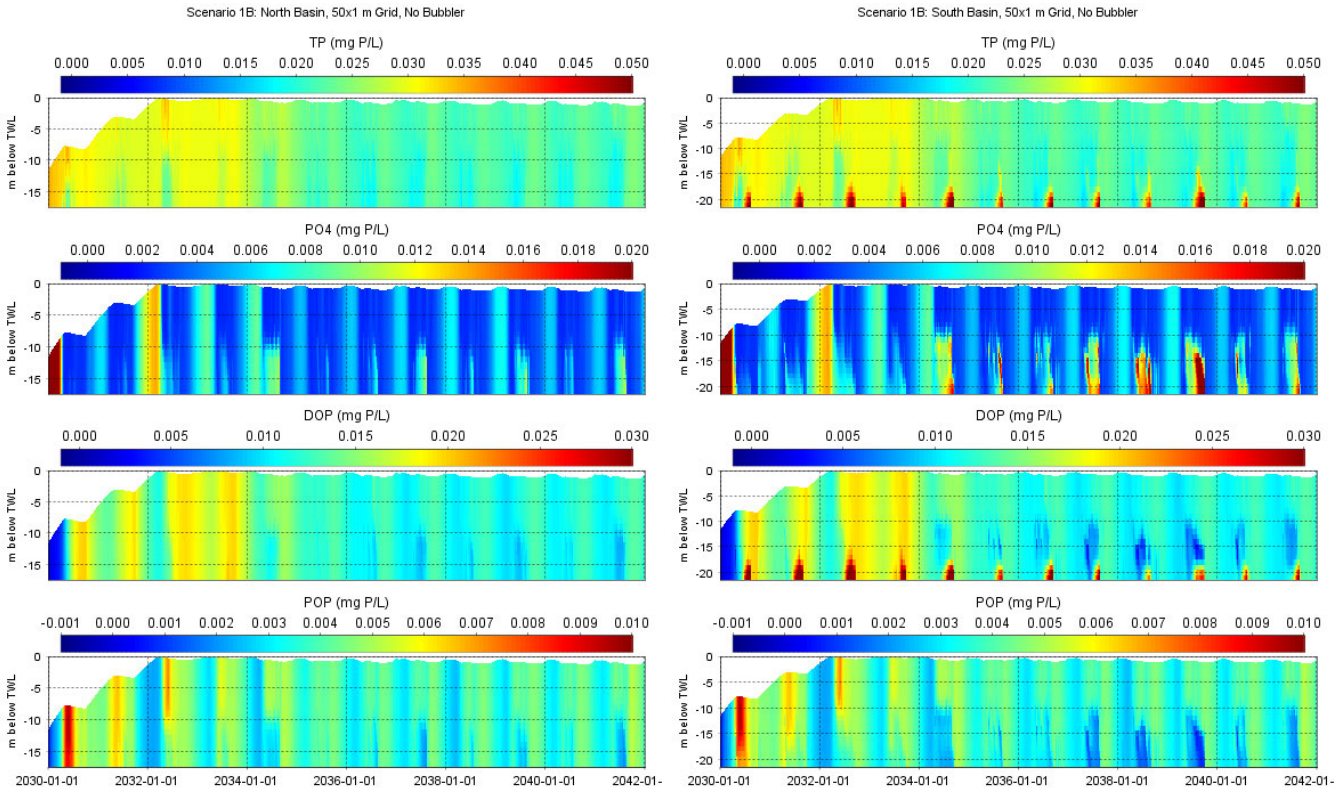

Figure 6.10 As Figure 6.7 for TP (top), PO4 (2nd panel), DOP (3rd panel) and POP (bottom).

Pseudocolour plots at deep locations in both basins of the state variables of NO3, NH4, DON and PON, and the derived variable TN, in the absence of bubbler operations for scenario 1B are illustrated in Figure 6.11. The simulation forecasts that TN and NO3 continually decreased from the elevated levels of ~7.5 mg N/L at the onset of the 'fill' stage to ~1 mg during the 'recycled' stage. Similar to organic C (Figure 6.9) and P (Figure 6.10) dynamics, DON and PON were lower during the 'recycled' and 'classic' stages than the 'fill' stage. Elevated NH4, and to a lesser degree DON, in the deep pocket of the south basin below -17 m TWL occurred during seasonal stratification because of low DO and subsequent high sediment fluxes during all 3 stages. DO in the bottom waters of the north basin remained sufficiently high because of basin scale mixing (and associated downward fluxes of atmospheric sourced DO) that maintained low NH4 (and DON) due to minimal sediment release fluxes.

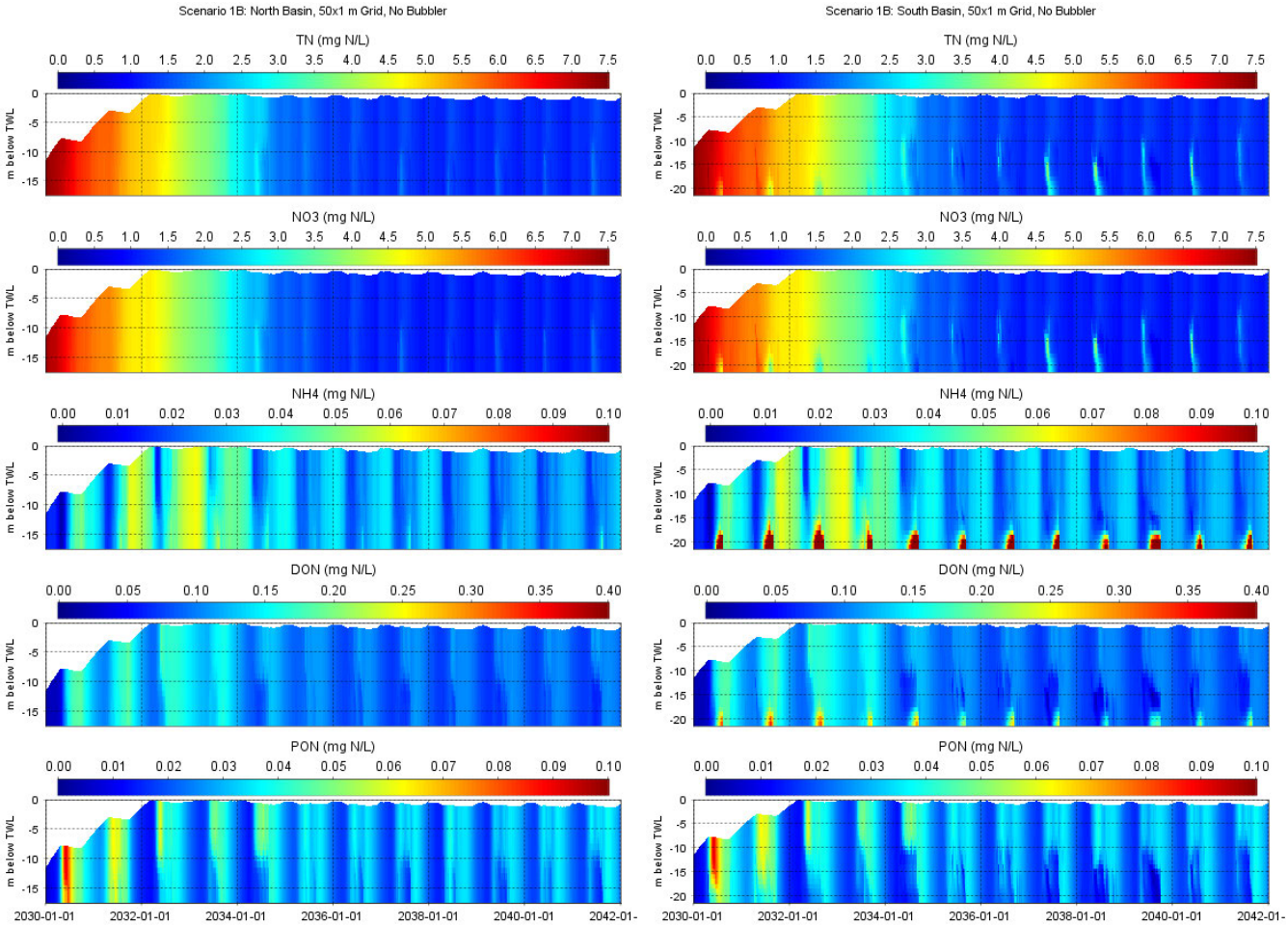

Figure 6.11 As Figure 6.7 for TN (top), NO3 (2nd panel), NH4 (3rd panel), DON (4th panel) and PON (bottom).

Pseudocolour plots at deep locations in both basins of the state variables of clay, silt and SiO2, and the derived variables of SS_{Inorg} and the PAR extinction coefficient, in the absence of bubbler operations for scenario 1B are illustrated in Figure 6.12. The simulation forecasts that most of the simulated inorganic TSS (~0.2 mg/L) is comprised of clay with minor contributions from silt. The PAR extinction coefficient is primarily related to algal and DOC levels rather than TSS. Hence, elevated PAR extinction coefficient values are simulated to occur throughout the water column during the spring algal bloom (period of no to weak stratification) and above the seasonal thermocline during the summer because of higher phytoplankton biomass. SiO2 is simulated to be lower during the 'classic' than 'recycled' stages due to spring diatom uptake and subsequent loss via settling to the sediments that strip this determinand from the water column. Low levels during the 'classic' stage are not materially replenished by the short ~1 month duration of 'top-up' winter spring inputs. In contrast, SiO2 levels are replenished to a degree during the 'recycled' stage with continuous inputs via the RW and springs inlet, which is evident in the elevated concentrations during seasonal thermal stratification below the thermocline in which the inlet water are discharged.

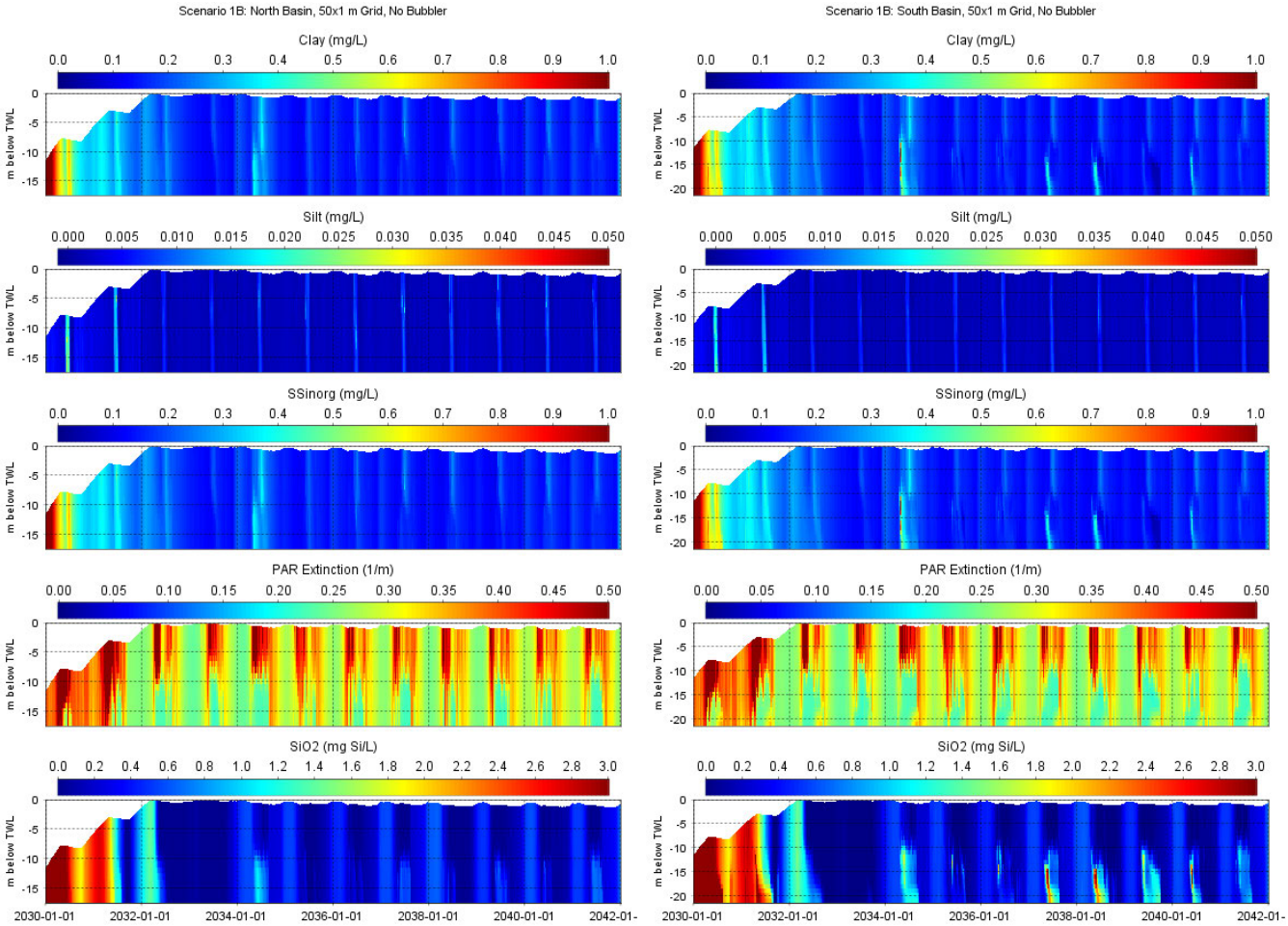

Figure 6.12 As Figure 6.7 for clay (top), silt (upper middle), TSS (middle), PAR extinction coefficient (lower middle) and SiO_2 (bottom).

Pseudocolour plots at deep locations in both basins of the state variables of Ca, Na, Cl and SO4 in the absence of bubbler operations for scenario 1B are illustrated in Figure 6.12. Ca, Cl and SO4 all decrease from levels characteristic of the springs during the 'fill' stage to concentrations more akin to the RW during the 'recycled' phase. Na levels of the springs and RW are similar, though seasonal variations are greater in the RW which is also forecast to occur in the reservoir.

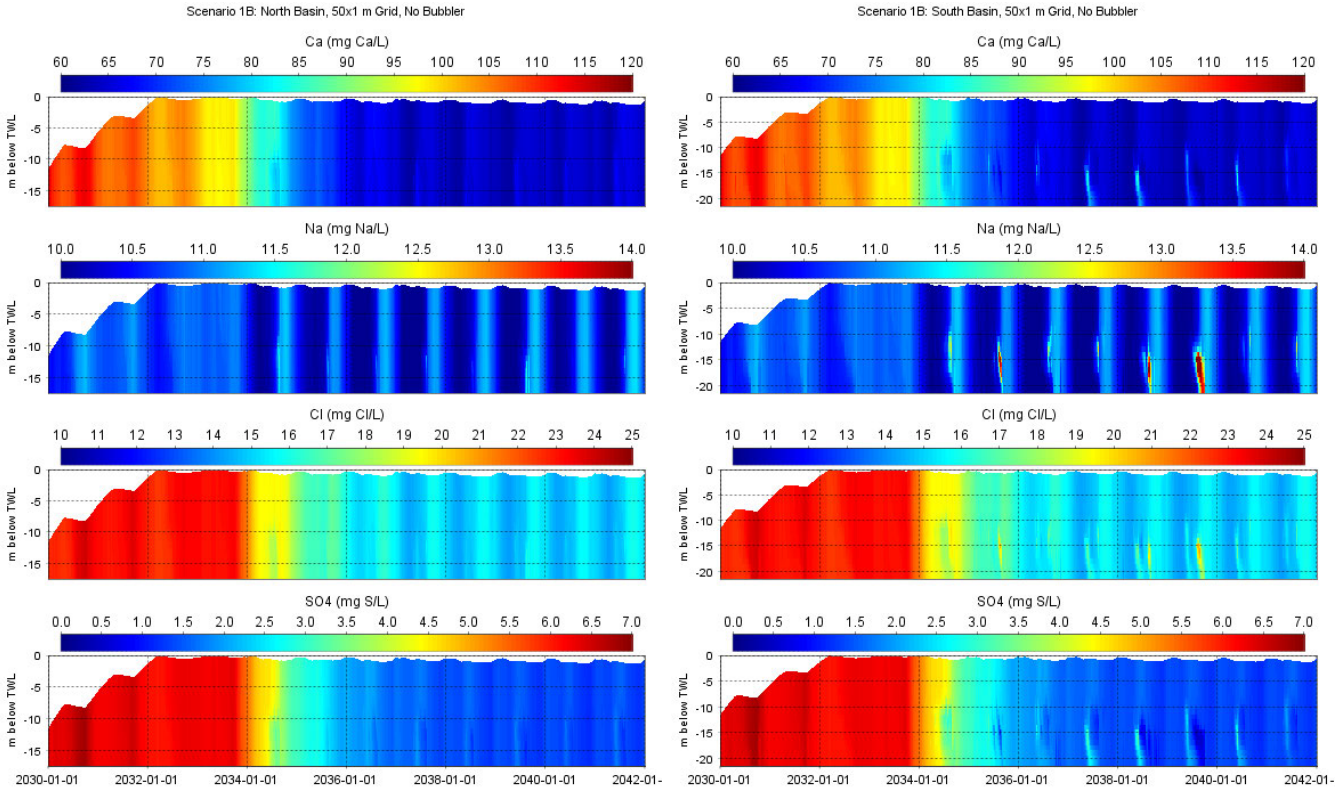

Figure 6.13 As Figure 6.7 for Ca (top), Na (upper middle), Cl (lower middle) and SO_4 (bottom).

6.2.2 Vertical profiles with bubbler operations

Pseudocolour plots of the simulated hydrodynamic state variables described previously in Sections 6.1.2 and 6.1.3 (i.e. T, tracers, RT) and DO (state variable) and DOSAT (derived variable) at deep water locations in both basins with nighttime bubbler operations (0600-1800 from April-August) for scenario 1B are illustrated in Figure 6.14. The simulation forecasts that:

– Nighttime bubbler operations prevent seasonal thermal stratification in both basins during all 3 stages ('fill', 'classic', 'recycled').

– As forecasts without bubbler operations:

  - The proportions of the HTR volume that is comprised of inlet waters (i.e. comingled tracer) during the 'classic' and 'recycled' phases are ~70% and ~95%, respectively.
  - Streams (i.e. stream tracer) comprised up to ~15% of the HTR volume at the end of the 'classic' stage and ~5% during the 'recycled' stage.
  - Springs comprised ~70% of the HTR volume during the 'classic' stage and ~15% during the 'recycled' stage.
  - RW comprised ~80% of the HTR volume during the 'recycled' stage.
  - The RT increased to a maximum of ~1,000 days at the end of the 'classic' stage, and then decreased to ~400 days throughout the 'recycled' stage.

– DO was typically >10 mg/L and ~7-8 mg/L throughout the water column during the winter and summer, respectively. Nighttime bubbler operations were not only effective in maintaining a vertically well-mixed water column during the period of potential seasonal stratification (~April-August), but also maintained elevated DO levels throughout the water column. The south basin's deep pocket waters in excess of -17 m TWL below the bubbler line elevation are forecasted not to become anoxic with minimum DO levels of ~1-4 mg/L and of much shorter duration than in the absence of bubbler operations. Recall that a degree of conservativeness is

inherent with the coarse (50x50x1 m) grid simulations as lower DO levels are forecast than the fine grid (20x20x1 m) simulations as described in Appendix A.

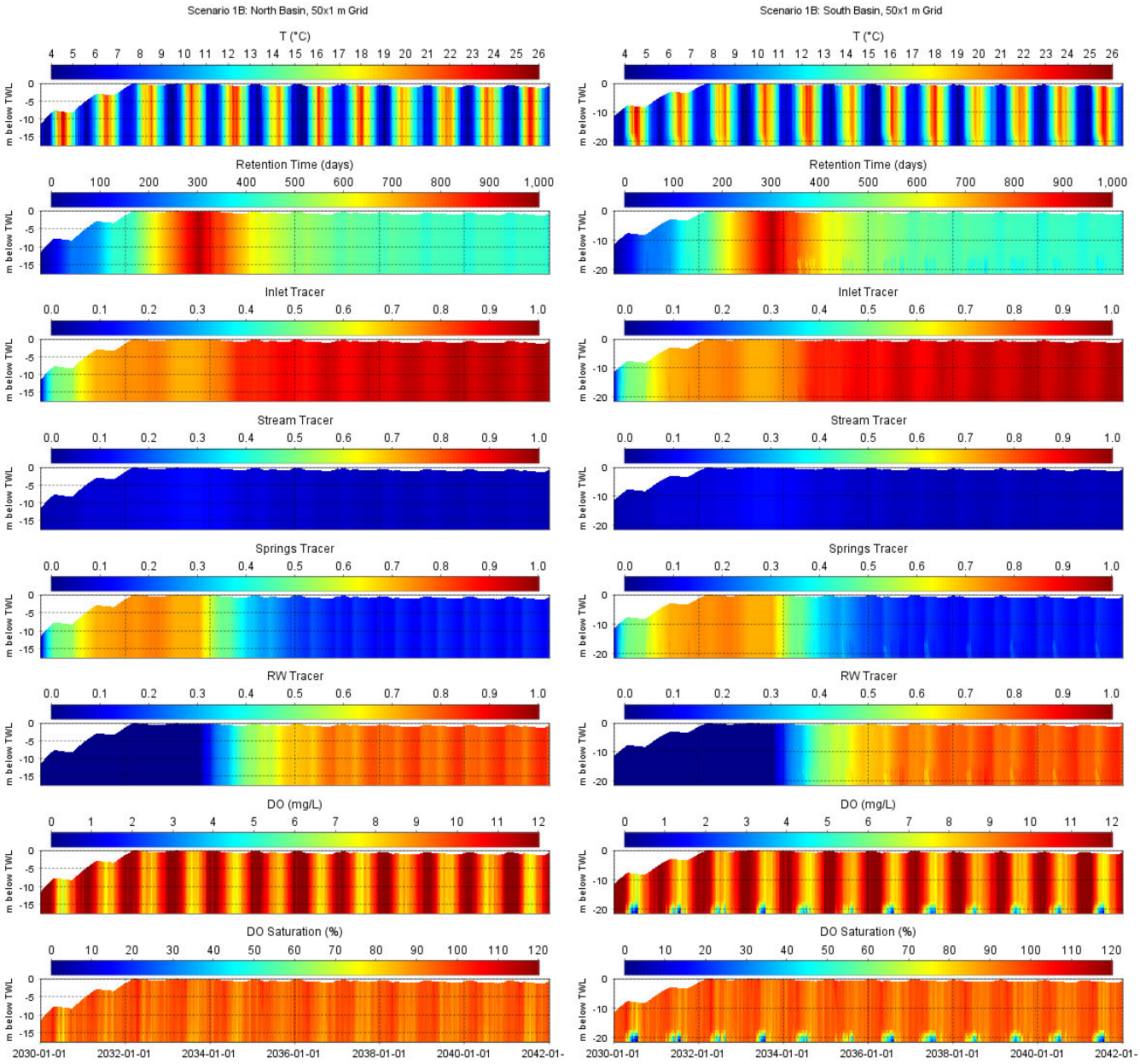

Figure 6.14 ***Pseudocolour plots of T (top), RT (2nd panel), conservative tracers of inlet (comingled) inflows (3rd panel), streams (4th panel), springs (5th panel) and RW (6th panel), DO (7th panel) and DOSAT (bottom) at deep locations in the north (left) and south (right) basins with bubbler operations for scenario 1B.***

Pseudocolour plots at deep locations in both basins of the simulated state variables of pH, DIC, DFE, PFE, DMN and PMN, and the derived variable of alkalinity with nighttime bubbler operations for scenario 1B are illustrated in Figure 6.15. The simulation forecasts that pH exhibited a similar interannual pattern as no bubbler operations (Figure 6.8) except for lower vertical variability due to a maintenance of a well mixed vertical column, which contrasts with the no mixing system forecasts where the absence of CO_2 exchange with the atmosphere in the waters below the seasonal thermocline lead to much lower pH in the north basin and much of the south basin. Again, in the deep water pocket of the south basin, there was an increase in the minimum pH from ~7.3-7.5 to ~7.5 as a result of the bubbler operations. As in the surface waters above the seasonal thermocline in the absence of bubbler operations, seasonal

pH variability is driven by elevated spring and summer algal productivity through uptake of CO_2 and the concomitant increase in pH. During lower winter algal productivity, CO_2 quasi-equilibrates with the atmosphere and in combination with low algal productivity yields seasonal minima in pH with and without mixing system operations. There were no forecasts of material vertical or horizontal gradients in pH, DIC and alkalinity in the main body of the reservoir with nighttime bubbler operations. Except in the small pocket of deep waters in the south basin below the elevation of the bubbler lines at ~-17 m TWL. Alkalinity and DIC are predicted to be substantially higher during the 'fill' and 'classic' stages because the springs (no RW inputs) are the dominant external input with much higher concentrations than RW. DFE and DMN levels were at/near ~0 mg/L, substantially lower than with no bubbler operations because of the maintenance of oxygenated bottom waters throughout the reservoir that prevented any material sediment fluxes. Though DMN levels in the south basin's deep pocket attained peak concentrations of 0.05-0.25 mg Mn/L for short periods during summer, this relatively small mass was rapidly dispersed through the water column with no material effect of reservoir concentrations. Oxygenated conditions throughout HTR promotes conditions for oxidised forms of particulate iron (PFE) and manganese (PMN), and non-detectable levels of reduced forms of dissolved forms of these metals (DFE, DMN).

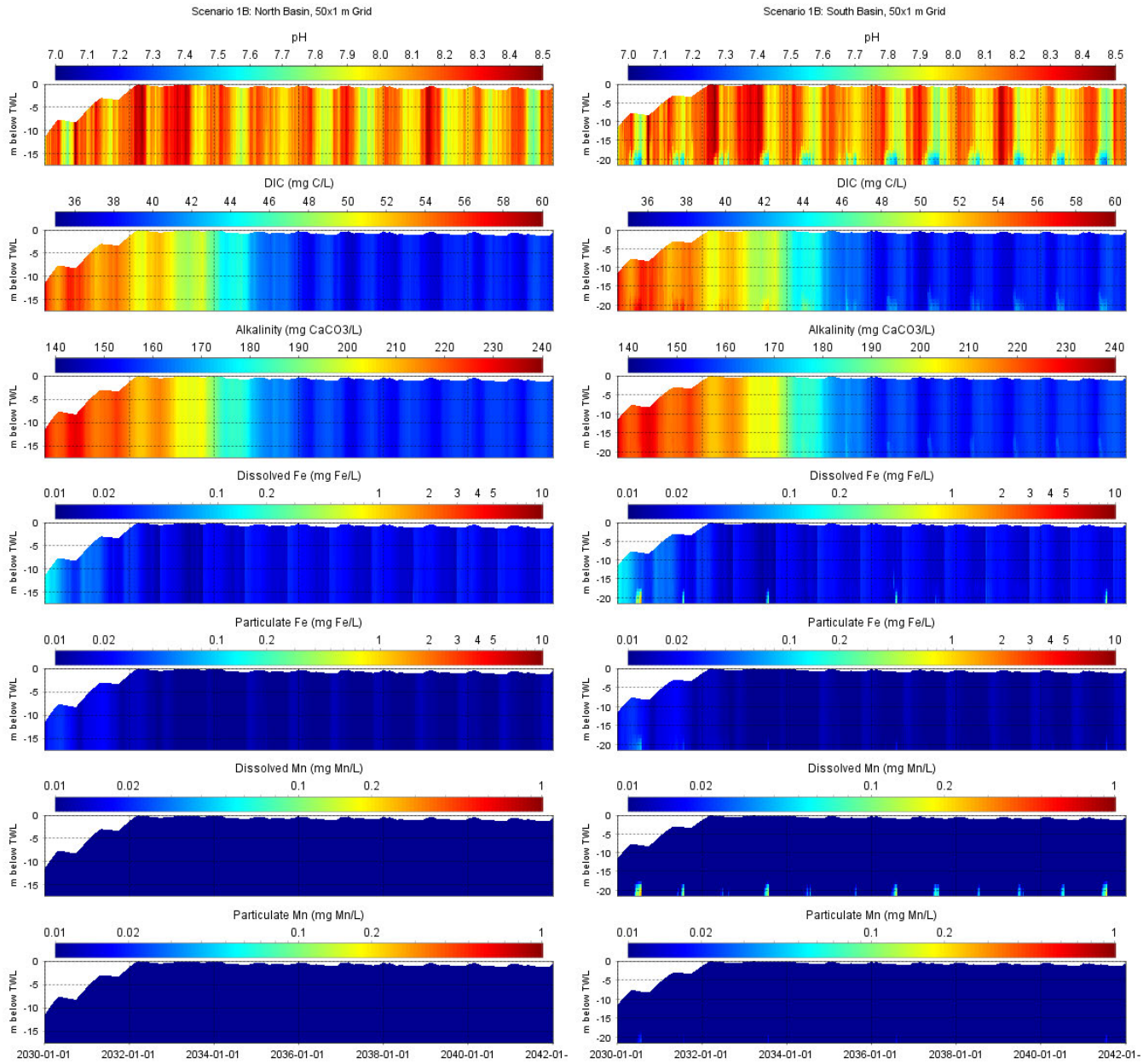

Figure 6.15 *As Figure 6.14 for pH (top), DIC (2nd panel), carbonate alkalinity (3rd panel), DFe (4th panel), PFe (5th panel), DMn (6th panel) and PMn (bottom).*

Pseudocolour plots at deep locations in both basins of the state variables of DOC and POC, and the derived variables of total algae, TOC and BOD, with nighttime bubbler operations for scenario 1B are illustrated in Figure 6.16. The simulation forecasts similar to the simulation with no bubbler operations (Figure 6.9) that total algal biomass, DOC, POC, TOC and BOD were greater over the 'fill' stage than the 'classic' and 'recycled' stages. Higher algal concentrations during the 'fill' stage were in large part fuelled by greater N external loading from the 6 months of autumn-winter springs inputs with substantially greater (~7.5 mg N/L) NO3 levels than the RW (~0.3 mg N/L). Vertical (through the water column) and horizontal (between deep waters of both basins) variability of DOC, POC, TOC and BOD was minimal with nighttime bubbler operations, whereas during summer in the absence of bubbler operations levels were generally higher in the epilimnion above the seasonal thermocline. Bubbler operations are predicted to moderately reduce peak summer algae levels through maintenance of well-mixed conditions (i.e. prevention of seasonal stratification). Generally, by maintaining vertically well-mixed conditions in reservoirs, bubble plume

destratification systems impart greater variability on the light levels experienced by algae in the absence of a seasonal thermocline, which generally yields two in-reservoir WQ benefits:

– Often deleterious algae are blue-green algae with buoyancy control via vacuoles. Buoyancy control provides a competitive advantage over other algae in seasonally stratified systems as during relatively calm conditions these algae can vertically migrate upwards to harvest more light and increase photosynthetic production. An effective bubble plume destratification system largely eliminates this competitive advantage.

– An additional benefit is that for the entire phytoplankton assemblage, effective bubble plume destratification systems generally result in algae spending a greater proportion of time in deeper waters with concomitant greater light limitation that generally lead to less algal biomass than in the absence of a bubbler.

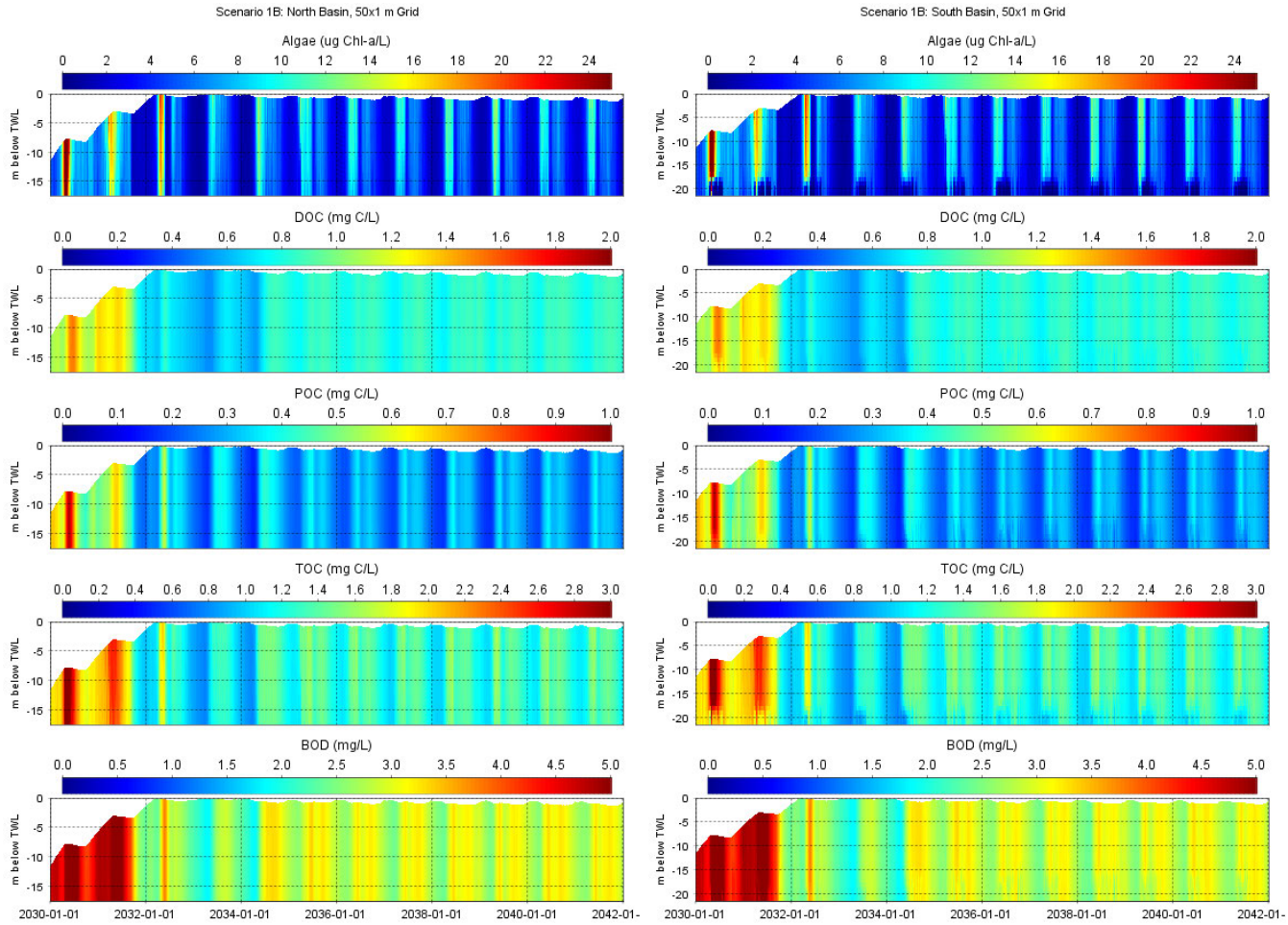

Figure 6.16 As Figure 6.14 for total algal biomass (top), DOC (2nd panel), POC (3rd panel), TOC (4th panel) and BOD (bottom).

Pseudocolour plots at deep locations in both basins of the state variables of PO4, DOP and POP, and the derived variable of TP, with nighttime bubbler operations for scenario 1B are illustrated in Figure 6.17. The simulation forecasts that similar to P dynamics with no bubbler operations (Figure 6.10), nighttime bubbler operations are predicted to yield higher TP, DOP, POP and PO4 during the 'fill' stage than the 'recycled' and 'classic' stages. Bubbler operations are predicted to maintain well-mixed and well oxygenated bottom waters throughout the reservoir with no (or very limited) build-up of elevated PO4 and DOP that was forecasted in the absence of bubbler operations, including a large reduction in the small deep hole of the south basin below -17 m TWL.

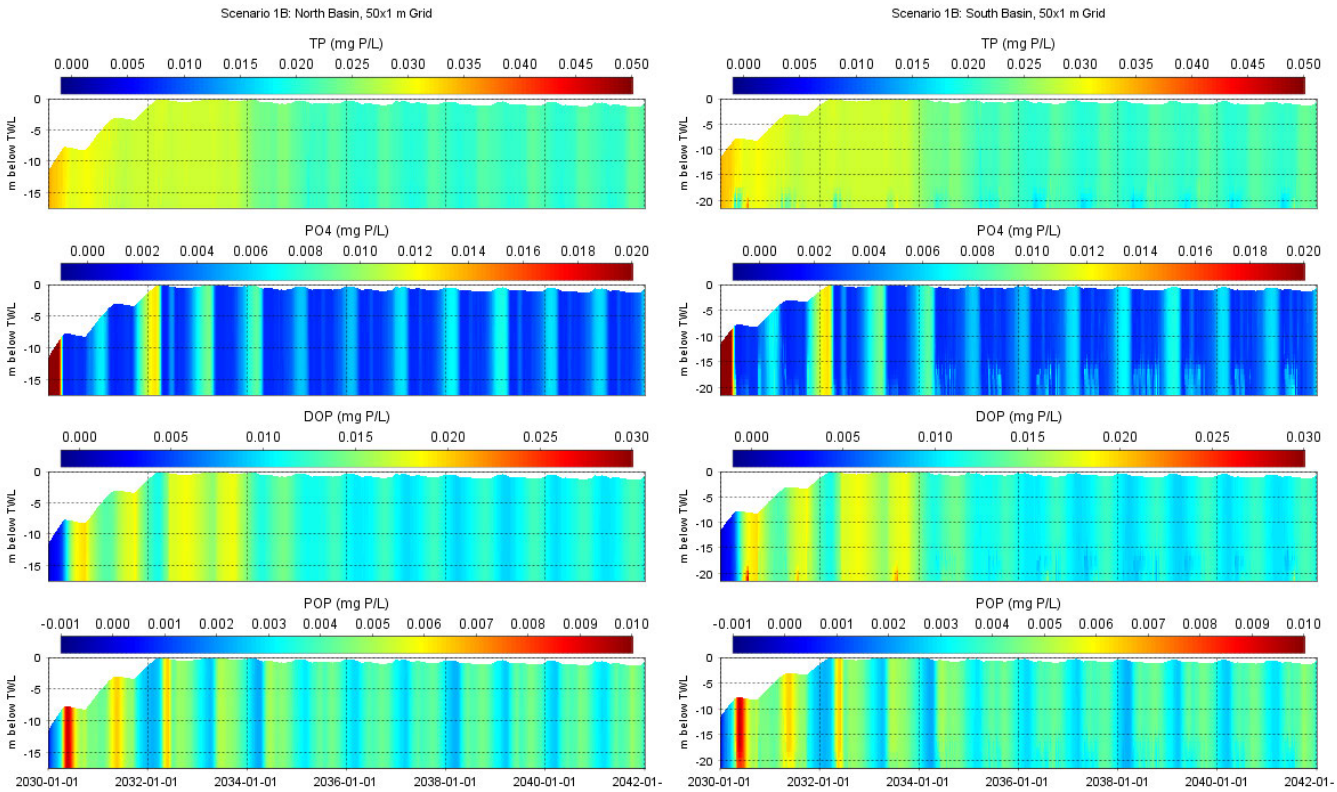

Figure 6.17 As Figure 6.14 for TP (top) , PO4 (2nd panel), DOP (3rd panel) and POP (bottom).

Pseudocolour plots at deep locations in both basins of the state variables of NO3, NH4, DON and PON, and the derived variable TN, with nighttime bubbler operations for scenario 1B are illustrated in Figure 6.18. The simulation forecasts that similar to N dynamics with no bubbler operations (Figure 6.11), NO3 decreased from ~7.5 mg N/L at the onset of the 'fill' stage to ~1-1.5 mg N/L during the 'recycled' stage. DON and PON were somewhat greater during the 'recycled' than 'classic' stage as with no bubbler operations. Further, DON and PON exhibited similar spatial-temporal patterns as organic C and P determinands, which are driven by the same processes. Bubbler operations maintained well-mixed and well oxygenated bottom waters in the south basin over the summer with minimal build-up of elevated NH4 and DON in the south basin that was predicted in the absence of bubbler operations.

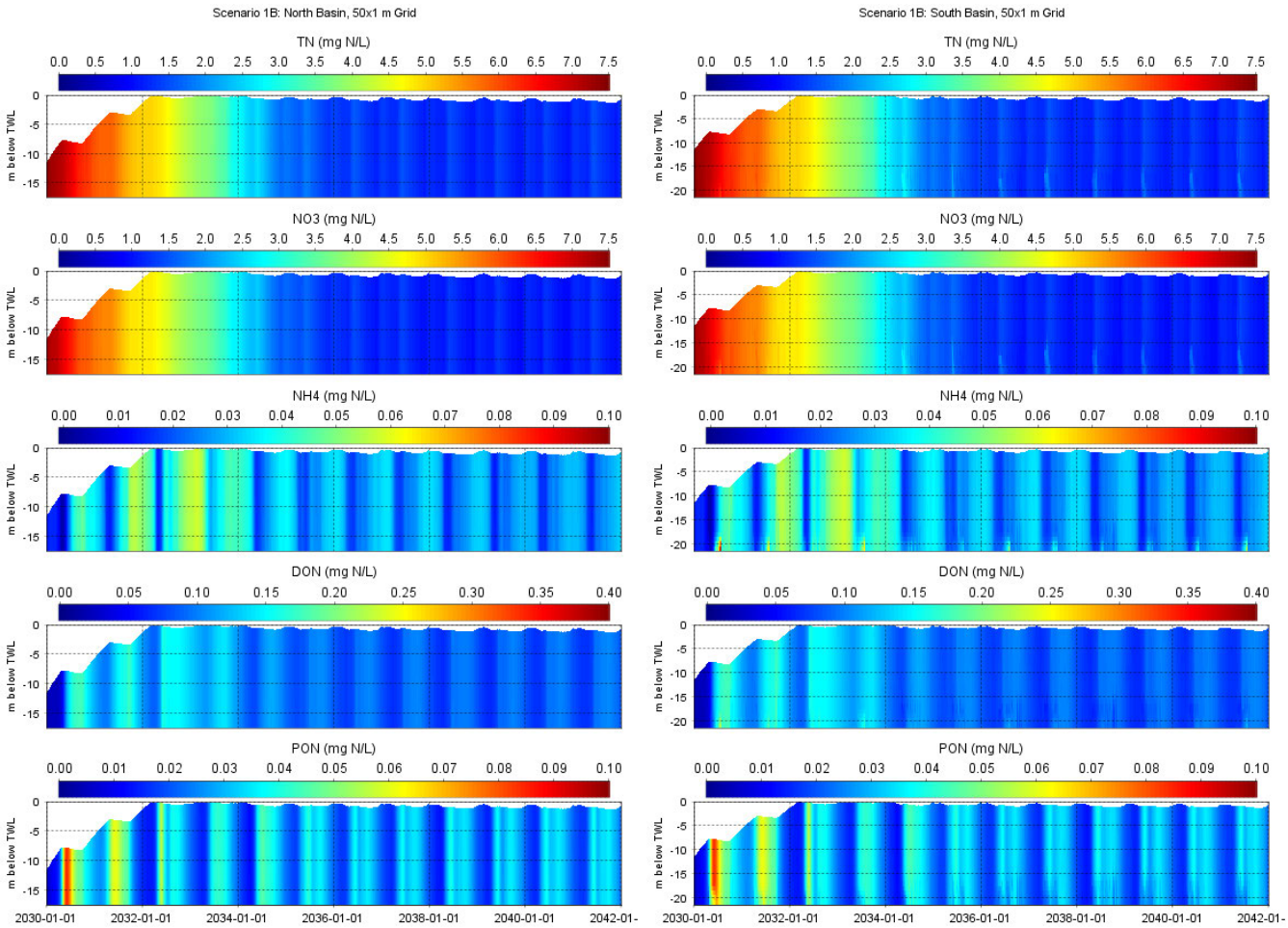

Figure 6.18 As Figure 6.14 for TN (top), NO3 (2nd panel), NH4 (3rd panel), DON (4th panel) and PON (bottom).

Pseudocolour plots at deep locations in both basins of the state variables of clay, silt and SiO2, and the derived variables of TSS and the PAR extinction coefficient, with nighttime bubbler operations for scenario 1B are illustrated in Figure 6.19. The simulation forecasts that simulated clay, silt and TSS levels are similar in magnitude and seasonality as those modelled in the absence of bubbler operations (Figure 6.12). Vertical variations are minimal over the summer as bubbler operations prevent the development of seasonal stratification and maintain a well-mixed water column. The PAR extinction coefficient is relatively vertically uniform through the water column at all times of year due to bubbler operations in contrast to elevated values in the epilimnion above the seasonal thermocline during the summer in the absence of bubbler operations due to elevated algal biomass, DOM and POM. Similar to forecasts in the absence of bubbler operations, SiO2 decreases from diatom uptake (typically in spring), which is not materially replenished during the 'classic' stage during the 1 month of spring 'top-up' external loading, but is so during the continuous inlet loads from RW and springs water into the south basin.

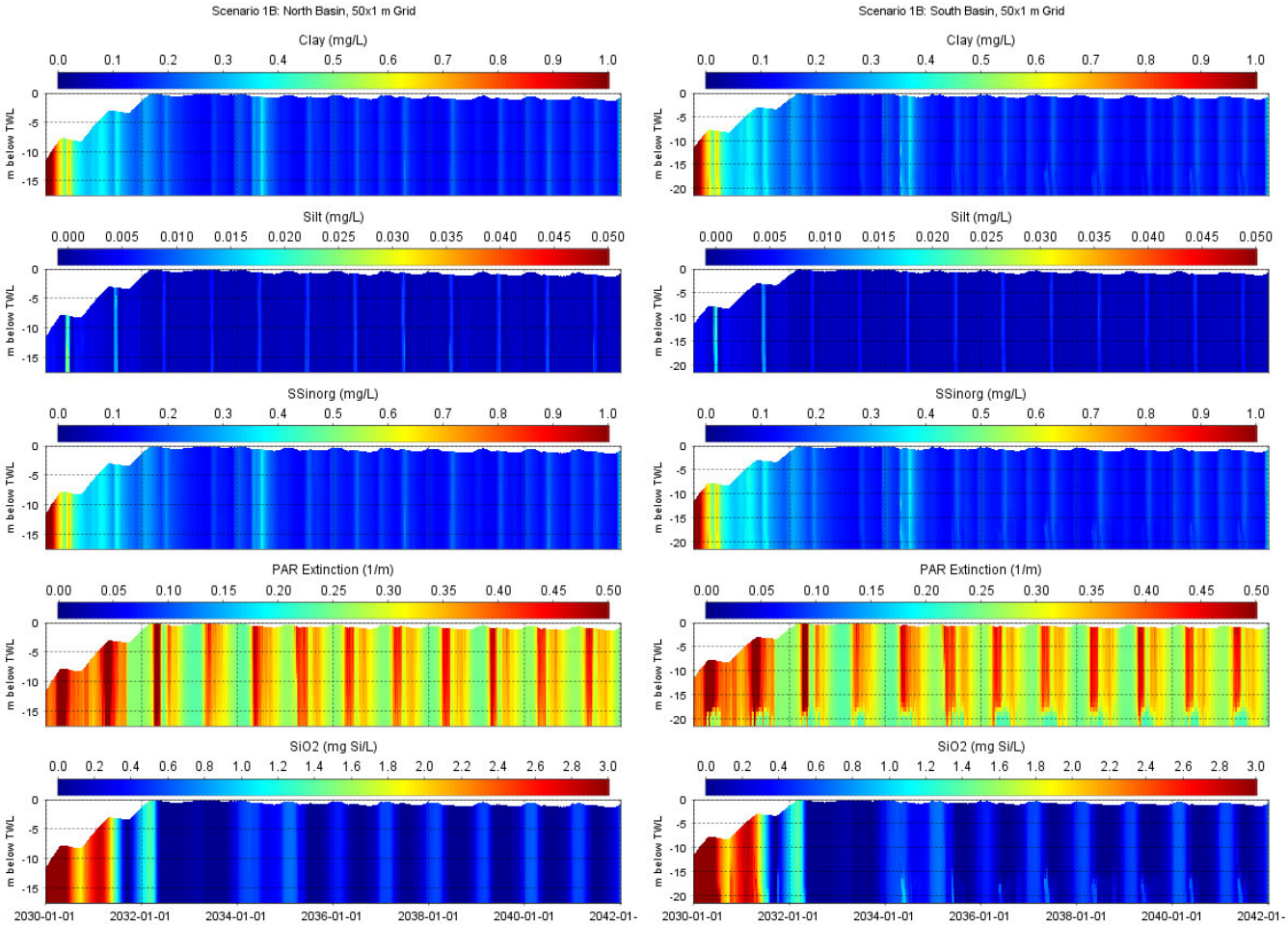

Figure 6.19 As Figure 6.14 for clay (top), silt (2nd panel), TSS (3rd panel), PAR extinction coefficient (4th panel) and SiO2 (bottom).

Pseudocolour plots at deep locations in both basins of the state variables of Ca, Na, Cl and SO4 in the absence of bubbler operations for scenario 1B are illustrated in Figure 6.12, which are similar to those described in the absence of bubbler operations (Figure 6.13).

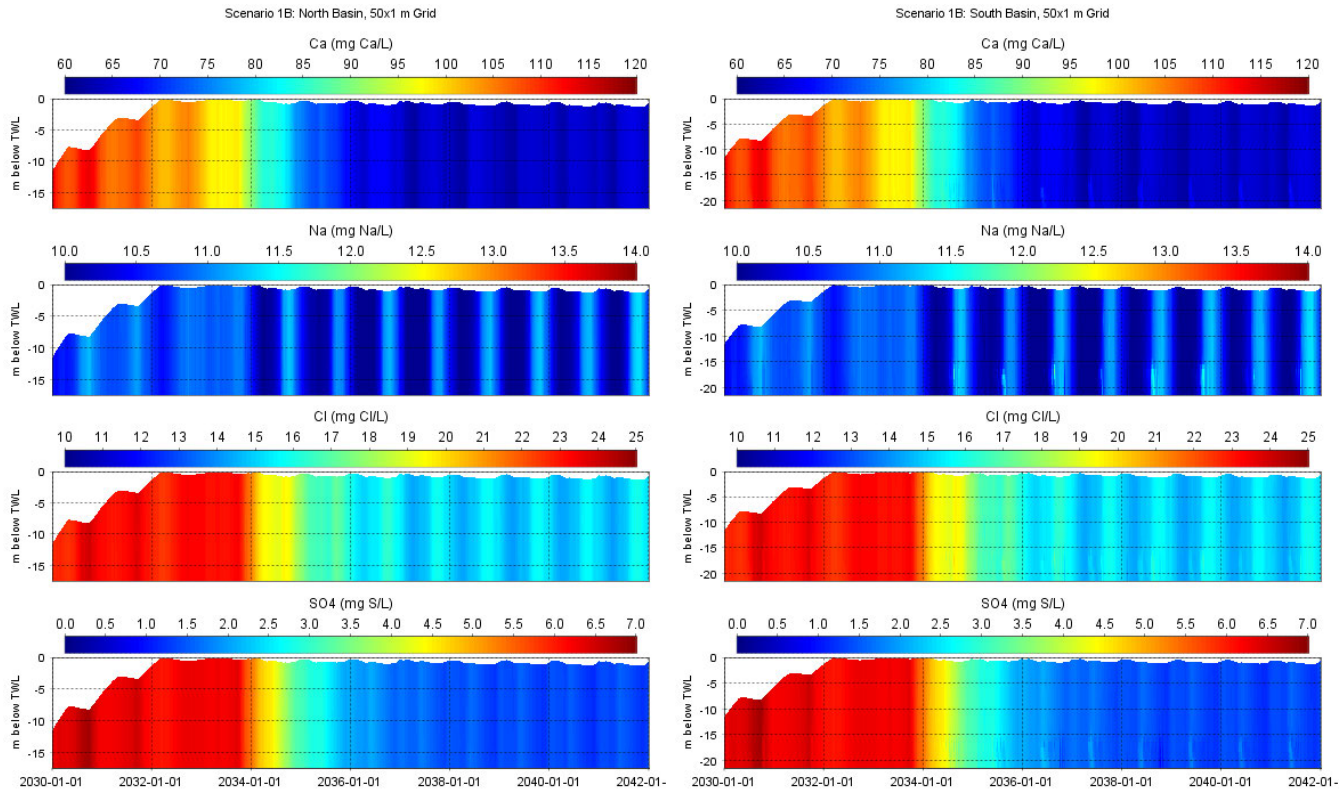

Figure 6.20 As Figure 6.14 for Ca (top), Na (upper middle), Cl (lower middle) and SO_4 (bottom).

6.2.3 Surface and bottom water quality without and with nighttime bubbler operations

Time series of state and derived variables are illustrated in this section as line plots at the following locations:

– The bottom waters immediately overlying the sediments at the deepest point in the south basin (~-22 m TWL). This location represents the region of the reservoir with the least vertical mixing intensity and the greatest influence from sediments. Though representative of a very small proportion of the deep waters and overall volume of HTR, it is the 'worst case' region of the reservoir from mixing intensity and WQ perspectives.

– The bottom waters immediately overlying the sediments at a deep point in the north basin (~-17 TWL). The north basin has an extensive deep water area, but all locations in this basin will have similar WQ. The sill that separates the two basins provides a physical setting for the WQ of the bottom waters to diverge as horizontal dispersion is physically impeded.

– The surface waters of the north basin at the representative deep water location described previously. Any location in the main body of the reservoir will have representative WQ of surface waters above the sill that separates the two basins. Due to HTR's relatively small size (horizontal length scale of ~1.5 km), horizontal dispersion time scales are short and maintain low horizontal WQ variability.

An overview of the WQ at these surface and bottom water locations without and with nighttime bubbler operations for scenario 1B includes:

– In the absence of bubbler operations, summer thermal stratification is relatively strong during all 3 stages, but persists later into the summer in the south than north basin (Figure 6.21). Seasonal thermal stratification does not occur with nighttime bubble operations, even in the south basin's deep water pocket.

– DO and DOSAT during bubbler operations are >8 mg/L and >90%, respectively, at the surface, the north basin's bottom waters, and much of the south basin's bottom waters, except for the small deep pocket where seasonal minima of ~1-4 mg/L and ~10-40% are predicted for brief periods, respectively (Figure 6.21). In the

absence of nighttime bubbler operations during seasonal stratification the bottom DO and DOSAT of the north basin attain seasonal minima of ~1-5 mg/L and ~10-60%, respectively, whereas in the south basin's deep pock the bottom waters become anoxic (DO and DOSAT of 0 mg/L and 0%, respectively) for several months each year.[26] There is a discernible improvement in the south basin's bottom DO from the 'classic' (2032-2033) to 'recycled' (2033 onwards) stages because of the direct injection of oxygenated inlet inflows.

– DIC and alkalinity are forecast to decrease from ~55 mg C/L and ~230 mg $CaCO_3$/L at the start of the 'fill' stage, respectively, to ~38 mg C/L and ~155 mg $CaCO_3$/L during the 'recycled' stage, respectively (Figure 6.22). This is largely driven by the change in the water balance of HTR from an annual 1 month 'top-up' of spring water ('classic' stage) to continuous inputs of springs water and RW ('recycled' stage). Peak spring-summer surface pH (~8.2-8.5) is driven by high algal productivity due to uptake of dissolved CO_2, whereas low algal productivity in winter yields seasonal minima in surface pH (~7.7-7.9).

– In the absence of nighttime bubbler operations during seasonal stratification, the anoxic conditions that develop at the bottom of the south basin's deep pocket is forecast to accumulate reduced dissolved forms of manganese (DMN) and iron (DFE) to peak concentrations of ~0.4-0.7 mg Mn/L and ~3-6 mg Fe/L, respectively (Figure 6.22). Maintenance of elevated bottom DO by nighttime bubbler operations effectively eliminates sediment releases of dissolved metals with resultant bottom DFE concentrations of ~0 mg Fe/L and short period spikes <0.2 mg Mn/L in the south basin's deep pocket.

– Nighttime bubbler operations are also predicted to cause a decrease in spring-summer peaks of algal biomass relative to no bubbler operations (Figure 6.23). The mechanism for this biomass reduction is greater light limitation where the elimination of seasonal stratification results in phytoplankton experiencing a lower average underwater PAR climate[27] and thereby lowering productivity. Relatedly, POC and DOC in the bottom waters are predicted to be less variable through the water column with bubbler operations. Greater vertical homogeneity of DOC and POC with nighttime bubbler operations yields concomitant BOD uniformity through the water column.

– The predicted effects of nighttime bubbler operations on P dynamics (Figure 6.24) include:

  - Elevated summer PO4 and DOP in the south basin's deep pocket in the absence of bubbler operations are greatly reduced with nighttime bubbler operations through maintenance of oxic water conditions overlying the deep water sediments that maintain low sediment releases.
  - Vertical variability in all P state variables is reduced with the elimination of seasonal stratification.

– The predicted effects of bubbler operations on N dynamics (Figure 6.25) include:

  - Elevated summer bottom NH4 and DON in the south basin's deep pocket in the absence of bubbler operations are greatly reduced with nighttime bubbler operations through maintenance of oxic water conditions overlying the deep water sediments that maintain low sediment releases.
  - Vertical variability in all N state variables is reduced with the elimination of seasonal stratification.
  - Regardless of bubbler operations a consistent decrease in NO3 is forecast from ~7.5 mg N/L at the onset of the 'fill' stage to ~1-1.5 mg N/L during the 'recycled' stage.

– As the primary water sources via the inlet (RW and springs water) have low inorganic particle (silt, clay) levels, TSS (inorganic suspended solids) is forecast to be low (<0.2 mg/L) without and with nighttime bubbler operations (Figure 6.26). The PAR extinction coefficient is predicted to be typically ~0. 25-0.5 1/m through the water column with nighttime bubbler operations due to vertical homogenisation of inorganic (clay, silt) and organic particles (e.g. POC), dissolved organic matter (e.g. DOC) and algae, all of which absorb underwater light.

– Nighttime bubbler operations through vertical homogenisation of the water column are predicted to reduce the accumulation of SiO2 in the bottom waters of the south basin during the period of seasonal thermal

[26] The SOD model parameter value of 1 g/m^2/d (Appendix B) is within the upper range of values. It is likely that the future HTR reservoir will have a lower SOD than adopted in this future reservoir forecast investigation so that anoxia may not occur and/or for a shorter duration in the absence of bubbler operations.

[27] During seasonal stratification phytoplankton largely maintained in suspension above the seasonal thermocline and thereby experience a high light climate, increased productivity and greater biomass.

stratification from direct hypolimnetic inputs from inlet inflows in the absence of bubbler operations (Figure 6.26).

– Ca, Na, Cl and SO4 were simulated conservative tracers to represent these determinands with typical values during the 'recycled' stage forecasted to be ~65 mg Ca/L, ~10.5 mg Na/L, ~15 mg Cl/L and ~1.5 mg SO4/L, respectively (Figure 6.27).

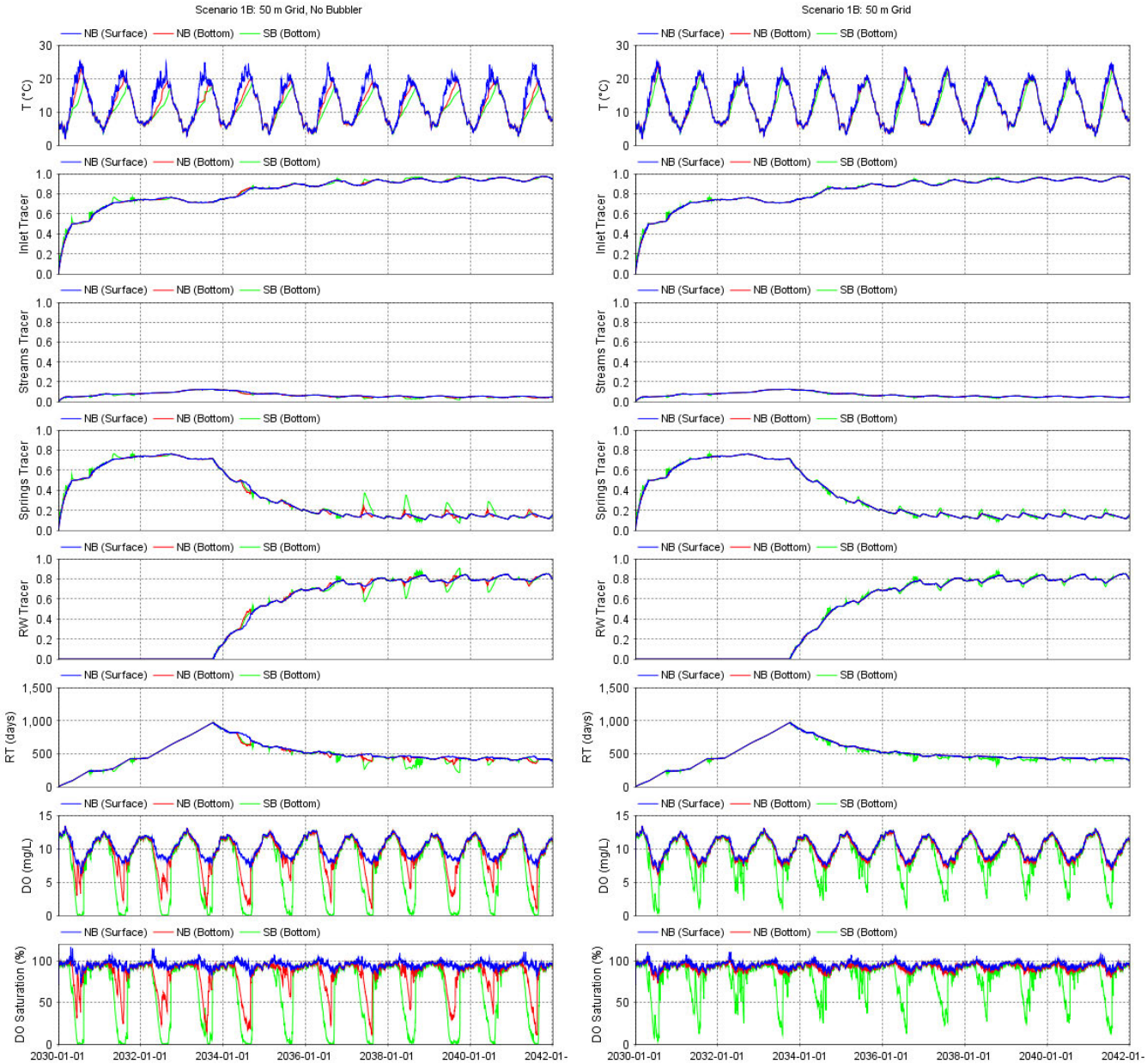

Figure 6.21 ***T (top), tracers (inlet [comingled] inflows [2nd panel] and streams [3rd panel]), RT (4th panel), DO (5th panel) and DOSAT (bottom) at the surface of the north basin (NB), and bottom waters at deep locations in NB and the south basin (SB) without (left) and with (right) nighttime bubbler operations for scenario 1B.***

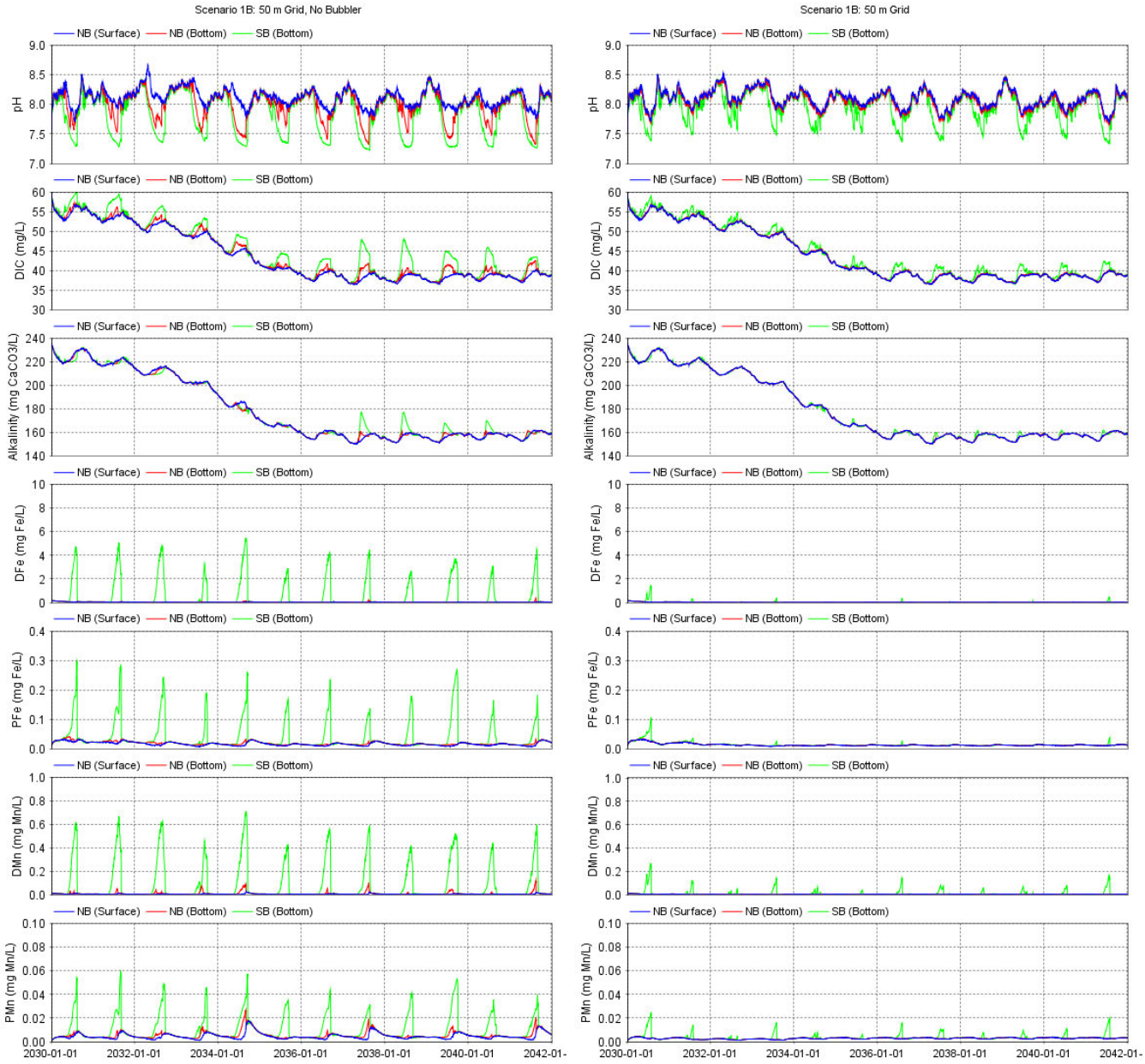

Figure 6.22 *As Figure 6.21 for pH (top), DIC (2nd panel), alkalinity (3rd panel), DFe (4th panel), PFe (5th panel), DMn (6th panel) and PMn (bottom).*

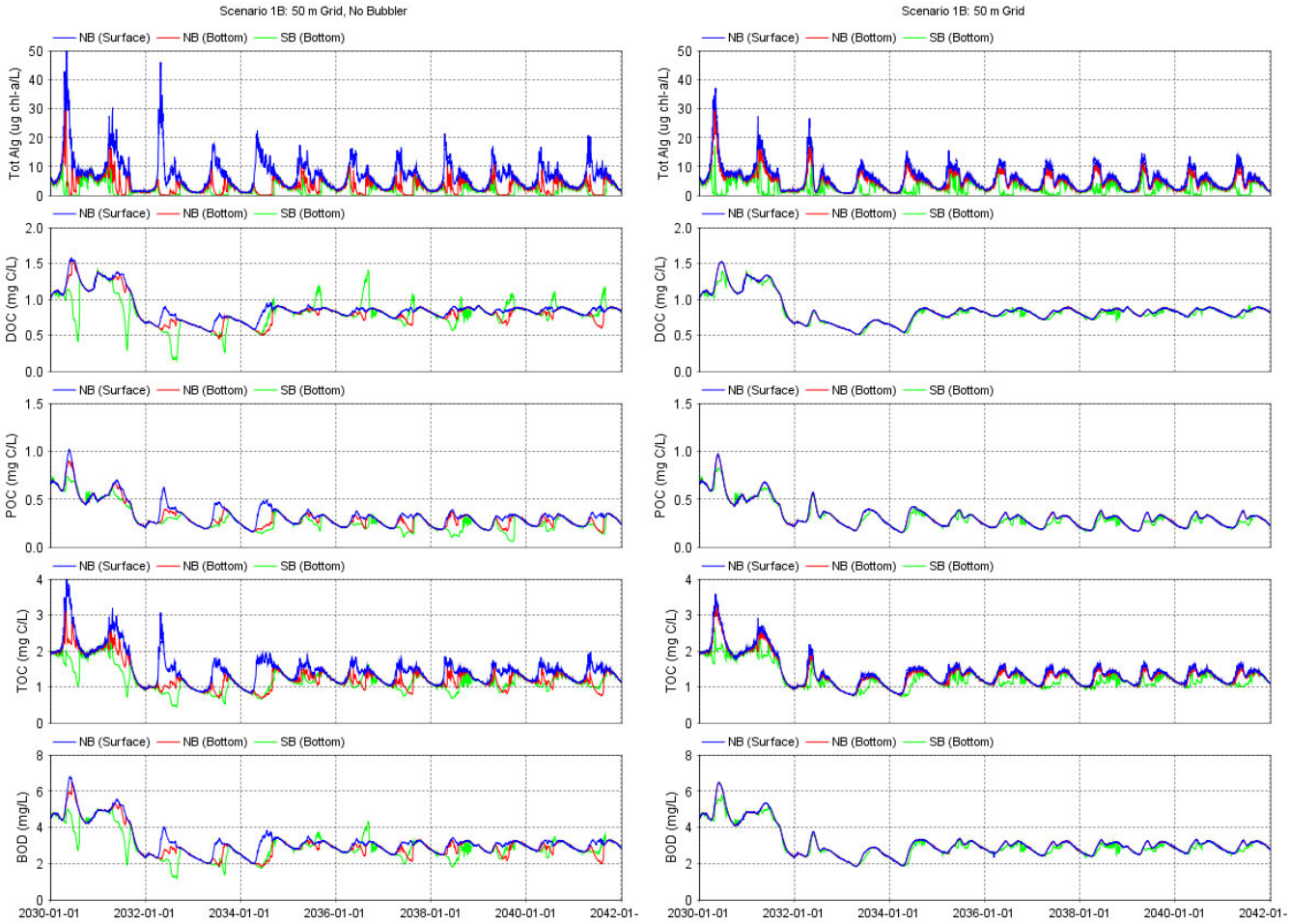

Figure 6.23 As Figure 6.21 for total chl-a (top), DOC (2nd panel), POC (3rd panel), TOC (4th panel) and BOD (bottom).

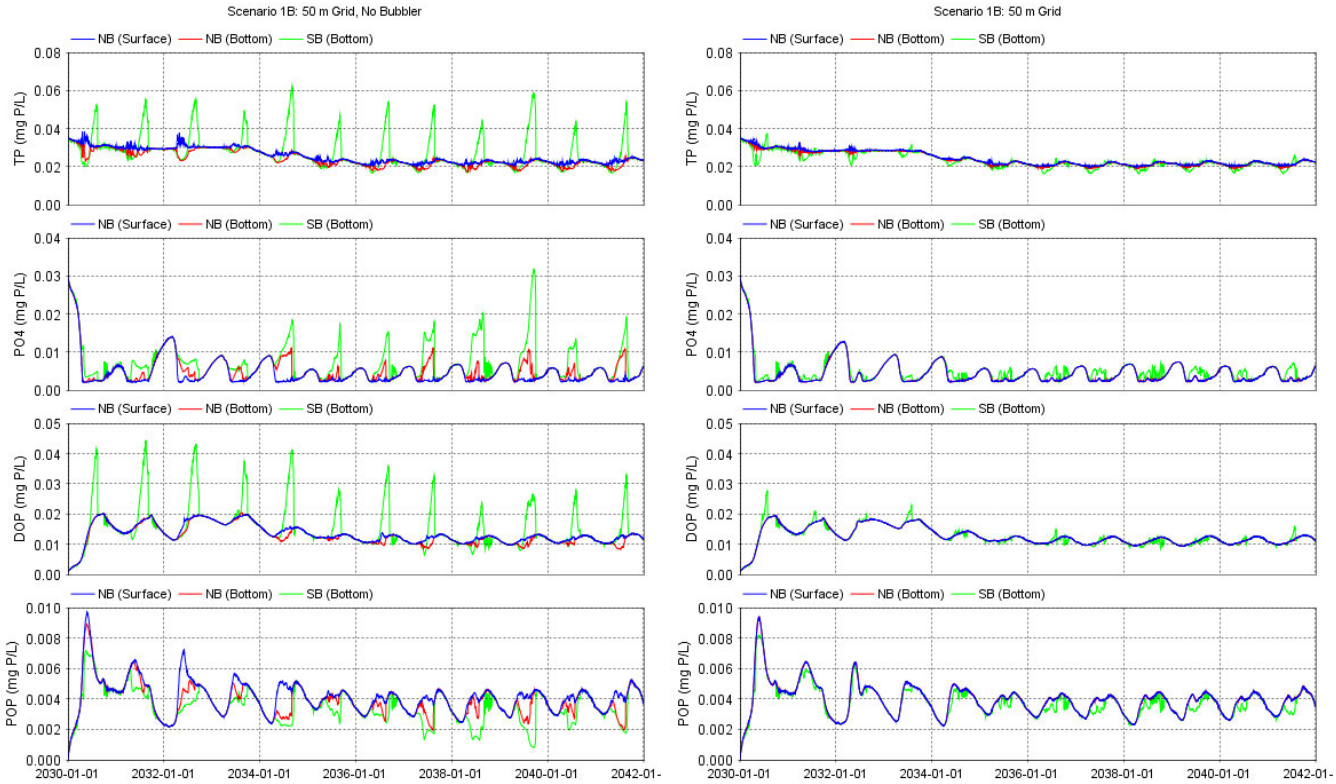

Figure 6.24 As Figure 6.21 for TP (top), PO4 (2nd panel), DOP (3rd panel) and POP (bottom).

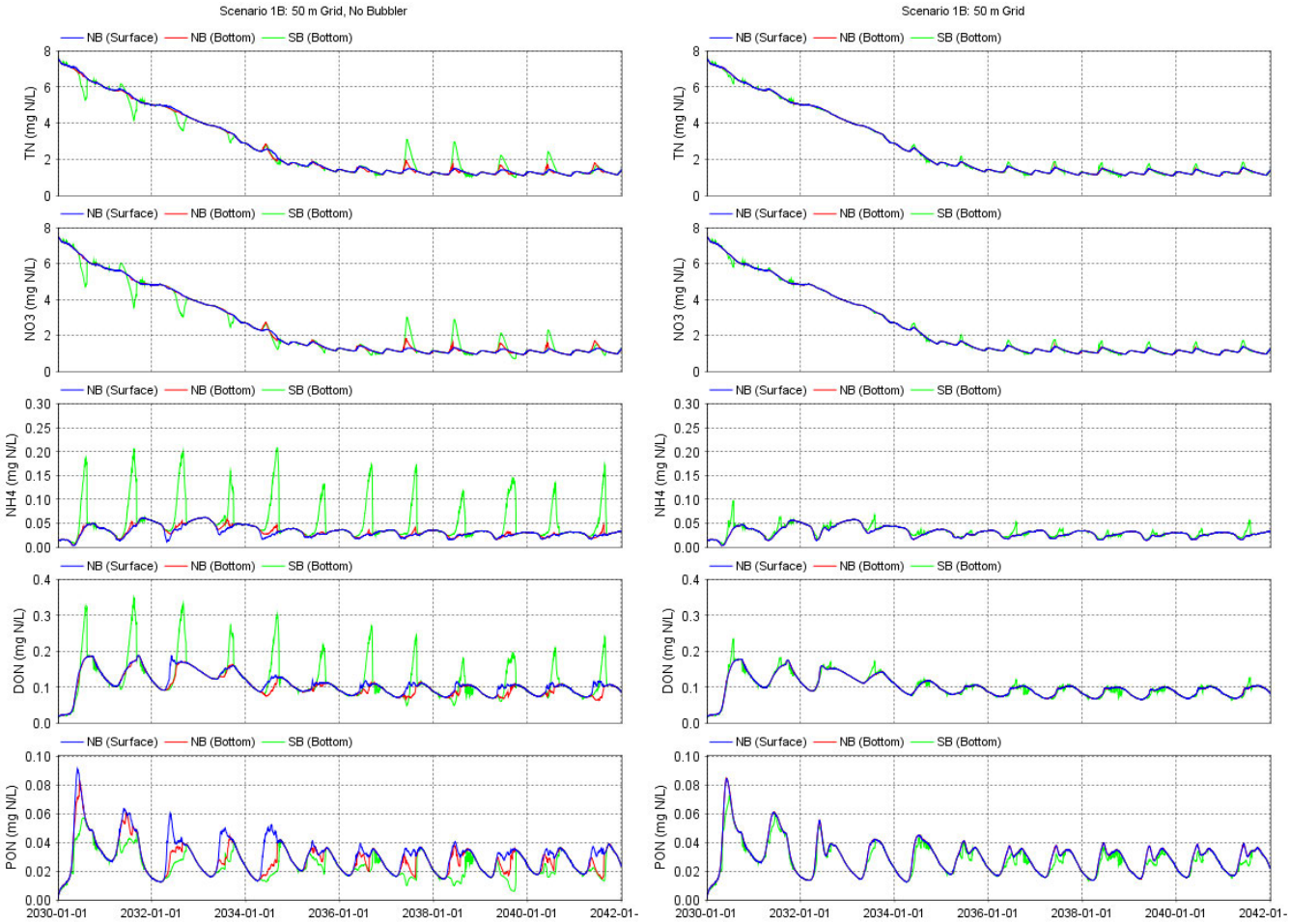

Figure 6.25 As Figure 6.21 for TN (top), NO3 (2nd panel), NH4 (3rd panel), DON (4th panel) and PON (bottom).

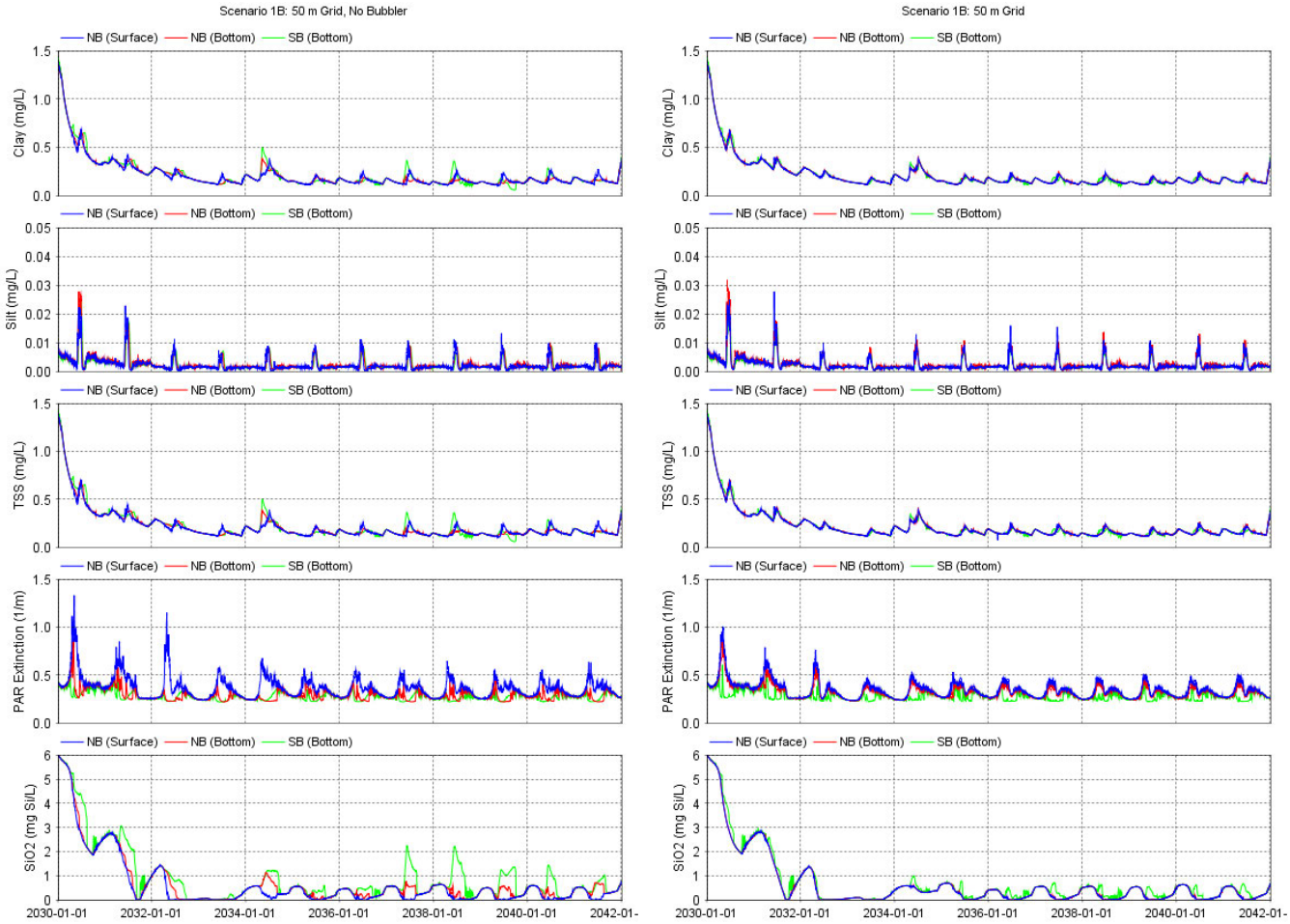

Figure 6.26 ***As Figure 6.21 for inorganic clay (top) and silt (2nd panel), TSS (3rd panel), PAR extinction coefficient (4th panel) and silicon dioxide (bottom).***

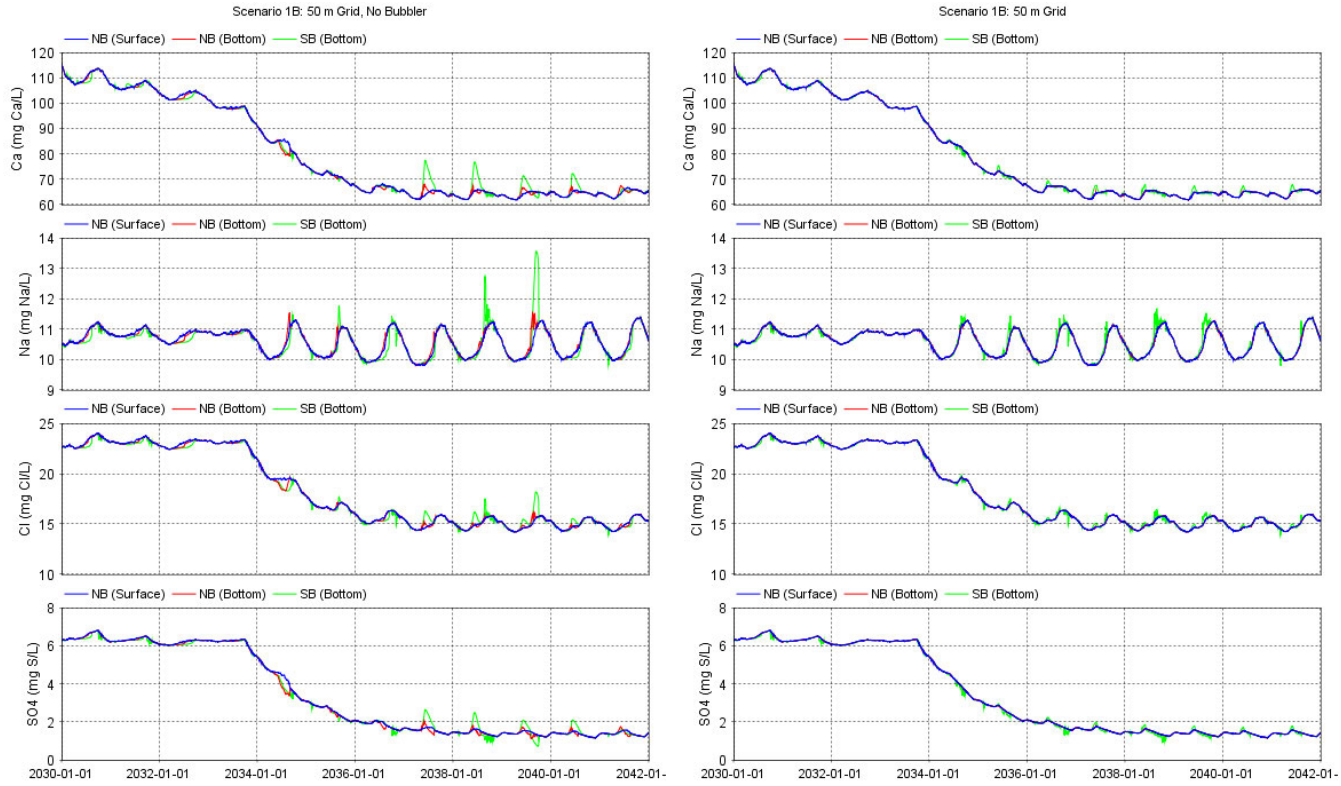

Figure 6.27 *As Figure 6.21 for Ca (top), Na (2nd panel), Cl (3rd panel) and SO4 (bottom).*

6.2.4 Nutrient limitation

For the 3 simulated algal groups both P- and N- limitation are forecast to occur in HTR's surface waters over the spring to early autumn period of elevated productivity and higher biomass during scenario 1B (Figure 6.28). These general patterns of nutrient limitation are predicted to occur across all 3 stages.

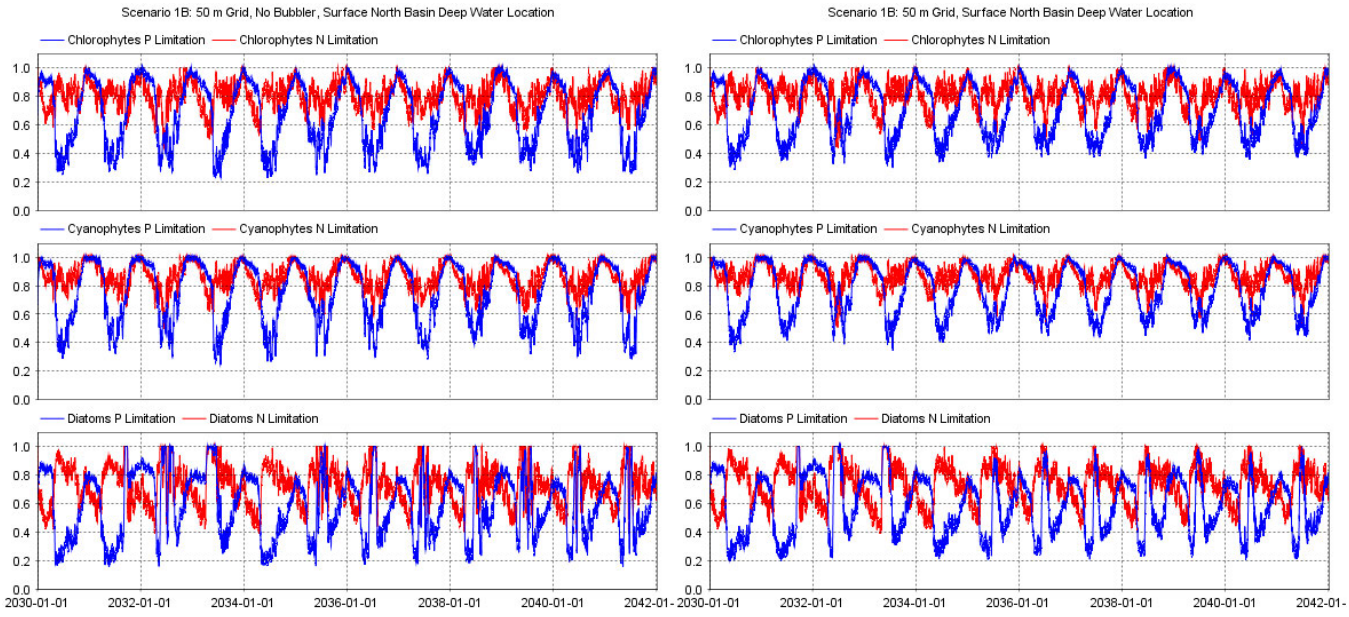

Figure 6.28 *P and N limitation of the three algal groups (chlorophytes top, cyanophytes middle, diatoms bottom) of simulations without (left) and with (right) nighttime bubbler operations for scenario 1B.*

6.2.5 Withdrawals

Scenario 1B withdrawals were from the high draw-off once HTR approached TWL, which generally extracts surface waters above the seasonal thermocline in the absence of bubbler operations. Similar withdrawal WQ between the 2 bubbler cases (no, nighttime) is predicted because simulated surface WQ in the absence of a mixing system is very similar as throughout the water column with nighttime bubbler operations (Figure 6.29). Though poor WQ is predicted in the south basin's deep waters without bubbler operations, this volume is small and readily diluted (see Section 9.3.2). The primary benefit from bubbler operations on withdrawal WQ are small reductions in the seasonal peaks of TOC and total algal biomass, and the elimination of seasonal thermal stratification that reduces the risk of deleterious WQ conditions (e.g. high dissolved metals, noxious blue-green algal bloom). The predicted withdrawal WQ envelopes for scenario 1B without and with nighttime bubbler operations are summarised in Section 9.5.

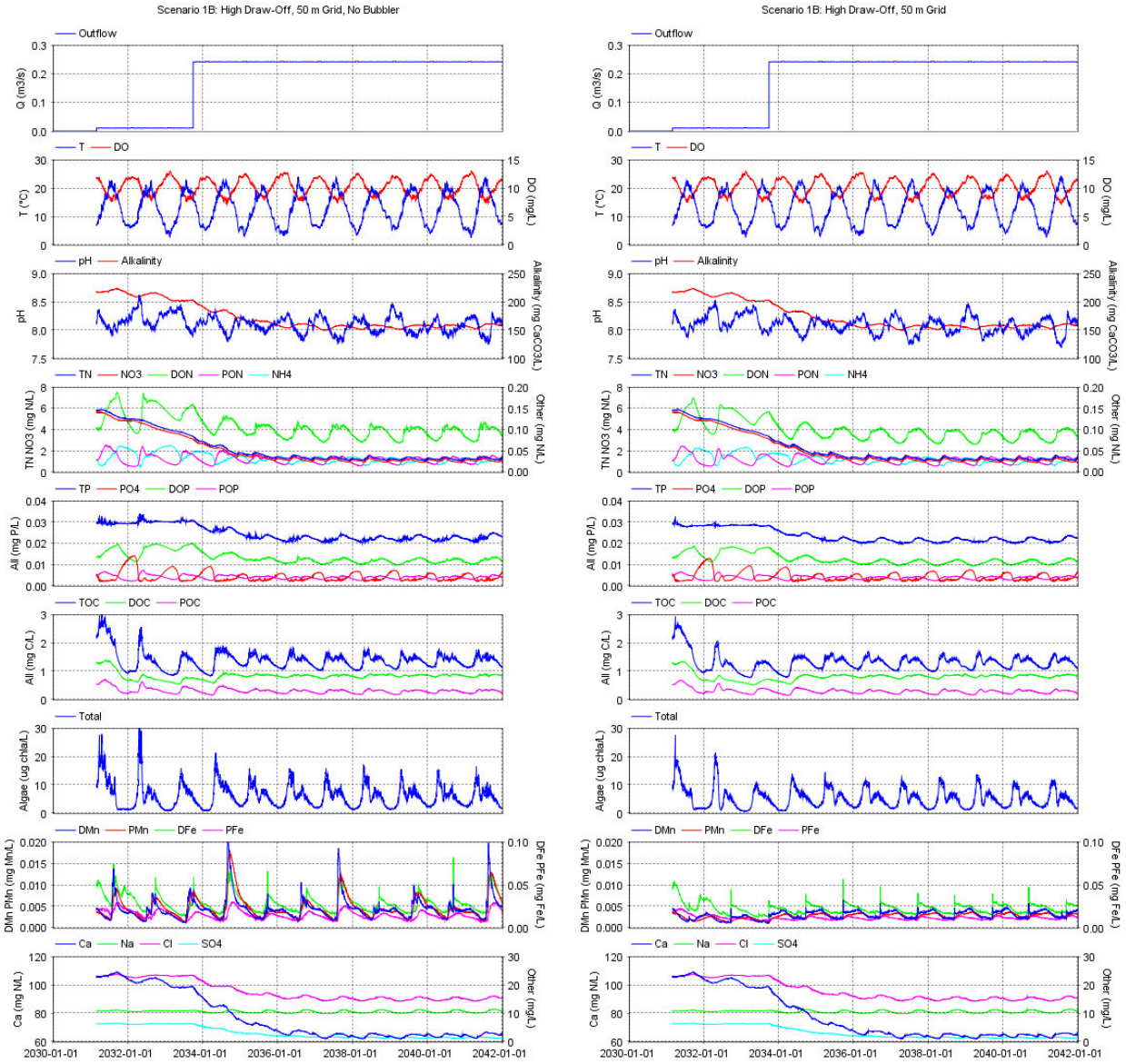

Figure 6.29 ***Withdrawal WQ for a number of determinands from the high draw-off outlet in the south basin without (left) and with (right) nighttime bubbler operations for scenario 1B.***[28]

[28] Purpose of plots to provide high level overview of any material changes in patterns or concentrations. Refer to north basin surface line plots of various WQ determinands in Section 0 for more detailed graphical presentation of patterns, which are similar to those in the withdrawals.

6.2.6 Comparison to Bewl Water reservoir monitoring data

Though there is no data to validate the future HTR WQ forecasts, the WQSG requested that a semi-quantitative comparison be carried out with a proximal reservoir. Monitoring data from Bewl Water reservoir, a nearby SW raw water supply storage, was selected as the most apt water body given its proximity to HTR and data availability[29].

Percentiles of forecasted withdrawal WQ (6 hour output intervals) of scenario 1B without and with nighttime bubbler operations during the 'classic' (October 2032-September 2033) and 'recycled' (January 2035-December 2041) stages were compared to near-surface (~4 m below TWL) Bewl Water measurements from May 2020-April 2023 (~monthly intervals) TWL (Figure 6.30) where:

– Forecasted T (both stages), pH (both stages), total algae as chl-a (both stages), NH4 ('recycled' stage), NO3 ('recycled' stage) and TP (both stages) were similar to Bewl Water measurements. Modelled HTR temperatures are similar to published measurements of southern England reservoirs (GHD 2023). Similarities in phytoplankton biomass are indicative of credible predictions by this investigation. Predicted HTR NO3, NH4 and TP during the 'recycled' stage compare reasonably well to Bewl Water measurements.
– Predicted NH4 ('classic' stage) and NO3 ('classic' stage) were much higher than Bewl Water measurements. Very high NO3 external loading from springs inputs during the 'fill' stage is the likely cause of this large discrepancy.
– TOC is forecasted to be lower than Bewl Water measurements during both the 'classic' and 'recycled' stages. The likely difference between the 2 water bodies is due to the low HTR concentrations in the primary inputs of RW (~0.4 mg C/L, Table 4.5) and springs (~0.6 mg C/L, Figure 4.12). Though higher levels occur in the HTR feeder streams (~10 mg C/L, Table 4.2), the loads are small due to the small contribution of this source to the overall water balance of the system.
– Total iron (TFe=PFE+DFE) and total manganese (TMn=TMN+DMN) are forecasted to be ~10 fold lower than Bewl Water measurements. RW TFe[30] and DMN of 0.05 mg Fe/L and 0.017 mg Mn/L, respectively (Table 4.5), are low and do not contribute substantive external metals loads. Though metal concentrations in the streams are substantially greater (~5 mg Fe/L, ~0.5 mg Mn/L, Table 4.5), their low contribution to HTR's water balance yields relatively small external loads to the reservoir. Internal loading of metals from the sediments during low DO conditions in the south basin's deep water pocket in the absence of a mixing system causes elevated DMN and DFE levels of ~0.4-0.7 mg Mn/L and ~3-6 mg Fe/L, respectively. Even in the absence of bubbler operations the high DFE and DMN concentrations in the south basin's deep waters has a minor effect on withdrawal WQ as it only represents a small proportion of the reservoir volume, where after the breakdown of summer stratification this relatively small 'pool' of elevated metals is readily dispersed (diluted) to low levels (see Section 9.3.2).

The simulated WQ of the withdrawals during the 'recycled' stage of scenario 1B have similar (T, pH, NO3, NH4, TP, chl-a) and lower (TOC, TFe, TMn) concentrations of determinands than Bewl Water reservoir surface measurements. However, given the substantive differences between the Bewl Water reservoir (in-stream reservoir, seasonal inflows) and HTR (off-stream reservoir, continuous inflows during the 'recycled' stage), the comparison has limited value other than demonstrating the HTR forecasts are plausible relative to a proximal reserovir. Nighttime bubbler operations have a small effect on the forecasted withdrawal WQ during the 'classic' and 'recycled' stages as maintenance of relatively homogeneous WQ throughout the reservoir is predicted to be similar to the surface WQ above the thermocline in the absence of bubbler operations.

[29] There was a substantive effort to no avail to identify reservoirs with data sets that could serve as improved analogues of the future Havant Thicket Reservoir than Bewl Water reservoir.
[30] Assumed TFe as not specified as DFE not defined in estimates provided by SW.

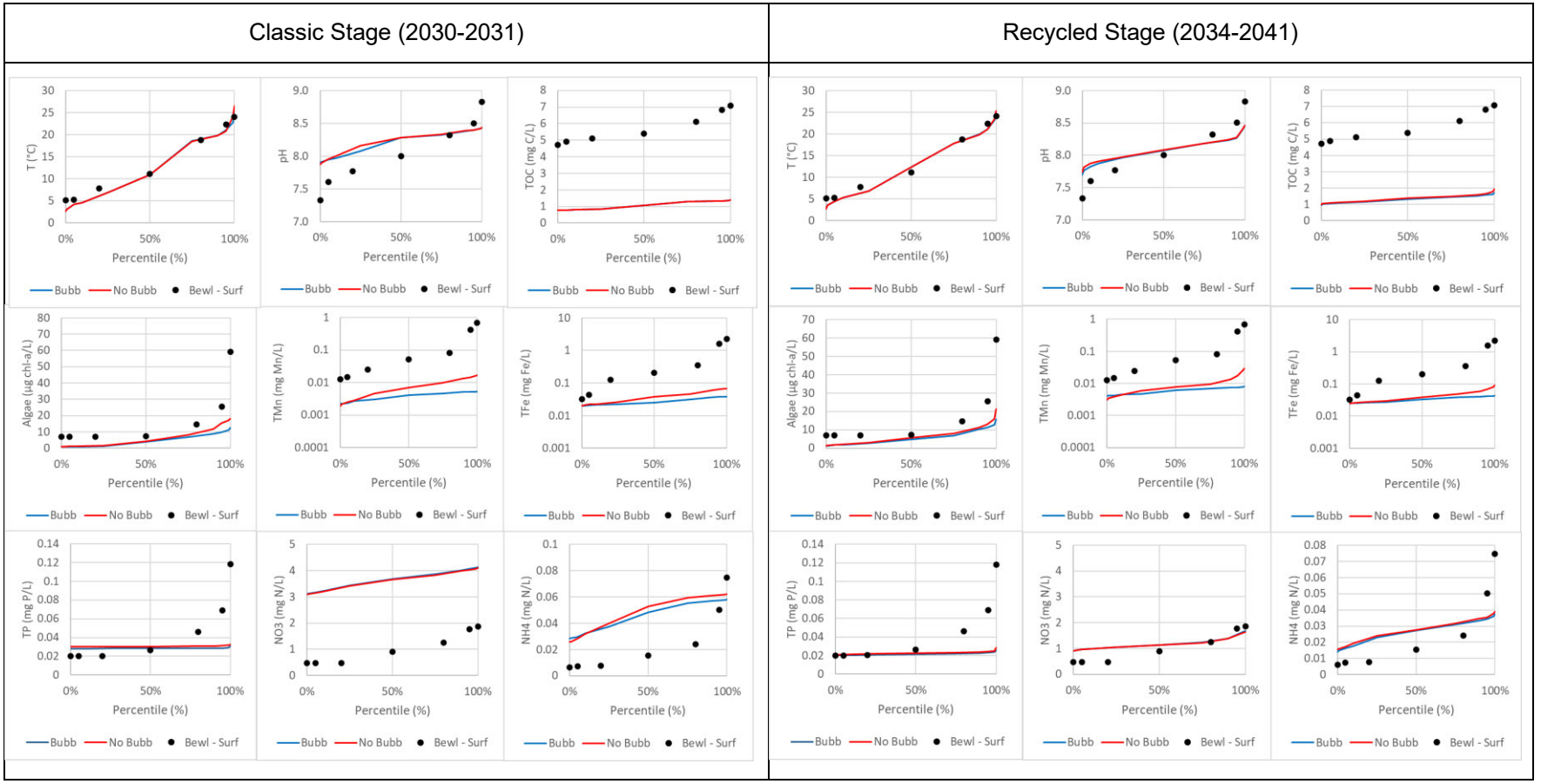

Figure 6.30 ***Percentile plots of simulated HTR withdrawal WQ with no and nighttime bubbler operations (lines) over the 'classic' (left) and 'recycled' (right) stages of scenario 1, and Bewl Water reservoir near-surface measurements (symbols).***

7. Effect of stabilisation on water quality with bubbler operations

7.1 Stabilisation effect on DO stratification

The greatest effect of stabilisation on the HTR WQ occurs during the first 2 years of the 'fill' stage because of the substantially higher SOD, DIM and DOM sediment fluxes than will occur post-stabilisation (see Section 4.5.2). Simulations with nighttime bubbler operations forecast that stabilisation will have a minimal effect on the temperature and seasonal stratification dynamics of scenario 1B (not shown), but differences in DO between the stabilisation and post-stabilisation periods in the south and north basins include (Figure 7.1):

– The first and second years of the reservoir's existence are forecast to have lower DO through the water column of the north basin and above -17 m TWL in the south basin by ~2 mg/L and ~1 mg/l, respectively, during the summer due to the stabilisation effect.

– The duration of anoxic bottom waters in the south basin's deep hole below -17 m TWL is extended by ~2-3 months during the first year, and ~1 month the second year.

– The vertical extent of anoxic waters in the south basin's deep hole extends upwards by ~1-2 m due to the stabilisation effect.

This modest DO deterioration is largely due to filling the reservoir over 3 consecutive winters that mutes the stabilisation effect relative to filling over 1 winter with very high SOD across the entire sediment area of the reservoir during the first year.

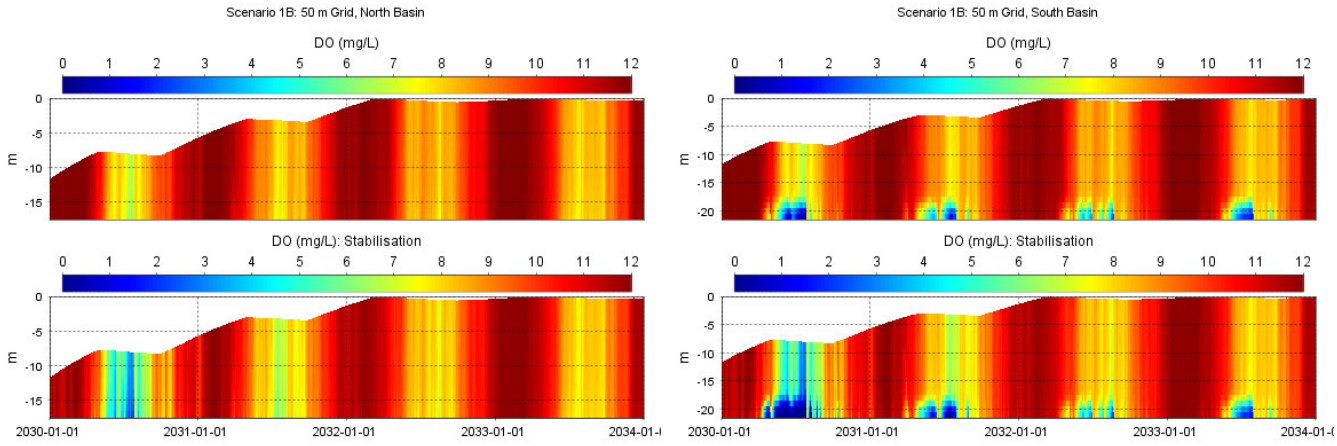

Figure 7.1 ***Pseudocolour plots of DO at deep locations in the north (left) and south (right panels) basins without (top) and with (bottom) estimates of stabilisation sediment fluxes for scenario 1B with bubbler operations from 2030-2033.***

7.2 Surface and bottom water quality

Time series of selected state (T, DO, PO4, DMN) and derived (total algal biomass) variables at the surface and bottom of the north (maximum depth of ~-17.5 m TWL) and south (maximum depth of ~-22 m TWL) basins nighttime bubbler operations further illustrate the modest degree of predicted stabilisation effects[31] on reservoir WQ (Figure 7.2) where:

[31] Section 4.5.2 provides the estimates of the elevated sediment fluxes over the stabilisation period for DOM (DOP, DON, DOC) and DIM (PO4, NH4, DIC) state variables.

- Differences in T between surface and bottom waters are minimal over seasonal and interannual time scales as described in Sections 6.2.2 and 6.2.3 for simulations with nighttime bubbler operations except less than ~-17 m TWL in the south basin below the bubbler line which remain cooler than the overlying waters during the period of reservoir heating from March to August.
- During the first and second year of filling, stabilisation effects materially and modestly lower DO of surface the surface and bottom waters, respectively, but subsequent years are very similar as described in Section 7.1.
- Post-stabilisation and stabilisation total algal biomass are very similar with and without the stabilisation during the first 6 years . Total algal biomass is substantially greater during the first 2 years and moderately higher during the third year, and then subsequently much lower.
- Increases in PO4 are forecast to be very moderate in the surface and bottom waters of both basins due to stabilisation effects.
- The extended period of low DO in the bottom waters of the south basin is forecast to double peak DMN levels during year 1 from ~0.2 mg Mn/L to ~0.5 mg Mn/L, and from ~0.1 mg Mn/L to ~0.2 mg Mn/L during year 2. In contrast, well-oxygenated bottom waters in the south basin during stabilisation is forecast to maintain very low DMN levels.
- Except for the materially lower DO during the first year of filling due to high SOD, generally nighttime bubbler operations are forecast to moderate potential stabilisation effects on reservoir WQ.

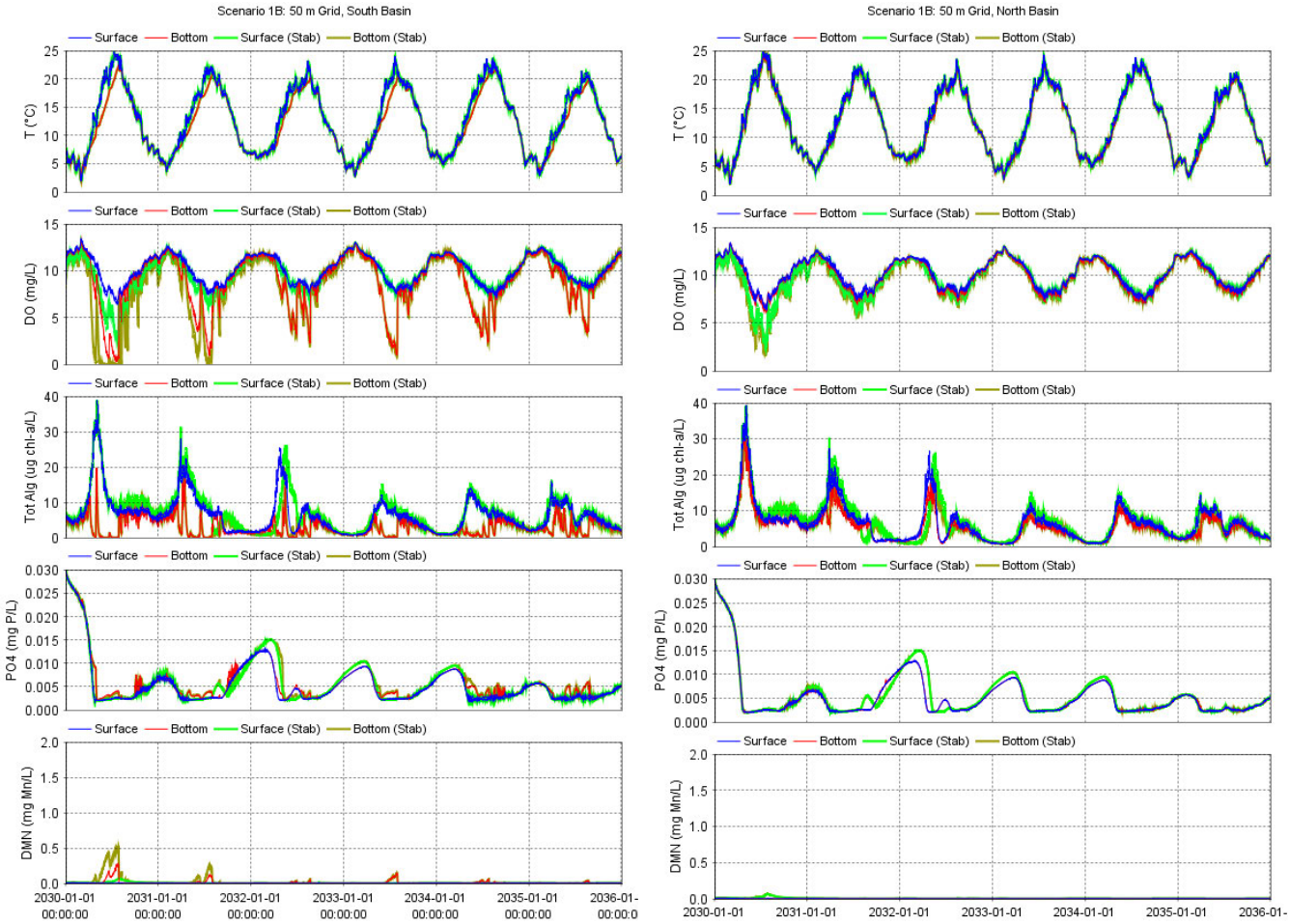

Figure 7.2 ***Comparison of selected simulated state variables (T [top], DO (2nd panel), total algae (3rd panel), PO4 [4th panel], DMN [bottom]) at the surface and bottom waters at deep water locations in the south (left) and north (right) basins with nighttime bubbler operations for coarse grid simulations of scenario 1B without and with stabilisation (Stab) estimates.***

7.3 Withdrawals

As with surface and bottom waters in the north and south basins, the stabilisation effect on withdrawal WQ with nighttime bubbler operations was relatively minor and limited primarily to a small reduction in DO during the first 2 years and a short-lived modest spike in DMN during the first summer (Figure 7.3). The predicted withdrawal WQ envelopes for scenario 1B with and without the stabilisation effect and nighttime bubbler operations are provided in Section 9.5.

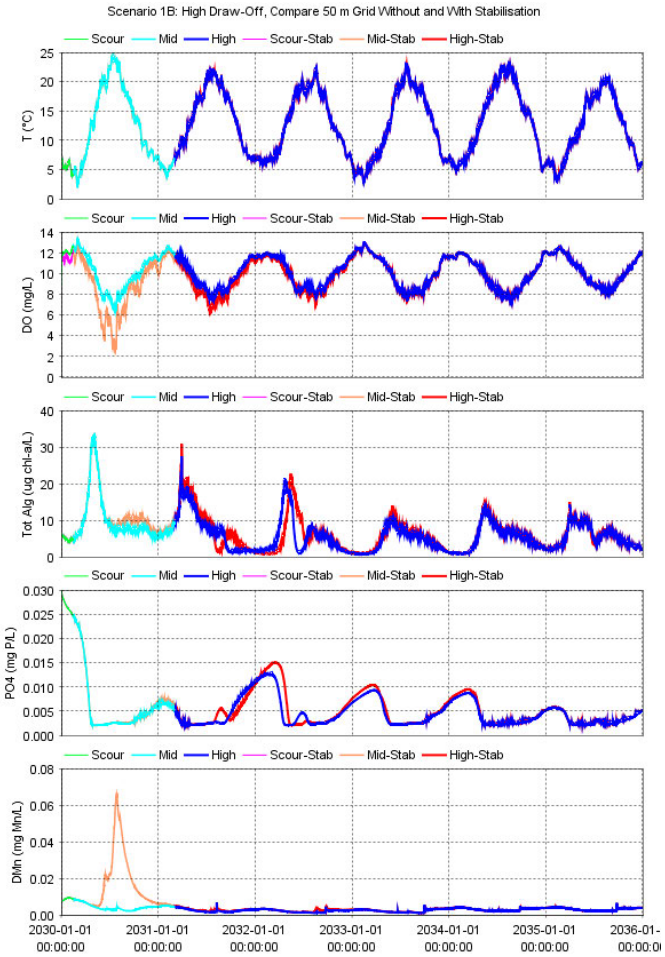

Figure 7.3 ***Comparison of selected simulated state variables (T [top], DO [2nd panel], total algae [3rd panel], PO4 [4th panel], DMN [bottom]) of the withdrawals with and without stabilisation effects and nighttime bubbler operations.***

8. Comparative analysis between baseline scenario 1B and other scenarios

In this section a comparative analysis of the scenarios that are outlined in Section 3 with baseline scenario 1B are provided. To simplify this comparative analysis, the following approach has been adopted:

– It is based solely on withdrawals for simulations with nighttime bubble plume operations (April-August). The DWSP mandates bubbler operations as the primary in-reservoir control measure to ameliorate WQ risks. Bubbler operations will eliminate persistent thermal stratification and maintain a relatively homogeneous WQ condition throughout the main body of the reservoir (Section 6). Hence, withdrawal WQ will also be representative of the characteristic forecasted WQ in the reservoir, as well as the forecasted WQ of raw water supply and environmental compensation flows.

– It is limited to a subset of hydrodynamic state variables (i.e. inlet and stream tracers, retention time) and determinands (i.e. T, DO, pH, alkalinity, total chl-a, TOC, TP, TN, NO3, TSS, SiO2) that may differ substantially between scenarios. A summary of forecasted determinand concentrations across the scenarios is summarised as a withdrawal WQ envelope for water supply, ecological acceptability metrics of the environmental compensation flows, and ecological status of the future reservoir in Sections 9.5, 9.6.2 and 9.6.3, respectively.

8.1 Scenario 4A: extended classic stage

Prior to consideration of RW inputs into HTR, this future water body was to be maintained primarily at/near TWL in a state of readiness as an emergency water supply in the event of a future drought through annual winter ‘top-ups’ with springs water of ~1 month duration. Scenario 4A, the extended classic, assumes no RW inputs at the projected start of October 2033 and that the reservoir is maintained at/near TWL for the next ~8 years. A comparison of the forecasted withdrawal WQ of scenarios 1B and 4A from October 2033 to December 2041 is provided in Figure 8.1 where:

– Temperature, DO, pH and TSS were nearly equivalent between the 2 scenarios.

– The inlet tracer decreased from ~95% over much of the ‘recycled’ stage of scenario 1B to ~50% at the end of scenario 4A due to no RW inputs and only sufficient springs inflows to maintain the reservoir at/near TWL. The stream tracer increased from ~5% over much of the ‘recycled’ stage of scenario 1B to ~35% at the end of scenario 4A, again due to the much lower inlet discharge because of no RW inputs. The retention time increased from ~400 days for much of the ‘recycled’ stage of scenario 1B to ~3,500 days at the end of scenario 4A, again due to the much lower inlet discharge due to no RW inputs and minimal withdrawals from the reservoir.

– Alkalinity levels decreased from ~150-160 mg $CaCO_3$/L for much of the ‘recycled’ stage of scenario 1B to ~140 mg $CaCO_3$/L at the end of the scenario 4B, again due to no RW inputs and dilution by rainfall and stream inputs (12.5 mg $CaCO_3$/L).

– In terms of algal biomass summer peaks of 11-14 µg chl-a/L and winter minima of 1-2 µg chl-a/L during scenario 4A were similar to the ‘recycled’ stage of scenario 1B.

– TOC during scenario 4A was ~0.1-0.2 mg C/L lower than much of the ‘recycled’ stage of scenario 1B, a small difference.

– TP was maintained at ~0.03 mg P/L during scenario 4A, substantially greater than the ~0.02 mg P/L for much of the ‘recycled’ stage of scenario 1B largely driven by the lower P concentrations of the RW.

– TN and NO3 during scenario 4A followed a similar trajectory as the ‘recycled’ stage of scenario 1 with a slightly lower concentration at the end of the simulations by ~0.5 mg N/L. A higher frequency of springs inputs with elevated NO3 levels (~7.5 mg N/L) led to greater seasonal variability in TN and NO3 during the ‘recycled’ stage of scenario 1B relative to scenario 4A, which again only had modest ‘top-up’ inputs of springs water once per year.

– Silica decreased substantially from seasonal peaks of ~1-1.3 mg Si/L during the 'recycled' stage of scenario 1A with continuous RW and/or springs inputs to very short duration winter peaks of ~0.1 mg Si/L due to limited springs inputs during scenario 1B.

In short, the WQ of baseline scenario 1B with moderate continuous RW (10-20 MLD) and 1-2 months per year of springs (15 MLD) inflows and moderate continuous withdrawals (20 MLD) is forecast to be very similar to that of the extended classic scenario 4A with 2-6 weeks per year of springs discharge (15 MLD) and minimal withdrawals (3 MLD for several months per year).

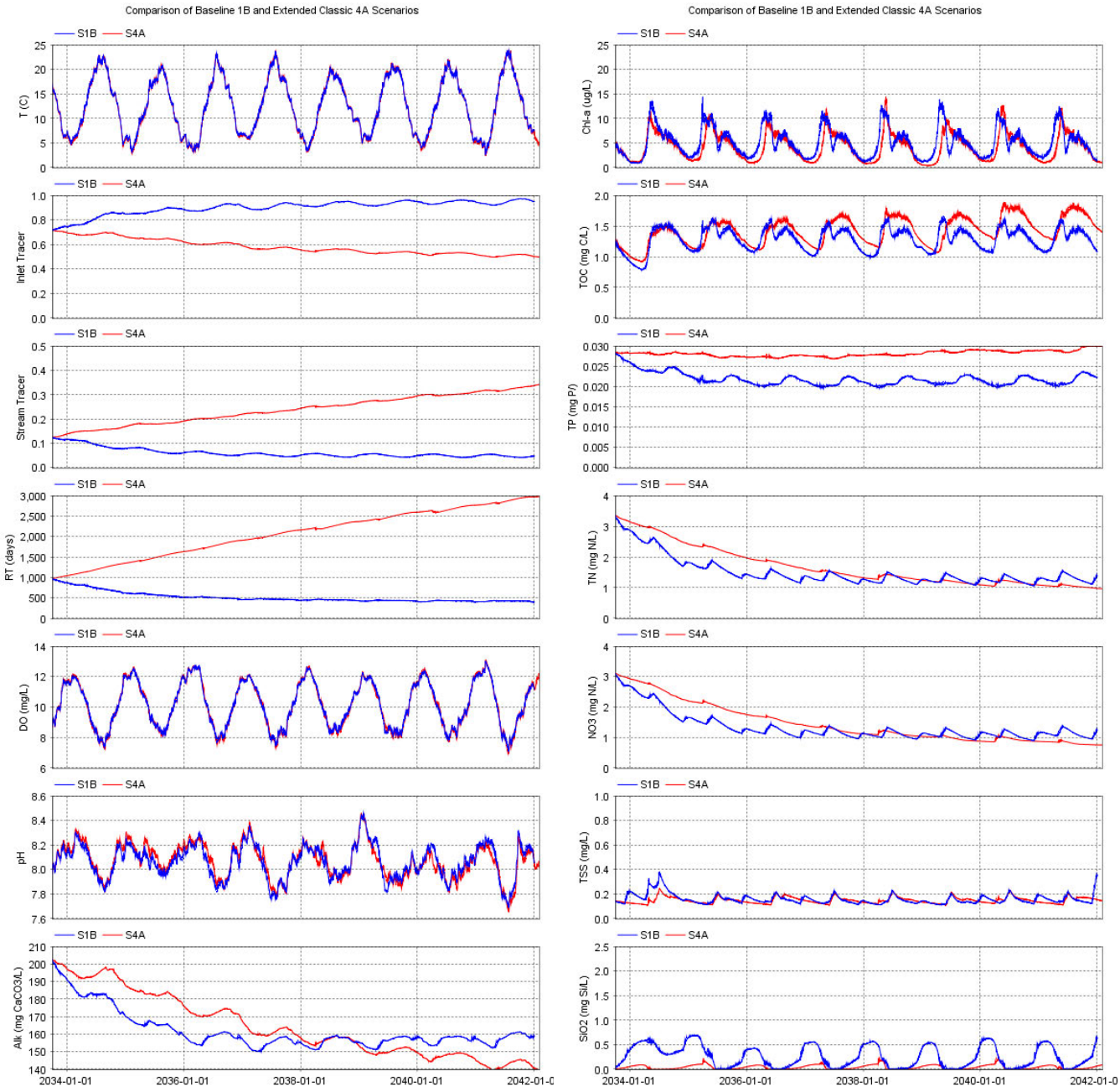

Figure 8.1 ***Comparison of selected hydrodynamic state variables and WQ determinands in the withdrawals from the high draw-off of scenario 1B (baseline) and scenario 4A (extended classic phase) with nighttime bubbler operations.***

8.2 Scenarios 2E-G: operational variations in inflows and withdrawals

Scenarios 2E (high yield with ~50 MLD withdrawals), 2F (moderate yield with ~30 MLD withdrawals maximising springs inputs) and 2G (moderate yield with ~30 MLD withdrawals maximising RW inputs) represent different operational strategies with variations in the mix of RW and springs inputs via the inlet and withdrawals from the reservoir over ~3 years of the 'recycled' stage from June 2037-May 2040 (Section 4.3.1.2.7). An additional year from 1 June 2040 to 31 May 2041 with the scenario 1B hydrology is incorporated into the simulations to evaluate the time scale for the reservoir to return to typical baseline conditions. Of particular interest is the high yield scenario 2E where a sizeable decrease in surface level necessitates withdrawals via the middle draw-off. A comparison of the forecasted withdrawal WQ of scenarios 2E, 2F and 2G relative to scenario 1B from June 2037 to May 2040 is provided in Figure 8.2 where:

– Temperature, DO and pH were nearly equivalent between the 4 scenarios.
– The inlet tracer increased from ~92-96% for scenario 1B to ~94-98% for scenarios 2F and 2G, and ~96-100% for scenario 2E, which simply reflects the much higher RW discharge via the inlet for these operational scenarios. The stream tracer decreased from ~4-6% for scenario 1B to ~2-4% for scenarios 2E-2G, because of the much higher inflows and withdrawals of the operational scenarios. The retention time decreased from ~425 days for scenario 1B to ~250 days for scenarios 2F and 2G, and ~175 days for scenario 2E, again because of the much higher inflows and withdrawals of the operational scenarios.
– Alkalinity levels of the withdrawals ranged from ~150-180 mg $CaCO_3$/L across the 4 scenarios. Scenarios 2E (high yield) and 2F (moderate yield maximising springs inputs) were ~10-20 and ~5-10 mg $CaCO_3$/L greater than scenarios 2G (moderate yield maximising RW inputs) and 1B (baseline RW).
– Peak algal biomass was ~20, 15 and ~12 µg chl-a/L for scenarios 2E, 2F and 2G, respectively. Scenario 2G had very similar algal biomass forecasts over the simulation duration as scenario 1B.
– TOC was similar across scenarios in the range of 1-2 mg C/L with scenarios 2E and 2F higher by up to ~0.4 and ~0.2 mg C/L than the very similar levels for 1B and 2G.
– TP was similar between the 4 scenarios at ~0.02 mg P/L, which indicates the strong influence of the average RW concentration of 0.017 mg P/L on the resultant reservoir levels.
– Typically, TN and NO3 were ~1 mg N/L except for peaks up to ~3.5 and ~2.5 mg N/L for scenarios 2E and 2F, respectively, in the third and final year of the operational scenarios due to elevated high NO3 springs inputs. In contrast, scenario 2G (moderate yield maximising RW inputs) was slightly lower by ~0.1 mg N/L over the 3 years to scenario 1B.
– TSS was higher by ~0.2-0.4 mg/L for scenarios 2E and 2F due to higher springs inputs via the inlet relative to scenarios 1B and 2G.,
– Silica increased from seasonal peaks of ~0.5 mg Si/L for scenarios 1B and 2G to up to ~2 and ~1-1.8 mg Si/L for scenarios 2E and 2G, respectively.

Though there is a large increase in the operational discharges into and from the reservoir via the inlet and high draw-off, respectively, between scenario 1B and scenarios 2E-2G, this is not forecasted to dramatically change the WQ dynamics of the reservoir with small to moderate predicted increases in alkalinity, algal biomass, TOC, TN, NO3, TSS and SiO2. The forecasted changes in the withdrawal WQ of these determinands for the 3 operational scenarios relative to scenario 1B are relatively modest.

Lastly, recall that the final year of the simulation of scenarios 2E-2G have the same hydrology as scenario 1B from 1 June 2040 to 31 May 2041. Inspection of Figure 8.2 shows that the WQ of the determinands over this final year of the operational scenarios rapidly converge to the levels of Scenario 1B as expected given the characteristic retention time of ~425 days for the baseline case.

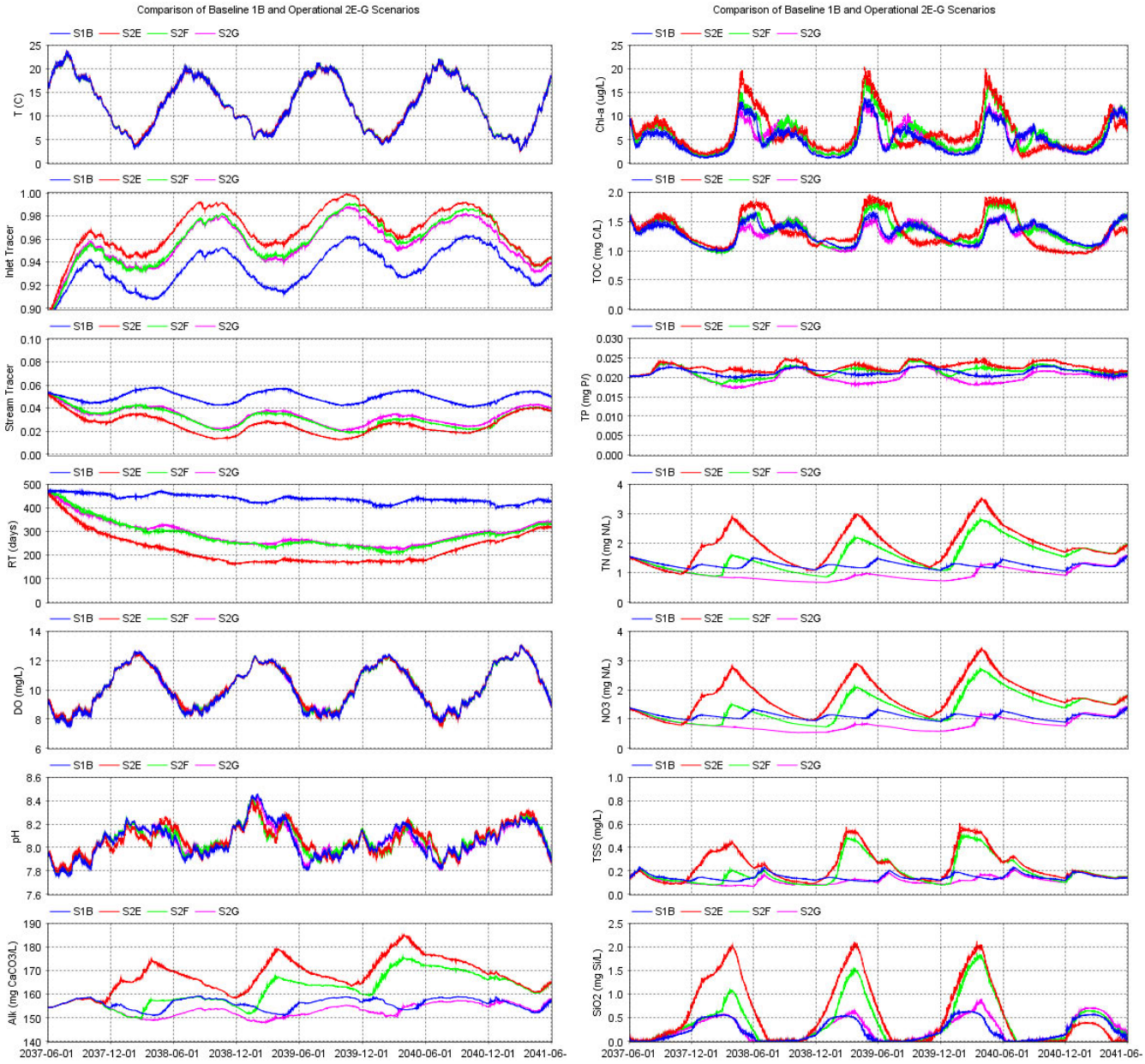

Figure 8.2 ***Comparison of selected hydrodynamic state variables and WQ determinands in the withdrawals from the high draw-off of scenario 1B (baseline); and scenarios 2E-G (variations in operational inputs of springs and recycled water).***

8.3 Scenarios 2H-J: variations in inflows and outflows during emergency drawdown in drought conditions

During emergency drawdown operations in drought conditions, as the reservoir volume (and surface) progressively decreases, the risk of unacceptable short-circuiting of recent RW inputs via the inlet in the south basin near the high and middle draw-offs that withdraw reservoir waters for water supply poses a risk. In this section scenarios 2H (maximum drawdown to ~31 m OD or -8.5 m TWL in December 2039), 2I (maximum drawdown to ~36 m OD or -3.5 m TWL from October-November 2039) and 2J (maximum drawdown to ~37 m OD or -2.5 m TWL from October-November 2039) are compared to baseline scenario 1B to forecast if the risk of short-circuiting is material. Recall that scenarios 2H-J are over nearly a 5 year period from 1 June 2037 to 28 February 2042. A comparison of the forecasted withdrawal WQ of drought scenarios 2H-2J relative to baseline scenario 1B is provided in Figure 8.3 for the same

simulated state variables (determinands) as described for operational scenarios 2E-G in Section 8.2 at/near TWL. Note that the drawdown of the reservoir for scenario 2H from August 2039 to February 2040 necessitated withdrawals from the middle draw-off. At other times during scenario 2H, and at all times for scenarios 2I-2J, withdrawals were from the high draw-off. A summary of the WQ forecasts of the selected determinands across the 4 scenarios include:

– Temperature, DO and pH were nearly equivalent between the 4 scenarios.
– The inlet tracer increased from ~92-96% for scenario 1B to ~94-99% for scenarios 2I and 2J, and ~96-100% for scenario 2H, which simply reflects the much higher RW discharge via the inlet for these drought scenarios. The stream tracer decreased from ~4-6% for scenario 1B to ~1-3% for scenarios 2H-2J, because of the much higher RW and springs inflows, and withdrawals of the drought scenarios. The retention time decreased from ~425 days for scenario 1B to ~150 days for scenarios 2I and 2J, and ~50 days for scenario 2H, again because of the much higher inflows and withdrawals of these drought scenarios. The retention time forecasts indicate that there is sufficient horizontal (~200 m) and vertical (~5 m) separation distance between the RW and springs inlet location and the middle draw-off to eliminate the risk of short-circuiting across the range of scenarios that have been considered in this investigation.
– Alkalinity levels of the withdrawals ranged from ~150-180 mg $CaCO_3$/L across the 4 scenarios. Scenarios 2H (large maximum drawdown) and 2I (moderate maximum drawdown) were ~10-15 and ~5-10 mg $CaCO_3$/L greater than scenarios 2J (low maximum drawdown) and 1B (baseline RW).
– Peak algal biomass was ~22, 17 and ~12 µg chl-a/L for scenarios 2H, 2I and 2J, respectively. Scenario 2J had very similar algal biomass forecasts over the simulation duration as scenario 1B.
– TOC was similar across scenarios in the range of 1-2 mg C/L with scenarios 2H and 2I greater by up to ~0.4 and ~0.2 mg C/L, respectively, than the very similar levels for scenarios 1B and 2J.
– TP was similar between the 4 scenarios at ~0.02 mg P/L, which indicates the strong influence of the average RW concentration of 0.017 mg P/L on the resultant reservoir levels.
– Typically, TN and NO3 were ~1 mg N/L except for peaks up to ~3.5 and ~2.5 mg N/L for scenarios 2H and 2I, respectively, due to elevated high NO3 springs inputs. In contrast, scenario 2J was ~0.2 mg N/L lower than scenario 1B.
– TSS increased by ~0.2-0.4 mg/L for scenarios 2H and 2I due to higher springs inputs via the inlet relative to scenarios 1B and 2J.
– Silica increased from seasonal peaks of ~0.5 mg Si/L for scenarios 1B and 2J to up to ~2 and ~1-1.8 mg Si/L for scenarios 2H and 2I, respectively.

Similar to the findings of the operational scenarios, though there is a large increase in the operational discharges into and from the reservoir via the inlet and high draw-off (and middle draw-off for scenario 2H), respectively, between scenario 1B and drought scenarios 2H-2J, which is not forecasted to dramatically change the WQ dynamics of the reservoir with small to moderate predicted increases in alkalinity, algal biomass, TOC, TN, NO3, TSS and SiO2. The forecasted changes in the withdrawal WQ of these determinands across the 3 drought scenarios relative to scenario 1B are relatively modest. Perhaps most importantly, a minimum retention time of ~50 days was forecast during maximum drawdown of the reservoir for scenario 2H with water extracted from the middle draw-off, which indicates a minimal risk of short-circuiting.

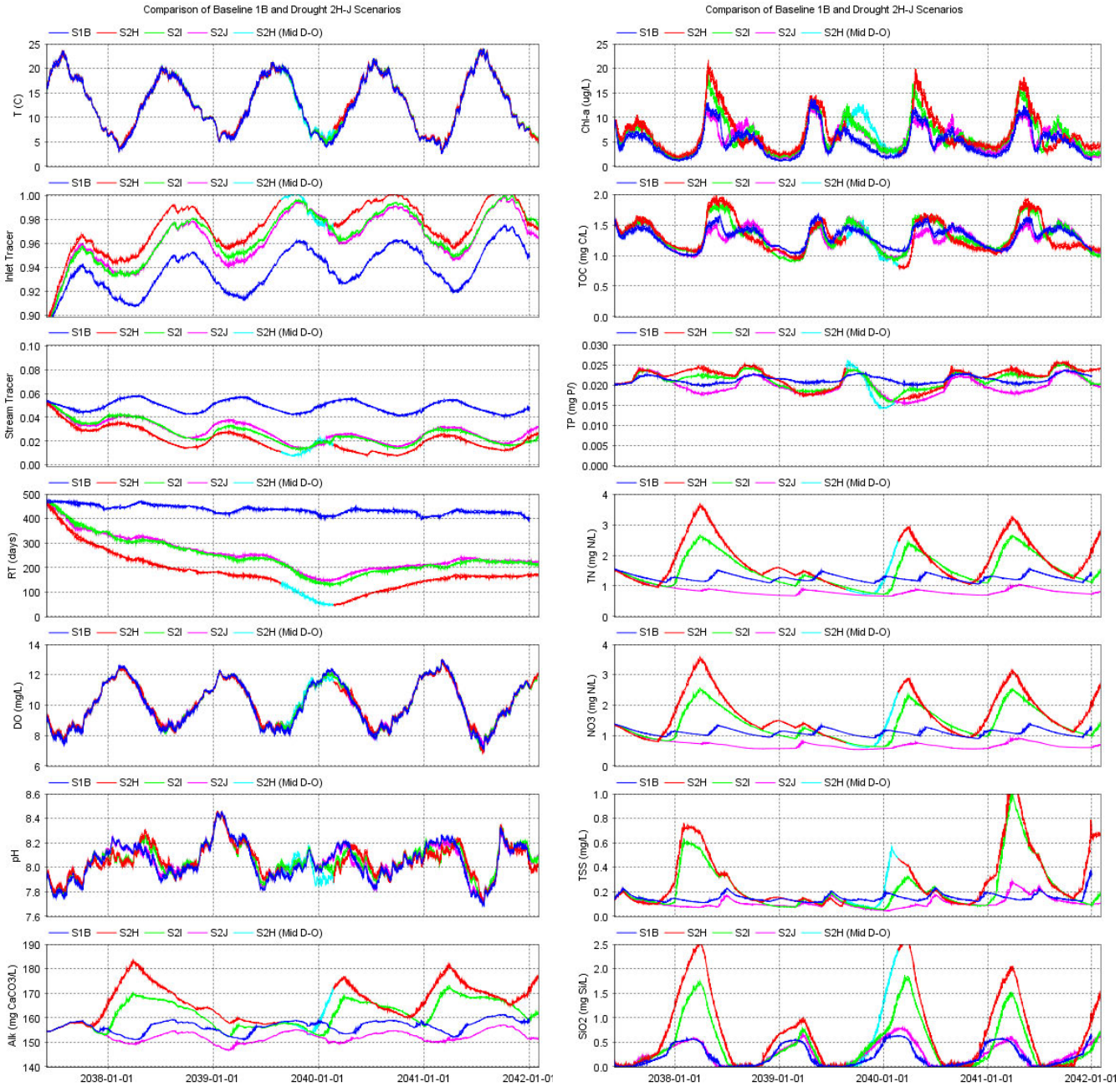

Figure 8.3 ***Comparison of selected hydrodynamic state variables and WQ determinands in the withdrawals of operational scenarios 2H-J during drought conditions and a period of emergency reservoir drawdown for water supply and baseline scenario 1B with nighttime bubbler operations from April-August.***

9. Discussion

9.1 Reservoir bathymetry

The reservoir's bathymetry provides a physical setting for horizontal WQ variability to develop in the deep waters over seasonal stratified periods in the absence of bubbler operations because:

– The sill is a physical barrier that prevents horizontal exchange between the deep waters of the 2 basins with predicted divergence in bottom water WQ in the absence of bubbler operations. In contrast, bubbler operations are forecast to effectively reduce (largely eliminate) spatial WQ variability through maintaining vertical homogeneity throughout the main body of the reservoir.

– Though the north basin (maximum depth ~17 m) will be less deep than the south basin (maximum depth ~22 m), it has a much larger area of deep sediments (i.e. north and south basin areas with depths >15 m ~17.7 ha and ~4.4 ha, respectively) and thereby has potential for greater internal loading via sediment releases.

– However, the larger north basin will also have higher vertical mixing intensity from wind-induced basin scale mixing processes (e.g. internal wave and boundary mixing due to larger size) during seasonal stratification in the absence of bubbler operations. The higher vertical mixing intensity in the north basin is anecdotally illustrated in Figure 6.7 that shows the decrease in DO below the thermocline in the absence of bubbler operations for scenario 1B persists for a shorter duration and remains higher than the south basin. The lower mixing intensity in the south basin is forecast to result in anoxia (DO ~0 mg/L) during seasonal stratification in the absence of bubbler operations with the build-up of elevated concentrations of DFE (~5 mg Fe/L) and DMN (~0.5 mg Mn/L) in the bottom waters relative to the north basin (higher DO maintains DMN of ~0.01 mg Mn/L and DFE of 0 mg Fe/L).

– The south basin's deep hole with a maximum depth of ~-22 m TWL (~17.5 m OD) is the only region of the reservoir that has the potential to develop poor WQ because:

  - Basin scale mixing will not occur over its limited areal extent, so natural ambient rates of mixing will be low.
  - The bubble plume destratification system will be placed at a consistent elevation of ~-17 m TWL (~22.5 m OD) and thereby not promote or influence any material artificial mixing.

  However, volumetrically this south basin deep hole only represents ~1.5% (120 ML) of the reservoir, and therefore is not likely to have a material effect on the overall reservoir and withdrawal WQ.

The current design of the reservoir bathymetry is undergoing updates in effort to source appropriate material for the dam embankments, which will likely include:

– A large channel through the sill between the two basins to a depth of ~-17.5 m (i.e. lake bed elevation of the north basin) TWL that will provide connectivity and a horizontal exchange pathway. This is anticipated to improve the overall reservoir WQ whereby the more highly oxygenated bottom waters of north basin can readily be transported to the south basin's bottom waters.

– Elimination of the south basin's deep hole so that the lake bed is at an elevation of ~-17.5 m TWL (22.5 OD) as the north basin, which will allow:

  - The bubble plume destratification system to effectively maintain vertically well mixed conditions throughout the main body of the reservoir.
  - Natural basin scale mixing processes to function effectively across the entirety of the reservoir's deep bottom waters.

This change to the reservoir bathymetry is anticipated to remove the WQ risks (albeit minor) associated with the current south basin's deep hole.

9.2 Model grid size

A comparison of coarse (50x50x1 m) and fine (20x20x1 m) grid simulations in Section 5 indicate that:

– The predicted reservoir WQ throughout most of the reservoir is in good agreement between the 2 grids except for the south basin's deep hole below -17 m TWL (22.5 m OD). The fine grid simulations are able to resolve the hydrodynamics of this deep hole adequately so that elevated DO and low DMN are predicted to be similar to the bottom waters of the north basin. In contrast, the coarse grid simulation does not adequately resolve the hydrodynamics in the deep hole with insufficient mixing modelled that leads to low DO and elevated sediment DMN fluxes.
– Because the volume of the deep hole below -17 m TWL only represents 1.5% of the reservoir's volume at TWL, the numerical artefact from poor simulated hydrodynamics of this region is muted due to the large degree of dilution that occurs when this poor WQ pool is mixed throughout the water body. As a consequence, the predicted withdrawal WQ is very similar between the grid sizes.
– The poorer simulated WQ in the south basin's deep hole with the coarse grid is conservative in terms of DWSP and environmental considerations relative to the fine grid.

Simulations with the coarse grid are appropriate for the time (~12 years) and space (~1.5 km basin, ~22 m maximum depth) scales of this investigation because model runs are ~2% of the duration of those with the fine grid. It is recommended that any scenarios over long interannual time scales utilise the coarse grid, as temporal and spatial WQ variability is captured adequately.

Simulations with the fine model grid are appropriate for the evaluation of short to moderate duration (<1 year) simulations that require higher spatial resolution. Examples include the GHD (2025a) updates to the bubble plume destratification system and the GHD (2025b) inlet location options analysis, both of which were <1 year simulation duration.

Lastly, the updates to the reservoir morphology will include the removal of the south basin's deep hole as described in Section 9.1. The scenarios in this investigation will likely have to be re-evaluated with the new reservoir morphology. It is anticipated that this new reservoir morphology of the south basin will be a constant ~-17 m TWL across the deepest portion similar to north basin. If so, it is likely that the coarse grid will be able to properly resolve the hydrodynamics across the entire reservoir and WQ comparisons with the fine grid simulation will be nearly equivalent.

9.3 Summary of forecasts

9.3.1 Scenarios 1B and 1BS: fill stage

The 'fill' stage is a less critical period than the 'classic' and 'recycled' stages because the reservoir is unlikely to be used for water supply purposes. However, the withdrawal WQ for downstream compensation flows to Riders Lane Stream needs to be ecologically acceptable. Except for the first year, the stabilisation effect forecast for scenario 1BS during the 'fill' stage is predicted to have ae relatively modest impact on the WQ of the reservoir and withdrawals relative to scenario 1B (no stabilisation effect) as described in Section 7 because:

– The highest stabilisation SOD and dissolved matter (e.g. PON, DON) sediment fluxes will occur during the first year that terrestrial soils, organic matter and vegetation are freshly inundated (see Section 4.5.2). As filling of the reservoir will occur over 3 consecutive winters, these high first year fluxes of freshly inundated areas are spread out over time as different depth bands of the reservoir are filled. This contrasts with many new reservoirs that are filled in a single year whereby the highest SOD and dissolved sediment fluxes occur simultaneously over the entire water body during the first year.
– Relatively low terrestrial vegetation biomass will be inundated because the reservoir's footprint is largely comprised of grassland and the excavation of the borrow pits to create the reservoir embankments will remove much of the terrestrial-derived organic matter (see Section 4.5.2).

Further, nighttime bubbler operations during the 'fill' stage are forecast to maintain a vertically well-mixed reservoir that promotes downward fluxes of atmospheric DO that maintains relatively low sediment fluxes and thereby concentrations of dissolved metals (i.e. DFE, DMN), nutrients (PO4, NH4) and organic matter (DOP, DON and DOC) (Section 7). The first year of the scenario 1BS 'fill' stage with the stabilisation effect is forecast to have a material deleterious impact on the DO throughout most of the reservoir (minimum DO during peak summer T over the entire reservoir surface and north basin bottom waters of 7 and 2 mg/L without and with stabilisation effect, respectively, Figure 7.2). The bottom waters in the south basin's deep hole is the only region of the reservoir that develops very poor WQ (i.e. anoxia for ~3-4 months and DMN up to 0.5 mg Mn/L, see Section 7). The stabilisation effect during the second and third years of the scenario 1BS 'fill' stage throughout the reservoir and bottom waters of south basin's deep hole are much more muted, and similar to the WQ forecasts of scenario 1B without stabilisation effects. In short, nighttime bubbler operations are predicted to maintain elevated DO through the water column and low reduced dissolved metals concentrations over the last two-thirds of the 'fill' stage, and therefore maintain acceptable WQ for releases to Riders Lane Stream and within the reservoir. However, the first year of the 'fill' stage may have unacceptable WQ for environmental compensation flows and will need to be adaptively managed in regards to potential releases to Riders Lane Stream.

9.3.2 Scenario 1B: recycled stage

The scenario 1B 'classic' stage when the reservoir is maintained at/near TWL to serve as an emergency water supply during drought conditions is for only a short duration (1 March 2032 to 30 September 2033, ~1.5 years). Hence, discussion of the 'classic' stage is provided on the basis of 'extended classic' scenario 4A (Section 9.3.3).

The scenario 1B 'recycled' stage extends just over 8 years from 1 October 2033 to 31 December 2041 with continuous RW inputs (~10-20 MLD), episodic springs inputs (~1 month duration via the inlet twice a year at ~15 MLD) and continuous withdrawals (~20 MLD). The reservoir retention time (water age) during the scenario 1B 'recycled' stage attains a quasi-equilibrium value of ~425 days (~1.2 year) (Section 6.1). External TP loads[33] are dominated by RW inputs during the scenario 1B 'recycled' stage, while TN loads are dominated by the episodic high nitrate springs inputs and secondarily by RW inputs (Figure 4.16). Further, the magnitude of external TN and TP loading of N and P will be much greater during the 'recycled' than the 'filling' and 'classic' stages (Figure 4.17), which will be largely offset by external losses from the high continuous withdrawals. HRRM treatment of RW (average TN and TP of 0.67 mg N/L and 0.017 mg P/L, respectively, Table 4.5) prior to discharge into the reservoir via the south basin inlet yields much lower TN and TP concentrations than the springs (TP of 0.03 mg P/L in Table 4.10, NO3 of 6-9 mg N/L in Figure 4.12). The outcome of the variations in the water balance and determinand concentrations of the RW and springs yields very similar reservoir and withdrawal WQ between the scenario 1B 'recycled' stage and the scenario 4A 'extended classic' case (see Figure 8.1).

As noted beforehand, the only region of poor WQ during the scenario 1B 'recycled' stage is the accumulation of high DFE and DMN in the south basin's bottom waters (up to ~-17 m TWL just below the elevation of the bubble plume mixing system) represents only ~1.5% (~120 ML) of the reservoir volume at TWL. Conservatively, assuming no oxidation of this pool of elevated dissolved metals when mixing of this pool occurs during the autumn, a dilution of >50 fold (100%/1.5%) will reduce simulated peaks of DMN (~0.5 mg Mn/L) and DFE (~5 mg Fe/L) to low levels of ~0.01 mg Mn/L and ~0.1 mg Fe/L, respectively, in reasonable agreement with modelled peak withdrawal concentrations (Figure 6.29).

9.3.3 Scenario 4A: extended classic

The extended classic scenario 4A represents the initial operational premise of HTR where the reservoir would be maintained at/near TWL with minimal withdrawals (i.e. continuous withdrawals of ~1 MLD for environmental compensation flows to Riders Lane Stream, and ~3-4 months of ~3 MLD withdrawals for spring-summer 'sweetening flows' to Farlington water treatment plant) and ~1 month 'top-ups' of the reservoir at ~15 MLD with springs water via

[33] External load sources considered were RW, springs, streams, birds and rain.

the inlet (~15 MLD for ~1 winter month per year) (see Section 4.3.1.2.9, are summarised with the extended classic scenario 4A (Section 9.3.3).

Atkins (2020) developed a simple TP mass balance model for operational conditions similar to the 'classic' stage based on stochastic outputs from the PYWR water resources model over a 1,000 year duration that included periods of drought and refill. The most sensitive process was sediment exchange where median TP concentrations varied from ~0.01 mg P/L to ~0.03 mg P/L for no and high sediment flux estimates, respectively. In this investigation, the predicted withdrawal TP for scenario 4A was ~0.03 mg P/L for the 'extended classic' case, which is at the upper range of the Atkins (2020) predictions. Interestingly, the simulated withdrawal TP of ~0.03 mg P/L scenario 4A was nearly equivalent to the springs water input concentrations via the south basin inlet.

As noted in Section 9.3.2, the withdrawal WQ of the extended classic scenario 4A and the 'recycled' stage of scenario 1B are very similar. It is likely that the combination of the nearly 50% lower average RW TP concentration of 0.017 mg P/L relative to that of the springs water of 0.03 mg P/L, and the high external TP losses via the sizeable continuous withdrawals of ~15 MLD, yield similar WQ forecasts for the reservoir and withdrawals.

9.3.4 Scenarios 2E-G: variations in operational discharges of inflows and withdrawals

Increased operational discharges into and from the reservoir for scenarios 2E-G relative to scenario 1B were forecasted to have a relatively modest effect on the baseline 'recycled' stage WQ with small to moderate increases in alkalinity, algal biomass, TOC, TN, NO3, TSS and SiO2. Further, the final year of these operational scenarios utilised the scenario 1B hydrology model inputs, which forecast rapid convergence to WQ concentrations of scenario 1B 'recycled' stage. In short, these operational scenarios demonstrate that increases of the inflows into and withdrawals from the reservoir, and variations in the proportion of source waters (i.e. springs versus RW), have a relatively modest effect on WQ and that the response time to return to baseline WQ with baseline hydrology is on the order of ~1 year.

9.3.5 Scenarios 2H-J: emergency water supply during drought conditions

Similar to operational scenarios 2E-G, though there is a large increase in the operational discharges into and from the reservoir via the inlet and high draw-off (and middle draw-off for scenario 2H), respectively, between scenario 1B and drought scenarios 2H-2J, this is not forecasted to dramatically change the reservoir WQ with small to moderate predicted increases in alkalinity, algal biomass, TOC, TN, NO3, TSS and SiO2. Perhaps most importantly, a minimum retention time of ~50 days was forecast during the period of sizeable reservoir drawdown of the surface to -8.5 m TWL (31 m OD) for scenario 2H with water extracted from the middle draw-off (note minimum surface level for middle draw-off withdrawals is 30 m OD or -9.5 m TWL). This was the most extreme drought scenario considered in terms of drawdown of the surface level, which indicates a minimal risk of short-circuiting with the current reservoir morphology, inlet location and withdrawal operational rules.

9.4 Mixing system: key in-reservoir control measure

The comparisons of the simulated WQ of scenario 1B with and without nighttime bubbler operations demonstrate that this stipulated DWSP in-reservoir control measure is forecast to eliminate seasonal stratification, maintain a well oxygenated reservoir and promote relatively homogeneous WQ in both the south and north main basins. Further, bubbler-induced mixing in the south basin promotes the mixing and dilution of RW and springs water via the inlet in the same basin to maintain acceptable WQ and to reduce the risk of short-circuiting to the high and middle draw-offs. Through maintaining minimal WQ variations through the main body of the reservoir, bubble plume destratification operations also are forecast to provide less short-term variability in the withdrawals for raw water supply and environmental compensation flows. An additional benefit in the elimination of seasonal stratification via bubbler operations is that the competitive advantage of blue-green algae with vertical migration capabilities is greatly reduced,

thereby typically promoting more desirable phytoplankton assemblages. For all of these reasons, bubbler operations has been mandated as the primary in-reservoir control measure in the DWSP to manage WQ.

9.5 Withdrawal WQ envelope

The withdrawal WQ envelope for selected determinands is defined as the range of the maximum and minimum simulated values across all scenarios in this investigation, which is summarised in Table 9.1. The maximum and minimum values were calculated on the basis of 6 hourly model outputs of the simulated withdrawal WQ over the following periods for each of the scenarios:

– Scenarios 1B (baseline) and 4A (extended classic) from 1 January 2034 to 31 December 2041 that corresponds to the ‘recycled’ stage of 1B.
– Scenarios 2E-2G from 1 June 2037-31 May 2040 that corresponds to the 3 years after the onset variations in operational inflow and withdrawal discharge relative to scenario 1B.
– Scenarios 2H-2J from 1 June 2037-31 May 2041 that corresponds to the 4 years after the onset variations in operational inflow and withdrawal discharge in response to drought conditions relative to scenario 1B.

Scenario 4A is the only case that represents the ‘classic’ stage where the WQ envelope for al the other scenarios (1B, 2E-2J) are during the ‘recycled’ stage. The ‘fill’ stage is not reported as withdrawals for water supply will be highly unlikely over this period.

Refer to Section 9.7.1 for recommendations on the use of these withdrawal WQ envelope forecasts.

Table 9.1 ***Withdrawal WQ envelope: maximum and minimum simulated levels of selected determinands (RT, T, S, Chl-a, TN, TP, TOC, BOD, TSS, pH, Alkalinity, Total Fe, Total Mn, Ca, Na, Cl and SO_4) for scenarios 1B and 4A from January 2034-December 2041, 2E-G from June 2037-May 2040, and 2H-J from June 2037-May 2041. WQE is the overall 'water quality envelope' defined as the range of maximum and minimum values of the selected determinands across all scenarios.***

Determinand	Maximum									Minimum								
	1B	4A	2E	2F	2G	2H	2I	2J	WQE	1B	4A	2E	2F	2G	2H	2I	2J	WQE
RT (days)										393	1042	161	205	216	47	128	144	**47**
T (°C)	23.9	24.0	23.6	23.6	23.6	23.6	23.6	23.6	**24.0**	2.7	2.4	3.7	3.6	3.5	2.9	3.0	2.8	**2.4**
S (psu)	0.30	0.26	0.30	0.30	0.30	0.30	0.30	0.30	**0.30**	0.27	0.21	0.28	0.28	0.28	0.28	0.28	0.28	**0.21**
Chl-a (µg/L)	14.4	14.6	20.6	18.6	12.9	21.7	19.0	13.0	**21.7**	0.8	0.4	1.9	1.5	1.6	1.8	1.6	1.5	**0.4**
TN (mg N/L)	2.88	3.14	3.52	2.81	1.58	3.64	2.69	1.58	**3.64**	1.06	0.97	0.95	0.86	0.67	0.73	0.73	0.67	**0.67**
TP (mg P/L)	0.026	0.030	0.025	0.024	0.024	0.026	0.024	0.024	**0.030**	0.020	0.027	0.020	0.018	0.017	0.014	0.016	0.015	**0.014**
TOC (mg C/L)	1.7	1.9	2.0	1.9	1.6	2.0	1.9	1.6	**2.0**	0.8	0.9	1.0	1.0	1.0	0.8	0.9	0.9	**0.8**
BOD (mg/L)	3.4	4.2	3.7	3.6	3.4	3.8	3.7	3.4	**4.2**	1.9	2.2	2.3	2.3	2.3	1.8	2.1	2.2	**1.8**
SS_{Inorg} (mg/L)	0.4	0.2	0.6	0.5	0.2	1.3	1.1	0.3	**1.3**	0.1	0.1	0.1	0.1	0.1	0.1	0.1	0.0	**0.1**
SS_{Total} (mg /L)[34]	2.0	1.9	2.8	2.5	1.7	3.0	2.7	1.8	**3.0**	0.6	0.5	0.8	0.6	0.6	0.6	0.6	0.6	**0.5**
pH	8.5	8.5	8.4	8.4	8.4	8.5	8.5	8.5	**8.5**	7.7	7.7	7.8	7.8	7.8	7.8	7.8	7.8	**7.7**
Alkalinity (mg $CaCO_3$/L)	191	198	185	175	158	183	174	158	**198**	150	139	154	150	148	153	152	147	**139**
Total Fe (mg Fe/L)	0.110	0.107	0.077	0.104	0.152	0.124	0.105	0.148	**0.152**	0.024	0.017	0.025	0.025	0.025	0.025	0.025	0.025	**0.017**
Total Mn (mg Mn/L)	0.014	0.012	0.012	0.015	0.020	0.019	0.014	0.020	**0.020**	0.004	0.002	0.005	0.005	0.005	0.005	0.005	0.005	**0.002**
Ca (mg Ca/L)	91.0	96.5	82.7	76.7	64.9	81.8	75.7	64.9	**96.5**	61.8	68.4	62.7	60.3	58.6	60.3	60.2	57.8	**58.6**
Na (mg Na/L)	11.4	12.2	12.5	12.1	11.9	13.0	12.3	12.3	**13.0**	9.8	10.8	9.8	9.6	9.5	7.7	8.8	8.6	**7.7**
Cl (mg Cl/L)	21.4	25.5	17.8	16.6	16.4	17.8	17.0	16.6	**25.5**	14.2	22.8	14.6	13.1	12.8	11.4	11.6	11.1	**11.4**
SO_4 (mg S/L)	5.4	7.2	3.1	2.5	1.8	3.1	2.4	1.8	**7.2**	1.1	6.3	0.7	0.7	0.5	0.3	0.4	0.3	**0.3**

[34] SS_{Total} estimated as SS_{Inorg} + POC x 2 mg/1 mg C + Chl-a x 0.001 mg chl-a/µg chl-a x 40 mg C/mg chl-a x 2 mg/mg C

9.6 Assessment of WQ Forecasts with The Water Framework Directive (England and Wales) 2015

9.6.1 Approach

The Water Framework Directive (WFD) objective is for all water bodies to attain 'good ecological status' by 2027. For Heavily Modified Water Bodies (HMWB) like the Hermitage Stream catchment (of which Riders Lane Stream is a tributary) the objective is to attain 'good ecological potential', which also requires the successful implementation of HMWB Mitigation Measures.

Only the Environment Agency can formally calculate the WFD water body status, and where data exist this is normally based on 3 years of monitoring. Refer to the end of this section for the HTR locations where the WFD water body status of the withdrawals (for discharge to Riders Lane Stream) and reservoir is evaluated. The forecasted WQ from 2027-2041 was estimated on a year-by-year basis with The Water Framework Directive (Standards and Classification) Directions (England and Wales) 2015 ('the WFD Directions').

It has been assumed that HTR will, in future, be considered as a WFD 'lake' water body, whilst the Hermitage Stream and its tributaries (i.e. Riders Lane Stream) will remain a HMWB. The 2015 WFD Directions provide numeric standards (or methods to calculate) of a determinand to delineate as a 'high', 'good', 'moderate' and 'poor' water body status. In this assessment, a fifth status category was included, namely 'bad', which is consistent with WFD-UKTAG (2014) where the defined standards for 'high', 'good', 'moderate' and 'poor' water body status represent the boundaries (e.g. if TP metric>high standard then high status water body, if good standard<TP metric<high standard then good status water body, if TP metric<poor standard then bad status water body). The scheme in Table 9.2 was used to categorise a water body's status in terms of a determinand's standards in this investigation.

Table 9.2 Categorisation scheme of a water body's status on basis of the 2015 WFD Direction's standards.

Status	River Determinands of T, BOD, NH_X, PO_4 Lake Determinands of TP & NH_X	River Determinand of DOSAT Lake Determinands of DO & EQR_{Chl-a}
High	Metric < High Standard	Metric > High Standard
Good	High Standard > Metric > Good Standard	High Standard > Metric > Good Standard
Moderate	Good Standard > Metric > Moderate Standard	Good Standard > Metric > Moderate Standard
Poor	Moderate Standard > Metric > Poor Standard	Moderate Standard > Metric > Poor Standard
Bad	Metric > Poor Standard	Metric < Poor Standard

The 2015 WFD Directions default to WFD-UKTAG (2014) for evaluation of the biological status in lakes. The WFD-UKTAG (2014) Ecological Quality Ratio for Phytoplankton Biomass (EQR_{Chl-a}) metric on the basis of chl-a was evaluated here. The EQR for Phytoplankton Trophic Index (EQR_{PTI}) requires species level measurements which cannot be evaluated here as only three generic algal groups were modelled. The EQR for Cyanobacteria Bloom Intensity (EQR_{Cyan}) requires greater certainty in predicted blue-green algal levels than those in this investigation. As the modelling framework here only provides credible forecasts of total algal biomass as chl-a (see Section 1.4), the EQR_{Chl-a} is adopted as the only in-lake biological standard.

For river assessments, the 2015 WFD Directions stipulate that metrics on the basis of measured (or modelled) concentrations are compared to a determinand's standards. The forecasted withdrawals, primarily from the high draw-off, are used in this assessment.

For lake assessments, the 2015 WFD Directions stipulate that metrics on the basis of measured (or modelled) concentrations through the water column (except for DO where if the lake stratifies then a representative hypolimnetic value is to be used) are compared to a determinand's standards. In this investigation a simplified and conservative approach is adopted whereby:

– The annual metric for the $EQC_{Chl\text{-}a}$ is based on the simulated surface layer chl-a concentration at 2 deep water locations (at/near maximum depths) in the south and north basins. This is a conservative measure as chl-a is generally higher at the surface than at depth (i.e. metric value will be greater for the surface than through the water column).
– The annual metrics for the determinands of TP and NH_X are based on simulated surface layer concentrations as this is typically the monitoring depth on which metrics are based (P. Daldorph, pers. comm.).
– The annual metric for DO is based on the simulated bottom layer concentrations of the south (maximum depth of 22 m) and north (maximum depth of 17.5 m) basins. In the absence of bubbler operations during seasonal stratification the WQ of the deep waters of the two basins are forecast to diverge (Section 9.3.2), hence evaluation of both basins. This is a highly conservative measure as typically bottom layer DO levels in the south basin are the lowest in the reservoir in the absence of bubbler operations during seasonal stratification.

9.6.2 Environmental compensation flow releases

The river standards and status categorisation of the 2015 WFD Directions relevant to forecasts of HTR withdrawals (as environmental compensation flows to Riders Lane Stream) are summarised in Table 9.3, Table 9.4, Table 9.5,

Table 9.6, Table 9.7 and Table 9.8 for the determinands of DOSAT, BOD, total ammonia (NH_X), pH, filterable reactive phosphorus (FRP or PO_4) and temperature (T), respectively. Standards for acid neutralising capacity (ANC) were not evaluated here due to the very low risk of acidification in the future reservoir.

Table 9.3 WFD river categorisation and standards for determinand DOSAT.

	WFD Sch. 2, Sec. 1, Table 1: River Categorisation for DO_{sat} Standard		WFD Sch. 3, Part 1, Sec. 1, Table 1: DOSAT (%) Standard of Rivers (Annual 10th Percentile)				
Stage	**River Type**	**Criteria Summary**	**High**	**Good**	**Moderate**	**Poor**	**Bad**
Classic	Type 7	Alkalinity >200 mg $CaCO_3$/L	70	60	54	45	
Recycled	Type 5	Elevation <80 m Alkalinity 100-200 mg $CaCO_3$/L	70	60	54	45	
Standard Implementation Rules ->			≥70	≥60 & <70	≥54 & <60	≥45 & <54	*<45*

Table 9.4 As Table 9.3 for determinand BOD.

	WFD Sch. 2, Sec. 1, Table 1: River Categorisation for BOD Standard		WFD Sch. 3, Part 1, Sec. 1, Table 2: BOD (mg/L) Standard of Rivers (Annual 90th Percentile)				
Stage	**River Type**	**Criteria Summary**	**High**	**Good**	**Moderate**	**Poor**	**Bad**
Classic	Type 7	Alkalinity >200 mg $CaCO_3$/L	4	5	6	7.5	
Recycled	Type 5	Elevation <80 m Alkalinity 100-200 mg $CaCO_3$/L	4	5	6	7.5	
Standard Implementation Rules ->			≤4	>4 & ≤5	>5 & ≤6	>6 & ≤7.5	>7.5

Table 9.5 As Table 9.3 for determinand NH_X.

	WFD Sch. 2, Sec. 1, Table 1: River Categorisation for NH_X Standard		WFD Sch. 3, Part 1, Sec. 1, Table 7: NH_X (mg N/L) Standard of Rivers (Annual 90th Percentile)				
Stage	**River Type**	**Criteria Summary**	**High**	**Good**	**Moderate**	**Poor**	**Bad**
Classic	Type 7	Alkalinity >200 mg $CaCO_3$/L	0.3	0.6	1.1	2.5	
Recycled	Type 5	Elevation <80 m Alkalinity 100-200 mg $CaCO_3$/L	0.3	0.6	1.1	2.5	
Standard Implementation Rules ->			≤0.3	>0.3 & ≤0.6	>0.6 & ≤1.1	>1.1 & ≤2.5	>2.5

Table 9.6 As Table 9.3 for determinand pH.

	WFD Sch. 3, Part 1, Sec. 1, Table 3: River Categorisation for pH Standard	
Stage	**High & Good (Annual 5th Percentile)**	**High & Good (Annual 95th Percentile)**
Classic & Recycled	6	9
Standard Implementation Rules ->	≥6	≤9

Table 9.7 As Table 9.3 for determinand FRP (PO_4).

	WFD Sch. 3, Part 1, Sec. 1, Table 5: FRP [PO_4] (mg P/L) Standard of Rivers (Annual Mean)				
Stage	**High**	**Good**	**Moderate**	**Poor**	**Bad**
Classic & Recycled	0.048	0.088	0.210	1.086	
Standard Implementation Rules ->	≤High	>High & ≤Good	>Good & ≤Moderate	>Moderate & <Poor	≥Poor

Table 9.8 As Table 9.3 for determinand T.

	Categorisation of River by Potential Fishery	WFD Sch. 3, Part 1, Sec. 1, Table 6: T (°C) Standard of Rivers (Annual 98th Percentile)				
Stage	**River Type**	**High**	**Good**	**Moderate**	**Poor**	**Bad**
Classic & Recycled	Cyprinid Fishery	25	28	30	32	
Standard Condition Rules ->		≤25	>25 & ≤28	>28 & ≤30	>30 & ≤32	>32

Application of the 2015 WFD Directions river standards to the forecasted WQ of the withdrawals across a range of simulations on an annual basis up to 12 years (i.e. simulation duration of scenario 1B) is summarised Appendix C. Application of the 2015 WFD Directions river standards to the forecasted withdrawals across the scenarios of this investigation over appropriate periods for each scenario is summarised in Table 9.9. All determinands meet a 'high' water body status except for BOD for the scenario 4A extended classic case. However, the WFD Directions stipulate BOD is not be used in classifying the status of water bodies.

Table 9.9 River water body status assessment of withdrawals over appropriate periods for each scenario.

Scenario	Years	DO_{Sat} (%) - Annual 10th %ile	BOD– (mg/L) - Annual 90th %ile	NH_x (mg N/L) Annual 90th %ile	pH Annual 5th %ile	pH Annual 95th %ile	FRP (mg P/L) Annual mean	T (°C) Annual 98th %ile
1	2036-41[35]	90	3.2	0.033	7.8	8.3	0.004	22.6
4A		89	4.0	0.054	7.8	8.3	0.005	22.7
2E	2038-39[36]	91	3.5	0.024	7.9	8.3	0.005	20.9
2F		91	3.3	0.027	7.9	8.3	0.004	20.9
2G		91	3.2	0.027	7.9	8.3	0.004	20.8
2H	2038-41[37]	91	3.4	0.023	7.9	8.3	0.005	22.5
2I		91	3.4	0.025	7.9	8.2	0.004	22.6
2J		91	3.2	0.025	7.8	8.2	0.004	22.6

9.6.3 Reservoir

The lake standards and status categorisation of the 2015 WFD Directions relevant for the reservoir are summarised in Table 9.10, Table 9.11, Table 9.12 andTable 9.13 for the determinands of TP, NH_X, DO and $EQR_{Chl\text{-}a}$, respectively.

[35] Summary metrics over 6 years (2036-2041) of long 12 and ~8 year simulation durations of scenarios 1B and 4A, respectively.
[36] Summary metrics over 2 years (2038-2039) of short 3 year simulation durations of scenarios 2E-G.
[37] Summary metrics over 4 years (2038-2041) of moderate ~5 year simulation durations of scenarios 2H-J.

Table 9.10 WFD lake categorisation and Standards for determinand TP.

	WFD Sch. 2, Sec. 2, Table 5: Lake Categorisation for TP Standard	WFD Sch. 3, Part 1, Sec. 2, Table 5: TP (µg P/L) Standard of Lakes (Annual Mean)				
Stage	**Lake Type**	**High**	**Good**	**Moderate**	**Poor**	**Bad**
Classic & Recycled	High Alkalinity, Shallow, Region 2[38]	25	35	70	140	
Standard Implementation Rules ->		≤25	>25 & ≤35	>35 & ≤70	>70 & <140	≥140

Table 9.11 WFD lake categorisation and Standards for determinand NH_X.

	WFD Sch. 2, Sec. 2, Table 1: Lake Categorisation for NH_X Standard		WFD Sch. 3, Part 1, Sec. 2, Table 9: NH_X (mg N/L) Standard of Lakes (Annual 90th Percentile)				
Stage	**River Type**	**Criteria Summary**	**High**	**Good**	**Moderate**	**Poor**	**Bad**
Classic	Type 7	Alkalinity >200 mg $CaCO_3$/L	0.3	0.6	1.1	2.5	
Recycled	Type 5	Elevation <80 m Alkalinity 100-200 mg $CaCO_3$/L	0.3	0.6	1.1	2.5	
Standard Implementation Rules ->			≤0.3	>0.3 & ≤0.6	>0.6 & ≤1.1	>1.1 & ≤2.5	>2.5

Table 9.12 WFD lake categorisation and Standards for determinand DO.

	Categorisation of Lakes by Potential Fishery	WFD Sch. 3, Part 1, Sec. 2, Table 18: DO (mg/L) Standard of Lakes (Annual Mean July/August)				
Stage	**River Type**	**High**	**Good**	**Moderate**	**Poor**	**Bad**
Classic & Recycled	Cyprinid Fishery	8	6	4	1	
Standard Condition Rules ->		≥8	≥6 & <8	≥4 & <6	≥1 & <4	<1

Table 9.13 UKTAG-WFD (2014) lake categorisation and Standards for $EQR_{Chl\text{-}a}$.

	UKTAG-WFD (2014) Lake Categorisation for EQR_{Chla}	UKTAG-WFD (2014) S Table 3: $EQR_{Chl\text{-}a}$ of Lakes (Annual Basis)				
Stage	**Lake Type**	**High**	**Good**	**Moderate**	**Poor**	**Bad**
Classic & Recycled	High Alkalinity, Shallow[39]	0.55	0.32	0.16	0.05	
Standard Implementation Rules ->		≥0.55	≥0.32 & <0.55	≥0.16 & <32	≥0.05 & <0.16	*<0.05*

Application of the 2015 WFD Directions lake standards to the forecasted WQ of the north and south basins across a range of simulations on an annual basis up to 12 years (i.e. simulation duration of scenario 1B) is summarised in Appendix D. Application of the 2015 WFD Directions lake standards to the forecasted WQ of the north and south basins over an appropriate period for each scenario is summarised in Table 9.14. The general findings include:

– NH_X in both basins is forecast to meet always high status across all scenarios.
– TP was forecast with a high status for all scenarios except for the extended classic scenario 4B with a good status.
– DO was forecast with a high status in the north basin for all scenarios except the extended classic scenarios with a good status. In contrast, the bottom waters in the deep south basin hole had a moderate-good status across years, which is likely due to poor simulated hydrodynamics in this region of the reservoir with the model (see Section 9.2).
– $EQR_{Chl\text{-}a}$ is forecast to have high status for scenarios 1B, 4A, 2G and 2J. whereas the two high inflow and withdrawal discharge scenaros (2E and 2H) have a good status in both basins.

[38] High alkalinity >1,000 uEq/L, shallow is lake with 3-15 m depth (HTR 8.7 m), region 2 same as Bewl Water in WFD Schedule 6.
[39] High alkalinity >1 mEq/L, shallow is lake with mean depth of 3-15 m, and lake with this classification has a colour <30 HU.

Table 9.14 ***Lake water body status assessment for scenarios over appropriate years ($Bottom_{SB}$=maximum depth layer of south basin, $Bottom_{NB}$=maximum depth layer of north basin, $Surface_{SB}$=surface layer of south basin, $Surface_{NB}$=surface layer of north basin) with metrics determined over the final 6 years of each scenario (2036-2041).***

Scenario	Years	$Surface_{SB}$ NH_x (mg N/L) Annual 90th %ile	$Surface_{NB}$ NH_x (mg N/L) Annual 90th %ile	$Surface_{SB}$ TP (µg P/L) Annual Mean	$Surface_{NB}$ TP (µg P/L) Annual Mean	$Bottom_{SB}$ DO (mg/L) - Annual July-August	$Bottom_{NB}$ DO (mg/L) - Annual July-August	$Surface_{SB}$ Annual EQR_{Chl-a}	$Surface_{NB}$ Annual EQR_{Chl-a}
1B	2036-41[35]	0.033	0.033	21	21	5.5	8.0	0.72	0.71
4A		0.054	0.054	28	28	5.4	7.9	0.98	0.97
2E	2039-40[36]	0.029	0.023	21	23	6.8	8.3	0.54	0.53
2F		0.026	0.026	21	21	6.3	8.3	0.54	0.61
2G		0.025	0.025	20	19	6.4	8.4	0.64	0.64
2H	2038-41[37]	0.023	0.023	20	20	6.3	8.1	0.52	0.51
2I		0.024	0.025	21	21	5.9	8.1	0.55	0.55
2J		0.025	0.025	20	20	6.1	8.2	0.61	0.61

9.7 Recommendations

9.7.1 Use of modelling outcomes for DWSP and environmental regulatory purposes

There are uncertainties in the forecasts of this investigation as model calibration-validation could not be carried out on a reservoir that does not yet exist (Sections 1.4, 2.1.2 and 4.5.1). However, use of literature-based model parameter values (Appendix B), implementation of an industry-standard model for lakes and reservoirs (Section 2.2), and model inputs on the basis of the best available information (Section 4), all provide a degree of credibility in regards to the predicted withdrawal WQ across a range of operational ('fill', 'classic' and 'recycled' stages) regimes.

Recognising that DWSP is generally qualitative in nature that relies largely on professional judgement and experience, the forecasted withdrawal WQ from this investigation provides additional quantitative information to support this traditional approach. The predicted withdrawal WQ at 6 hourly intervals for all of the simulated state and derived variables have been provided in digital format to PW and SW for these purposes, and to allow further evaluation of the WQ envelope (Section 9.5) and the ecological status of the withdrawals for compensation flows (Section 9.6).

Because the reservoir will be filled over 3 consecutive winters, high SOD and sediment fluxes of DIM and DOM due to the stabilisation effect are staggered in time, which diminishes its influence on generating poor WQ in the reservoir and withdrawals relative to a case where the reservoir is filled in 1 year. Hence, the stabilisation effect on the reservoir is forecasted to be minor and of relatively short duration.

9.7.2 Use of modelling outcomes for in-reservoir and downstream environmental release regulatory compliance

In addition to the provision of the forecasted withdrawal WQ time series in digital format (Section 9.7.1), the predicted reservoir WQ at ~4 m intervals through the water column at 2 deep water locations in the north and south basins have also been provided in digital format to SW and PW to further inform in-reservoir environmental considerations. An initial assessment of the WQ ecological status of the reservoir on the basis of the 2015 WFD Directions is provided in Section 9.6. This information is provided in this report as a summary of the modelling findings in a format suitable for further evaluation of the ecological status of the reservoir (Section 9.6.3) and the withdrawals to serve as environmental compensation flows (Section 9.6.2).

9.7.3 Final modelling update of scenarios

As described in Section 9.1, the current design of the reservoir bathymetry is undergoing further updates. Upon finalisation of the reservoir bathymetry design, it is recommended that the scenarios in this investigation are re-run and provided in a Final Update Report.

10. References

Absalon D, M Matysik, A Woznica, B Lozowski, W Jarosz, R Ulanczyk, A Babzynska & A Paserbinski (2020) Multi-Faceted Environmental Analysis to Improve the Quality of Anthropogenic Water Reservoirs (Paprocany Reservoir Case Study). Sensors (20) 2626; doi:10.3390/s20092626.

Allan M, DP Hamilton & K Muraoka (2018) A coupled hydrodynamic-ecological model to test management options for restoration of lakes Onoke and Wairarapa. Environmental Research Institute Report No. 111. Prepared for Greater Wellington Regional Council by The University of Waikato, Hamilton, New Zealand.

Atkins (2020) Water quality modelling report. Havant Thicket Reservoir Project Environmental Statement Volume Appendix A15.3. Prepared for Portsmouth Water. Doc No HTR-ATK-RZ-RE-RP-Z-0008 Rev C02. 1 September 2020.

Atkins (2021) Havant Thicket Reservoir Project - MRW+ Volume 2 Scope Document. Prepared for Portsmouth Water Ltd. Doc No HTR-ATK-RZ-RE-SP-Z-0001. April 2021. Version C02.

Beutel MW (2003) Hypolimnetic Anoxia and Sediment Oxygen Demand in California Drinking Water Reservoirs, Lake and Reservoir Management, 19:3, 208-221, DOI: 10.1080/07438140309354086.

Beutel M & IA Hannoun (2007) Evaluation of hypolimnetic oxygen demand in a large eutrophic raw water reservoir, San Vicente Reservoir, Calif. J. Env. Eng. 133(2):130-138.

Brodzeller J & P McGinley (2016) A CE-QUAL-W2 model for dissolved oxygen in the Big Eau Pleine Reservoir, Wisconson USA. Report prepared for Big Eau Pleine Citizens Organisation. https://www3.uwsp.edu/cnr-ap/watershed/Documents/BEP_FinalReport_Draft_July11_2016.pdf.

Bruce LC, DP Hamilton, J Imberger, G Gal, M Gophen, T Zohary & KD Hambright (2006) A numerical simulation of the role of zooplankton in C, N and P cycling in Lake Kinneret, Israel. Ecol. Model. 193:412-436.

Butler, JN (1982) Carbon dioxide equilibria and their applications. Addison-Wesley, Massachusetts, USA.

Caramatti I (2021) 3D modelling of spatiotemporal variability of ice cover, water exchange and phytoplankton distribution in lower Lake Constance. PhD Dissertation. University of Konstanz. 2021.

Cerco CF & TM Cole (1994) Three-dimensional eutrophication model of Chesapeake Bay. Volume 1: Main Report. Prepared for USEPA and USACE. Technical Report EL-94-4. 658 pp.

Chung EU, FA Bombardelli & SG Schladow (2009) Modelling linkages between sediment resuspension and water quality in a shallow, eutrophic, wind-exposed lake. Ecol. Model. 220: 1251-1265.

Cui Y, Z Guangwei, H Li, L Luo, X Cheng, Y Jin & D Trolle (2016) Modelling the response of phytoplankton to reduced external nutrient load in a subtropical Chinese reservoir using DYRESM-CAEDYM, Lake and Reservoir Management, 32:2, 146-157, DOI: 10.1080/10402381.2015.1136365/.

Dallimore C, BR Hodges & J Imberger (2003) Coupling an underflow model to a 3D hydrodynamic model. ASCE Journal of Hydraulic Engineering. 129(10):748-757. **http://doi.org/10.1061/(ASCE)0733-9429(2003)129:10(748)**.

Droop, MR (1974) The nutrient status of algal cells in continuous culture. J. Mar. Biol. Assoc. UK 54, pp. 825–855.

Ghane A (2022) Phosphorus and oxygen dynamics between fall and spring turnover events in a small Canadian shield lake. PhD Dissertation at Civil Engineering Department of Queen's University, Kingston, Ontario, Canada. February 2022.

Gharehchaman BZ (2021) Three-dimensional hydrodynamic and ecosystem modeling of warm-monomictic reservoirs (Maroon and Abolabbas, Iran) under the impact of 21st century climate change. PhD Dissertation. University of Kassel. November 2021.

GHD (2023) Havant Thicket Reservoir water quality modelling report – evaluation of the concept design of the bubble plume destratification system. Prepared for Future Water MJJV Limited. April 2023.

GHD (2024) Havant Thicket Reservoir: Water quality modelling of recycled water inputs. Prepared for Future Water MJJV Limited. June 2024.

GHD (2025a) Havant Thicket Reservoir water quality modelling report – Update of concept design of the mixing system. Prepared for Future Water MJJV Limited. April 2025.

GHD (2025b) Havant Thicket Reservoir water quality modelling report – Outfall location options analyses. Prepared for Future Water MJJV Limited. April 2025.

GHD (2025c) Havant Thicket Reservoir Project – Comparative analysis of GHD (2024) Scenarios 1 and 4 with updates to model and water quality inputs. Technical Memorandum prepared for Future Water MJJV Limited. May 2025.

Gorka, M, SE Sauer, D Lewicka-Szczebak & J Mriusz-Orion (2011) Carbon isotope signature of dissolved inorganic carbon (DIC) in precipitation and atmospheric CO_2. Environmental Pollution 159: 294-301.

Gunnison D, JH Brannon, RL Chen, I Smith Jr & TC Sturgis (1984) Richard B. Russel Dam and Reservoir: potential water quality effects of initial filling and decomposition of vegetation. Miscellaneous Paper E-84-2 by USACE Waterways Experiment Station Environmental Laboratory.

Hipsey, MR & DP Hamilton (2008) Computational Aquatic Ecosystem Dynamics Model: CAEDYM v3. Prepared by Centre for Water Research, University of Western Australia. November 2, 2008.

Hodges B & C Dallimore (2023) Aquatic Ecosystem Model: AEM3D – v1.2 Hydrodynamics Science Manual. Prepared for HydroNumerics. 29 September 2023.

Hodges BR, J Imberger, A Saggio & KB Winters (2000) Modeling basin-scale internal waves in a stratified lake. Limnol. Oceanogr. 45(7):1603-1620.

Jellison R & JM Melack (1993) Meromixis and vertical diffusivities in hypersaline Mono Lake, California. Limnol. Oceanogr. 38:1008–1019.

Johnson C, M Ulrich, L Sigg & D Imboden (1991) A mathematical model of the manganese cycle in a seasonally anoxic lake. Limnol. Oceanogr. 36(7):1415-26.

Jones, HD, S Ozkundakci, S Kochendoerfer, C McBride & D Hamilton (2014) Lake Rotokakahi water quality modelling. ERI Report 32 by University Waikato for Bay of Plenty Regional Council.

Krueger KM, CE Vavrus, ME Lofton, RP McClure, P. Gantzer, CC Carey & ME Schreiber (2020) Iron and manganese fluxes across the sediment-water interface in a drinking water reservoir. Water Research 182:1-14.

Lee, C, DJ Scwab, D Bletsky, J Stroud & B Lesht (2007) Numerical modelling of mixed sediment resuspension, transport, and deposition during the March 1998 episodic events in southern Lake Michigan. J Geophy Res 112, C02018, doi:10.1029/2005JC03491.

McBride, CG, K Muraoka & D Hamilton (2016) A water quality model of Lake Tkitapu. ERI Report 71 by University of Waikato for Bay of Plenty Regional Council.

McBride, CG, MG Allan & D Hamilton (2019) Assessing the effects of nutrient load reductions to Lake Roturua: Model simulations for 2001-2015. ERI Report 124 by University of Waikato for Bay of Plenty Regional Council.

Missaghi S & M Hondzo (2010) Evaluation and application of a three-dimensional water quality model in a shallow lake with complex morphometry. Ecological modelling 221:1512-1525.

Munger, ZW, CC Carey, AB Gerling, KD Hamre, JP Doubek, SD Klepatzki, RP McClure & ME Schreiber (2016) Effectiveness of hypolimnetic oxygenation for preventing accumulation of Fe and Mn in a drinking water reservoir. Wat. Res 106:1-14.

Neal, C, M Neal, B Reynolds, SC Maberly, L May, RC Ferrier, J Smith & JE Parker (2005) Silicon concentrations in UK waters. J Hydrology 304:75-93.

Neretin LN, C Pohl, G Jost, T Leipe & F Pollehne (2003) Manganese cycling in the Gotland Deep, Baltic Sea. Mar. Chem. 82(3-4) 125-43.

Pickering S (1994) Prospect Reservoir sediment metal and nutrient release studies. Australian Water and Technology Report DSQ11WS, Sydney, Australia.

Rhee, GY & EJ Gotham (1981) The effect of environmental factors on phytoplankton growth: temperature and the interactions of temperature with nutrient limitation. Limnol. Oceanogr. 26:635–648.

Riley, JP & G Skirrow (1974) Chemical Oceanography Academic Press, London.

Romero JR, JP Antenucci & J Imberger (2004) One- and three-dimensional biogeochemical simulations of two differing reservoirs. Ecol. Model. 174:143-160.

Saddek T & X Casamitjana (2015): Application of the DYRESM–CAEDYM model to the Sau Reservoir situated in Catalonia, Spain, Desalination and Water Treatment, DOI: 10.1080/19443994.2015.1053530.

Scott JT & SD Patterson (2022) Lake Wister Water Quality Modelling in Support of Nutrient and Sediment TMDL Development. Report Prepared for Poteau Valley Improvement Authority and Oklahoma Department of Environmental Quality. 5 July 2022. pvia.org/lake-modeling-report-final.

Stantec (2022) Technical Note: Analysis of Nutrient Input from Birds using the [Havant Thicket] reservoir. 31 March 2022.

Steinsberger T, B Muller, C Gerber, B Shafei & M Schmid (2019) Modeling sediment oxygen demand in a highly productive lake under various trophic scenarios. PLoS ONE 14(10): e0222318. **https://doi.org/10.1371/journal.pone.0222318**.

Stuart, ME & PL Smedley (2009) Baseline groundwater chemistry: the Chalk aquifer of Hampshire. British Geological Survey Open Report. OR/09/052 61 pp.

Suranjana S, S Morrthi, X Wu, J Wang, S Nadiga, P Tripp, D Behringer, YT Hou, HY Chuang, M Iredell, M Ek, J Meng, R Yang, MP Mendez, H Van Den Dool, Q Zhang, W Wang, M Chen & E Becker (2014). The NCEP Climate Forecast System Version 2. Journal of Climate, Volume 27, pp 2185-2208.

Trammer AW, CL Marti, D Tonina, R Benjankar, D Weigel, L Vihena, C McGrath, P Goodwin, M Tiedmann, J McKean & J. Imberger (2018) A hierarchical modelling framework for assessing physical and biochemical characteristics of a regulated river. Ecol. Model. 368: 78-93.

Trolle D, H Skovgaard & E. Jeppesen (2008) The Water Framework Directive: Setting the phosphorus loading target for a deep lake in Denmark using the 1D lake ecosystem model DYRESM–CAEDYM. Ecol. Model. (2008), doi:10.1016/j.ecolmodel.2008.08.005.

Urban NR, C Dinkel & B Wehrli (1997) Solute transfer across the sediment surface of a eutrophic lake: I. Porewater profiles from dialysis samplers. Aquat. Sci. 59(1), 1-25.

Wang M, BZ Houlton, S Wang, C Ren, HJM van Grinsven, C Chen, J Xu & B Gu (2021). Human-caused increases in reactive nitrogen burial in sediment of global lakes. The Innovation 2(4), 100158.

Wanninkhof, R (1992) Relationship between windspeed and gas exchange over the ocean. J. Geophys. Res. (Oceans) 97(C5):7373–7382.

Weiss, RF (1974) Carbon dioxide in water and seawater: the solubility of a non-ideal gas. Marine Chem. 2:203–215.

WFD-UKTAG [Water Framework Directive – United Kingdom Technical Advisory Group] (2014) UKTAG Lake Assessment Method Phytoplankton: Phytoplankton Lake Assessment Tool with Uncertainty Module (PLUTO). July 2014.

Zhang F (2021) The dynamics of manganese in a monomictic water supply reservoirs and its impacts on water treatment processes. PhD Thesis. Griffith University, QLD Australia.

Zhang J, N He, C Liu, L Xu, Z Chen, Y Li, R Wang, G Yu, W Sun, C Xiao, HYH Chen & PB Reich (2020) Variation and evolution of C:N ratio among different organs enable plants to adapt to N-limited environments. Glob Change Biol. 26:2534–2543. https://doi.org/10.1111/gcb.14973.

Appendices

Appendix A

Comparison of Coarse and Fine Grid Simulations over 12 Years of Scenario 1B

A-1 Introduction

A comparison coarse and fine grid simulations of the surface and bottom waters, and withdrawals, for scenario 1B with nighttime bubbler operations is provided in this section. The objective is to further verify the coarse grid adequately simulates WQ concentrations in the reservoir and withdrawals as simulations with the fine grid as presented in GHD (2024) Appendix A.

A-2 Surface and bottom water quality

Time series of selected simulated state (T, DO, PO4, DMN) and derived (total algal biomass) variables at the surface and bottom waters of the north and south basins are compared between the coarse (50 m) and fine (20 m) horizontal grids. The surface and bottom waters with the fine grid are reproduced well by the coarse grid (Figure B-1). In fact, the coarse grid is generally more conservative in terms of forecasting poorer WQ than the fine grid (e.g. lower DO and longer anoxic duration in south basin with substantially higher DMN).

Along with GHD (2024) Appendix A, this appendix's findings supports the use of the coarse grid simulations to characterise in-reservoir WQ in a conservative manner.

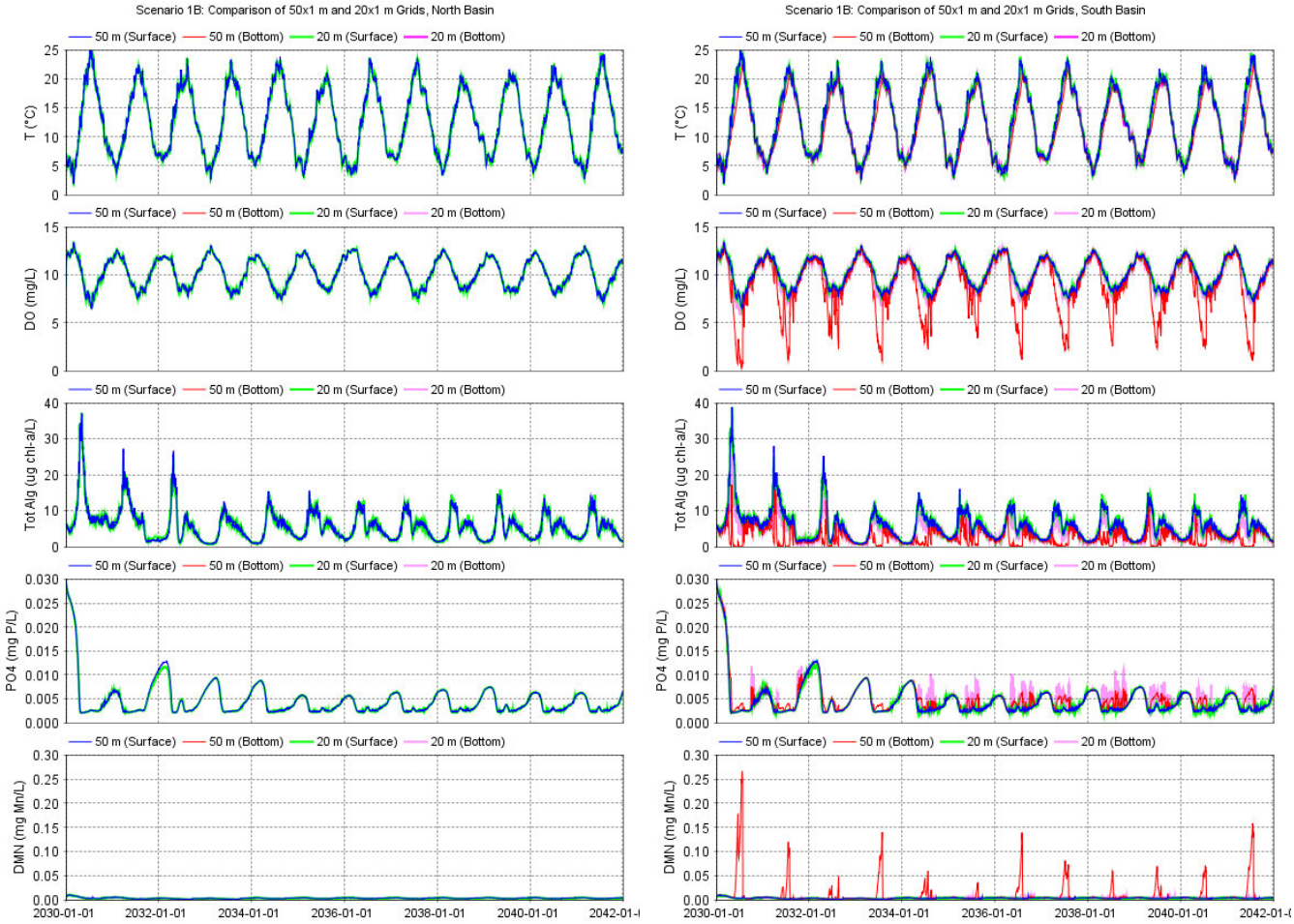

Figure A.1 ***Comparison of selected simulated state variables (T, DO, total algae, PO4, DMN) at the surface (0 m below water level) and bottom waters at deep water locations in the north (left) and south (right) basins for coarse and fine grid simulations of scenario 1B.***

A-3 Withdrawals

As with the surface and bottom water WQ forecasts in both of HTR's basins in the previous section, there is good agreement between the coarse and fine grid simulated withdrawal WQ of scenario 1B with nighttime bubbler operations (Figure B.2).

Along with GHD (2024) Appendix A, this section demonstrates that the use of the coarse grid simulations in this investigation is appropriate to define the WQ envelope of the withdrawals (Section 9.5) and to evaluate the environmental acceptability of compensation flows to Riders Lane Stream (Section 9.6).

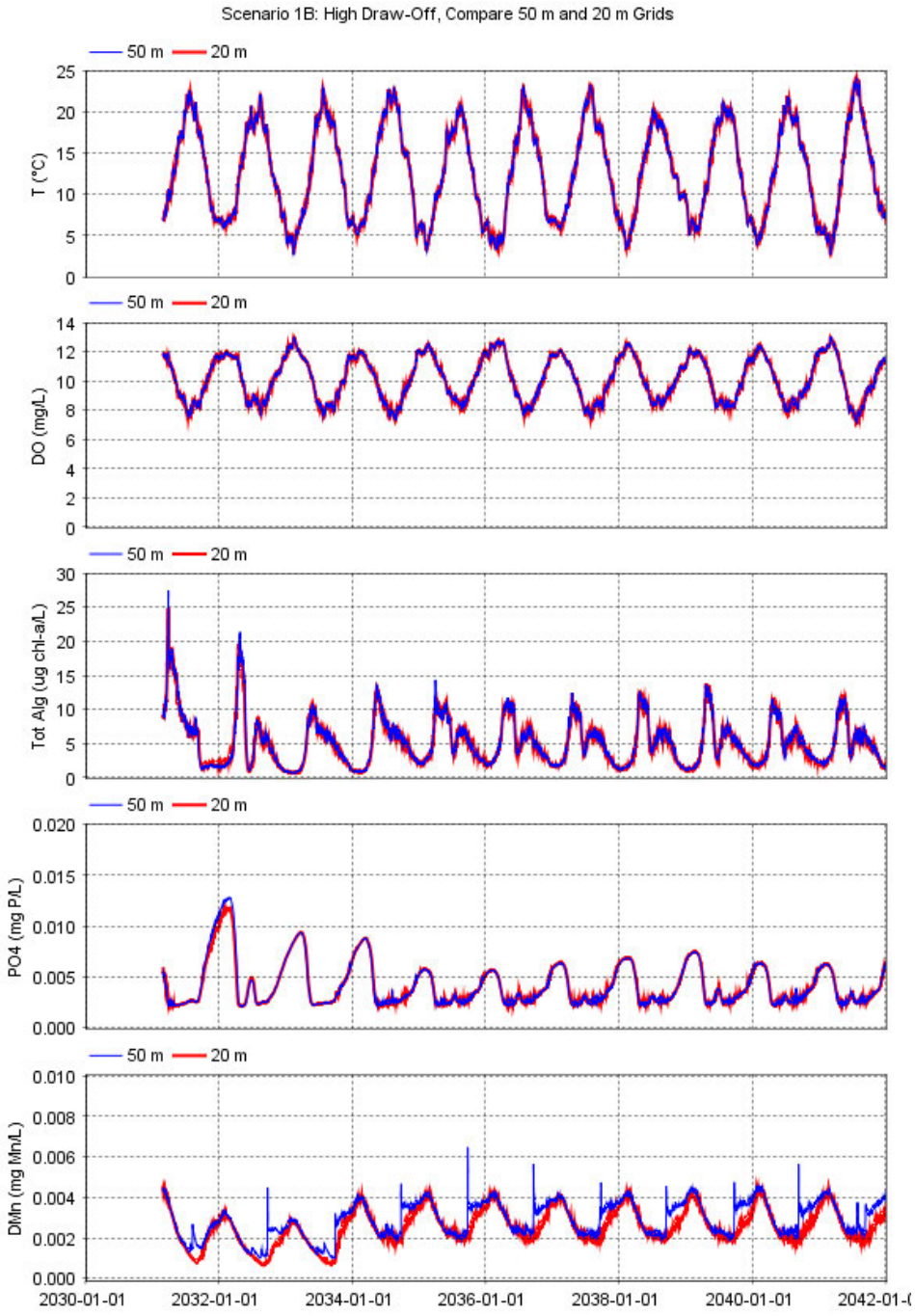

Figure A.2 ***Comparisons of coarse and fine grid simulations of selected WQ state variables of the withdrawals from the high draw-off outlet for scenario 1B.***

Appendix B

WQ Parameter Values

Table B.1 ***Parameters, values, units, and references/justifications of model WQ processes. Italic and italic underlined values are assumed to equal and to scale to another parameter value, respectively. Yellow shading are sediment fluxes that are adjusted for stabilisation phase effects (see Section 4.5.2). Updates to GHD (2024) parameter values are in red parentheses.***

Parameter	Value	Units	References and Justification
Carbon (State Variables DOC, POC, DIC, pH)			
Ionic Strength	0.008		Assigned: 0.008 due to high inputs of spring and recycled water. Ionic strength estimates on basis of EC from streams, springs and HIGHLY MINERALISED recycled water are 0.003, 0.008 and 0.008, respectively.
DOC Sediment Flux Temperature Multiplier	1.05		Assigned: 1.05 for all sediment fluxes as consistent published/unpublished values Allan et al (2018) 1.06 (2x NZ lakes) Bruce et al (2006) 1.05 (Israel lake) Missaghi & Hondzo (2010) 1.05 (MN USA shallow lake) Romero J. (unpubl. data) 1.05 for Pickering (1994) NSW Australia reservoir DOC sediment flux data Tranmer et al (2018) 1.05 (ID USA reservoir)
DOC Maximum Sediment Flux Rate @ 20°C	0.1	g C/m^2/d	Assigned: 0.1 g/m2/d as a conservative value greater than published/unpublished values Missaghi & Hondzo (2010) 0.0005 g/m^2/d (MN USA shallow lake) Romero J. (unpubl. data) 0.075 g/m^2/d with linear inverse Michaelis-Menten relation for Pickering (1994) Australian reservoir DOC sediment flux data (DO<5 mg/L) with DO ½ saturation=1 mg/L, a=-0.1, b=1.1 and minimum flux rate of 0 g/m^2/day (r^2=99%)
DOC Sediment Flux DO ½ Saturation Constant	1	mg O_2/L	Assigned: 1 mg/L as highest of published/unpublished values Missaghi & Hondzo (2010) 0.005 mg/L (MN USA shallow lake) Romero (unpubl. data) 1 mg/L for Pickering (1994) NSW Australian reservoir DOC sediment flux data Tranmer et al (2018) 0.5 mg/L (ID USA reservoir)
DIC Sediment Flux Temperature Multiplier	*1.05*		*Assumed: 1.05 for all sediment flux rates as DOC*
DIC Maximum Sediment Flux Rate @ 20°C	*0.375*	*g C/m^2/d*	*Scaled: As 1x O2 moles of SOD yields 1x C moles from aerobic respiration, DIC flux estimated as 0.375 (=12 g C/32 g O2) of SOD*
DIC Sediment Flux DO ½ Saturation Constant	*0.5*	*mg O_2/L*	*Assumed: Same value as SOD, the primary sediment source process*
DOC Specific Light Attenuation Coefficient	0.01	(1/m)/(mg /L)	Assigned: Estimate
DOC Mineralisation Rate @ 20°C	0.01	1/d	Assigned: 0.01 1/d as upper range of published values Allan et al (2018) DON->NH4 0.005 1/d (2x NZ lakes) Ghane (2022) 0.01 1/d (Canadian shield lake) Missaghi & Hondzo (2010) 0.011 (MN USA shallow lake) Romero et al (2004) POP->FRP, PON->NH4 0.01 1/d (2x NSW Australia reservoirs) Tranmer et al (2018) 0.003 1/d for DON->NH4 (2x NZ lakes)
DOC Mineralisation DO ½ Saturation	2	mg O_2/L	Assigned: 2 mg/L as median of published values Bruce et al (2006) 2.5 mg/L (Israel Lake) Missaghi & Hondzo (2010) 1.5 mg/L (MN USA shallow lake)
DOC Mineralisation Temperature Multiplier	1.08		Assigned: 1.08 as available published value Romero et al (2004) POM->Inorganic dissolved matter 1.08 (2x NSW Australia reservoirs)
Nitrogen (State Variables NO3, NH4, DON, PON, IN_FDI, IN_CHL, IN_CYA)			
NH4 Sediment Flux Temperature Multiplier	*1.05*		*Assumed: 1.05 as DOC* Additional references:

Parameter	Value	Units	References and Justification
			Romero (unpubl. data) 1.05 for Pickering (1994) NSW Australia reservoir NH_4 sediment flux data Missaghi & Hondzo (2010) 1.05 (MN USA shallow lake)
NH4 Maximum Sediment Flux Rate @ 20°C	0.015	g $N/m^2/d$	Assigned: 0.015 g/m2/d of Romero (unpubl. data) similar to typical oligo & meso- trophic reservoirs Allan et al (2018) 0.01-0.03 $g/m^2/d$ (2x NZ lakes) Beutal & Hannoun (2007) 0.016-0.070 $g/m^2/d$ (CA USA eutrophic reservoir) Bruce et al (2006) 0.05 $g/m^2/d$ (Israel lake) Ghane (2022) 0.007 $g/m^2/d$ (Canadian shield lake) Missaghi & Hondzo (2010) 0.09 $g/m^2/d$ (MN USA shallow lake) Romero (unpubl. data) 0.015 $g/m^2/d$ with linear inverse Michaelis-Menten relation for Pickering (1994) Australian reservoir NH_4 sediment flux data with DO ½ Saturation=1 mg/L, a=-0.1, b=1.1 and minimum flux rate of 0 $g/m^2/day$ (r^2=0.99) Romero et al (2004) 0.01 $g/m^2/d$ (2x NSW Australia reservoirs) Scott & Patterson (2022) 0.05 $g/m^2/d$ (OK USA Reservoir) Trammer et al (2018) 0.019 $g/m^2/d$ (ID USA reservoir)
NH4 Sediment Flux DO ½ Saturation Constant	1	mg O_2/L	Assigned: 1 mg/L of Romero (unpubl. data) at upper range of published values Bruce et al (2006) 1 mg/L (Israel lake) Missaghi & Hondzo (2010) 0.5 mg/L (MN USA shallow lake) Romero (unpubl. data) 1 mg/L for Pickering (1994) NSW Australian reservoir sediment flux data Scott & Patterson (2022) 0.5 mg/L (OK USA reservoir) Tranmer et al (2018) 0.5 mg/L (ID USA reservoir)
NO3 Sediment Flux Temperature Multiplier	*1.05*		*Assumed: 1.05 for all sediment flux rates as DOC* Additional references: Missaghi & Hondzo (2010) 1.05 (MN USA shallow lake) Romero (unpubl. data) 1.05 best fit of Pickering (1994) NSW Australia reservoir NO_3 sediment flux data
NO3 Maximum Sediment Flux Rate @ 20°C	-0.01	g $N/m^2/d$	Assigned: -0.01 $g/m^2/d$ in mid-range of published/unpublished values Allan et al (2018) -0.03 to -0.04 $g/m^2/d$ (2x NZ lakes) Ghane (2022) 0.007 $g/m^2/d$ (Canadian shield lake) Missaghi & Hondzo (2010) 0.03 $g/m^2/d$ (MN USA shallow lake) Romero (unpubl. data) -0.0115 $g/m^2/d$ with linear inverse Michaelis-Menten relation for Pickering (1994) NSW Australia reservoir NO_3 sediment flux data with DO ½ Saturation=0.5 mg/L, a=-0.1, b=1.1 and maximum flux rate of 0 $g/m^2/day$ (r^2=0.99) Scott & Patterson (2022) -0.001 $g/m^2/d$ (OK USA reservoir)
NO3 Sediment Flux DO ½ Saturation Constant	0.5	mg O_2/L	Assigned: 0.5 mg/L of Romero (unpubl. data) in range of published values Missaghi & Hondzo (2010) 0.03 mg/L (MN USA shallow lake) Romero (unpubl. data) 0.5 mg/L for Pickering (1994) NSW Australia reservoir NO_3 sediment flux data Scott & Patterson (2022) 0.5 mg/L (OK USA reservoir)
DON Sediment Flux Temperature Multiplier	*1.05*		*Assumed: 1.05 for all sediment flux rates as DOC* Additional reference: Missaghi & Hondzo (2010) 1.05 (MN USA shallow lake)
DON Maximum Sediment Flux Rate @ 20°C	*0.0175*	*g $N/m^2/d$*	*Scaled to DOC Maximum Sediment Flux Rate as Redfield ratio of 106 mol C:16 mol N or 0.175 mg N/1 mg C*
DON Sediment Flux DO ½ Saturation Constant	*1*	*mg O_2/L*	*Assumed: 1.05 as DOC* Additional reference: Scott & Patterson (2022) 0.5 mg/L (OK USA Reservoir)
Nitrification Rate @ 20°C	0.02	1/d	Assigned: 0.02 1/d typically used in applications Allan et al (2018) 0.1 1/d (2x NZ lakes) Bruce et al (2006) 0.015 1/d (Israel lake) Cui et al (206) 0.05 1/d (China sub-tropical reservoir)

Parameter	Value	Units	References and Justification
			Gharehchaman (2021) 0.02 1/d (2x Iran reservoirs) Ghane (2022) 0.32 1/d (Canadian shield lake) Hamilton & Schladow (1997) 0.02 1/d (NSW Australia reservoir) Missaghi & Hondzo (2010) 0.25 1/d (MN USA shallow lake) Romero et al (2004) 0.02 1/d (2x NSW Australia reservoirs) Saddek & Casamitjana (2015) 0.02 1/d (Spain reservoir) Steinsberger et al (2019) 0.02 1/d Tranmer et al (2018) 0.05 1/d (ID USA reservoir)
Nitrification Temperature Multiplier	1.07		Assigned: 1.07 within range of published values Allan et al (2018) 1.07 (2x NZ lakes) Bruce et al (2006) 1.08 (Israel lake) Gharehchaman (2021) 1.08 (2x Iran reservoirs) Saddek & Casamitjana (2015) 1.08 (Spain reservoir)
Nitrification DO ½ Saturation Constant	1	mg O_2/L	Assigned: 1 mg/L within range of published values Allan et al (2018) 0.5 mg/L (2x NZ lakes) Bruce et al (2006) 0.5 mg/L (Israel lake) Gharehchaman (2021) 0.5 mg/L (2x Iran reservoirs) Ghane (2022) 2 mg/L (Canadian shield lake) Missaghi & Hondzo (2010) 0.75 mg/L (MN USA shallow lake) Romero et al (2004) 2 mg/L (2x NSW Australia reservoirs) Saddek & Casamitjana (2015) 2 mg/L (Spain reservoir)
Denitrification Rate @ 20°C	0.02	1/d	Assigned: 0.02 mg/L within range of published values Allan et al (2018) 0.08 1/d (2x NZ lakes, unlikely high value) Bruce et al (2006) 0.08 1/d (Israel lake, unlikely high value) Cui et al (2018) 0.01 1/d (China sub-tropical reservoir) Gharehchaman (2021) 0.01 1/d (2x Iran reservoirs) Ghane (2022) 0.0012 1/d (Canadian shield lake) Missaghi & Hondzo (2010) 0.15 1/d (MN USA shallow lake, unlikely high value) Romero et al (2004) 0.01 1/d (2x NSW Australia reservoirs) Steinsberger et al (2019) 0.02 1/d
Denitrification Temperature Multiplier	1.07		Assigned: 1.07 within range of published values Allan et al (2018) 1.07 (2x NZ lakes) Bruce et al (2006) 1.08 (Israel lake) Gharehchaman (2021) 1.08 (2x Iran reservoirs)
Denitrification DO ½ Saturation Constant	0.5	mg O_2/L	Assigned 0.5 mg/L as most published values Allan et al (2018) 0.5 mg/L (2x NZ lakes) Bruce et al (2006) 0.5 mg/L (Israel Lake) Ghane (2022) 0.5 mg/L (Canadian shield lake) Missaghi & Hondzo (2010) 0.44 mg/L (MN USA shallow lake) Romero et al (2004) 0.5 mg/L (2x NSW Australia reservoirs)
DON Mineralisation Rate @ 20°C	*0.01*	*1/d*	*Assumed: 0.01 1/d as DOC* Additional references: Allan et al (2018) 0.005 1/d (2x NZ lakes) Cui et al (2016) 0.004 1/d (China subtropical reservoir) Ghane (2022) 0.016 1/d (Canadian shield lake) Missaghi & Hondzo (2010) 0.08 1/d (MN USA shallow lake) Romero et al (2004) PON->NH4 0.01 1/d (2x NSW Australia reservoirs) Tranmer et al (2018) 0.003 1/d (ID USA reservoir)

Parameter	Value	Units	References and Justification
DON Mineralisation DO ½ Saturation Constant	*2*	*mg O_2/L*	*Assumed:* 2 mg/L as *DOC* Additional references: Bruce et al (2006) 2.5 mg/L (Israel Lake) Missaghi & Hondzo (2010) 1.5 mg/L (MN USA shallow lake) Saddek & Casamitjana (2015) 3 mg/L (Spain reservoir)
DON Mineralisation Temperature Multiplier	*1.08*		*Assumed: 1.08* as *DOC*
Phosphorus (State Variables PO4, DOP, POP, IP_FDI, IP_CHL, IP_CYA)			
PO4 Sediment Flux Temperature Multiplier	*1.05*		*Assumed: 1.05 for all sediment flux rates as DOC* Additional references: Missaghi & Hondzo (2010) 1.05 (MN USA shallow lake) Romero (unpubl. data) 1.05 best fit of Pickering (1994) NSW Australia reservoir PO_4 sediment flux data Saddek & Casamitjana (2015) 1.05 (Spain reservoir)
PO4 Maximum Sediment Flux Rate @ 20°C	0.003	g P/m^2/d	Assigned: 0.003 g/m^2/d of Romero (unpubl. data) within range of published values Allan et al (2018) 0.002-0.007 g/m^2/d (2x NZ lakes) Beutal & Hannoun (2007) 0.01-0.029 g/m^2/d (CA USA eutrophic reservoir) Bruce et al (2006) 0.0008 g/m^2/d (Israel lake) Ghane (2022) 0.0032 mg N/m^2/d (Canadian shield lake) Missaghi & Hondzo (2010) 0.04 g/m^2/d (MN USA shallow lake) Romero et al (2004) 0.0005 g/m^2/d (2x NSW Australia reservoirs) Romero (unpubl. data) 0.003 g/m^2/d with linear inverse Michaelis-Menten relation for Pickering (1994) NSW Australia reservoir PO_4 sediment flux data with DO ½ Saturation=0.5 mg/L, a=-0.1, b=1.1 and minimum sediment flux rate of 0 g/m^2/d (r^2=0.99) Saddek & Casamitjana (2015) 0.005 g/m^2/d (Spain reservoir) Scott & Patterson (2022) 0.003 g/m^2/d (OK USA reservoir) Trammer et al (2018) 0.0001 g/m^2/d (ID USA reservoir) Trolle et al (2008) 0.004 g/m^2/d (Denmark mesotrophic lake)
PO4 Sediment Flux DO ½ Saturation Constant	0.5	mg O_2/L	Assigned: 0.5 mg/L of Romero (unpubl. data) at lower range of published values Adopt 0.5 mg O2/L Allan et al (2018) 1.5-3.5 mg/L (2x NZ lakes) Bruce et al (2006) 3 mg/L (Israel lake) Missaghi & Hondzo (2010) 1 mg/L (MN USA shallow lake) Romero (unpubl. data) 0.5 mg/L for Pickering (1994) NSW Australia reservoir PO_4 sediment flux data Scott & Patterson (2022) 0.5 mg/L (OK USA reservoir) Trammer et al (2018) 0.5 mg/L (ID USA reservoir) Trolle et al (2008) 0.1 mg/L (Denmark mesotrophic lake)
DOP Sediment Flux Temperature Multiplier	*1.05*		*Assumed: 1.05 for all sediment flux rates as DOC* Additional reference: Missaghi & Hondzo (2010) 1.05 (shallow USA lake)
DOP Maximum Sediment Flux Rate @ 20°C	*0.0025*	*g P/m^2/d*	*Scaled to DOC Maximum Sediment Flux Rate as Redfield ratio of 106 mol C:1 mol P or 0.025 mg P/1 mg C*
DOP Sediment Flux DO ½ Saturation Constant	*1*	*mg O_2/L*	*Assumed: 1 mg/L* as *DOC* Additional reference: Scott & Patterson (2022) 0.5 mg/L (OK USA Reservoir)
DOP Mineralisation Rate @ 20°C	*0.01*	*1/d*	*Assumed: 0.01 1/d* as *DOC* Additional references: Allan et al (2018) 0.05 1/d (2x NZ lakes) Cui et al (2016) 0.01 1/d (China subtropical lake) Ghane (2022) 0.01 1/d (Canadian shield lake)

Parameter	Value	Units	References and Justification
			Missaghi & Hondzo (2010) 0.25 1/d (MN USA shallow lake) Romero et al (2003) POP->PO4 0.01 1/d (2x NSW Australia reservoirs) Saddek & Casamitjana (2015) 0.075 1/d (Spain reservoir) Tranmer et al (2018) 0.01 1/d (ID USA reservoir) Trolle et al (2008) 0.01 1/d (Denmark mesotrophic lake)
DOP Mineralisation DO ½ Saturation Constant	*2*	*mg O_2/L*	*Assumed: 2 mg/L* as *DOC* Additional references: Bruce et al (2006) 2.5 mg/L (Israel Lake) Missaghi & Hondzo (2010) 1.5 mg/L (MN USA shallow lake)
DOP Mineralisation Temperature Multiplier	*1.08*		*Assumed: 1.08* as *DOC* Additional reference: Romero et al (2006) POP->PO4 1.08 (2x NSW Australia reservoirs)
Silica (State Variable SiO2)			
SiO_2 Sediment Flux Temperature Multiplier	*1.05*		*Assumed: 1.05 for all sediment flux rates as DOC* Additional reference: Romero (unpubl. data) 1.05 best fit of Pickering (1994) NSW Australia reservoir SiO_2 sediment flux data
SiO_2 Maximum Sediment Flux Rate @ 20°C	0.03	g Si/m^2/d	Assigned: 0.03 g/m^2/d of Romero (unpubl. value) Romero (unpubl. data) 0.03 g/m^2/d with linear inverse Michaelis-Menten relation for Pickering (1994) NSW Australia reservoir SiO_2 sediment flux data with DO ½ Saturation=0.5 mg/L, a=-0.1, b=1.1 and minimum sediment flux rate of 0 g/m^2/d (r^2=0.99)
SiO_2 Sediment Flux DO ½ Saturation Constant	0.5 (1)	mg O_2/L	Assigned: Updated value based on calibration/validation of reservoirs since GHD (2024) Previously Assigned: 0.5 mg/L of Romero (unpubl. data)
Particulate Organic Matter (State Variable POM)			
POM Stokes Law Particle Settling Density	1,040	kg/m^3	Assigned: 1,040 kg/m^3 at lower range of published values Bruce et al (2006) 1080 kg/m^3 (Israel lake) Missaghi & Hondzo (2010) 1040 kg/m^3 (MN USA shallow lake)
POM Stokes Law Particle Settling Diameter	5	µm	Assigned: 5 um at lower range of published values Bruce et al (2006) 15 µm (Israel lake) Missaghi & Hondzo (2010) 5 µm (MN USA shallow lake)
POM Critical Shear Stress for Resuspension	0.01	N/m^2	Assigned: Critical shear stress parameter of 0.01 N/m^2 for sediments at low range of published values Chung et al (2009): 0.04 N/m^2 (CA USA Salton Sea) Lee et al (2007): 0.05 N/m^2 (MI USA Lake Michigan) GHD (2023) & Appendix B: No resuspension simulated Simulated differences minimal over range of 1-0.0001 N/m^2
POM Maximum Resuspension Rate	0.01	g/m^2/d	Assigned: Adopted maximum sediment total resuspension rate of ~0.1 g/m^2/d where assume ~10% POM in upper sediments Chung et al (2009) 0.075 g/m^2/d (CA USA Salton Sea)
POM Resuspension Half Saturation Constant	50	g/m^2	Assigned: Estimate based on half the areal mass of an assumed ~1 mm active resuspension layer in upper sediments and ~10% particulate organic matter (~100 g/m^2)
POM Specific Light Attenuation Coefficient	0.02	(1/m)/(mg /L)	Assigned: Estimate
POM Decomposition Rate @ 20°C	0.02	1/d	Assigned: 0.02 1/d within range of published values Allan et al (2018) POP->DOP 0.005 1/d, PON->DON 0.004 1/d (2x NZ lakes) Bruce et al (2006) POC->DOC 0.001 1/d, PON->NH4 0.02 1/d, POP->PO4 0.01 1/d (Israel lake)

Parameter	Value	Units	References and Justification
			Gharehchaman (2021) 0.01 1/d (2x Iran reservoirs) Ghane (2022) 0.07 1/d (Canadian shield lake) Missaghi & Hondzo (2010) POC->DOC 0.07 1/d, PON->DON 0.005 1/d, POP-DOP 0.03 1/d (MN USA shallow lake) Romero et al POP->PO4 & PON->NH4 0.01 1/d (2x NSW Australia reservoirs) Saddek & Casamitjana (2015) 0.2 1/d (Spain reservoir) Tranmer et al (2018) POP->DOP 0.05 1/d, PON->DON 0.01 1/d (ID USA reservoir) Trolle et al (2008) 0.01 1/d (Denmark mesotrophic lake)
POM Decomposition DO ½ Saturation Constant	2	mg O_2/L	Assigned: 2 mg/L within range of published values Bruce et al (2006) 2.5 mg/L (Israel lake) Saddek & Casamitjana (2015) 3 mg/L (Spain reservoir) Missaghi & Hondzo (2010) 1.5 mg/L (MN USA shallow lake)
POM Decomposition Temperature Multiplier	1.08		Assigned: 1.08 at lower range of published values Bruce et al (2006) 1.18 (Israel lake) Romero et al (2004) 1.08 (2x NSW Australia reservoirs)
Dissolved Oxygen (State Variable DO)			
DO Sediment Flux Temperature Multiplier	*1.05*		*Assumed: 1.05* as *DOC* Additional references: Ghane (2022) 1.05 (Canadian shield lake) Missaghi & Hondzo (2010) 1.05 (MN USA shallow lake) Saddek & Casamitjana (2015) 1.07 (Spain reservoir) Trolle et al (2008) 1.05 (Denmark mesotrophic lake)
DO Maximum Sediment Flux Rate @ 20°C	1	g O_2/m^2/d	Assigned: 1.0 g/m^2/d with standard Michaelis-Menten formulation in upper range of published values as a conservative measure. This parameter is often referred to as the Sediment Oxygen Demand (SOD). Allan et al (2018) 1.65 g/m^2/d (2x NZ lakes) Beutel (2003) range of 0.08-0.76 g/m^2/d (Reservoirs CA USA w/ flux chamber) Beutal & Hannoun (2007) SOD5 (SOD @ 5 mg O2/L) of 0.1 (low turbulence) to 0.6 (high turbulence) g/m^2/d in reservoir arms and 0.2 (low turbulence) to 1.0 (high turbulence) g/m^2/d in profundal depths (CA USA eutrophic reservoir) Brodzeller J & P McGinley (2016) 0.35-0.6 g/m^2/d (WI USA reservoir) Bruce et al (2006) 1.5 g/m^2/d (Israel lake) Cui et al (2016) 1.2 g/m^2/d (China sub-tropical reservoir) Gharehchaman (2021) 0.3 g/m^2/d (2x Iran reservoirs) Ghane (2022) 0.5 g/m^2/d (Canadian shield lake) Krueger et al (2020) 0.47-0.70 g/m^2/d (WV USA reservoir w/ flux chamber) Missaghi & Hondzo (2010) 1.3 g/m^2/d (MN USA shallow lake) Romero et al (2004) 0.3 g/m^2/d (2x NSW Australia reservoirs) Saddek & Casamitjana (2015) 3.2 g/m^2/d (Spain reservoir) Scott & Patterson (2022) 0.62 g/m^2/d (OK USA reservoir) Trammer et al (2018) 1.2 g/m^2/d (ID USA reservoir) Trolle et al (2008) 0.7 g/m^2/d (Denmark mesotrophic lake) Urban et al (1997) 0.08 g/m^2/d (Switzerland lake w/ flux chamber)
DO Sediment Flux DO ½ Saturation Constant	0.5	mg O_2/L	Assigned: 0.5 mg/L with standard Michaelis-Menten formulation in lower range of published values as a conservative measure Allan et al (2018) 0.25 mg/L (2x NZ lakes) Bruce et al (2006) 0.5 mg/L (Israel lake) Gharehchaman (2021) 5 mg/L (2x Iran reservoirs) Missaghi & Hondzo (2010) 0.7 mg/L (MN USA shallow lake) Saddek & Casamitjana (2015) 0.2 mg/L (Spain reservoir)

Parameter	Value	Units	References and Justification
			Scott & Patterson (2022) 0.5 mg/L (OK USA Reservoir) Trammer et al (2018) 0.5 mg/L (ID USA reservoir) Trolle et al (2008) 0.4 mg/L (Demark mesotrophic lake)
Diatoms (State Variable FDIAT)			
DIATOM Carbon to Chl-a Ratio	40	mg C/mg Chla	Assigned: 40 mg C/mg Chla as most published value, assigned to all phytoplankton groups Absalon (2020) 40 mg C/mg Chla (Poland reservoir) Caramatti (2021) 40 mg C/mg Chla (Lake Constance) Ghane (2022) 40 mg C/mg Chla (Canadian shield lake) Romero et al (2004) 40 mg C/mg Chla (2x NSW Australia reservoirs) Scott & Patterson (2022) 32 mg C/mg Chla (OK USA reservoir)
DIATOM Maximum Growth Rate @ 20°C	1.4	1/d	Assigned: 1.4 1/d within range of published values Absalon (2020) 3.2 1/d (Poland reservoir) Allan et al (2018) 1.4-1.6 (2x NZ lakes) Caramatti (2021) 1.2 1/d (Lake Constance) Cui et al (2016) 1.0 1/d (China sub-tropical reservoir) Ghane (2022) 1.4 1/d (Canadian shield lake) Romero et al (2004) 1.3 1/d (2x NSW Australia reservoirs) Scott & Patterson (2022) 1.8 1/d (OK USA reservoir) Trammer (2018) 1.7 1/d (ID USA reservoir)
DIATOM Initial Slope of PI Curve	60	$\mu E/m^2/s$	Assigned: 60 $\mu E/m^2/s$ within range of selected values Absalon (2020) 80 $\mu E/m^2/s$ (Poland reservoir) Allan et al (2018) 20 $\mu E/m^2/s$ (2x NZ lakes) Caramatti (2021) 10 $\mu E/m^2/s$ (Lake Constance) Cui et al (2016) 180 $\mu E/m^2/s$ Ghane (2022) 70 $\mu E/m^2/s$ (Canadian shield lake) Romero et al (2004) 60 $\mu E/m^2/s$ (2x NSW Australia reservoirs) Scott & Patterson (2022) 20 $\mu E/m^2/s$ (OK USA Reservoir)
DIATOM Growth Temperature Multiplier	1.06		Assigned: 1.06 at upper range of published values Allan et al (2018) 1.05-1.06 (2x NZ lakes) Caramatti (2021) 1.05 1/d (Lake Constance) Ghane (2022) 0.93 (Canadian shield lake) Tranmer et al (2018) 1.06 (ID USA reservoir)
DIATOM Growth Standard Temperature	15	°C	Assigned: 15°C within range of published values Absalon (2020) 15°C (Poland reservoir) Allan et al (2018) 18-20°C (2x NZ lakes) Bruce et al (2006) 20°C (Israel lake) Caramatti (2021) 12°C (Lake Constance) Cui et al (2016) 15°C (China sub-tropical reservoir) Ghane (2022) 23°C (Canadian shield lake) Romero et al (2004) 16°C (2x NSW Australia reservoirs) Scott & Patterson (2022) 12°C (OK USA reservoir) Tranmer et al (2018) 25°C (ID USA reservoir)
DIATOM Growth Optimum Temperature	20	°C	Assigned: 20°C within range of published values Absalon (2020) 18°C (Poland reservoir) Allan et al (2018) 23-29°C (2x NZ lakes) Bruce et al (2006) 20°C (Israel lake) Caramatti (2021) 16°C (Lake Constance) Cui et al (2016) 20°C (China sub-tropical reservoir)

Parameter	Value	Units	References and Justification
			Ghane (2022) 29°C (Canadian shield lake) Romero et al (2004) 20°C (2x NSW Australia reservoirs) Scott & Patterson (2022) 23°C (OK USA reservoir) Tranmer et al (2018) 28°C (ID USA reservoir)
DIATOM Growth Maximum Temperature	30	°C	Assigned: 30°C within range of published values Absalon (2020) 30°C (Poland reservoir) Allan et al (2018) 33-34°C (2x NZ lakes) Bruce et al (2006) 27.5°C (Israel lake) Caramatti (2021) 30°C (Lake Constance) Cui et al (2016) 28°C (China sub-tropical reservoir) Ghane (2022) 35°C (Canadian shield lake) Romero et al (2004) 29°C (2x NSW Australia reservoirs) Scott & Patterson (2022) 30°C (OK USA reservoir) Tranmer et al (2018) 35°C (ID USA reservoir)
DIATOM Minimum Internal P:Chla Ratio	0.3	mg P/mg Chla	Assigned: 0.3 mg P/mg Chla within range of published values, assigned to all phytoplankton groups Absalon (2020) 0.62 mg P/mg Chla (Poland reservoir) Allan et al (2018) 0.22-0.35 mg P/mg chla (2x NZ lakes) Bruce et al (2006) ~0.48 mg P/mg Chla (Israel lake assuming a 40 mg C:1 mg Chla ratio) Caramatti (2021) 0.4 mg P/mg Chla (Lake Constance) Cui et al (2016) 0.1 mg P/mg Chla (China sub-tropical reservoir) Ghane (2022) 0.208 mg P/mg Chla (Canadian shield lake) Scott & Patterson (2022) 0.25 mg P/mg Chla (OK USA reservoir)
DIATOM Maximum Internal P:Chla Ratio	1.2	mg P/mg Chla	Assigned: 1.2 mg P/mg Chla within range of published values, assigned to all phytoplankton groups Absalon (2020) 0.64 mg P/mg Chla (Poland reservoir) Allan et al (2018) 1.1-2 mg P/mg Chla (2x NZ lakes) Bruce et al (2006) ~3.4 mg P/mg Chla (Israel lake assuming a 40 mg C:1 mg Chla ratio) Caramatti (2021) 0.8 mg P/mg Chla (Lake Constance) Cui et al (2016) 2.3 mg P/mg Chla (China sub-tropical reservoir) Ghane (2022) 0.5 mg P/mg Chla (Canadian shield lake) Scott & Patterson (2022) 1.3 mg P/mg Chla (OK USA reservoir)
DIATOM Maximum P Uptake Rate	0.5	mg P/mg Chla/d	Assigned: 0.5 mg P/mg Chla/d within range of published values, assigned to all phytoplankton groups Allan et al (2018) 0.24-0.25 mg P/mg Chla/d (2x NZ lakes) Bruce et al (2006) ~0.5 mg P/mg Chla/d (assuming a 40 mg C:1 mg chla ratio) Caramatti (2021) 1.8 mg P/mg Chla/d (Lake Constance) Cui et al (2016) 1.85 mg P/mg Chla/d (China sub-tropical reservoir) Ghane (2022) 0.59 mg P/mg Chla/d (Canadian shield lake)
DIATOM Growth P ½ Saturation Constant	0.007	mg P/L	Assigned: 0.007 mg P/L within range of published values Absalon (2020) 0.001 mg P/L (Poland reservoir) Allan et al (2018) 0.004-0.01 mg P/L (2x NZ lakes) Bruce et al (2010) 0.0015 mg P/L (Israel lake) Caramatti (2021) 0.005 mg P/L (Lake Constance) Cui et al (2016) 0.01 mg P/L (China sub-tropical reservoir) Ghane (2022) 0.006 mg P/L (Canadian shield lake) Romero et al (2004) 0.007 mg P/L (2x NSW Australia reservoirs) Scott & Patterson (2022) 0.01 mg P/L (OK USA reservoir) Trammer (2018) 0.006 mg P/L (ID USA reservoir)
DIATOM Minimum Internal N:Chla Ratio	2.5	mg N/mg Chla	Assigned: 2.5 mg N/mg Chla within range of published values, assigned to all phytoplankton groups Absalon (2020) 2.7 mg N/mg Chla (Poland reservoir) Allan et al (2018) 3-3.4 mg N/mg Chla (2x NZ lakes)

Parameter	Value	Units	References and Justification
			Bruce et al (2006) ~3 mg N/mg Chla (Israel lake assuming a 40 mg C:1 mg Chla ratio) Caramatti (2021) 4 mg N/mg Chla (Lake Constance) Cui et al (2016) 2.5 mg N/mg Chla (China sub-tropical reservoir) Ghane (2022) 1 mg N/mg Chla (Canadian shield lake) Scott & Patterson (2022) 2 mg N/mg Chla (OK USA reservoir)
DIATOM Maximum Internal N:Chla Ratio	5	mg N/mg Chla	Assigned: 5 mg N/mg Chla within range of published values, assigned to all phytoplankton groups Absalon (2020) 5 mg N/mg Chla (Poland reservoir) Cui et al (2016) 4.5 mg N/mg Chla (China sub-tropical reservoir) Allan et al (2018) 3.5-10 mg N/mg Chla (2x NZ lakes) Bruce et al (2006) ~4.5 mg N/mg Chla (Israel lake assuming a 40 mg C:1 mg chla ratio) (Israel lake) Caramatti (2021) 9 mg N/mg Chla (Lake Constance) Ghane (2022) 5 mg N/mg Chla (Canadian shield lake) Scott & Patterson (2022) 4.5 mg N/mg Chla (OK USA reservoir)
DIATOM Maximum N Uptake Rate	1	mg N/mg Chla/day	Assigned 1 mg N/mg Chla/d within range of published values, assigned to all phytoplankton groups Allan et al (2018) 1.4-3.3 mg N/mg Chla/d (2x NZ lakes) Caramatti (2021) 9.5 mg N/mg Chla/d (Lake Constance) Cui et al (2016) 0.58 mg N/mg Chla/d (China sub-tropical reservoir) Bruce et al (2006) ~4.4 mg N/mg Chla/d (assuming a 40 mg C:1 mg chla ratio) (Israel lake) Ghane (2022) 4 mg N/mg Chla/d (Canadian shield lake) Scott & Patterson (2022) 3.5 mg N/mg Chla/d (OK USA reservoir)
DIATOM Growth N ½ Saturation Constant	0.06	mg N/L	Assigned: 0.06 mg N/L within range of published values Absalon (2020) 0.04 mg N/L (Poland reservoir) Allan et al (2018) 0.05-0.065 mg N/L (2x NZ lakes) Caramatti (2021) 0.02 mg NL (Lake Constance) Cui et al (2016) 0.099 mg N/L (China sub-tropical reservoir) Ghane (2022) 0.045 mg N/L (Canadian shield lake) Romero et al (2004) 0.06 mg N/L (2x NSW Australia reservoirs) Scott & Patterson (2022) 0.045 mg N/L (OK USA reservoir) Trammer (2018) 0.075 mg N/L (ID USA reservoir)
DIATOM Growth Si ½ Saturation Constant	0.3	mg Si/L	Assigned: 0.3 mg Si/L within range of published/unpublished values Cui et al (2016) 0.2 mg Si/L (China sub-tropical reservoir) Ghane (2022) 0.2 mg Si/L (Canadian shield lake) Jones et al (2014) 0.2 mg Si/L (NZ lake) McBride et al (2016) 0.2 mg Si/L (NZ lake) Romero et al (2004) 0.3 mg/L (2x NSW Australia reservoirs) but not reported
DIATOM Total Loss Rate (Respiration+Excretion+Mortality) Rate @ 20°C	0.16	1/d	Assigned: 0.16 1/d at upper range of published values Absalon (2020) 0.2 1/d (Poland reservoir) Allan et al (2018) 0.08-0.16 1/d (2x NZ lakes) Caramatti (2021) 0.15 1/d (Lake Constance) Cui et al (2016) 0.06 1/d (China sub-tropical reservoir) Ghane (2022) 0.09 1/d (Canadian shield lake) Romero et al (2004) 0.14 1/d (2x NSW Australia reservoirs) Scott & Patterson (2022) 0.12 1/d (OK USA reservoir) Trammer (2018) 0.11 1/d (ID USA reservoir)
DIATOM Total Loss Rate Temperature Multiplier	1.08		Assigned: 1.08 within range of published values Absalon (2020) 1.07 (Poland reservoir) Allan et al (2018) 1.06-1.10 (2x NZ lakes) Bruce et al (2006) 1.12 (Israel lake) Caramatti (2021) 1.06 (Lake Constance)

Parameter	Value	Units	References and Justification
			Romero et al (2004) 1.08 (2x NSW Australia reservoirs) Trammer (2018) 1.07 (ID USA reservoir)
DIATOM Fraction of Total Loss Rate to Respiration	0.69		Assigned: 0.69 within range of published values, assigned to all phytoplankton groups Allan et al (2018) 0.7-0.79 (2x NZ lakes) Bruce et al (2006) 0.4 m/d (Israel lake) Ghane (2022) 0.3 (Canadian shield lake) Jones et al (2014) 0.8 (NZ lake) McBride et al (2016) 0.7 (NZ lake) McBride et al (2019) 0.9 (NZ lake)
DIATOM Fraction of Total Loss Rate less Respiration to Mortality (to particulate organic matter)	0.67		Assigned: 0.67 within range of published values, assigned to all phytoplankton groups Allan et al (2018) 0.26-0.7 (2x NZ lakes) Bruce et al (2006) 0.9 (Israel lake) Ghane (2022) 0.6 (Canadian shield lake) Jones et al (2014) 0.7 (NZ lake) McBride et al (2019) 0.95 (NZ lake)
DIATOM Fraction of Total Loss Rate less Respiration to Excretion (to dissolved organic matter)	0.33		Assigned: 0.33 within range of published values, assigned to all phytoplankton groups Allan et al (2018) 0.3-0.74 (2x NZ lakes) Bruce et al (2006) 0.1 (Israel lake) Ghane (2022) 0.4 (Canadian shield lake) Jones et al (2014) 0.3 (NZ lake) McBride et al (2016) 0.7 (NZ lake) McBride et al (2019) 0.05 (NZ lake)
DIATOM Constant Settling Velocity	0.5	m/d	Assigned: 0.5 m/d within range of published values, similar to unreferenced laboratory measurements, and similar to stoke settling velocity assuming 20 µm and 1,020 kg/m^3 particle diameter and density, respectively Bruce et al (2006) 1.6 m/d (Israel Lake) Caramatti (2021) 0.3 m/d (Lake Constance) Ghane (2022) 0.07 m/d (Canadian shield lake) Romero et al (2004) 0.05 m/d (2x NSW Australia reservoirs) Scott & Patterson (2022) 0.5 m/d (OK USA reservoir) Trammer (2018) 0.2 m/d (ID USA reservoir)
DIATOM Critical Shear Stress for Resuspension	*0.01*	*N/m^2*	*Assigned: As POM*
DIATOM Maximum Resuspension Rate	$1x10^{-5}$	g/m^2/d	Assigned: Adopted maximum sediment total resuspension rate of ~0.1 g/m^2/d where assume ~0.01% diatoms in upper sediments Chung et al (2009) 0.075 g/m^2/d (CA USA Salton Sea)
DIATOM Resuspension Half Saturation Constant	0.05	g/m^2	Assigned: Estimate based on half the areal mass of an assumed ~1 mm active resuspension layer in upper sediments with ~0.01% diatoms (~0.1 g/m^2)
DIATOM Specific Light Attenuation Coefficient	0.02	(1/m)/(µg Chla/L)	Assigned: 0.02 1/m/(µg Chla/L) within range of published values, assigned to all phytoplankton groups Absalon (2020) 0.04 1/m/(µg Chla/L) (Poland reservoir) Cui et al (2016) 0.01 1/m/(µg Chla/L) (China sub-tropical reservoir) Ghane (2022) 0.02 1/m/(µg Chla/L) (Canadian shield lake) Value of 0.02 1/m/(µg Chla/L) in Romero et al (2004) but not reported
Green Algae (GA, Chlorophytes) (State Variable CHLOR)			
GA Carbon to Chl-a Ratio	*40*	*mg C/mg Chla*	*Assumed: 40 mg C/mg* Chla *for all phytoplankton groups as for diatoms* Additional references Absalon (2020) 40 mg C/mg Chla (Poland reservoir)

Parameter	Value	Units	References and Justification
			Romero et al (2004) 40 mg C/mg Chla (2x NSW Australia reservoirs) Scott & Patterson (2022) 27 mg C/mg Chla (OK USA reservoir)
GA Maximum Growth Rate @ 20°C	1	1/d	Selected: 1.0 1/d within range of published values Absalon (2020) 1.5 1/d (Poland reservoir) Allan et al (2018) 1-1.5 1/d (2x NZ lakes) Romero et al (2004) 0.8 1/d (2x NSW Australia reservoirs) Scott & Patterson (2022) 1.8 1/d (OK USA reservoir)
GA Initial Slope of PI Curve	90	µE/m^2/s	Assigned: 90 µE/m^2/s within range of published values Absalon (2020) 100 µE/m^2/s (Poland reservoir) Allan et al (2018) 30-80 µE/m^2/s (2x NZ lakes) Romero et al (2004) 100 µE/m^2/s (2x NSW Australia reservoirs) Scott & Patterson (2022) 20 µE/m^2/s (OK USA reservoir)
GA Growth Temperature Multiplier	*1.06*		*Assumed: 1.06 for all phytoplankton groups as for diatoms* Additional references Allan et al (2018) 1.06-1.08 (2x NZ lakes) Romero et al (2004) 1.08 (2x NSW Australia reservoirs)
GA Growth Standard Temperature	20	°C	Assigned: 20°C within range of published values Absalon (2020) 17°C (Poland reservoir) Allan et al (2018) 20°C (2x NZ lakes) Romero et al (2004) 20°C (2x NSW Australia reservoirs) Scott & Patterson (2022) 12°C (OK USA reservoir)
GA Growth Optimum Temperature	28	°C	Assigned: 28°C within range of published values Absalon (2020) 24°C (Poland reservoir) Allan et al (2018) 26-30°C Romero et al (2004) 28°C (2x NSW Australia reservoirs) Scott & Patterson (2022) 23°C (OK USA reservoir)
GA Growth Maximum Temperature	35	°C	Assigned: 35°C within range of published values Absalon (2020) 30°C (Poland reservoir) Allan et al (2018) 34°C (2x NZ lakes) Romero et al (2004) 35°C (2x NSW Australia reservoirs) Scott & Patterson (2022) 30°C (OK USA reservoir)
GA Minimum Internal P:Chla Ratio	*0.3*	*mg P/mg Chla*	*Assumed: 0.3 mg P/mg Chla for all phytoplankton groups as for diatoms* Additional references Absalon (2020) 0.3 mg P/mg Chla (Poland reservoir) Allan et al (2018) 0.2-1.8 mg P/mg Chla (2x NZ lakes) Scott & Patterson (2022) 0.25 mg P/mg chla (OK USA reservoir)
GA Maximum Internal P:Chla Ratio	*1.2*	*mg P/mg Chla*	*Assumed: 1.2 mg P/mg Chla for all phytoplankton groups as for diatoms* Additional references Absalon (2020) 1 mg P/mg Chla (Poland reservoir) Allan et al (2018) 2.1-2.2 mg P/mg Chla (2x NZ lakes) Scott & Patterson (2022) 1.3 mg P/mg Chla (OK USA reservoir)
GA Maximum P Uptake Rate	*0.5*	*mg P/mg Chla/d*	*Assumed: 0.5 g P/mg Chla/d for all phytoplankton groups as for diatoms* Additional reference Allan et al (2018) 0.15-0.22 g P/mg Chla/d (2x NZ lakes)
GA Growth P ½ Saturation Constant	0.005	mg P/L	Assigned: 0.005 mg P/L within range of published values Absalon (2020) 0.001 mg P/L (Poland reservoir)

Parameter	Value	Units	References and Justification
			Allan et al (2018) 0.004-0.005 mg P/L (2x NZ lakes) Romero et al (2004) 0.005 mg P/L Scott & Patterson (2022) 0.01 mg P/L (OK USA reservoir)
GA Minimum Internal N:Chla Ratio	*2.5*	*mg N/mg Chla*	*Assumed: 2.5 mg N/mg Chla for all phytoplankton groups as for diatoms* Additional references Absalon (2020) 3 mg N/mg Chla (Poland reservoir) Allan et al (2018) 2-3.1 mg N/mg Chla (2x NZ lakes) Scott & Patterson (2022) 2 mg N/mg Chla (OK USA reservoir)
GA Maximum Internal N:Chla Ratio	*5*	*mg N/mg Chla*	*Assumed: 5 mg N/mg Chla for all phytoplankton groups as for diatoms* Additional references Absalon (2020) 5 mg N/mg Chla (Poland reservoir) Allan et al (2018) 3.5-11.5 mg N/mg Chla (2x NZ lakes) Scott & Patterson (2022) 4.5 mg N/mg Chla (OK USA reservoir)
GA Maximum N Uptake Rate	*1*	mg N/mg Chla/d	*Assumed: 1 mg N/mg Chla/d for all phytoplankton groups as for diatoms* Additional references Adopt 1 mg N/mg Chla/d for all phytoplankton groups as for diatoms Allan et al (2018) 1.6-3.8 mg N/mg Chla/d (2x NZ lakes) Scott & Patterson (2022) 3.5 mg N/mg Chla/d (OK USA reservoir)
GA Growth N ½ Saturation Constant	0.06	mg N/L	Assigned: 0.06 mg N/L at upper range of published values Absalon (2020) 0.05 mg N/L (Poland reservoir) Allan et al (2018) 0.004-0.06 mg N/L (2x NZ lakes) Romero et al (2004) 0.06 mg N/L (2x NSW Australia reservoirs) Scott & Patterson (2022) 0.045 mg N/L (OK USA reservoir)
GA Total Loss Rate (Respiration+Excretion+Mortality) Rate @ 20°C	0.16	1/d	Assigned: 0.16 1/d within range of published values Absalon (2020) 0.2 1/d (Poland reservoir) Allan et al (2018) 0.11-0.13 1/d (2x NZ lakes) Romero et al (2004) 0.09 1/d (2x NSW Australia reservoirs) Scott & Patterson (2022) 0.12 1/d (OK USA Reservoir)
GA Respiration Temperature Multiplier	1.07		Assigned: 1.07 within range of published values Absalon (2020) 1.08 (Poland reservoir) Allan et al (2018) 1.06-1.07 (2x NZ lakes) Romero et al (2004) 1.08 (2x NSW Australia reservoirs)
GA Fraction of Total Loss Rate to Respiration	*0.69*		*Assigned: 0.69 for all phytoplankton groups as for diatoms* Additional references Allan et al (2018) 0.64-0.7 (2x NZ lakes) Jones et al (2014) 0.8 (NZ lake) McBride et al (2016) 0.7 (NZ lake) McBride et al (2019) 0.9 (NZ lake)
GA Fraction of Total Loss Rate less Respiration to Mortality (to particulate organic matter)	*0.67*		*Assigned: 0.67 for all phytoplankton groups as for diatoms* Additional references Allan et al (2018) 0.17-0.67 (2x NZ lakes) Jones et al (2014) 0.7 (NZ lake) McBride et al (2016) 0.3 (NZ lake) McBride et al (2019) 0.9 (NZ lake)
GA Fraction of Total Loss Rate less Respiration to Excretion (to dissolved organic matter)	*0.33*		*Assigned: 0.33 for all phytoplankton groups as for diatoms* Additional references Allan et al (2018) 0.33-0.83 (2x NZ lakes)

Parameter	Value	Units	References and Justification
			Jones et al (2014) 0.3 (NZ lake) McBride et al (2016) 0.7 (NZ lake) McBride et al (2019) 0.1 (NZ lake)
GA Constant Settling Velocity	0.2	m/s	Assigned: 0.2 m/d within range of published values, similar to unreferenced laboratory measurements, and similar to stoke settling velocity assuming 15 µm and 1,020 kg/m^3 particle diameter and density, respectively Allan et al (2018) 0-0.66 m/d (2x NZ lakes) Romero et al (2004) 0.02 m/d (2x NSW Australia reservoirs) Scott & Patterson (2022) 0.5 m/d (OK USA reservoir)
GA Critical Shear Stress for Resuspension	*0.01*	*N/m^2*	*Assigned: As POM*
GA Maximum Resuspension Rate	*1x10^{-5}*	*g/m^2/d*	*Assigned: As diatoms*
GA Resuspension Half Saturation Constant	0.05	g/m^2	Assigned: Estimate based on half the areal mass of an assumed ~1 mm active resuspension layer in upper sediments with ~0.01% green algae (~0.1 g/m^2)
GA Specific Light Attenuation Coefficient	*0.02*	*(1/m)/(µg Chla/L)*	*Assigned: 0.02 1/m/(µg Chla/L) for all phytoplankton groups as for diatoms* Additional references Absalon (2020) 0.04 1/m/(µg Chla/L) (Poland reservoir) Value of 0.02 1/m/(µg Chla/L) in Romero et al (2004) but not reported Cui et al (2016) 0.01 1/m(µg CYANO Chla/L) (China sub-tropical reservoir)
Blue-Green Algae (BGA, Cyanobacteria) (State Variable CYANO)			
BGA Carbon to Chl-a Ratio	*40*	*mg C/mg Chla*	*Adopt 40 mg C/mg Chla for all phytoplankton groups as for diatoms* Additional references Absalon (2020) 40 mg C/mg Chla (Poland reservoir) Caramatti (2021) 40 mg C/mg Chla (Lake Constance) Ghane (2022) 40 mg C/mg Chla (Canadian shield lake) Romero et al (2004) 40 mg C/mg Chla (2x NSW Australia reservoirs) Scott & Patterson (2022) 80 mg C/mg Chla (OK USA reservoir)
BGA Maximum Growth Rate @ 20°C	0.8	1/d	Assigned: 0.8 1/d within range of published values Absalon (2020) 1.0 1/d (Poland reservoir) Allan et al (2018) 0.5-0.6 1/d (2x NZ lakes) Caramatti (2021) 1.3 1/d (Lake Constance) Cui et al (2016) 0.7 1/d (China sub-tropical lake) Ghane (2022) 0.8 1/d (Canadian shield lake) Romero et al (2004) 1.1 1/d (2x NSW Australia reservoirs) Scott & Patterson (2022) 1.2 1/d (OK USA reservoir) Trammer (2018) 0.75 (ID USA reservoir)
BGA Initial Slope of PI Curve	130	µE/m^2/s	Assigned: 130 µE/m^2/s within range of published values Absalon (2020) 150 µE/m^2/s (Poland reservoir) Allan et al (2018) 150-190 µE/m^2/s (2x NZ lakes) Caramatti (2021) 150 µE/m^2/s (Lake Constance) Cui et al (2016) 180 µE/m^2/s (China sub-tropical reservoir) Ghane (2022) 130 µE/m^2/s (Canadian shield lake) Romero et al (2004) 130 µE/m^2/s (2x NSW Australia reservoirs) Scott & Patterson (2022) 60 µE/m^2/s (OK USA reservoir)
BGA Growth Temperature Multiplier	1.08		Assigned: 1.08 within range of published values Allan et al (2018) 1.08-1.09 (2x NZ lakes) Caramatti (2021) 1.09 1/d (Lake Constance) Ghane (2022) 1.08 (Canadian shield lake)

Parameter	Value	Units	References and Justification
			Romero et al (2004) 1.08 (2x NSW Australia reservoirs) Trammer et al (2018) 1.06-1.09 (ID USA reservoir)
BGA Growth Standard Temperature	20	°C	Assigned: 20C within range of published values Absalon (2020) 20°C (Poland reservoir) Allan et al (2018) 20°C (2x NZ lakes) Caramatti (2021) 20°C (Lake Constance) Cui et al (2016) 20°C (China sub-tropical reservoir) Ghane (2022) 24°C (Canadian shield lake) Romero et al (2004) 20°C (2x NSW Australia reservoirs) Scott & Patterson (2022) 20°C (OK USA reservoir) Tranmer et al (2018) 20°C (ID USA reservoir)
BGA Growth Optimum Temperature	30	°C	Assigned: 30C within range of published values Absalon (2020) 20°C (Poland reservoir) Allan et al (2018) 27-34°C (2x NZ lakes) Caramatti (2021) 16°C (Lake Constance) Cui et al (2016) 28°C (China sub-tropical reservoir) Ghane (2022) 30°C (Canadian shield lake) Romero et al (2004) 30°C (2x NSW Australia reservoirs) Scott & Patterson (2022) 28°C (OK USA reservoir) Tranmer et al (2018) 33°C (ID USA reservoir)
BGA Growth Maximum Temperature	39	°C	Assigned: 39C within range of published values Absalon (2020) 35°C (Poland reservoir) Allan et al (2018) 39-41°C (2x NZ lakes) Caramatti (2021) 30°C (Lake Constance) Cui et al (2016) 35°C (China sub-tropical reservoir) Ghane (2022) 39°C (Canadian shield lake) Romero et al (2004) 39°C (2x NSW Australia reservoirs) Scott & Patterson (2022) 40°C (OK USA reservoir) Tranmer et al (2018) 39°C (ID USA reservoir)
BGA Maximum Internal P:Chla Ratio	*0.3*	*mg P/mg Chla*	*Assigned: 0.3 mg P/mg Chla for all phytoplankton groups as for diatoms* Additional references Absalon (2020) 0.1 mg P/mg Chla (Poland reservoir) Allan et al (2018) 0.22-0.49 mg P/mg Chla (2x NZ lakes) Caramatti (2021) 0.8 mg P/mg Chla (Lake Constance) Cui et al (2016) 0.03 mg P/mg Chla (China sub-tropical reservoir) Ghane (2022) 0.16 mg P/mg Chla (Canadian shield lake) Scott & Patterson (2022) 0.5 mg P/mg Chla (OK USA reservoir)
BGA Minimum Internal P:Chla Ratio	*1.2*	*mg P/mg Chla*	*Assigned: 1.2 mg P/mg Chla for all phytoplankton groups as for diatoms* Additional references Absalon (2020) 1.5 mg P/mg Chla (Poland reservoir) Allan et al (2018) 1-2 mg P/mg Chla (2x NZ lakes) Caramatti (2021) 1.2 mg P/mg Chla (Lake Constance) Cui et al (2016) 2.6 mg P/mg Chla (China sub-tropical reservoir) Ghane (2022) 1 mg P/mg Chla (Canadian shield lake) Scott & Patterson (2022) 2 mg P/mg Chla (OK USA reservoir)
BGA Maximum P Uptake Rate	*0.5*	*mg P/mg Chla/d*	*Assigned: 0.5 mg P/mg Chla/d for all phytoplankton groups as for diatoms* Additional references Allan et al (2018) 0.3-0.39 mg P/mg Chla/d (2x NZ Lakes) Caramatti (2021) 2.2 mg P/mg Chla/d (Lake Constance)

Parameter	Value	Units	References and Justification
			Cui et al (2016) 1.1 mg P/mg Chla/d (China sub-tropical reservoir) Ghane (2022) 0.59 mg P/mg Chla/d (Canadian shield lake) Scott & Patterson (2022) 0.3 mg P/mg chla/d (OK USA reservoir)
BGA Growth P ½ Saturation Constant	0.005	mg P/L	Assigned: 0.005 mg P/L within range of published values Absalon (2020) 0.001 mg P/L (Poland reservoir) Allan et al (2018) 0.003-0.006 mg P/L (2x NZ lakes) Caramatti (2021) 0.003 mg P/L (Lake Constance) Cui et al (2016) 0.01 mg P/L (China sub-tropical reservoir) Ghane (2022) 0.007 mg P/L (Canadian shield lake) Romero et al (2004) 0.008 mg P/L (2x NSW Australia reservoirs) Scott & Patterson (2022) 0.006 mg P/L (OK USA reservoir) Trammer (2018) 0.005 mg P/L (ID USA reservoir)
BGA Maximum Internal N:Chla Ratio	*2.5*	*mg N/mg Chla*	*Assigned: 2.5 mg N/mg Chla for all phytoplankton groups as for diatoms* Additional references Absalon (2020) 2.5 mg N/mg Chla (Poland reservoir) Allan et al (2018) 2.9-3.5 mg N/mg Chla (2x NZ lakes) Caramatti (2021) 5 mg N/mg Chla (Lake Constance) Cui et al (2016) 2 mg N/mg Chla (China sub-tropical reservoir) Ghane (2022) 1 mg N/mg Chla (Canadian shield lake) Scott & Patterson (2022) 2.5 mg P/mg Chla (OK USA reservoir)
BGA Minimum Internal N:Chla Ratio	*5*	*mg N/mg Chla*	*Assigned: 5 mg N/mg Chla for all phytoplankton groups as for diatoms* Additional references Absalon (2020) 5 mg N/mg Chla (Poland reservoir) Allan et al (2018) 5-9.5 mg N/mg Chla (2x NZ lakes) Caramatti (2021) 9 mg N/mg Chla (Lake Constance) Cui et al (2016) 4 mg N/mg Chla (China sub-tropical reservoir) Ghane (2022) 5 mg N/mg Chla (Canadian shield lake) Scott & Patterson (2022) 4 mg P/mg Chla (OK USA reservoir)
BGA Maximum N Uptake Rate	*1*	*mg N/mg Chla/d*	*Assigned: 1 mg N/mg Chla /day for all phytoplankton groups as for diatoms* Additional references Allan et al (2018) 1.5-3.3 mg N/mg Chla (2x NZ lakes) Caramatti (2021) 10 mg N/mg Chlad (Lake Constance) Cui et al (2016) 0.75 mg N/mg Chla (China sub-tropical reservoir) Ghane (2022) 4 mg N/mg Chla (Canadian shield lake) Scott & Patterson (2022) 1.5 mg P/mg Chla (OK USA reservoir)
BGA Growth N ½ Saturation Constant	0.03	mg N/L	Assigned: 0.03 mg N/L within range of published values Absalon (2020) 0.04 mg N/L (Poland reservoir) Allan et al (2018) 0.017-0.033 mg N/L (2x NZ lakes) Caramatti (2021) 0.015 mg N/L (Lake Constance) Cui et al (2016) 0.098 mg N/L (China sub-tropical reservoir) Ghane (2022) 0.045 mg N/L (Canadian shield lake) Romero et al (2004) 0.03 mg N/L (2x NSW Australia reservoirs) Scott & Patterson (2022) 0.0001 mg N/L (OK USA reservoir) Trammer (2018) 0.045 mg N/L (ID USA reservoir)
BGA Total Loss Rate (Respiration+Excretion+Mortality) Rate @ 20°C	0.12	1/d	Assigned: 0.12 1/d within range of published values Absalon (2020) 0.2 1/d (Poland reservoir) Allan et al (2018) 0.078-0.09 1/d (2x NZ lakes) Caramatti (2021) 0.08 1/d (Lake Constance) Cui et al (2016) 0.093 1.d (China sub-tropical reservoir)

Parameter	Value	Units	References and Justification
			Ghane (2022) 0.125 1/d (Canadian shield lake) Romero et al (2004) 0.07 1/d (2x NSW Australia reservoirs) Scott & Patterson (2022) 0.05 1/d (OK USA reservoir) Trammer (2018) 0.074 1/d (ID USA reservoir)
BGA Respiration Temperature Multiplier	1.06		Assigned: Adopt 1.06 within range of published values Absalon (2020) 1.03 (Poland reservoir) Allan et al (2018) 1.03-1.06 (2x NZ lakes) Caramatti (2021) 1.09 (Lake Constance) Romero et al (2004) 1.08 (2x NSW Australia reservoirs) Trammer (2018) 1.04 (ID USA reservoir)
BGA Fraction of Total Loss Rate to Respiration	*0.69*		*Assigned: 0.69 for all phytoplankton groups as for diatoms* Additional references Allan et al (2018) 0.1-0.78 (2x NZ lakes) Bruce et al (2006) 0.4 Ghane (2022) 0.5 Jones et al (2014) 0.8 (NZ lake) McBride et al (2019) 0.6 (NZ lake)
BGA Fraction of Total Loss Rate less Respiration to Mortality (to particulate organic matter)	*0.67*		*Assigned: 0.67 for all phytoplankton groups as for diatoms* Additional references Allan et al (2018) 0.43-0.9 (2x NZ lakes) Bruce et al (2006) 0.9 Ghane (2022) 0.3 Jones et al (2014) 0.7 (NZ lake) McBride et al (2019) 0.99 (NZ lake)
BGA Fraction of Total Loss Rate less Respiration to Excretion (to dissolved organic matter)	*0.33*		*Assigned: 0.33 for all phytoplankton groups as for diatoms* Additional references Allan et al (2018) 0.1-0.57 (2x NZ lakes) Bruce et al (2006) 0.1 Ghane (2022) 0.7 Jones et al (2014) 0.3 (NZ lake) McBride et al (2016) 0.7 (NZ lake) McBride et al (2019) 0.01 (NZ lake)
BGA Constant Settling Velocity	0.1	m/d	Assigned: 0.1 m/d though greater than published values, but similar to stoke settling velocity assuming 10 µm and 1,020 kg/m^3 particle diameter and density, respectively Ghane (2022) 0.04 m/d (Canadian shield lake) Romero et al (2004) 0.01 m/d (2x NSW Australia reservoirs)
BGA Critical Shear Stress for Resuspension	*0.01*	*N/m^2*	*Assigned: As POM*
BGA Maximum Resuspension Rate	*1x10^{-5}*	*g/m^2/d*	*Assigned: As diatoms*
BGA Resuspension Half Saturation Constant	0.05	g/m^2	Assigned: Estimate based on half the areal mass of an assumed ~1 mm active resuspension layer in upper sediments with ~0.01% blue-green algae (~0.1 g/m^2)
BGA Specific Light Attenuation Coefficient	*0.02*	*(1/m)/(µg Chla/L)*	*Adopt 0.02 1/m/(µg Chla/L) for all phytoplankton groups as for diatoms* Additional references Absalon (2020) 0.04 1/m/(µg Chla/L) (Poland reservoir) Cui et al (2016) 0.02 1/m(µg CYANO Chla/L) (China sub-tropical reservoir) Ghane (2022) 0.02 1/m/(µg Chla/L) (Canadian shield lake)
Clay Inorganic Particles (State Variable SSOL1)			

Parameter	Value	Units	References and Justification
CLAY Stokes Law Settling Density	2650	kg/m^3	Assigned: Inorganic particle density (quartz)
CLAY Stokes Law Settling Diameter	1	µm	Assigned: Clay particle at lower range of particle diameters of 1 um
CLAY Critical Shear Stress for Resuspension	*0.01*	*N/m^2*	*Assigned: As POM*
CLAY Maximum Resuspension Rate	0.05	g/m^2/d	Assigned: Adopted maximum sediment total resuspension rate of ~0.1 g/m^2/d where assume ~50% clay in upper sediments Chung et al (2009) 0.075 g/m^2/d (CA USA Salton Sea)
CLAY Resuspension Half Saturation Constant	500	g/m^2	Assigned: Estimate based on half the areal mass of an assumed ~1 mm active resuspension layer in upper sediments and ~34% clay (~1,000 g/m^2)
CLAY Specific Light Attenuation Coefficient	0.05	(1/m)/(mg/L)	Assigned: Assumed value
Silt Inorganic Particles (State Variable SSOL2)			
SILT Stokes Law Particle Density	2650	kg/m^3	Assigned: Inorganic particle density (quartz)
SILT Stokes Law Particle Diameter	4	µm	Assigned: Very fine silt particle at lower range of particle diameters of 4 um
SILT Critical Shear Stress for Resuspension	*0.01*	*N/m^2*	*Assigned: As POM*
SILT Maximum Resuspension Rate	0.05	g/m^2/d	*Assigned: As CLAY*
SILT Resuspension Half Saturation Constant	500	g/m^2	Assigned: Estimate based on half the areal mass of an assumed ~1 mm active resuspension layer in upper sediments and ~30% silt (~1,000 g/m^2)
SILT Specific Light Attenuation Coefficient	0.05	(1/m)/(mg/L)	Assigned: Assumed value
Manganese (State Variables DMn, PMn)			
DMn Maximum Oxidation (Coagulation) Rate @ 20°C	0.0175 (0.05)	1/d	Assigned: Updated value based on calibration/validation of reservoirs since GHD (2024) Previously Assigned: 0.0175 1/d, which is half of the Johnson et al (1991) published value as a conservative measure. The coagulation rate in this context represents the conversion of dissolved reduced manganese (MnIV or DMn) to particulate oxidized manganese (MnII or PMn). Johnson et al (1991) coagulation coefficient 0.035 1/d (Switzerland lake) Zhang et al (2022) coagulation coefficient 0.35 1/d (VIC Australia reservoir) (Note this is very likely a typo in the dissertation and ought to be 0.035 1/d) Munger et al (2016) determined half-times of reduced DMn in the range of 10-60 days, which is equivalent to 0.069-0.012 1/d exponential rate.
DMn Oxidation (Coagulation) DO ½ Saturation Constant	1 (3)	mg O_2/L	Assigned: Updated value based on calibration/validation of reservoirs since GHD (2024) Previously Assigned: 1 mg/L on basis of published value Johnson et al (1991) 1 mg/L
DMn Oxidation (Coagulation) Temperature Multiplier	1.05		Assigned: Assumed 1.05
PMn Maximum Reduction Rate @ 20°C	*0.00875 (0.05)*	1/d	Assigned: Assumed 50% of oxidation (coagulation) rate
PMn Reduction DO ½ Saturation Constant	0.25 (3)	mg O_2/L	Assigned: Updated value based on calibration/validation of reservoirs since GHD (2024) Previously Assigned: Assumed very low DO that yields redox conditions
PMn Reduction Temperature Multiplier	1.05		Assigned: Assumed 1.05
DMn Maximum Sediment Flux Rate @ 20°C	0.1 (0.055)	g Mn/m^2/d	Assigned: Updated value based on calibration/validation of reservoirs since GHD (2024) Previously Assigned: 0.1 g/m^2/d that is greater than published/unpublished values as conservative measure Beutal & Hannoun (2007) 0.028-0.050 g/m^2/d (CA USA eutrophic reservoir)

Parameter	Value	Units	References and Justification
			Johnson et al (1991) 0.011-0.055 g/m^2/d (Switzerland lake) Kreuger et al (2020) 0.034-0.062 g/m^2/d (VA USA reservoir, flux chamber) Romero (unpubl. data) 0.07 g/m^2/d with linear inverse Michaelis-Menten relation for Pickering (1994) Australia reservoir DMn sediment flux data with DO ½ saturation=1 mg/L, a=-0.1, b=1.1, temperature multiplier=1.05 and minimum flux rate of 0 g/m^2/d (r^2-0.99)
DMn Sediment Flux DO ½ Saturation Constant	1 (3)	mg O_2/L	Assigned: Updated value based on calibration/validation of reservoirs since GHD (2024) Previously Assigned: 1 mg/L as published values Johnson et al (1991) 1 mg/L Romero (unpubl. data) 1 mg/L for Pickering (1994) NSW Australian reservoir sediment flux data
DMn Sediment Flux Temperature Multiplier	*1.05*		*Assigned: Assumed 1.05 for all sediment flux rates as DOC*
PMn Stokes Law Particle Density	3,000	kg/m^3	Assigned: 3000 kg/m^3 as published/unpublished value Neretin et al (2003) estimated density of birnessite of 3000 kg/m^3
PMN Stokes Law Particle Diameter	4 (1.5)	µm	Assigned: Updated value based on calibration/validation of reservoirs since GHD (2024) Previously Assigned: 4 µm as published value Neretin et al (2003) estimated spherical diameter of 4 µm
PMn Critical Shear Stress for Resuspension	*0.01*	*N/m^2*	*Assigned: As POM*
PMn Maximum Resuspension Rate	0.0001	g/m^2/d	Assigned: Adopted maximum sediment total resuspension rate of ~0.1 g/m^2/d where assume ~0.1% PMn in upper sediments Chung et al (2009) 0.075 g/m^2/d (CA USA Salton Sea)
PMn Resuspension Half Saturation Constant	1	g/m^2	Assigned: Estimate based on half the areal mass of an assumed ~1 mm active resuspension layer in upper sediments and ~0.1% manganese (~3 g/m^2)
PMn Specific Light Attenuation Coefficient	0.02	1/m/(mg PMN/L)	Assigned: Assumed value
Iron (State Variables DFE, PFE)			
DFe Maximum Oxidation (Coagulation) Rate @ 20°C	*0.035* (0.02)	*1/d*	Assigned: Updated value based on calibration/validation of reservoirs since GHD (2024) *Previously Assigned: Assumed published coagulation rate of Mn* Munger et al (2016) determined half-time of reduced FMn in range of 1-6 days, which is equivalent to exponential rate of 0.69-0.12 1/d exponential rate
DFe Oxidation (Coagulation) DO ½ Saturation Constant	*1*	*mg O_2/L*	*Assigned: Assumed as Mn*
DFe Oxidation (Coagulation) Temperature Multiplier	*1.05*		*Assigned: Assumed as Mn*
PFEe Maximum Reduction Rate @ 20°C	*0.0175 (0.01)*	*1/d*	*Scaled: Assumed 50% of oxidation (coagulation) rate*
PFe Reduction DO ½ Saturation Constant	1	mg O_2/L	Assigned: Assumed higher DO threshold than PMN
PFe Reduction Temperature Multiplier	*1.05*		*Assigned: Assumed as Mn*
DFe Maximum Sediment Flux Rate @ 20°C	1 (0.5)	g Fe/m^2/d	Assigned: Updated value based on calibration/validation of reservoirs since GHD (2024) Previously Assigned: 1 g/m^2/d that is greater than published/unpublished values as conservative measure Beutal & Hannoun (2007) 0.003-0.007 g/m^2/d (CA USA eutrophic reservoir) Cervo & Cole (1996) 0.55 g/m^2/d (Chesapeake Bay USA) Kreuger et al (2020) 0.34-0.56 g/m^2/d (VA USA reservoir, flux chamber) Romero (unpubl. data) 0.72 g/m^2/d with linear inverse Michaelis-Menten relation for Pickering (1994) Australia reservoir sediment flux data with DO ½ saturation=0.3 mg/L, a=-0.1, b=1.1, temperature multiplier=1.05 and

Parameter	Value	Units	References and Justification
			minimum flux rate of 0 g/m^2/d (r^2-0.99) Urban et al (1997) 0.05 g/m^2/d (Switzerland lake, flux chamber)
DFe Sediment Flux DO ½ Saturation Constant	0.3 (1)	mg O_2/L	Assigned: Updated value based on calibration/validation of reservoirs since GHD (2024) Previously Assigned: 0.3 mg/L as unpublished value Romero (unpubl. data) 0.3 mg/L for Pickering (1994) Prospect Reservoir sediment flux data
DFe Sediment Flux Temperature Multiplier	*1.05*		*Assigned: Assumed 1.05 for all sediment flux rates as DOC*
PFe Stokes Law Particle Density	*3000*	*kg/m^3*	*Assigned: Assumed as Mn*
PFEe Stokes Law Particle Diameter	*4 (1.5)*	µm	*Assigned: Assumed as Mn*
PFe Critical Shear Stress for Resuspension	*0.01*	N/m^2	*Assigned: Assumed as POM*
PFe Maximum Resuspension Rate	0.005	g/m^2/d	Assigned: Adopted maximum sediment total resuspension rate of ~0.1 g/m^2/d where assume ~5% PFe in upper sediments Chung et al (2009) 0.075 g/m^2/d (CA USA Salton Sea)
PFe Resuspension Half Saturation Constant	50	g/m^2	Assigned: Estimate based on half the areal mass of an assumed ~1 mm active resuspension layer in upper sediments and ~5% iron (~100 g/m^2)
PFe Specific Light Attenuation Coefficient	*0.02*	*1/m/(mg PMN/L)*	*Assigned: Assumed as Mn*

Appendix C

Annual 2015 WFD Direction Metrics for Environmental Compensation Flows

Table C.1 River water body status assessment of withdrawals on annual basis for scenario 1B.

Year	Stage	DO_{Sat} (%) - Annual 10^{th} %ile	BOD– (mg/L) - Annual 90^{th} %ile	NH_x (mg N/L) Annual 90^{th} %ile	pH Annual 5^{th} %ile	pH Annual 95^{th} %ile	FRP (mg P/L) Annual mean	T (C) Annual 98^{th} %ile
2030	Fill	87	6.2	0.045	7.8	8.3	0.009	23.9
2031	Fill	90	5.2	0.055	7.9	8.3	0.005	21.7
2032	Fill-Classic	90	3.4	0.053	8.0	8.4	0.006	21.6
2033	Classic-Recycled	90	2.9	0.057	7.9	8.4	0.005	22.2
2034	Recycled	89	3.3	0.041	7.9	8.3	0.004	22.5
2035	Recycled	92	3.2	0.035	8.0	8.2	0.003	20.4
2036	Recycled	90	3.2	0.034	7.8	8.3	0.004	22.7
2037	Recycled	89	3.2	0.034	7.8	8.3	0.004	22.9
2038	Recycled	91	3.2	0.033	7.9	8.2	0.004	19.8
2039	Recycled	90	3.2	0.032	7.8	8.4	0.004	20.6
2040	Recycled	90	3.2	0.030	7.9	8.2	0.004	21.3
2041	Recycled	89	3.2	0.031	7.8	8.3	0.004	23.1
Assessment Summary -->		*High*	*High*	*High*	*High*	*High*	*High*	*High*

Table C.2 As Table D.1 for scenario 4A.

Year	Stage	DO_{Sat} (%) - Annual 10^{th} %ile	BOD– (mg/L) - Annual 90^{th} %ile	NH_x (mg N/L) Annual 90^{th} %ile	pH Annual 5^{th} %ile	pH Annual 95^{th} %ile	FRP (mg P/L) Annual mean	T (C) Annual 98^{th} %ile
2034	Extended Classic	88	3.3	0.052	7.9	8.3	0.004	22.5
2035	Extended Classic	91	3.5	0.054	8.0	8.3	0.004	20.4
2036	Extended Classic	89	3.6	0.054	7.9	8.3	0.004	22.7
2037	Extended Classic	88	3.8	0.054	7.8	8.3	0.004	22.9
2038	Extended Classic	90	3.8	0.053	7.9	8.2	0.005	19.9
2039	Extended Classic	90	3.8	0.055	7.9	8.4	0.005	20.7
2040	Extended Classic	90	4.1	0.051	7.8	8.1	0.004	21.3
2041	Extended Classic	88	4.2	0.054	7.7	8.2	0.005	23.1
Assessment Summary -->		*High*	*Good-High*	*High*	*High*	*High*	*High*	*High*

Table C.3 As Table D.1 for scenario 2E.

Year	Stage	DO_{Sat} (%) - Annual 10^{th} %ile	BOD– (mg/L) - Annual 90^{th} %ile	NH_x (mg N/L) Annual 90^{th} %ile	pH Annual 5^{th} %ile	pH Annual 95^{th} %ile	FRP (mg P/L) Annual mean	T (C) Annual 98^{th} %ile
2038	Recycled	92	3.5	0.023	7.9	8.2	0.005	19.6
2039	Recycled	91	3.6	0.022	7.9	8.3	0.006	20.5
Assessment Summary -->		*High*	*High*	*High*	*High*	*High*	*High*	*High*

Table C.4 As Table D.1 for scenario 2F.

Year	Stage	DO_{Sat} (%) - Annual 10^{th} %ile	BOD– (mg/L) - Annual 90^{th} %ile	NH_x (mg N/L) Annual 90^{th} %ile	pH Annual 5^{th} %ile	pH Annual 95^{th} %ile	FRP (mg P/L) Annual mean	T (C) Annual 98^{th} %ile
2038	Recycled	92	3.2	0.026	7.9	8.2	0.004	19.7
2039	Recycled	91	3.5	0.025	7.9	8.4	0.004	20.6
Assessment Summary -->		*High*	*High*	*High*	*High*	*High*	*High*	*High*

Table C.5 As Table D.1 for scenario 2G.

Year	Stage	DO_{Sat} (%) - Annual 10^{th} %ile	BOD– (mg/L) - Annual 90^{th} %ile	NH_x (mg N/L) Annual 90^{th} %ile	pH Annual 5^{th} %ile	pH Annual 95^{th} %ile	FRP (mg P/L) Annual mean	T (C) Annual 98^{th} %ile
2038	Recycled	92	3.2	0.026	8.0	8.2	0.004	19.6
2039	Recycled	91	3.2	0.024	7.9	8.4	0.004	20.6
Assessment Summary -->		*High*	*High*	*High*	*High*	*High*	*High*	*High*

Table C.6 As Table D.1 for scenario 2H.

Year	Stage	DO_{Sat} (%) - Annual 10^{th} %ile	BOD– (mg/L) - Annual 90^{th} %ile	NH_x (mg N/L) Annual 90^{th} %ile	pH Annual 5^{th} %ile	pH Annual 95^{th} %ile	FRP (mg P/L) Annual mean	T (C) Annual 98^{th} %ile
2038	Recycled	92	3.7	0.024	7.9	8.3	0.006	19.6
2039	Recycled	93	2.8	0.020	7.9	8.4	0.004	20.5
2040	Recycled	91	3.3	0.019	7.9	8.1	0.006	21.1
2041	Recycled	90	3.6	0.024	7.8	8.2	0.006	23.0
Assessment Summary -->		*High*	*High*	*High*	*High*	*High*	*High*	*High*

Table C.7 As Table D.1 for scenario 2I.

Year	Stage	DO_{Sat} (%) - Annual 10^{th} %ile	BOD– (mg/L) - Annual 90^{th} %ile	NH_x (mg N/L) Annual 90^{th} %ile	pH Annual 5^{th} %ile	pH Annual 95^{th} %ile	FRP (mg P/L) Annual mean	T (C) Annual 98^{th} %ile
2038	Recycled	91	3.6	0.027	7.9	8.2	0.005	19.7

Year	Stage	DO_{Sat} (%) - Annual 10^{th} %ile	BOD– (mg/L) - Annual 90^{th} %ile	NH_x (mg N/L) Annual 90^{th} %ile	pH Annual 5^{th} %ile	pH Annual 95^{th} %ile	FRP (mg P/L) Annual mean	T (C) Annual 98^{th} %ile
2039	Recycled	92	3.1	0.024	7.9	8.4	0.004	20.6
2040	Recycled	91	3.3	0.022	7.9	8.1	0.004	21.3
2041	Recycled	90	3.6	0.024	7.8	8.2	0.004	23.1
Assessment Summary -->		*High*	*High*	*High*	*High*	*High*	*High*	*High*

Table C.7 As Table D.1 for scenario 2J.

Year	Stage	DO_{Sat} (%) - Annual 10^{th} %ile	BOD– (mg/L) - Annual 90^{th} %ile	NH_x (mg N/L) Annual 90^{th} %ile	pH Annual 5^{th} %ile	pH Annual 95^{th} %ile	FRP (mg P/L) Annual mean	T (C) Annual 98^{th} %ile
2038	Recycled	92	3.2	0.027	8.0	8.2	0.004	19.6
2039	Recycled	92	3.1	0.025	7.9	8.4	0.004	20.5
2040	Recycled	91	3.1	0.023	7.9	8.2	0.003	21.2
2041	Recycled	90	3.2	0.024	7.8	8.2	0.004	23.0
Assessment Summary -->		*High*	*High*	*High*	*High*	*High*	*High*	*High*

Appendix D

Annual 2015 WFD Direction Metrics for Reservoir

Table D.1 Lake water body status assessment on annual basis for scenario 1B (Bottom$_{SB}$=maximum depth layer of south basin, Bottom$_{NB}$=maximum depth layer of north basin, Surface$_{SB}$=surface layer of south basin, Surface$_{NB}$=surface layer of north basin).

Year	Stage	Surface$_{SB}$ NH_x (mg N/L) Annual 90th %ile	Surface$_{NB}$ NH_x (mg N/L) Annual 90th %ile	Surface$_{SB}$ TP (µg P/L) Annual Mean	Surface$_{NB}$ TP (µg P/L) Annual Mean	Bottom$_{SB}$ DO (mg/L) - Annual July-August	Bottom$_{NB}$ DO (mg/L) - Annual July-August	Surface$_{SB}$ Annual EQR_{Chl-a}	Surface$_{NB}$ Annual EQR_{Chl}
2030	Fill	0.045	0.045	31	31	4.4	7.4	0.36	0.36
2031	Fill	0.055	0.055	29	29	4.9	7.9	0.55	0.55
2032	Fill-Classic	0.053	0.053	29	29	6.5	8.3	0.80	0.80
2033	Classic-Recycled	0.057	0.057	28	28	4.8	7.9	0.98	0.97
2034	Recycled	0.041	0.041	24	24	5.4	7.6	0.80	0.80
2035	Recycled	0.035	0.035	22	22	6.2	8.4	0.63	0.62
2036	Recycled	0.034	0.034	21	21	4.7	8.0	0.67	0.67
2037	Recycled	0.034	0.034	21	21	5.3	7.8	0.73	0.73
2038	Recycled	0.033	0.033	21	21	6.3	8.4	0.77	0.77
2039	Recycled	0.032	0.032	22	22	5.9	8.3	0.74	0.74
2040	Recycled	0.030	0.030	21	21	6.2	8.1	0.70	0.69
2041	Recycled	0.031	0.031	22	22	4.8	7.6	0.69	0.68
Assessment Summary -->		*High*	*High s*	*High RECYCLED*	*High RECYCLED*	*Moderate-Good*	*Good-High*	*High RECYCLED*	*High RECYCLED*

Table D.2 As Table E.1 for scenario 4A.

Year	Stage	Surface$_{SB}$ NH_x (mg N/L) Annual 90th %ile	Surface$_{NB}$ NH_x (mg N/L) Annual 90th %ile	Surface$_{SB}$ TP (µg P/L) Annual Mean	Surface$_{NB}$ TP (µg P/L) Annual Mean	Bottom$_{SB}$ DO (mg/L) - Annual July-August	Bottom$_{NB}$ DO (mg/L) - Annual July-August	Surface$_{SB}$ Annual EQR_{Chl-a}	Surface$_{NB}$ Annual EQR_{Chl-a}
2034	Extended Classic	0.052	0.052	28	28	7.6	7.5	0.82	0.82
2035	Extended Classic	0.054	0.054	28	28	8.4	8.4	0.79	0.79
2036	Extended Classic	0.054	0.054	27	28	7.9	7.9	0.92	0.92
2037	Extended Classic	0.054	0.054	28	28	7.7	7.8	0.94	0.93
2038	Extended Classic	0.053	0.054	28	28	8.3	8.3	1.09	1.08
2039	Extended Classic	0.055	0.055	29	28	8.2	8.1	1.14	1.14
2040	Extended Classic	0.051	0.051	29	29	8.0	8.1	0.88	0.87
2041	Extended Classic	0.054	0.054	29	29	7.4	7.4	0.92	0.92
Assessment Summary -->		*High*	*High*	*Good*	*Good*	*Moderate-Good*	*Good-High*	*High*	*High*

Table D.3 As Table E.1 for scenario 2E.

Year	Stage	$Surface_{SB}$ NH_x (mg N/L) Annual 90th %ile	$Surface_{NB}$ NH_x (mg N/L) Annual 90th %ile	$Surface_{SB}$ TP (µg P/L) Annual Mean	$Surface_{NB}$ TP (µg P/L) Annual Mean	$Bottom_{SB}$ DO (mg/L) - Annual July-August	$Bottom_{NB}$ DO (mg/L) - Annual July-August	$Surface_{SB}$ Annual EQR_{Chl-a}	$Surface_{NB}$ Annual EQR_{Chl-a}
2038	Recycled	0.023	0.023	22	22	6.9	8.4	0.54	0.53
2039	Recycled	0.022	0.023	23	23	6.7	8.2	0.51	0.51
Assessment Summary -->		*High*	*High*	*High*	*High*	*Good*	*High*	*Good*	*Good*

Table D.4 As Table E.1 for scenario 2F.

Year	Stage	$Surface_{SB}$ NH_x (mg N/L) Annual 90th %ile	$Surface_{NB}$ NH_x (mg N/L) Annual 90th %ile	$Surface_{SB}$ TP (µg P/L) Annual Mean	$Surface_{NB}$ TP (µg P/L) Annual Mean	$Bottom_{SB}$ DO (mg/L) - Annual July-August	$Bottom_{NB}$ DO (mg/L) - Annual July-August	$Surface_{SB}$ Annual EQR_{Chl-a}	$Surface_{NB}$ Annual EQR_{Chl-a}
2038	Recycled	0.026	0.026	20	20	6.5	8.4	0.62	0.62
2039	Recycled	0.025	0.025	22	22	5.9	8.2	0.58	0.58
Assessment Summary -->		*High*	*High*	*High*	*High*	*Moderate-Good*	*High*	*High*	*High*

Table D.5 As Table E.1 for scenario 2G.

Year	Stage	$Surface_{SB}$ NH_x (mg N/L) Annual 90th %ile	$Surface_{NB}$ NH_x (mg N/L) Annual 90th %ile	$Surface_{SB}$ TP (µg P/L) Annual Mean	$Surface_{NB}$ TP (µg P/L) Annual Mean	$Bottom_{SB}$ DO (mg/L) - Annual July-August	$Bottom_{NB}$ DO (mg/L) - Annual July-August	$Surface_{SB}$ Annual EQR_{Chl-a}	$Surface_{NB}$ Annual EQR_{Chl-a}
2038	Recycled	0.026	0.025	20	20	6.5	8.5	0.64	0.64
2039	Recycled	0.025	0.026	20	20	6.2	8.0	0.63	0.63
Assessment Summary -->		*High*	*High*	*High*	*High*	*Good*	*High*	*High*	*High*

Table D.6 As Table E.1 for scenario 2H.

Year	Stage	$Surface_{SB}$ NH_x (mg N/L) Annual 90th %ile	$Surface_{NB}$ NH_x (mg N/L) Annual 90th %ile	$Surface_{SB}$ TP (µg P/L) Annual Mean	$Surface_{NB}$ TP (µg P/L) Annual Mean	$Bottom_{SB}$ DO (mg/L) - Annual July-August	$Bottom_{NB}$ DO (mg/L) - Annual July-August	$Surface_{SB}$ Annual EQR_{Chl-a}	$Surface_{NB}$ Annual EQR_{Chl-a}
2038	Recycled	0.024	0.024	23	23	6.7	8.4	0.56	0.55
2039	Recycled	0.020	0.020	20	19	6.9	8.4	0.46	0.45
2040	Recycled	0.019	0.020	19	19	6.5	8.2	0.54	0.51
2041	Recycled	0.024	0.024	24	23	5.1	7.5	0.50	0.49
Assessment Summary -->		*High*	*High*	*High*	*High*	*Moderate-Good*	*Good-High*	*Good-High*	*Good-High*

Table D.7 As Table E.1 for scenario 2I.

Year	Stage	$Surface_{SB}$ NH_x (mg N/L) Annual 90th %ile	$Surface_{NB}$ NH_x (mg N/L) Annual 90th %ile	$Surface_{SB}$ TP (µg P/L) Annual Mean	$Surface_{NB}$ TP (µg P/L) Annual Mean	$Bottom_{SB}$ DO (mg/L) - Annual July-August	$Bottom_{NB}$ DO (mg/L) - Annual July-August	$Surface_{SB}$ Annual EQR_{Chl-a}	$Surface_{NB}$ Annual EQR_{Chl-a}
2038	Recycled	0.027	0.027	22	22	6.5	8.3	0.60	0.59
2039	Recycled	0.024	0.025	20	20	6.2	8.4	0.55	0.54
2040	Recycled	0.022	0.022	20	20	6.2	8.1	0.54	0.52
2041	Recycled	0.024	0.025	23	23	4.8	7.5	0.51	0.51
Assessment Summary -->		*High*	*High*	*High*	*High*	*Moderate-Good*	*Good-High*	*Good-High*	*Good-High*

Table D.8 As Table E.1 for scenario 2J.

Year	Stage	$Surface_{SB}$ NH_x (mg N/L) Annual 90th %ile	$Surface_{NB}$ NH_x (mg N/L) Annual 90th %ile	$Surface_{SB}$ TP (µg P/L) Annual Mean	$Surface_{NB}$ TP (µg P/L) Annual Mean	$Bottom_{SB}$ DO (mg/L) - Annual July-August	$Bottom_{NB}$ DO (mg/L) - Annual July-August	$Surface_{SB}$ Annual EQR_{Chl-a}	$Surface_{NB}$ Annual EQR_{Chl-a}
2038	Recycled	0.027	0.027	20	20	6.6	8.5	0.66	0.66
2039	Recycled	0.025	0.025	20	20	7.0	8.4	0.59	0.58
2040	Recycled	0.023	0.022	18	19	6.3	8.2	0.59	0.58
2041	Recycled	0.024	0.024	20	20	4.7	7.7	0.59	0.59
Assessment Summary -->		*High*	*High*	*High*	*Good*	*Moderate-Good*	*Good-High*	*High*	*High*

www.ghd.com

The Power of Commitment